FINAL REPORT
VOLUME 4

THE DEVELOPMENT OF QUALIFICATION STANDARDS FOR CAST SUPER DUPLEX STAINLESS STEEL (2507 WROUGHT EQUIVALENT)

OCTOBER 1, 2000 - SEPTEMBER 30, 2005

VASUDEVAN HARIHARAN
CARL D. LUNDIN

MATERIALS JOINING GROUP
MATERIALS SCIENCE AND ENGINEERING
THE UNIVERSITY OF TENNESSEE, KNOXVILLE

CARL D. LUNDIN
PROFESSOR OF METALLURGY

MATERIALS JOINING GROUP
MATERIALS SCIENCE AND ENGINEERING
THE UNIVERSITY OF TENNESSEE
KNOXVILLE 37996-2200

TELEPHONE (865) 974-5310
FAX (865) 974-0880

lundin@utk.edu

FOREWARD

The final report for the DOE Grant DE-FC36-00 IDI13975 consists of five volumes. The volumes provide in depth information on Cast Duplex and Cast Super Duplex Stainless Steels. Volume 1 is entitled "Metallurgical Evaluation of Cast Duplex Stainless Steels and their Weldments" involves comparison of selected grades of Duplex Stainless Steels and their welds with their wrought counterparts regarding corrosion performance, mechanical properties and weldability. Volume 2 entitled "The Development of Qualification Standards for Cast Duplex Stainless Steel" involves inter-laboratory testing and Volume 3 "The Development of Qualification Standards for Cast Super Duplex Stainless Steel" provides information on the testing of Super Duplex Stainless Steels to ASTM A923. Volume 4 is the "Guidance Document for the Evaluation of Super Duplex Stainless Steel" and involves the applicability of ASTM A923 to the Cast Super Duplex materials. Volume 5 is the data package for the incorporation of ASTM A890-5A material into the ASTM A923.

In volume 1 selected grades of Duplex Stainless Steel castings and their welds, in comparison with their wrought counterparts, were evaluated, regarding corrosion performance, mechanical properties and weldability. Multiple heats of cast duplex stainless steel were evaluated in the as-cast, solution annealed static cast and solution annealed centrifugal cast conditions, while their wrought counterparts were characterized in the solution annealed condition and in the form of as-rolled plate. Welding, including extensive assessment of autogenous welds and a preliminary study of composite welds, Shielded Metal Arc Weld (SMAW), was performed. The evaluations included Critical Pitting Temperature (CPT) testing, Intergranular Corrosion (IGC) testing, ASTM A923 (Methods A, B and C), Charpy impact testing, weldability testing (ASTM A494), ferrite measurement and microstructural evaluations.

Volume 2 deals with the Development of Qualification Standards for Cast Duplex Stainless Steel (A890-4A) which is equivalent to wrought 2205. This volume involves

iii

testing of cast Duplex Stainless Steel to several ASTM specifications, formulating and conducting industry round robin tests and studying the reproducibility of the results. ASTM E562 (Standard Test Method for Determining Volume Fraction by Systematic manual Point Count) and ASTM A923 (Standard Test Methods for Detecting Detrimental Intermetallic Phase in Wrought Duplex Austenitic/Ferritic Stainless Steels) were the specifications utilized in conducting this work. An ASTM E562 industry round robin, ASTM A923 applicability study, ASTM A923 industry round robin, and an ASTM A923 study of the effectiveness of existing foundry solution annealing procedures for producing cast Duplex Stainless Steel without intermetallic phases were implemented.

Volume 3 comprises of the Development of Qualification Standards for Cast Super Duplex Stainless Steel (A890-5A) which is equivalent to wrought 2507. The objective of this work was to determine the suitability of ASTM A923 "Standard Test methods for Detecting Detrimental Intermetallic Phase in Duplex Austenitic-Ferritic Stainless Steels" for 25 Cr Cast Super Duplex Stainless Steels (ASTM A890-5A). The various tests which were carried out were ASTM A923 Test Method A, B and C (Sodium Hydroxide Etch Test, Charpy Impact Test and Ferric Chloride Corrosion Test), ferrite measurement using Feritscope®, ASTM E562 Manual Point Count Method and X-Ray Diffraction, hardness measurement using Rockwell B and C and microstructural analysis using SEM and EDS.

Volume 4 is the guidance document for the evaluation of cast Super Duplex Stainless Steel which deals with the various evaluation methods which were defined and used for the work on volume 3 for the "Development of Qualification Standards for Cast Super Duplex Stainless Steel alloy A890-5A (2507 Wrought Equivalent)". The document explains in detail each test which was conducted. It also includes some of the results which were acquired during this work.

Volume 5 is the Data Package for the evaluation of Super Duplex Stainless Steel Castings prepared at the end of work comprised in volumes 3 and 4. The document deals

with the various evaluation methods used in the work documented in volume 3 and 4. This document covers materials regarding evaluation of the A890-5A material in terms of inclusion in ASTM A923. The various tests which were conducted on the A890-5A material are included in this document.

Abstract

The objective of the program is to determine the suitability of ASTM A923 "Standard Test methods for Detecting Detrimental Intermetallic Phase in Wrought Duplex Austenitic-Ferritic Stainless Steels" for 25 Cr Cast Super Duplex Stainless Steels (ASTM A890-5A).

Different tests were carried out on the materials procured from various steel foundries as stated in the ASTM A923. The foundries were designated as Foundry A, B, C and D. All the materials were foundry solution annealed. Materials from Foundry D were solution heat treated at The University of Tennessee also and then they were subjected to heat treatment schedule which was derived from the testing of wrought DSS to establish the A923 specification. This was possible because the material from the same heat was sufficient for conducting the full scope of heat treatment. This was done prior to carrying out various other tests.

Charpy samples were machined. The Ferrite content was measured in all the Charpy samples using Feritscope® and ASTM E562 Manual Point Count Method. After the ferrite content was measured the samples were sent to AMC-Vulcan, Inc. in Alabama to conduct the Charpy impact test based on ASTM A923 Test Method B. This was followed by etch testing and corrosion analysis based on ASTM A923 Test Methods A and C respectively at University of Tennessee. Hardness testing using Rockwell B and C was also carried out on these samples. A correlation was derived between all the three test methods and the best method for evaluating the presence of intermetallic in the material was determined. The ferrite content was correlated with the toughness values.

Microstructural analysis was carried out on the etch test samples using Scanning Electron Microscopy in order to determine if intermetallic phases were present. The fracture surfaces from Charpy test specimens were also observed under SEM in order to determine the presence of any cracks and whether it was a brittle or a ductile fracture. A correlation was carried out between the ferrite content, hardness values and the type of fracture. SEM was also carried out on the corrosion samples in order to see the difference on the surface after corrosion analysis has been carried out. Energy Dispersive

Spectroscopy was carried out on the material acquired from Foundry D in order to determine the variation in the amount of the chemical composition of various elements when the material is subjected to different heat treatment schedules.

X-Ray analysis was also carried out in order to verify whether it is possible to identify the different phases present in the material. Volume percentage of ferrite was also calculated from X-Ray diffraction and compared with the Feritscope® and ASTM E562 Manual Point Count data in order to determine whether X-Ray Diffraction is a suitable method for carrying out qualitative analysis of different phases present.

From the various tests that were conducted, it was concluded that since ASTM A923 Methods adequately identifies the presence of intermetallic phases in A890 – 5A grade Cast Super Duplex Stainless Steel A890 – 5A can be directly included in ASTM A923. Correlation was determined between all the ASTM A923 Test Methods A, B and C and Test Method B were identified as the best method for detecting the presence of detrimental intermetallic phases. The micrographs from the A890-4A grade (now in ASTM A923) were identified as applicable for the A890-5A grade to compare and detect the presence of intermetallic phases. Using these micrographs one can verify whether an A890-5A sample has an unaffected, affected or a possibly affected structure. It was also observed that when compared to the A890-4A grade A890-5A grade is more sensitive to heat treatment. From the ferrite and hardness measurement a correlation was developed between toughness, volume percentage ferrite and hardness of the material. From SEM and EDS the type of intermetallic phase present and its chemical composition was determined. The best method for calculating volume percentage ferrite was determined between the Feritscope®, ASTM E562 Manual Point Count and X-Ray Diffraction.

The test data will be submitted to ASTM to support the adoption of the ASTM A890-5A Cast Super Duplex in the A923 specification.

Table of Contents

x

List of Tables

List of Figures

I. Introduction

Steel can be defined as an alloy of iron (Fe) and carbon (C) with carbon content less than 1.7%. Stainless steel is the term for a whole group of corrosion-resistant steels, containing at least 11% of chromium.

The earliest steels were martensitic and ferritic Fe-Cr steels. Later on Austenitic Stainless Steel was developed which contained a Cr content of 18-28% and Ni 8% or more. This steel began to be used widespread due to its ease of production and fabrication, particularly welding[2]. But it was sensitive to grain boundary carbide precipitation during heat treatment and welding, and sensitive to intergranular corrosion attack. This lead to the development of another category of steels called Duplex Stainless Steels[2].

With the addition of Ni to the ferritic steels the structure changes to ferritic and austenitic. Typical content is 18 - 28% Cr and 4 - 7% Ni. Duplex as the name implies has two phases - Austenite and Ferrite and both the phases should be in equal proportion of (50% - 50%) in order to exhibit the best performance characteristics.

The first reference to Duplex stainless steels appeared in 1927 when Bain and Griffith published data on ferritic - austenitic structures[2]. Soon it was exploited by various countries like France, Germany, Sweden and the USA. From the early 1970s various different grades of wrought and cast Duplex Stainless Steels have been developed. Since Duplex Stainless Steels are relatively new materials, there is a limitation in its use due to the lack of specifications and fabrication details. Data related to corrosion resistance are also very limited which tends to reduce its usage in various fields. Two of the main factors which cause cast Duplex Stainless Steels to perform less than the desired level is the in appropriate austenite-ferrite balance and precipitation of detrimental intermetallic phases during the casting or subsequent welding process.

The objective of this program is to develop a data package for Super Duplex Cast Alloy A890-5A (wrought equivalent 2507) suitable for acceptance of the alloy in ASTM specification A923 (Standard Test Methods for Detecting Detrimental Intermetallic Phase in Wrought Duplex Austenitic-Ferritic Stainless Steels) and to formulate a guidance document to assist specifiers and engineers for properly employing Super Duplex Stainless material (Figure 1). The previous work in this program on cast alloy A890-4A (wrought equivalent 2205) was sufficient to affect the successful inclusion of this cast alloy into ASTM A923.
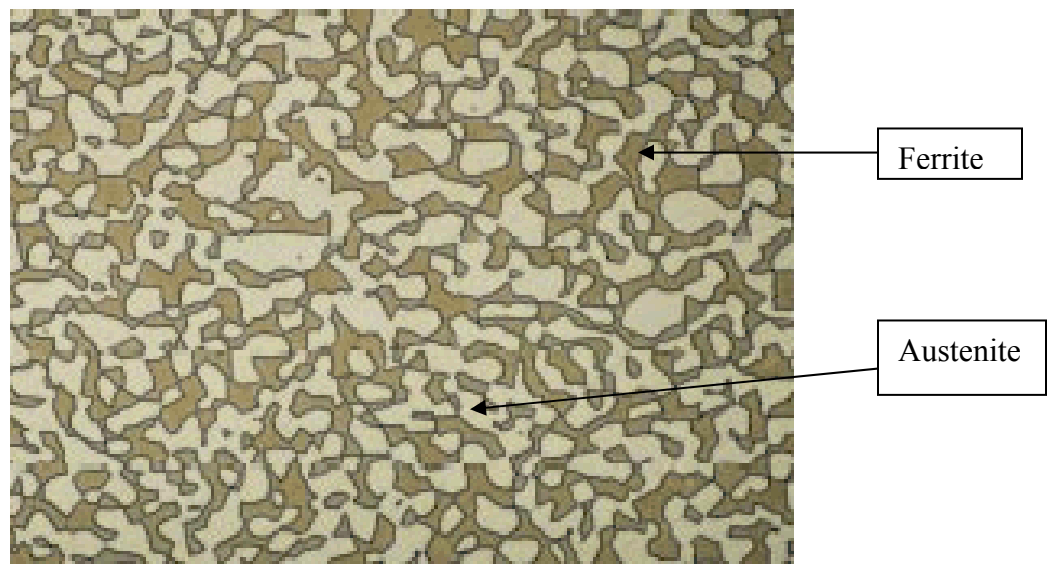
Figure 1: 2507 Microstructure (After Sandvik Steel [92])

II. Literature Review

1. Types of Stainless Steels

1) Ferritic Low Chromium Steels
2) Martensitic chromium steels
3) Austenitic steels and alloys
4) Martensitic Austenitic steels
5) Precipitation Hardening steels
6) Austenitic - Ferritic steels or Duplex

1.1. Ferritic Chromium Steels

The Ferritic class of stainless steels normally has a chromium content of 12 - 18% and often a small amount of other alloying elements. These steels keep their ferritic structure after rapidly cooling from high temperature and they are therefore not hardenable. They are magnetic. They are sensitive to intergranular corrosion after heat treatment and welding but in modern variants (ELI = Extra Low Interstitials, i.e. carbon and nitrogen) this problem largely has been overcome.

1.2 Martensitic Chromium Steels

The Martensitic class of stainless steels has a Cr content of less than 20% with a C of more than 0.15%. This makes them hardenable which means when they are rapidly cooled of from the fully austenitic high temperature phase, hard and brittle martensite is formed. The hardness can then be reduced and toughness improved to the required levels by tempering.

They have moderate corrosion resistance which is best in the annealed condition. They show relatively poor weldability and are magnetic.

1.3 Austenitic Steels and Alloys

The Austenitic class of stainless steels has a Cr content of 18-28% and Ni 8% or more. The basic steel has 18% Cr and 8% Ni - often called 18/8 steel (i.e. AISI Type 304) which has some variants. By adding 2-3% Mo the next series of stainless steels, the 18/8/Mo steels (i.e. AISI Type 316) often referred to as "acid proof". These steels are not hardenable by heat treatment.

1.4. Martensitic Austenitic Steels

Standard austenitic steels are transformed to martensitic when deformed i.e. they are so called TRIP steels (Transformation Induced by Plasticity). This means that deformation induces martensite formation which means that steels with 18% Cr and 10% Ni will have martensitic content about 50% when delivered in the hard condition. Examples are 5R10 (304/304H), 12R10 (302), 11R51 (302) and 5R60 (316).

1.5 Precipitation Hardening Steels

This series of stainless steels have a higher Cr content of above 16%. Ni above 7% and approximately 1% of Al. The Al is added to form precipitated nickel-aluminum particles. In the annealed condition the structure is austenitic but during cold deformation the austenitic structure is transformed to harder phase of martensite. It can be drawn to wire and coiled to springs. These are age hardened through a precipitation reaction which occurs at a temperature range of 850°F to 1150°F.

1.6   Austenitic - Ferritic Steels or Duplex

1.6.1   Development of Duplex Stainless Steels

Avesta Jernverk in 1929 was the first to produce the first commercial grade called 453E with approximate composition of 25%Cr-5%Ni. Soon after in 1932 and 1933 a modified grade with 25%Cr-5%Ni-1%Mo (grade 453S) was marketed. Applications included coolers of Brobeck type (plate and forgings), autoclaves for gunpowder production (castings) and valves for sulphite pulping (castings).

Another record of early duplex dates back to 1933, when an error during the melting of an 18%Cr-9%Ni-2.5%Mo grade at the Firminy works of the J.Holtzer Company, France, led to a 20%Cr-8%Ni-2.5%Mo steel. Subsequent analysis of the castings found that it had a high volume fraction of ferrite in an austenite matrix and was not sensitive to intergranular corrosion (IGC) in various corrosive media. One of the first patents was issued in France in 1936.

In the 1950s there was a burst of activities in the field of high chrome low nickel stainless steels due to the nickel shortage. This lead to the development of Uranus 50 (UR50) with 20 - 35% ferrite (UNS S32404). In 1959 the grade CD4MCU (25%-Cr5%-Ni2%-Mo3%Cu) was developed by the Alloy Casting Institute. However, it was brittle and didn't have good weldability. Hence the chromium content was reduced to 22-23% and a quench annealing treatment was used to increase the ductility.

In the 1960s the carbon content was reduced to 0.03%. 3RE60 one of the earliest of this kind proved to be the solution for chloride induced stress corrosion cracking in austenite materials.

In 1970s the 22Cr type (2205) was developed in Germany and Sweden i.e. DIN 1.4462 or UNS S31803. The composition range was wide giving a higher ferrite HAZ upon welding. This caused corrosion problems. Most producers use narrower range of composition than the standards would indicate as suitable[1].

With the introduction of AOD/VOD (Argon-Oxygen-Decarburization/Vacuum-Oxygen-Decarburization) the chemistry and the thermal treatment of the steels improved.

The oxygen, sulphur, carbon and residual elements could be controlled at low levels and nitrogen could be added without much cost penalty. This reduced the overall cost of Duplex Stainless Steel making[2].

Slowly, in the 1980s, the importance and advantages of nitrogen was better understood. Its effect on the structural balance in the HAZ and on corrosion resistance came into play. The 25Cr grade (2507 Super Duplex Stainless Steel) was also developed in the 1980s. Some developed from casting grade like S32750, while others, directly as a weldable wrought grade like S32750. These super duplex contain about 25%Cr, 6-7%Ni, 3-4%Mo, 0.2-0.3%N, 0.2%Cu and 0.2%W. A Lean alloy grade was also developed in the 1980s. The lower alloy content, in particular Mo, meant they were cheaper but they had a lower pitting resistance. They compete with the higher austenite like 304L and 316L on the grounds of better chloride SCC and strength and similar pitting resistance. Table 1 shows different kinds of duplex base materials and their compositions.

Table 1: Range of Typical Base Materials (After G.B Holloway & J.C.M.Farrar [118])

Standard		Product	Commercial	Typical Analysis, wt%						PRE*
UNS	EN	Form	Grades	Cr	Ni	Mo	Cu	W	N	
S31803	1.4462	Wrought	UR 45N SAF2205	22	5	3	-	-	0.15	33
S32205	1.4462	Wrought	2205 UR45N+	23	5	3	-	-	0.18	35
J92205	-	Cast	2205	22	5	3	-	-	0.18	35
S32750	1.4410	Wrought	SAF2507 UR45N+	25	5	4	-	-	0.25	41
J93404	1.4469	Cast	2507	25	7	4.5	-	-	0.25	41
S32760	1.4501	Wrought	Zeron 100	25	7	3.5	0.7	0.7	0.25	40
J93380	1.4508	Cast	Zeron 100	25	7	3.5	0.7	0.7	0.25	40
S32550	1.4507	Wrought	Ferralium 255 UR52N	25	7	3	1.5	-	0.15	38
S32550	1.4507	Wrought	Ferralium SD40 UR52N+	26	7	3.5	1.5	-	0.25	41
(J93370)	1.4515 1.4517	Cast	CD4MCuN	25	5	2	3	-	0.20	40

1.6.2 Classification of Duplex Stainless Steels

1. **Low cost molybdenum free DSS of the type 23Cr-4Ni-0.1N** - These are grouped as 2304 duplex grades and provide alternatives to AISI 304 and 316. However the market for this has declined.

2. **22Cr-5Ni-3Mo-0.17N** - These steels which include the SAF Alloy 2205 (cast ASTM A890-4A) are the most popular and least expensive. These alloys have a Pitting Resistance Equivalent Number (PREN) ranging from 30 to 36 and corrosion resistance which is between AISI 316 and 6Mo super austenitic stainless steels.

$$PREN = Cr + 3.3 \, Mo + 16N$$

3. **25 Cr with varying contents of Mo and N also containing Cu and W as alloy elements -** Wrought Ferralium 255 and cast ASTM A890-1B fall in this category. These have a PREN ranging from 32 to 40.

4. **Super DSS of the type 25Cr-7Ni-3.5Mo-0.27N** having PREN values greater than 40. SAF Alloy 2507 (cast ASTM A890-5A) and Zeron 100 (Cast ASTM A890-6A) fall in this category[3].

1.6.3. Application of Duplex Stainless Steels

Chemical and Petrochemical

Grades S31500 and S32304 have been used for clean duties replacing austenitic grades in hot aqueous chloride media in brackish waters, hot coastal conditions tubing was made from grade S31803/S32205. This grade is used for reactors, heat exchangers, storage tanks in production of detergent, plastic production like polypropylene, steam sterilization of byproducts and sodium cyanide production. S32550 is used in phosphoric

and sulphuric acid production, where chlorides and fluorides are present combined with erosion and wear conditions such as in pumps, agitator blades and shafts[4]. 2205 and 2507 are used in terephtalic acid plants to control the corrosion due to acetic acid at high temperature. UR 52N (UNS S32520) is used as an alternate to super austenite and rubber lining to prevent corrosion from phosphoric acid.

Oil and Gas

It's used for tubing purposes in North Sea. They are used in down hole, wellheads and flow line application. They are also used in water injection compression and sea water lift pumps. Bolts in S32205/S31803 and S32760 are used which opens up the possibility of using piping systems at lower temperature. They are also used in architectural applications such as blast and weather walls. Sprint Metal developed SDSS grade D58 to make wirelines to fight the stresses in the chloride and H_2S environments[6].

Pulp and Paper

They are used in suction rolls, chemical pulping, bleaching, Chemi-Thermo Mechanical Pulping (CTMP), pulp storage tanks, paper machines and steam plant.

Power Generation

They are used in sea water cooling systems or in the handling of geothermal fluids. They are used in FGD systems mainly in North America and Europe. 255 DSS was used in FGD systems as retrofit absorber lining.

Marine Transportation

They have replaced 316L (N) and 317L (N) as there high strength to weight ratio maximized cargo capacity through a reduction in wall thickness. They are also employed

in making of propeller shafts, steering propellers, thrusters, water jet engines and other products subjected to high mechanical load. UNS S31803 (UR 45N) are used to make tanks for carrying chemicals. UNS S32304 (UR 35N) is used as an alternative to carbon coated product carriers[7,99].

Refinery Plants

2507 type has been used in the overhead systems and preheat trains to prevent the corrosion due to ammonia, hydrogen chloride and hydrogen sulphide[90].

a) **Environmental Protection Plant**

Duplex containing copper are used in sulphur containing liquids as they are more resistant to Sulphur otherwise it would lead to SO_2 which is harmful to environment[8].

b) **Other Applications**

They are also used in mining, food industry for making storage tanks and in structures in particular for bridges where corrosion of steels is difficult to avoid.

1.6.4. Manufactures of Duplex Stainless Steels

1. Avesta Sheffield Ltd
2. Creusot-Loire Industrie
3. Valourec
4. Summitomo Metal Industries
5. Wier Materials Ltd
6. DMV Stainless/Feroni
7. Krupp Stahl
8. Haynes International
9. Boehler Edelstahl
10. Mannesmann
11. AB Sandvik Stell
12. Fabrique de Fer
13. Nippon Kokan
14. TEW
15. Steel Foundries for Castings
16. Sprint Metal[9]

2. Metallurgy of Duplex Stainless Steels

The presence of ferrite with austenite not only provides better intergranular corrosion resistance but also improves stress corrosion cracking resistance compared to fully austenitic stainless steels[10]. In addition, ferrite also improves the hot cracking resistance and also the weld metal properties.

However, the presence of ferrite in austenite may also cause complex metallurgical reactions that include the formation of a variety of secondary phases, all of which have adverse effects on corrosion resistance and on the mechanical properties particularly impact toughness. Figure 2 shows the precipitates in DSS and it is evident that most of these precipitates concern ferrite and ferrite promoting elements such as Cr, Mo and W. The figure also shows that almost all these reactions take place over the temperature range of 300 - 1000°C.

The various phases that are formed are:

1. Sigma phase
2. Chi phase
3. R phase
4. phi phase
5. Tou phase
6. Secondary austenite
7. Cr_2N
8. CrN
9. M_7C_3
10. $M_{23}C_6$
11. Cu

Table 2 shows the crystallographic data for various phases that could be observed in Duplex Stainless Steels.

Table 2: Crystallographic Date for Various Phases Observed in Duplex Stainless Steels (After Charles J. [15])

Type of Precipitate	Lattice Type	Space Group	Lattice Parameter (Å)	Formation Range (°C)
Ferrite (δ)	BCC	Lm3m	a=2.86-2.88	
Austenite (γ)	FCC	Fm3m	a=3.58-3.62	<1250
Secondary Austenite (γ$_2$)	FCC	Fm3m	a=3.58-3.62	Type 1=<650 Type 2=650-800 Type 3=700-900
Sigma (σ)	Tetragonal	P4$_2$/mnm	a=8.79, c=4.54	600-1000
Chi (χ)	Cubic	L43m	a=8.92	700-900
Laves (R)	Rhombohedral	R3	a=10.9, c=19.34	550-650
Π-Nitride	Cubic	P4,32	a=6.47	550-600
Cr$_2$N	Hexagonal	P31m	a=4.80, c=4.47	700-950
M$_{23}$C$_6$	Cubic	Fm3m	a=10.56-10.65	650-950
M$_7$C$_3$	Hexagonal	Pnma	a=4.52,b=6.99, c=12.11	950-1050
Tau (Ѓ)	Orthorhombic	Fmmm	a=4.05, b=4.84, c=2.86	550-650
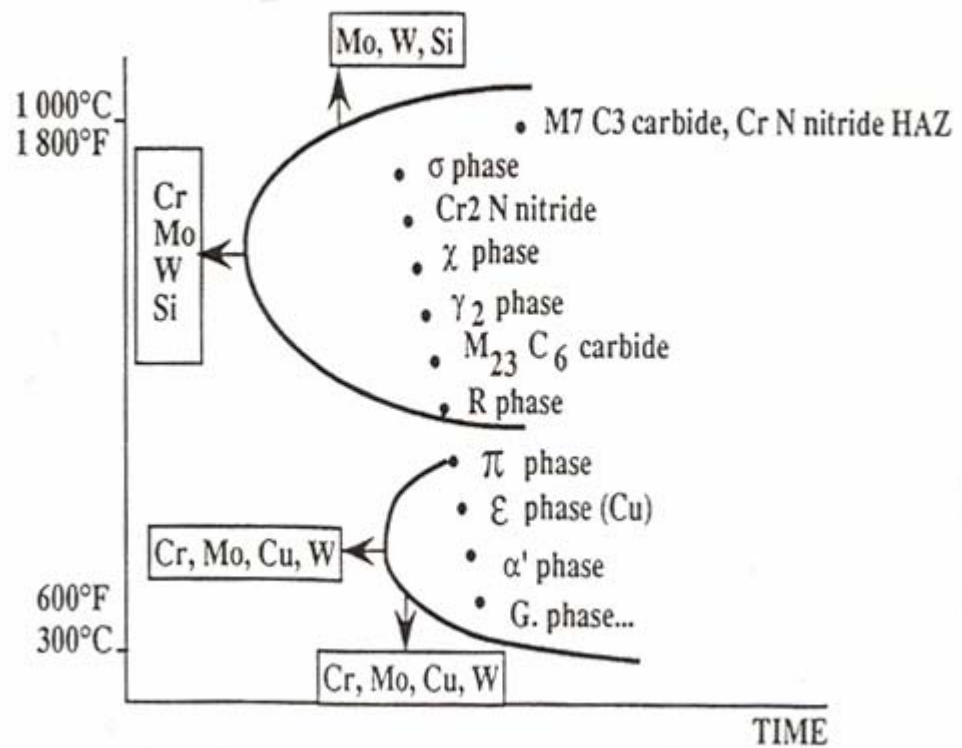
Figure 2: Possible Secondary Phases in Duplex Stainless Steels (After Charles J [10])

2.1. Sigma Phase

The deleterious Cr and Mo rich sigma phase is a hard embrittling precipitate, which forms between 650 and 1000°C[11-17]. It leads to the decrease in both impact properties and ductility. It is detrimental to corrosion properties due to its chemical composition which is Fe-30Cr-4Ni and 4-7Mo but sometimes as high as 10Mo, depending on the original Mo composition of the alloy.

At 900°C ferrite decomposition to sigma takes place in as little as 2 minutes in super duplex alloy whereas in austenite it takes a very long time due to the pre requirement of $M_{23}C_6$ particles[18,19]. According to Charles[10], Machado et al.[21] and Atamert et al.[22] it is due to the similar composition of ferrite and sigma. The diffusion of ferrite forming elements such as Cr, Mo and W in ferrite is 100 times faster than that in austenite and also that the ferrite/austenite interface is favorable for sigma phase nucleation. Ferrite phase is also thermodynamically metastable where sigma phase precipitates.

Sigma phase has been found to nucleate at various locations in Duplex Stainless Steel at a temperature above 750°C[10,13,17,21,23]. Nilsson and Wilson[11] and Josefsson et al.[16] conducted isothermal phase transformation using SAF 2507. It was found that sigma phase nucleated preferentially at ferrite/ferrite/austenite triple points and grew along ferrite/ferrite boundaries. Atamert and King[22] showed that sigma phase nucleated at austenite - ferrite and ferrite - ferrite interfaces; similar to Nilsson and Wilson's results. They also suggested that nucleation is heterogeneous in nature and does not depend on the crystallographic orientation relationships between the phases. They also showed that absence of any intergranular precipitate of sigma phase is indeed a proof of heterogeneous nucleation and that the rate-controlling step is nucleation. Redjaimia et al.[33] and Wang et al.[17] performed isothermal transformation studies on 23Cr-5Ni-3Mo and Zeron 100. They found that sigma phase nucleates on $M_{23}C_6$ carbides or co-precipitates with secondary austenite. They suggested that nucleation and growth depends on the crystallographic orientation relationship which was in contradiction to the findings of Atamert and King. According to the TEM study carried out by O.Smuk, P.Nenonen

and H.Haenninen[24] on DUp 27 and SAF 2507 they showed that sigma phase precipitated at temperature above 800°C by the mechanism of eutectoid reaction of the ferrite decomposition into sigma and secondary austenite.

Lai et al.[23] and Wang et al.[17] both show that the morphology of sigma phase is different when it precipitates at the ferrite/austenite or ferrite/ferrite interface or co-precipitates with secondary austenite. When using SEM-EDX techniques to identify sigma phase, the ratio of iron-chrominum-molybdenum is often used to determine whether the precipitate is sigma or any other secondary phase. The identification based only on chemical composition is not recommended by Wang[17] and Gooch[25], who said that it may vary with different temperature ranges. In addition other phases like chi phase have similar compositions. Thorvaldsson et al.[26] compared composition of sigma phase in different alloy system and observed significant variation. He suggested that identification should also be based on crystallographic criteria as chi phase which has similar composition has a different crystal structure[11,15,16].

The formation of sigma phase is encouraged by the presence of Cr, Mo, Si and Mn[27,28]. Hence the matrix surrounding the sigma phase is depleted in Cr and Mo which is detrimental to corrosion resistance. It was found that it is more stable than chi and R phase. In fact these two phases dissolve and convert into sigma after long time aging.

Solution annealing has to be applied to remove sigma phase in the as cast or as rolled materials. A fast cooling rate is required after solution annealing in order to achieve complete of sigma phase. Solution annealing at higher temperature decreases the formation of sigma phases[12,13,14,16,17] because the solution annealing temperature tends to increase the volume fraction of ferrite, which consequently is diluted with respect to ferrite forming elements thereby suppressing sigma formation.

2.2. Chi Phase

Chi Phase is commonly found in duplex but is usually present in much smaller quantity than sigma phase[12,13,14,30,32,25,34]. It is as harmful to toughness and corrosion resistance as sigma. It has an equivalent amount of Cr but has larger quantity of Mo

(~20%) hence is more detrimental to pitting corrosion resistance. It forms between 700 and 900°C. But it precipitates faster at 800 to 850°C. However, upon long term aging it converts into sigma phase. It forms on the ferrite/austenite interface and grows into ferrite. However the cube-cube orientation relationship ensures continuity between chi and ferrite matrix.

It is impossible to distinguish between chi and sigma using optical light microscopy. But TEM can be used as they have different crystal structures. Chi causes much brighter contrast than sigma. It was indicated by Nilsson et al. that for tungsten-containing super DSS the tungsten content in chi is also substantially higher than sigma. It was shown by C.S.Lee, J.S.Ahn, K.A.Lee, K.T.Kim, C.G.Park and K.Y.kim[31] that for a duplex containing tungsten (1.6Mo-4.3W) the ductility and toughness deterioration were restrained as sigma phase precipitate was retarded by the formation of chi phase.

2.3. R Phase

The R Phase precipitates between 550 to 800°C. It is Mo rich having a composition of 30Fe-25Cr-35Mo-6Ni-4Si. They form at inter and intragranular sites[33] and is most deleterious to pitting corrosion resistance. The most rapid and stable growth is at the temperature 550 - 650°C. At higher temperature it is converted to sigma after ageing. It has an irregular shape and uneven contrast in TEM. This information can be used when SEM/EDX are used.

O.Smuk, P.Nenonen and H.Haenninen[24] showed that oxide particles resulting from powder contaminations serve as nucleation sites for the formation of R Phase in SAF 2507 after 600°C /10h and 700°C/2 h. aging treatments and in Dup 27 it precipitates as particle at phase and grain boundary after 700°C/2 h.

2.4. Π Phase

Π Phase is recognized as a nitride and has a chemical composition of $Fe_7Mo_{13}N_4$. It was found that it contains 28%Fe, 35%Cr, 3%Ni and 34%Mo. It shows

an even contrast in the TEM. It forms at about 600°C. It is detrimental to toughness and corrosion resistance[14,16]. It is identified[34] at intergranular sites in duplex weld metal after an isothermal heat treatment at 600°C for several hours[51].

2.5. Ѓ Phase

Ѓ Phase is formed in the temperature range of 550 to 650°C on heat treatment for several hours. It can lead to the formation of heavily faulted needle-like Ѓ phase on a ferrite/ferrite boundary[51].

2.6. Secondary Austenite

Secondary Austenite is also a transformation product of ferrite[12,14,17,23,30,35,38]. The reason that this is termed secondary austenite is because of its FCC crystal structure, which is the same as that of primary austenite. The difference between primary and secondary austenite is the chemical composition.

Secondary austenite can precipitate through three mechanisms in delta ferrite:

1) Eutectoid reaction
2) Widmannstätten precipitates
3) Martensitic shear process

The eutectoid reaction is facilitated by rapid diffusion along ferrite/austenite boundaries. This reaction occurs in the temperature range 700-900°C. Since sigma phase is rich in Cr, Mo and Si the secondary austenite which surrounds sigma phase, is depleted in these elements. It was shown by Nilsson et al.[30] and Lai et al[23] that's during sigma precipitation, nickel is rejected to adjacent regions within ferrite and subsequently secondary austenite is enriched with Ni.

Between 650-700°C at which diffusion is more rapid, secondary austenite forms as Widmannstätten precipitates having various morphologies. This type obeys Kurdjumov Sachs (K-S) relationship and also shows significantly higher nickel content than the surrounding ferrite, indicating that the transformation is diffusion assisted.

Below 650°C ferrite is transformed into secondary austenite via a mechanism that shows similarities with martensite formation. This type precipitates isothermally and shows no difference in composition compared with ferrite, thus indicating the transformation is diffusionless. The orientation obeys Nishiyama-Wasserman (N-W) relation. Nilsson et al, added that diffusion controlled transformation occurs to some extent below 650°C.

A fourth and fifth mechanism, both similar to the first mechanism, were observed by Lai et al.[23] and Nilsson and Wilson[13]. Lai[23] showed that the formation of secondary austenite can be associated with the formation of Cr-rich carbides. It was argued that the formation of Cr-rich carbides leads to a loss of Cr from the vicinity of the boundary within ferrite phase and the depletion of chromium promotes the formation of secondary austenite. Hence it was leaner in Cr, Mo as well as in N which resulted in a drastic decrease in pitting corrosion resistance.

It is mostly found at austenite/ferrite phase boundaries or at the interior of ferrite grains[13,22,30]. Four types of morphologies were observed by Lai[23]:

1) Bulging (globular) γ2 originating at the original alpha/austenite interface which grows into alpha.
2) Widmannstätten γ2 originating at the original alpha/alpha interface which grows into alpha.
3) Cellular γ2 originating at the original alpha/gamma or alpha/alpha interface which grows with sigma during eutectoid decomposition of alpha into a cellular gamma plus alpha mixture.
4) Needle shaped γ2 originating within the alpha grains with a preferred orientation growth direction.

According to Nilsson et al.[13,22,30] the first two morphologies are more frequently observed. It was noted that Widmannstätten type secondary austenite is actually two austenite crystals separated by a twin boundary and for an unknown reason, this type of secondary austenite has an even lower concentration of Cr than the globular type of austenite. O.Smuk, P.Nenonen and H.Haenninen[24] showed that in SAF 2507 the secondary austenite forms after a 600°C/10 h and 700°C/2h aging treatment.

2.7. Nitrides Cr_2N and CrN

The precipitation of Cr_2N is in a temperature range of 700-900°C[21,13,14,39,42]. The formation of Cr_2N is due to the rapid cooling from a high solution temperature because super saturation of nitrogen in ferrite occurs. In other words with increased cooling time, precipitated Cr_2N is also diminished due to nitrogen's increasing solubility associated with the increasing amounts of austenite, produced from the ferrite to austenite transformation[39].

Machado et al.[21] and Kokawa et al.[42] studied the morphologies of Cr_2N and found that elongated Cr_2N particles often precipitate intergranularly either at ferrite/ ferrite grain boundaries or ferrite/austenite phase boundaries. After welding[43] the formation of CrN is favored in the heat affected zone. It has a cubic structure.

2.8. Carbides $M_{23}C_6$ and M_7C_3

Carbides play a less important role in super duplex than in the duplex because of the low carbon content. According to Nilson[14], no precipitation of carbides of any kind was observed in SAF 2507. M_7C_3 forms between 950 to 1050°C at the ferrite austenite grain boundaries[45]. As its formation takes 10 minutes it can be avoided by normal quenching techniques.

Duplex grades with carbon content of about 0.03% the carbide $M_{23}C_6$ rapidly precipitates between 650 and 950°C requiring less than a minute to form at 800°C. Precipitation occurs at ferrite austenite boundaries where Cr rich ferrite intersects with

carbon rich austenite. It can also be found[28] at the ferrite-ferrite and austenite-austenite boundaries and to a lesser degree inside the ferrite and austenite grains. The different precipitation morphologies are cuboidal, acicular and cellular. They act as initiation sites for pitting and intergranular corrosion.

2.9. Cu-rich Epsilon Phase

In alloys containing copper and/or tungsten[14,36,46,47], other hardening mechanisms occur. In the case of super saturation of the ferrite due to the decrease in solubility at lower temperatures leads to the precipitation of extremely fine Cu-rich epsilon phase particles after 100 hours at 500°C[51], which significantly extend the low temperature hardening range of duplex[46].

According to Ravindranath et al.[36] and Sriram and Tromans[47], the Cu rich phases are very fine and are often attacked by electrolytic thinning thus leaving holes at grain boundaries. Soylu and Honeycombe[46] showed that copper precipitates can refine the microstructure particularly austenite. In an experiment with 30Cr-8Ni-3Cu alloy these authors found that copper precipitates took place with multi twinned morphology before the ferrite to austenite transformation. The subsequent transformation nucleated on the finely dispersed copper particles resulting in a fine, homogeneously distributed, twinned austenite morphology. It was thus suggested that such a refinement would lead to a higher strength and greater toughness as well as improved corrosion resistance but no data is available on this till date.

2.10. G Phase

Spinodal decomposition of ferrite occurs in the temperature range of 300-500°C. In this range there is precipitation of G phase. It causes embrittlement. However as duplex are not applied in this temperature range it is not of much concern.

3. Microstructural Investigation Techniques

The evaluation of duplex microstructures requires proper etching techniques for light optical microscopy and scanning electron microscopy. Various etchants and electro-chemical etching techniques have been developed to help reveal duplex microstructures[16,36,47].

Some of the most often mentioned etchants and their effects are as follows:

1) Ravindranath and Malhotra[36] etched samples electrolytically in 10% KOH solution. The cell voltage was kept at 5V. The etchant colored the ferrite yellow, sigma phase reddish brown and the carbide black. The austenite phase remained unattacked in etching.

2) Nilson et al.[30] developed a two step electrolytic etching technique, which also employs KOH, to obtain contrast from intermetallic phase. The two step electrolytic etching technique involving dilute nitric acid (HNO_3) to make phase boundaries visible, followed by saturated KOH to enhance the contrast of the precipitates. The authors also utilized a dye etchant called Beraha etchant to produce as-welded microstructures with secondary austenite in high contrast. The etchant consists of 2.2g $(BH_4)HF_2$, 0.2g $K_2S_2O_5$, 18 ml HCl, 100 ml distilled H_2O. Etching for a time in the range 10 to 20 seconds colors ferrite blue while austenite remains virtually uncolored.

3) Cheng et al. applied a solution made of 50g $K_3Fe(CN)_6$, 30 g KOH and 100 ml distilled water. Heating is required for this solution.

4) Sriram and Tromans[47] used kalling's reagent, which does not require either electrolytic set up or heating. kalling's reagent is an acid chloride solution (1.5 g

CuCl$_2$, 33 ml HCl, 33ml alcohol and 33ml distilled water) that etches ferrite dark and austenite light.

5) Electrolytic etching with 10% oxalic acid or 40% NaOH solution are also commonly applied methods for etching duplex. Glyceregia is another alternative for etching duplex.

It has been indicated that light optical microscopy is not sufficiently sensitive to identify secondary precipitates. SEM/EDX should be used as the back scatter image would tell us the various phases that are present in the sample. But some times SEM is not sufficient due to the similarity in chemical composition among different precipitates and difference in chemical composition for the same precipitate formed at different temperature. Thus, to precisely identify secondary particles, transmission electron microscopy (TEM) is necessary. A typical sample thinning solution consists of 20% perchloric acid, 10% glycerol and 70% ethyl alcohol. Thinning is usually done at 0°C and 25-45V using a twin jet polishing unit[21,41].

4. Alloying Effects

Secondary phases indicate that precipitation of secondary particle involve Cr, Mo, W, Cu, N and other alloying elements. Thus, it is important to understand the role that each element plays. Preventing secondary phases from forming is not the only concern when duplex is subjected to solution heat treatment or welding. A proper ferrite and austenite level is also needed to obtain excellent corrosion resistance and suitable mechanical properties. The effect of alloying elements on the ferrite and austenite and on corrosion properties is discussed below (Table 3).

Table 3: Influence of different alloying additions and Microstructure on the Pitting and Crevice Resistance of Duplex Stainless Steels (After Bernhardsson S [89])

Alloying	Effect	Reason	Practical Limitation
C	Negative	Causes precipitation of chromium carbides with accompanying chromium depleted zones	About 0.03% maxi
Si	Positive	Si Stabilizes the passive film	About 2% maximum, due to its effect on structural stability and on nitrogen solubility
Mn	Negative	Mn-rich sulphides act as initiation sites for pitting. Mn may also destabilize the passive film	About 2%. Higher level may increase the risk of intermetallic precipitation
S	Negative	Sulphides if not Cr-Ti or Ce rich, tend to initiate pitting attack	About 0.003%, if maximum pitting resistance required. For reasonable machining, up to 0.02% allowed
Cr	Positive	Cr stabilizes the passive film	Between 25 and 28% maximum depending on the Mo content. Higher Cr content increases the risk of intermetallic precipitation
Ni	Negative	Increased Ni, other elements constant, dilutes the γ- phase with regard to N, which in turn decreases the PRE of the γ- phase. If the alloy is very sensitive to precipitation of chromium nitrides, Ni can have a positive effect	Ni should primarily be used to give the alloy desired austenite content.
Mo	Positive	Mo stabilizes the passive film, either directly or through enrichment beneath the film	About 4-5% depending on the Cr content. Mo enhances the risk of intermetallic precipitation
N	Positive	N increases the PREN of the γ phase, not only be increasing the N content of that phase, but also by increasing the Cr and Mo contents through their partitioning coefficients	About 0.15% in Mo free grades. About 0.3% in super duplex and some in 0.4% in 25%Cr, high Mo, high Mn alloys
W	Positive	Probably same as Mo	Increases the tendency of intermetallic precipitation
Cu	Disputed	Marginal positive and negative effect	About 2.5% maximum. Higher levels reduce hot workability and undesirable hardenability

4.1. Chromium

Chromium improves the localized corrosion resistance, by the formation of a passive chromium rich oxy-hydroxide film[48]. Electrochemically this is achieved by extending the passive range[49] and reducing the rate of general corrosion (ipass). However, there is a limit to the Cr content so as not to enhance the rate of formation of sigma phase, which can markedly reduce the ductility, toughness and corrosion resistance[32]. The practical upper limit suggested by SCRATA is 27% (coupled with Mo in the 2-3% range)[50,51]. In addition in the heavy casting section it is held to a lower side to reduce cracking tendency in the as cast condition[50].

Equations have been developed in to quantify elemental effects (the so called chromium equivalents Cr_{eq}) of which the most favorable is:

$$Cr_{eq} = \%Cr + \%Mo + 0.7 * \%Nb$$

4.2. Molybdenum

It has a beneficial influence on the pitting and crevice corrosion resistance of an alloy in chloride solutions. Molybdenum extends the passive potential range and reduces the corrosion current density (imax) in the active range. It suppresses the sites of pitting corrosion by the formation of an oxy hydroxide or molybdate ion[52].

In high temperature sea water, the addition of at least 3% Mo is recommended to prevent crevice corrosion, while an upper limit of about 4% Mo has been quoted.

4.3. Nickel

Ni effect can be determined by using the equation

$$Ni_{eq} = \%Ni + 35\%C + 20\%N + 0.25\%Cu$$

Although it is not included in the PREN (PREN = %Cr+3.3%Mo+16%N or PREN = %Cr+3.3(%Mo+0.5%W)+16%N; refer to section 7.2) , it has a significant effect on the corrosion resistance and impact toughness as well as on the formation of secondary particles[32,50,54,55]. This is because it stabilizes austenite. With other elements held constant, the optimum pitting resistance, plus a good strength and ductility, can be achieved by adjusting the nickel content to give ferrite-austenite balance of approximately 50% each. Higher Ni would lead to an increase in austenite and hence there would be a greater concentration of Cr and Mo in the remaining ferrite. This highly alloyed ferrite is more susceptible to the precipitation of intermetallic phases at the temperature range of 650-950°C. High Ni promotes the formation of alpha prime[35] an embrittling intermetallic phase. According to Varol et al.[32], Ni effectively raises the temperature range over which sigma phase forms. Thus the standard postweld heat treatment used for alloys SAF 2205 can promote sigma phase formation and embrittlement. Consequently, higher heat treatment temperatures which usually cause higher ferrite content have to be utilized to dissolve all of the sigma phase. Low Ni levels can result in the formation of a high level of ferrite in the microstructure, thereby lowering toughness and corrosion resistance.

4.4. Nitrogen

Addition of nitrogen:

1) Improves localized corrosion resistance and raises the critical pitting temperature and is 16 times more effective than chromium in this respect.
2) Acts as a strong austenite former (in fact it is about 20 times more effective than Ni as an austenite stabilizer on weight percent basis[32]).
3) Increases the yield strength by solid solution strengthening, and unlike carbon does not promote any sensitization i.e. susceptibility to intergranular corrosion.

The proposed factor for nitrogen in the PREN relationship varies between 13 and 30 but the most widely used for duplex is 16. It partitions to the austenite due to the increases solubility in the phase and also concentrates at the metal passive film interface[57]. During prolonged passivation of stainless steels in acid solutions, surface nitrogen enrichment has been witnessed[58,59]. Nitrogen also increases the crevice corrosion resistance. This is due to nitrogen altering the crevice solution chemistry or by segregating to the surface, which is in keeping with the mechanism for enhanced pitting resistance[60,62].

It stabilizes the duplex against the precipitation of intermetallic phases[62] such as sigma and chi, by reducing chromium partitioning[63]. It is also reported the increasing the nitrogen content reduces the risk of nitride formation. This is due to an increase in austenite content and so a reduction in the distance between austenite islands. As it is a strong austenite formation its addition to duplex encourages austenite reformation in the Heat Affected Zone.

The introduction of nitrogen also introduces metallurgical complexity into the duplex. The solubility of nitrogen in liquid steel is the first concern. The importance of this is to prevent the occurrence of nitrogen degassing on casting solidification[64]. The nitrogen solubility in steels is highly composition dependent. It was found that increasing the $C^{34,64}$, Mo and Mn content resulted in an increase in the equilibrium nitrogen solubility of the steels, while increasing the Si, $Cu^{25,34,46}$ and $Ni^{32,64}$ content results in a decrease. This was contradictory to the results for $W^{32,64}$. Duplex has been made up of 0.87% N in a pressurized electroslag process[21].

SCRATA[50] in their 1991 "Material Fact Sheets" comments that the maximum nitrogen should be limited to 0.14%. However Anson et al.[64] have shown that it is possible to safely increase the level of nitrogen in a duplex at least for the 22Cr-5Ni-4Mo type. It has also been reported that castings can have nitrogen levels as high as 0.28% without gas porosity defects[68].

It was shown by Ogawa et al.[54,55] and Miura et al.[55] that increasing the nitrogen modifies the weld phase balance without further compositional change in austenite, while

increasing Ni decreased the nitrogen concentration in austenite due to dilution, with an increase in austenite.

4.5. Manganese

Manganese has little effect on the duplex phase balance, especially at the levels encountered and is extended from the Cr_{eq} and Ni_{eq}[65]. Nevertheless it would appear that Mn can increase the temperature range and formation of rate of detrimental sigma phase. Mn addition to stainless steels increase abrasion and wear resistance[67], and tensile properties without the loss of ductility[66]. It also increases the solid solubility of nitrogen and thus allows for increased nitrogen and thus allows for increased nitrogen contents to be achieved without the risk of out gassing. However, Mn-addition in excess 3% and 6% for nitrogen levels of 0.1% and 0.23% significantly decreases the critical pitting temperature (CPT), probably due to an increase in MnS inclusion which can act as initiation sites for pits[69]. The combined addition of N and Mn in duplex improves[28] pitting resistance and counteracts the singular problems associated with Mn.

4.6. Copper

Copper is a minor alloying element which is added to improve the corrosion rate in non-oxidizing environments such as sulphuric acid. In some 25% Cr duplex 1.5% Cu is added to obtain the optimum corrosion resistance in 70% H_2SO_4 at 60°C while for boiling HCl an addition of 0.5%Cu decreased both the active dissolution and crevice corrosion rates. Addition of Cu to duplex is limited to 2% since higher level would lead to precipitation hardening[70].

Copper appears to improve machinability in low oxygen and sulphur materials and can lead to hardening after exposure to the 300-600°C temperature ranges. This is due to the precipitation of Cu rich precipitates. This improves the abrasion corrosion resistance in duplex pump castings.

4.7. Tungsten

Tungsten addition of up to 2%[71,30,76] is allowed in duplex as it improves pitting resistance, i.e. extend the passive potential range and reduce ipass. It also increases the crevice corrosion resistance in heated chloride solutions[53]. This is due to the adsorption of tungsten into the passive layer without the modification of its oxide state. However in acid chloride solutions tungsten appears to pass through from the substrate into a passive film by interaction with water to form insoluble WO_3[73].

According to Nilsson et al.[30] and Hertzman et al.[74] tungsten is known to form intermetallic phases in the 700 to 1000°C temperature range and encourages formation of secondary austenite formation in the weld metal. According to J.S.kim, K.Y.Kim and J.S.Lee in 2507 tungsten has a strong effect in suppressing the brittle secondary phase precipitation, particularly in the early stage of aging. However, as the aging time is increased this is suppressed[75]. Levels between 1% and 3% have been shown to restrict the formation of sigma at the phase boundaries and instead the precipitation occurs at the intragranular sites. This is due to the large tungsten atom influencing the diffusion of Mo and W at the phase boundaries and thus nucleation of sigma. Nilson[30] and Ogawa et al.[76] indicated that the amount of Cr_2N tended to be increased by W additions. They suggested that the factors responsible for these phenomena are the reduction in the solubility of N in the ferrite phase by tungsten entering into solid solution and the reduction in the solubility limit of N in the steel as a whole with increased ferrite content.

4.8. Silicon

It is beneficial for concentrated nitric acid service and also enhances the high temperature oxidation resistance[67]. High silicon (3.5-5.5%) bearing duplex has been developed with increased pitting corrosion resistance and a claimed immunity to stress corrosion cracking. However, a high silicon level is a strong sigma former[68,50,72]. Taylor[68] indicates that silicon in combination with Molybdenum can be particularly dangerous.

SCRATA recommends that 0.5-0.6% Si content is the best choice for duplex stainless castings.

4.9. Carbon, Sulphur and Phosphorus

The carbon content of most wrought duplex stainless steels is limited to 0.02% or 0.03% primarily to suppress the precipitation of Cr-rich carbides which can act as initiation sites for pitting corrosion and intergranular attack.

Similarly P and S contents are controlled though not eliminated as the presence of some sulphur is important for weld bead penetration[67]. Level of C and S can be controlled by using the process of VOD or AOD, while phosphorus can be reduced using good melting practices.

4.10. Microsegregation of the Elements

Farrar[72] pointed out that it is the local microsegregation of chromium and molybdenum that controls the transformation of delta ferrite and formation of intermetallic phases. Farrar showed that the transformation from delta ferrite to austenite is accompanied by significant diffusion of both Cr and Mo across the austenite /ferrite boundary to the delta-ferrite and that the enrichment strongly influences the formation of intermetallic phases.

Atamert and King[77] found that Cr partitioning was not significantly influenced by temperature. Molybdenum however was found to partition to ferrite as temperature decreases. A strong partitioning of nickel to austenite was observed to decrease gradually with increasing temperature. Nitrogen was found to have the most profound effect on phase balance, increasing the amount of austenite and reducing the amount of ferrite. The partition coefficient of nitrogen is dependent on composition. Cr and Mn increase nitrogen solubility, which explains why super duplex can contain higher nitrogen contents than the lower chromium variants. It is also affected by temperature. During a solution anneal, even though the solubility of nitrogen in ferrite may increase, the volume

29

fraction of austenite decreases. This leads to an enrichment of nitrogen in the remaining austenite[49].

Ogawa and Koseki[54] found that among Cr, Mo and Ni, the microsegregation of Ni and Mo is more pronounced than that of Cr, and Ni is more pronounced than Mo. It was also found that the partitioning of Ni, Mo and Cr during ferrite solidification is not as great as in austenite solidification. They also showed that the partitioning of Cr, Mo and Ni between the ferrite and the austenite was not significant in welds. However an increase in Ni or N promoted the partitioning by raising the austenite transformation temperature. Again, nitrogen was found to have a dominant effect on the formation of weld metal austenite.

5. Physical And Mechanical Properties

5.1. Physical Properties

Duplex have low thermal expansion coefficients similar to carbon steels. This reduces the requirement for expansion joints and renders duplex suitable for thermal cycling conditions. The thermal conductivity is higher than for austenitic grades and this with higher mechanical strength, allows for thinner walled components in many applications such as pressure vessels and tubing. Duplex shows a degree of magnetism.

5.2. Tensile Properties

Duplex have higher proof strength (Rp) and tensile strength (Rm) values than most ferrite and austenitic grades[169,170]. The ultimate tensile strength is high, while the elongation is greater than 25%. This allows duplex to be used as thinner sections than austenitic grades[94]. The ability to work harden duplex alloys up to tensile strength (Rm) of 1200 MPa is exploited in the manufacture of wirelines, surgical prostheses etc.

5.3. Hardness

The hardness requirement approximately 28 on Rockwell C (HRC) depending on the alloy type. The hardness of solution annealed duplex and super duplex alloy are generally below this limit, unless subject to cold work or precipitation of intermetallic phases.

5.4. Impact Strength

High impact energies can be achieved in duplex as low as -100°C in the solution annealed and unwelded condition. Impact strength can be improved by reducing the oxygen content and by controlling the aluminum level[128]. There are a number of other factors[82] that affect the toughness of wrought duplex alloys. Any precipitation of intermetallic phases, such as sigma, chi etc., leads to a sharp decrease in toughness. This phenomenon is particularly important in the super duplex grades, in which the transformation is the most rapid.

In alloys containing copper, it is possible to undertake low temperature heat treatment to obtain appreciable hardening and wear resistance while maintaining satisfactory toughness.

Cold work reduces the room temperature impact strength of the duplex and increases the ductile to brittle transition temperature. The combination of cold work and ageing in the range 300-400°C leads to an even greater drop in the room temperature impact strength and in some heats of grade S31803 (Alloy 2205); it has been reported that[78] the ductile to brittle transition can be raised above ambient temperature.

Duplex should not be used beyond 300°C unless specific toughness evaluations are made. Particular attention should be paid to welds, where the initial impact strength should be sufficiently high to accommodate the drop which occurs due to service ageing. Indeed a limit of 250°C has been stated for welded structures[83].

5.5. Fatigue Properties

Materials with Rm greater than 1000Mpa, the value of fatigue limit is generally found to be less than 50% Rm. Similar results obtained in sea water type environments appear to show marked scatter[84] with some duplex and austenitic steels giving corrosion fatigue limits (CFLs) close to average fatigue limit in air (AFLA), whereas others hardly attain values equivalent to 0.4*AFLA (or 0.2*Rm).

The drop in fatigue strength in a corrosive environment is clearly linked to the intrinsic resistance of the materials to the corrosion mechanisms[165]. PREN >40 is necessary to ensure minimum risk of fatigue strength reduction in sea water while a PREN of around 32 is desirable to minimize the reduction in fatigue strength.

Chwee-Sim Goh and Tick-Hon Yip[158] studied the cyclic behavior of SAF 2507 under constant plastic-strain amplitudes. The cyclic hardening/softening curves show initial hardening, followed by softening and finally saturation behavior. Two regimes can be differentiated in the cyclic stress-strain curve (CSSC) of DSSS. The transition point at which the cyclic strain-hardening rate changes is identified to be $\varepsilon_p/2 = 7*10^{-3}$. TEM results showed that there is a close relationship between CSSC, hardening/softening curves and the dislocation substructure evolution.

In the low plastic strain amplitude regime of the CSSC, the dislocation activity in the austenite grains is found to be higher than that in the ferrite grains. At higher plastic strain amplitudes, low-energy dislocations were found in the ferrite grains, while clusters and bundles of dislocations can be observed in the austenite grains.

Dislocations were also found in the as received specimen of SDSS in the ferrite and austenite grains. The material did not receive any further heat treatment, as it was received in the annealed condition. The existing dislocations may have been produced during extrusion

.

6. Forming and Machining

6.1. Cold Forming

High forming pressure is required, greater than that for the 304 grades and more power is required. Local strains e.g. at the surface during bending of up to 60% can be tolerated in the base metal but the maximum permissible value is much lower in welds, particularly when the ductility of the weld metal has not been optimized by controlling the oxygen and hydrogen contents and by ensuring the absence of intermetallic phases[94].

Industrial experience has shown that, by taking a number of precautions similar to those used for high molybdenum and nitrogen austenitic alloys, cold drawing of the duplex grades can be performed without major difficulty. During the last 10 years Aker Maritime has used cold forming as an important process in the fabrication of pipes made up of duplex stainless steels[85].

6.2. Hot Forming and Superplasticity

Because of the two phases the duplex can be readily hot formed above 950°C. Indeed, they deform so easily that precautions must be taken to avoid creep during heat treatment. This can be overcome by using induction heating in the case of tubes. Superplasticity has even been shown[86] to be possible in duplex deformed above 900°C. This phenomenon requires low strain rates, temperature of at least 0.6 Tm (where Tm is the absolute melting temperature) and a very fine structure (grain size ≤ 1um).

L Duprex, B.C.De Cooman and N. Akdut[159] performed hot torsion test on the DSS of type EN1.4462 steel. The temperature was varied in the range from 950˚C to 1200˚C, while the strain rate was varied from 0.01/s to 2/s. The mean flow stress (MFS) was fitted to the hyperbolic sine function proposed by Sellars and Tegart. An activation energy for plastic deformation of Q_{HW} = 425 KJ/mol was obtained. The high value was explained by the fact that, in addition to the softening of ferrite (δ) and austenite (γ), there

was a decrease in the volume fraction of the high strength austenite with increasing temperature.

For higher value of Zener-Holomon parameter (Z), the MFS showed a linear dependence on ln(Z), which was related to be gradual disappearance of a yield-point-elongation-like effect was characterized by a nonstrengthening plateau during initial stages of plastic deformation. The strain to rupture and the dynamic softening were both found to decrease for higher value of ln(Z). Therefore the ductility was directly related to the amount of dynamic softening that is dynamic recrystallization (DRZ) of the austenite phase. At high strain rate significant dynamic softening was observed for temperatures above 1100˚C.

In ferrite the high stacking-fault energy (SFE) of ferrite results in the relative ease of dislocations to climb at high temperature. As a result, the build up of stress concentrations is slowed and very high ductility is obtained especially in hot torsion where the deformation is shear-like. It is generally accepted that strain partitioning between ferrite and austenite results in internal stresses at the phase boundaries, which may lead to crack formation.

It was also observed that for ln(Z) value below 36, the beginning of plastic deformation is characterized by strain partitioning between austenite and ferrite. The mechanical behavior is therefore determined by the recovery of ferrite resulting in a yield point elongation like plateau in the stress-strain curve.

6.3. Machinability

The lower alloyed duplex like the S32304, are comparatively easy to machine[79] and behave in a similar manner to austenitic grades 316 and 317 for machining with HSS and with 317LN and 317LMN for machining with cemented carbide tools. Modern duplex grades are much difficult to machine than the older grades by virtue of the higher austenite and nitrogen content. With increasing nitrogen and molybdenum machinability decreases rapidly. Thus super duplex are most difficult to machine.

Comparisons of duplex and austenitic grades with similar alloy content machining operations, such as end milling with HSS tools, the duplex grades are easier to machine. But intermittent cutting operations are more difficult for duplex than for austenitic alloys.

These differences are due to the higher strength of duplex and in particular the high temperature tensile strength. Other factors such as low fraction of non metallic inclusion and low carbon content also contribute. Improved machinability can be achieved by introducing non-metallic inclusions, such as sulphides. Nevertheless high sulphur grades will be sensitive to weld metal cracking and have a lower resistance to pitting corrosion[87]. Thus they should only be selected where welding is not envisaged and corrosion resistance is not paramount.

7. Corrosion

The most important alloying elements with respect to the localized corrosion properties of duplex are Cr, Mo and N whereas Ni acts to stabilize the austenite phase. This review will focus on various types of corrosion and the various corrosion tests.

7.1. General Corrosion

7.1.1. Sulphuric Acid

All duplex grades show a lower corrosion rates than 304L and 316L in dilute sulphuric acid[166,167]. Higher alloy grades are more resistant than alloy S32304[88,89].

The beneficial effect of copper, as an active alloying element in reducing acids, is illustrated by an improved performance of alloys S32550 and S32760 with between 0.5% and 2% Cu compared to alloy S32750 with no copper. The duplex alloy S32550 with up to 2.5% Cu can be used between 40% and 85% H_2SO_4[95]. The super duplex grade can be used at even higher concentration and temperatures out performing Ni based alloys like N08020 (Alloy 20Cb3) and offering similar resistance as special silicon austenitic

stainless steels. A good resistance has been obtained for S32550 at a flow rate of 10 m/s. At this rate it was found that the passivity was stabilized.

7.1.2 Hydrochloric Acid

It is extremely aggressive and stainless steels are therefore only resistant at lower concentrations. Grades S32205/S31803 offers similar resistance to 316L at low temperatures although the resistance is better at higher temperature. The super duplex are similar to austenitic alloys N08028 and S31254[95,96]. The best performance in HCl is shown by S32760 with Cu and W additions.

7.1.3. Nitric Acid

This leads to an oxidizing environment. In this Molybdenum has a strong negative effect, while chromium is beneficial. Hence it has been recommended that a limit of 2% Mo content should be considered[95], like S32950 or the low alloyed steel S32304 otherwise it would lead to intergranular corrosion.

7.1.4. Phosphoric Acid

Concentrated phosphoric acid is not very corrosive. Contaminants in wet process phosphoric acid, such as chlorides and fluorides, can lead to high corrosion rates. Duplex like S31803 and S32550, have been utilized in such media[91] e.g. as pumps and valves and in chemical tankers.

7.1.5. Organic Acids

Duplex and super duplex have good passivation properties in pure and contaminated acids[92]. Modern duplex S32205/S31803 are resistant in acetic acids whereas the austenitic grade 304L corrodes at high temperatures and may even crack at

high concentrations. In formic acid, most aggressive of all organic acids, most stainless steels and titanium corrode at intermediate concentration and high temperatures, but super duplex S32750 is resistant to the boiling point[93].

7.1.6. Sodium Hydroxide

Duplex can be applied in caustic environment at low concentrations. Studies in the pulp and paper industry have shown that duplex have much lower corrosion rates than standard austenitic grades in white liquors[94] (caustic environment with NaCl, Na_2CO_3, Na_2S, Na_2SO_4) of kraft digestors.

7.2. Localized Corrosion

7.2.1. Pitting Attack

The mathematical formula describing the relationship between the amount of Cr, Mo and N and the corrosion properties was found by Lorenz and Medawar. It is:

$$\textbf{PREN} = \textbf{\%Cr+3.3\%Mo+16\%N}$$

or

$$\textbf{PREN} = \textbf{\%Cr+3.3(\%Mo+0.5\%W)+16\%N}$$

It is used in ASTM A890-94a. However many researchers believe[14,47,54,95,96] that PREN calculated from the bulk alloy composition may be misleading in duplex due to the presence of two phases. It is important to consider the pitting resistance of ferrite and austenite individually due to partioning of the alloying elements between the phases especially if the heat treatment is not optimized. An adjustment to the chemical composition to meet a specified PREN can cause a grade to have an improper ferrite-austenite phase balance. The factors which affect pitting corrosion are:

1) **Balance ferrite and austenite** - Too much ferrite can cause the formation of Cr_2N and other intermetallic phases and too much austenite would lead to reduction in nitrogen and greater segregation of Cr and Mo.

2) **Control of Ni content** - This is necessary to have a proper balance of the phases.

3) **Proper heat treatment temperature** - Proper solution annealing temperature is required for the balance of the phases.

4) **Proper welding procedures** - This includes selecting proper welding parameters, joint geometry, heat input, filler metal and shielding /backing gases. Excessive dilution and extremely slow and fast cooling should be avoided.

5) **Proper pH** - The pH has a small effect on pitting resistance with lower pH conditions being more aggressive[89].

Improved resistance is obtained with higher alloy grades and modern grades with more nitrogen addition i.e., S31500, S32304 and S32900. Grade S32304 has similar resistance to the austenitic grade S31603 while super duplex S32750 are comparable to 6%Mo austenitic grade S31254.

7.2.2. Crevice Corrosion

Crevice corrosion can be formed at flanged joints, beneath weld spatter etc, and the tighter the gap the more likely that crevice corrosion will occur. For instance soft non metallic materials, which can mould to the metal surface, are severe crevice formers. The crevice corrosion resistance is related to the pitting resistance as the CCTs are roughly proportional to CPTs[89].

In practical experience it has been shown that grade S32205/S31803 and S32550 can suffer from crevice attack in 1 ppm chlorine at 16°C[101] and 0.8 ppm at 10°C[98], while super duplex are resistant at 45°C in sea water with 0.8 ppm chlorine.

7.3. Chloride Stress Corrosion Cracking

Work in 1950s and 1960s concluded that ferrite protects austenite against SCC, as it has a lower corrosion potential in an acidified crack solution, such that once a crack in austenite reaches ferrite, the mixed potential inside the crack is suppressed and the austenite is protected. Gunn[160] reports that the SCC resistance to laboratory weldments with "normal" ferrite levels is about equivalent to the resistance of base metal.

However in modern duplex cracking can occur preferentially in ferrite phase. This is because ferrite has at least 3%Ni in comparison to the ferrite based stainless steels which are nickel free. This makes ferrite phase susceptible[89] to SCC. Cottis and Newman explained the mechanism using appreciation of electrochemical behavior and mechanics of crack propagation through the two phases. The crack which reaches the austenite, to propagate through it requires the prevailing potential and pH to be favorable to cracking in this phase. However the ferrite would tend to leave the austenite intact unless the stress is sufficiently high to cause ductile tearing, which will require high stress intensities.

Superduplex grades like S32750 are resistant to cracking in aerated 10%Cl (i.e. 16.5% NaCl) with temperature approaching 300°C[89].

7.4. Sulphide Stress Corrosion Cracking

7.4.1. The Effect of H_2S

The resistance of duplex stainless steel to SCC in the presence of H_2S and Chloride is reduced, if compared to similar environments where only chloride is present. Increasing chloride concentration reduces the critical pH_2S which can be tolerated at a given temperature[100]. Higher pH_2S can be withstood at low and high temperatures as long as chloride contents are low i.e. below 0.1% NaCl.

7.4.2. Cathodic Protection

The cathodic protection is usually by aluminum alloy anodes with a potential of about -1000mv SCE. It has been shown that embrittlement occurs at -900mV SCE in cold worked material. The potential difference reduces the hydrogen charging of duplex[101] although this will depend on the separation distance between the anode and structure. Several works have shown that very small cracks originate in the ferrite and are blunted when they reach austenite; hence the finer the grain size, greater the resistance of duplex to hydrogen embrittlement. It has been found that cracks propagate under high loads[102] above Rp when austenite can be plastically deformed.

8. Corrosion Test Methods

8.1. Pitting Corrosion Tests

The most widely used pitting corrosion test is ferric chloride test per ASTM G48-92 Method A, in which samples are tested in 6% $FeCl_3$(by weight) solution at various temperatures. Compared to ASTM G48-76 Method A, the newest version has two important changes:

1) The title of Method A was changed from "Total Immersion Ferric Chloride Test" to "Ferric Chloride Pitting Test".
2) A new section "Significance and Use" was added.
3) An appendix titled "Recommended Standard Data Format for computerization of data from ASTM Standard Test method G48-XX" was added.

The ferric chloride pitting test can be used to rank alloys in two ways. One is to test alloys at the same temperature and compare the weight loss, and the second is to test alloys at the same temperature and see which alloy exhibits pitting. This is also called as

Critical Pitting temperature (CPT) test. It takes several tests to define the CPT for a given alloy and each pitting test is conducted for 24 hours[35,95].

Ferric chloride test also appears as Method C in ASTM 923-94 "Standard Test Methods for Detecting Detrimental Intermetallic Phase in wrought duplex". This standard applies only to two alloys (S31803 {Alloy 2205} and Cast A890-4A) and requires a test temperature of 25°C for the base metal and 22°C for the weld metal.

Another commonly used pitting corrosion test is called the cyclic polarization test. The test requires more expensive equipment than $FeCl_3$ test[103]. Another method is Zero Resistance Ammeter (ZRA). It is an electrochemical test. The advantage is that it determines the CPT in a short period of time.

8.2. Intergranular Corrosion (IGC) Tests

No standardized IGC test is available from ASTM for duplex. However, many researchers have adopted ASTM A 262 Practice B (boiling $Fe_2(SO4)_3$-50% H2SO4 for 120 hours) and practice C (boiling 65% HNO3 for 240 hours)[35,11,36,104].

Another popular IGC test method is called Electrochemical Potentiokinetic Reactivation (EPR) test[105,106]. This test is quantitative; is highly sensitive to a relatively small degree of chromium depletion; quite rapid and non-destructive[105]. The test has been incorporated as an ASTM standard practice G108-94, however for AISI 304 and 304L only. Otero et al.[105] found that EPR test can be used to determine the presence of sigma phase.

9. Welding

The following welding processes are suitable for duplex stainless steels:
1) SMAW - Shielded Metal Arc Welding (Stick electrode welding)
2) GTAW - Gas Tungsten Arc Welding
3) GMAW - Gas Metal Arc Welding
4) FCAW - Flux Cored Arc Welding

5) SAW - Submerged Arc Welding
6) PAW - Plasma Arc welding (Table 4)

The other welding processes such as resistance welding, laser welding, electron beam welding and friction welding are considered immature processes for welding duplex. The reason is that these processes are characterized by rapid cooling rates which lead to excessively high ferrite content in the weld and HAZ. Research has been in the field of laser welding by Kajo Grubic and Ivan Juragac[107] showed that the power of laser beam and welding speed have significant effects on the shape of a weldment, penetration depth and weld width. Welding without filler material, no matter what the parameters is highly coarsened ferritic structure is formed. In corrosion testing, corrosion damage appeared only in the weld metal at the center line of the weld. Hence laser welding, if used, should be used with filler metal only.

Electroslag welding is not suitable for welding because of its high heat input and extremely slow cooling rate. Of the processes stated above SMAW (MMA) and GTAW (TIG) are the most frequently used processes but now days MIG/MAG is used more frequently.

9.1. SMAW

It is a versatile welding process and can be used for welding at any position. In addition for repair welding of castings and other structures, SMAW is selected[108].

Either rutile or basic electrode is used for welding duplex. Welders prefer rutile coated welding consumables over basic electrode for good slag detachability (beneficial for root pass welding) and smooth weld based appearance but they have low impact toughness due to high silicon and oxygen content[109,110,111,112] and vice versa.

Moisture control is important to prevent hydrogen cracking and porosity[110,114]. One method is to re-dry electrodes for about two hours at 250-350°C before welding or to use extra-moisture resistant (EMR) electrodes which have a guaranteed low coating moisture content.

Table 4: Welding Processes Characteristics (After Nassau [128])

WELDING PROCESS	CHARACTERISTICS
Shielded Metal Arc Welding	Readily available, all positions, slag on weld to be removed, low deposition rate
Gas Tungsten Arc Welding	Requires good skill, most suitable for pipe welding, high effect of dilution in root runs, low deposition rate, can be mechanized/automated
Gas Metal Arc Welding	Requires good skill, more setup work, metal transfer depends on wire quality (spattering), commonly only for filling of joint, high deposition rate, can be automated
Flux Core Arc Welding	Limited availability of consumables, only for filling of joint, limited positional welding, high deposition rate, slag protection
Submerged Arc Welding	Only mechanized, required set-up arrangements, only downhand (flat) welding, high dilution affects weld properties, higher deposition rate, slag removal in joint may be difficult
Pulsed Arc Welding	Requires complex equipment, only mechanized welding, no filler metal added, plate composition determines weld properties, high welding speed

In SMAW, the weld pool is protected by gases and slag from the electrode covering. To maximize this protection, Holmberg[113] recommended that an arc as short as possible should be maintained. A long arc can produce weld porosity, excessive oxides, excessive heat input and reduced mechanical properties.

9.2. GTAW

It is slow but is ideal for making high-quality root passes in pipe welding. The process prevents residual slag, spatter, and oxidation of the inside root pass, with proper backing. Moreover, greater control and repeatability can be achieved by using an automated GTAW process. This process also provides the best impact toughness for the weld metal comparing to other processes. However if there is excessive dilution or improper backing and shielding gas then there is a decrease in the impact toughness.

To avoid dilution in the root pass, filler metal must be added. GTAW without filler metal (autogenous) is not recommended unless PWHT is planned[109,111,113]. Solution leads to the loss of nitrogen also which would result in high ferrite content in the weld. Thus an inert gas shielding may not be proper for GTAW. 5% N_2 into Ar (more than 5% will cause an unstable arc) and 100% N_2 as backing gas can be used. Heat input for GTAW and SMAW is nearly similar, i.e., 0.5-2.5 KJ/mm.

9.3. GMAW

This process is nowdays commonly used for welding of duplex and super duplex because it offers high weld metal quality, low fuel emission rate, higher efficiency and is cost effective. Pulsed arc GMAW gives the best and safest result because of better penetration profile. It has been the best choice for joining 13% Cr pipe using super duplex wire electrodes[115].

9.4. Narrow Gap GTA Welding of P/M Superduplex

It is the best method for welding thick wall P/M super duplex because

1) Improves the weld quality
2) Improves economic efficiency by lowering the joint volume and filler wire consumption
3) With pulsed welding current offers an easy way to control heat input
4) Lower heat input
5) Lower incidence of weld metal defects
6) Small consumption of shielding gas
7) Lower residual stress

But it requires more accurate joint preparation and alignment and more expensive shielding gas[116]. Flux is a great concern too for having lower weld metal oxygen content.

9.5. Other Welding Processes

Shielding gas and flux are a major concern for FCAW also. Filler metals are also limited for this process[108,117]. Dilution is a great concern for SAW and PAW. High current as well as incorrect nozzle positions can cause dilutions as high as 70%, which will produce a very coarse structure. For SAW, dilution can be controlled by proper weld preparation and heat input and careful management of interpass temperature. For PAW, nickel-base filler metal and /or postweld heat treatment should be considered. For all processes, to control the heat input, stringer beads should be used[123] (Welding duplex stainless steels - Jan Hilkes and Karel Bekkers).

One paper discussed a DSS Radial Friction Welding (RFW) procedure optimization effort aimed at increasing production rated and reducing installation costs of flowlines in the oil and gas industry. The pipe examined was 6-5/8 inch diameter with a 9/16 inch wall thickness. Welds were made without shield gas on 22% chromium DSS

using both matching and super duplex rings. The testing showed that the weld cycle time could be used to control the ferrite content in the weld to values of 49-63%, with no sigma present in the final product. No information could be found on whether or not this apparent production process improvement was implemented.

9.6. Filler Metals

Proper selection of filler metals is very important to maintain the mechanical and corrosion properties of the weld and HAZ. Filler metals that have a modified chemistry compared to base metal are generally accepted. It is modified to provide comparable mechanical properties and better corrosion resistance and to allow for the loss of particular elements in the arc[68]. Hence the filler metals have higher nickel content and nitrogen. Ni is added to control the ferrite content and increase the pitting corrosion resistance of weld metal.

Weld metal toughness is affected by not only the ferrite content but also oxygen content. Covered electrodes with high silicon content such as rutile electrodes also give high oxygen content in the weld metal. Basic covered electrodes give lower silicon and oxygen content[118] (Welding consumables for Duplex and super duplex - Optimizing properties after heat treatment - G.B Holloway & J.C.M.Farrar). Atamert et al.[127] found that weld metal oxygen content is inversely proportional to the flux basicity. He claimed that flux-cored weld wires with low oxygen concentration and optimum nitrogen solubility display excellent corrosion resistance and mechanical properties. Pak and Rigdal used consumable wires OK Tubrod 14.27 and OK Tubrod 14.37 and found that these wires can produce weld metals that fulfill the requirements of duplex welding.

G.B Holloway & J.C.M.Farrar compared different electrodes in the as welded and PWHT conditions for welding duplex and super duplex and found that:

1) Toughness always improves after solution treatment and quenching.
2) Tensile properties, in terms of proof strength and ultimate tensile strength are always reduced after solution annealing.

3) Weld metal ferrite content showed little reduction after solution annealing.

4) Overmatched consumables are now considered to be a viable option if proper welding procedure and heat treatment is used.

Ni- base filler metals are often used for corrosion resistance, especially for root passes where the dilutions the highest. However, Holmberg[127] stated that combination of Ni-base fillers in the root and duplex fillers in the intermediate passes and cap passes may result in brittle microstructures. Oedegaerd and Fager found that welding super duplex using high Ni filler metal produced Cr_2N in the reheated regions and resulted in lower toughness. Karlsson et al.[119] indicated that the newly developed OK92.95 can solve the above problem. He showed that the weld metal deposited with electrode OK92.95 has an impact toughness of>50J at -196 °C and CPT> 85 °C.

Although there has been many developments the development of welding filler electrodes/ wires for duplex and super duplex, the standardization of welding consumables is limited[108]. Van Nassau et al.[108] pointed out that covered electrodes can be made to the following drafts of national and international standards or working documents:

1) AWS A 5.4-92
2) AWS A 5.9-93
3) CEN (TC121 PREN)
4) IIW (Subcommittee IIE.Doc.II-E-11891)

9.7. Shielding and Backing Gas

Nitrogen is known to be the most beneficial on duplex. It has been shown that nitrogen addition to shielding and backing gases improves the pitting corrosion resistance compared to normal pure argon[120,133]. While backing gases are encouraged to be 100% N_2, nitrogen content in shielding gas has to be limited to below 5% due to weldability problems. It has been shown that level of nitrogen above 3% in argon can lead to

detrimental effects on weldability, particularly reflected in tungsten electrode contamination, unstable arc conditions, weld pool turbulence, spatter and weld metal porosity. Besides adding nitrogen to argon, helium and hydrogen can also be added. In general, more penetration can be achieved by helium and hydrogen. However if hydrogen is used in the shielding gas, ferrite content must be properly controlled to prevent hydrogen cracking. It also enhances nitrogen loss in the weld pool.

In GMAW oxidizing gas components such as oxygen and carbon dioxide are usually required to stabilize the arc. However, oxygen additions may result in lower weld metal toughness for duplex. Stenbacka et al.[125] emphasized that standard gases such as Ar+2%O2 and Ar+2%CO2 are not suitable in GMAW of 2205, 2507. A quaternary gas mixture containing Ar, 5%He, 2%CO_2 and 2%N_2 which is called Arcal 129 can be used.

For pulsed arc welding, Ar+2%CO_2 or 68%Ar+30%He+1%O_2 are suggested for 22%Cr duplex wire electrode. For super duplex 100% Ar gives a very good result with a weldment free from oxides and spatter. Ar+2%CO_2 can also be used as an alternative. For spray arc welding 69% Ar+30%He+1%O_2 can be used for 22%Cr duplex and Ar+2%CO_2 for super duplex electrode.

10. Welding Metallurgy

10.1 Heat Affected Zone

It is important to control the ferrite-austenite balance in the weld HAZ. Gooch[25], stated that intergranular corrosion resistance of duplex would deteriorate when the ferrite content is high. This can also lead to a decrease in impact toughness[41,129,130,132]. The high temperature HAZ can be defined as the zone next to fusion boundary which approaches the melting point and would become completely ferritic on heating. Low temperature HAZ is the zone where the phase balance has remained substantially unchanged.

Certain effects on HTHAZ may occur if welding is performed with fillers giving weld metals different nitrogen activities. Use of nickel base filler, such as type 625, will result in nitrogen migration into the fused region thereby increasing the ferrite level in the

HTHAZ[126]. In HTHAZ, lower temperature reaction may occur in rapidly cooled welds, such as nitride formation. In the interpass regions secondary austenite may precipitate. The LTHAZ is located away from the fusion boundary and may cause intermetallic phases. This is a problem encountered in highly alloyed super duplex.

For duplex ferrite content is a function of heat input/cooling rate. The lower the heat input, higher the ferrite content and which reduces the impact toughness[41,129,130,132]. Draugelates et al.[132] explained that the higher cooling rate suppresses the diffusion-controlled processes in austenite reformation, hence, the original phase ratio of ferrite to austenite is shifted towards higher ferrite content. Atamert and King[41] indicated that the decomposition of δ ferrite to $\delta+\gamma$ shows C curve kinetics. The transformation rate is fasted at approximately 850°C in Fe-C-Cr-Ni alloys. For super duplex the nose of the C-curve is at about 1050°C.

Welding parameters should be controlled to ensure that the overall cooling conditions are slow enough for adequate austenite formation in the HTHAZ and fast enough to avoid deleterious precipitation in the LTHAZ. Lippold et al. and Kirineva and Hannerz showed that the presence of chromium rich nitrides (Cr_2N) is observed over a wide range of cooling rates and the effect is particularly evident for microstructures with a high proportion of ferrite. Chromium-rich nitrides also decrease the impact toughness and reduce pitting resistance. Increased ferrite and nitrogen levels cause a risk of chromium nitride formation in ferrite, due to lower solubility of nitrogen in ferrite. A high cooling rate, reduce the tendency of sigma and chi precipitation.

Excessively high heat input, may not be beneficial. Although the ferrite content may be reduced by slower cooling rates, the risk of intermetallic precipitation increases. In addition high heat input usually results in material being at peak temperatures for longer times and thus substantial grain growth may occur which lowers the impact toughness[41, 133-134].

Lippold et al. investigated alloys SAF 2205, SAF 2507 and 52N+. It was found that alloy 2507 is less sensitive to microstructural degradation in the HAZ than alloy 2205 over a wide range of heat input and cooling rate. According to him the 2205 welds exhibit a wider more highly ferritic HAZ than the super duplex alloy 2507 is related to

greater temperature range between the solidus and ferrite solvus temperature for alloy 2205. A similar study was conducted by Kivineva and Hannerz who showed that at a similar cooling rate, more ferrite was found in the HAZ of SAF 2205 than in SAF 2507.

Hoffmeister and Lothongkum showed the effect of nitrogen in super duplex. It was found that increasing the nitrogen content not only raised the A4 temperature but also accelerated the ferrite to austenite transformation. It was also shown that medium nitrogen content such as 0.10% can be detrimental due to precipitation of Cr_2N when the cooling rate in high.

The welding thermal cycle peak temperature studied by researchers is 1350°C at which ferritization occurs even for super duplex. In general for a given cooling rate, higher the peak temperature, higher the ferrite content. However, heating rate and base metal structure also affect the final ferrite and austenite balance[41]. Atamert and King[40] and Lippold et al showed that fast heating rates retard the dissolution of the austenite and thus prevent high ferrite content in the HAZ. They also showed that for wrought materials the interphase spacing may also affect the ferrite and austenite content in HAZ.

High peak temperature causes grain growth problems in wrought materials; lower impact toughness[41,133,134]. However it is not the only factor. Ferrite grain growth highly depends on heat input and cooling rate. Higher the heat input, greater is the grain growth in the HAZ. It is also controlled by dissolution of austenite. Atamert and King[40] indicated that when the spacing between austenite particles is large, grain growth is extensive. According to Ferreira and Hertzman[134] larger the grain size, lower the austenite content.

The above discussion is limited to single pass welding. In multipass weld deposits, the HAZ from the first cycle can be reheated by subsequent passes, to a degree dependent on the position of the HAZ relative to the heat source. In multipass welds the underlying weld metal is also reheated by the deposition of each subsequent pass. Atamert et al. and King characterized four regions in their analysis. It was found that the region 2 has lower austenite volume, which is not desirable due to reduced toughness and corrosion resistance. They did a computer modeling and found out that this region can be eliminated; at least for GTA welding.

A maximum interpass temperature of 150°C is recommended for multipass welding of duplex . This is because for a given heat input, a higher interpass temperature results in a slower cooling rate which for duplex may cause precipitation of various undesirable secondary phases. Farrar and Karlsson suggested that 23%Cr Mo free and 22% Cr have a maximum interpass temperature of 200°C whereas 150°C is the maximum interpass temperature for super duplex and other 25%Cr such as Ferralium 255.

10.2 Weld Fusion Zone (FZ)

Weld metal will exhibit segregation of alloying elements. However, the primary solidification phase with duplex is ferrite and this causes minimum segregation of chromium and molybdenum during solidification [54]. At low heat input the ferrite-austenite transformation is controlled by nitrogen. At high heat input there is sufficient time for diffusion of Cr, Mo and Ni to occur, and therefore there would be significant alloy difference of the two phases[25,135].

Welding without the addition of filler metal or excessive dilution with base metal can produce brittle weld metal with high ferrite content and hence should be avoided unless there is going to be postweld solution annealing. If the filler composition has more Ni it would[135]:

1) Promote austenite formation and will result in the reduction of nitrogen content in the austenite and thus lower the corrosion resistance of austenite and hence of weld metal.

2) Promote greater concentration of ferrite stabilizing elements (Cr, Mo) in the remaining ferrite. Hence it is more susceptible to the precipitation of sigma phase in the range of 650-950°C. Ni also widens the temperature range over which sigma phase is formed. The standard 1040° C PWHT used for alloy 2205 can promote sigma phase and embrittlement[32]. Consequently higher PWHT temperature must be used to dissolve sigma phase (1100 to 1150°C).

However, if the dilution from the parent steel is low, ferrite level can be too low to even satisfy weld metal strength requirement.

10.3. Effect of Solution Annealing Heat Treatment

Duplex can form harmful intermetallic phases during slow cool. It can lead to undesirable mechanical properties and poor corrosion resistance. The influence of elements on the on the stability of secondary phases has a bearing on selecting the solution annealing temperatures for duplex.

10.4. Effect of Heat Treatment Temperature

Higher solution annealing temperatures were found to give higher ferrite content in the HAZ thereby reducing the impact toughness, ductility and corrosion resistance. The other effects were:

1) Lowering of the partioning coefficients[37]. As a result the material is less sensitive to intermetallic phase transformations but more sensitive to secondary austenite and Cr_2N formation[37,38].

2) A decrease in chromium content and increase nickel content in the ferrite[19]. Lai et al.[19] demonstrated that this affect slows the formation of sigma phase which is consistent with Charles[37] and Kuroda and Mastsuda[38].

3) Changes the ferrite and austenite morphologies. Radenkovic et al.[136] observed that morphology of the austenite changes from a discontinuous network to continuous grain boundary morphology. In addition the initially irregular shape boundaries become smoother as the solution annealing temperature increases. Kuroda and Mastsuda[38] also noted that the grain size increases with increasing peak temperature.

10.5. Effect of Heat Treatment Variables

Higher the solution annealing temperature, stronger the effect of time on the ferrite content. Grain growth is also faster at higher temperatures, which makes heat treatment at excessive temperatures undesirable. Kotecki[153] examined the step annealing/cooling procedures using SAF 2205 weld metal but there was no advantage or disadvantage observed.

11. Ferrite Prediction and Measurement

The measurement of ferrite content of duplex is a necessity from the specification and service performance consideration standpoints. Ferrite measurement evolved after the realization that austenitic weld metal containing a moderate amount of ferrite was free from hot cracking related weld defects. In duplex appropriate ferrite content is required to achieve an excellent combination of strength, toughness and corrosion resistance. Low level of ferrite may lead to low strength, undesirable corrosion resistance and may not prevent hot cracking. High level may lead to reduction in toughness, undesirable pitting and intergranular corrosion resistance and also cold cracking embrittlement.

The earliest work on ferrite prediction was carried out by Schaeffler in 1949 on weld metals. His work was modified by Delong[81] which was further modified by Kotecki[137]. This involves Schaeffler diagram which requires calculating chromium and a nickel equivalent for each base metal and proposed filler metal.

11.1. The Schoefer Diagram

The Schoefer diagram was adopted by ASTM and used in specification A800. This diagram requires that all the ferrite stabilizing elements be converted into Cr_{eq} and all the austenite stabilizing as Ni_{eq}.

$$Cr_{eq} = Cr+1.5Si+1.4Mo+Nb-4.99$$
$$Ni_{eq} = Ni+30C+0.5Mn+26(N-0.02)+2.77$$

Here the elemental concentrations are given by weight percent.

ASTM A800-91 states that the Schoefer diagram is applicable to alloys containing elements in the following ranges:

Carbon   0.20 max

Manganese   2.00 max

Silicon   2.00 max

Chromium   17.0 to 28.0

Nickel   4.0 to 13.0

Molybdenum   4.00 max

Columbium   1.00 max

Nitrogen   0.20 max

Thus, it is evident that for modern duplex especially super SAF 2507, nitrogen which is a strong austenite promoter, Mo which is a ferrite promoter, can easily exceed Schoefer diagram maximum limitations.

11.2. The WRC-1992

For the WRC the Cr eq and the Ni eq are calculated as:
$$\mathbf{Cr_{eq} = Cr+Mo+0.7Nb}$$
$$\mathbf{Ni_{eq} = Ni+35C+20N+0.25Cu}$$

The significant addition in developing the -1992 was the addition of Cu to Ni eq. Lake[140] developed data on the evaluation effect of Cu. Using Lake's data Kotecki[141] proposed a coefficient of 0.25 for Cu. He pointed out that the WRC-1992 only offers predications over a limited Cr eq and Ni eq range 17-31 and 9-8.

In WRC ferrite content is expressed in terms of ferrite number which is an arbitrate number based on magnetic response but in Schoefer diagram it is expressed as volume percent. However, as far as modifications to the Cr and NI equivalents are concerned, the most significant difference is the disappearance of Mn and Si.

According to Lotecki and Siewert[138] and Szumachowski and Kotecki the removal of Mn was due to:

1) Mn does not promote the high temperature formation of austenite at the expense of ferrite, and thus the effect of Mn on ferrite content is very small.

2) The effect of Mn is even smaller when the ferrite content is represented in ferrite number instead of ferrite percentage.

Kotecki[91] found that the coefficient of 1.5 for silicon indicated by Schaeffler diagram overstates the effect. In a study of six welds spanning 0.34 to 1.38 wt% Si, Kotecki determined a coefficient of 0.1. It was shown by Takemoto et al. that the effect of Si is small below 2 wt %Si, but greater at higher silicon content.

Kotecki felt that a number of alloy elements have not been considered in the WRC-1992 diagram like silicon. Elements like tungsten and titanium were not considered. According to him WRC-1992 does not well address the cooling rate effects.

11.3. Ferrite Measurement

11.3.1. Point Count

Point counting per ASTM E562 has been the traditional method used to determine the ferrite content of duplex and weld metal in terms of volume fraction or ferrite percentage. This involves preparing a specimen using standard metallographic procedures, selecting a proper magnification, grid and finally counting intersections of the grid with the ferrite phase. The disadvantages associated are:

1) Destructive
2) Time consuming
3) Not accurate

Color etching techniques, which usually color the ferrite, are encouraged in applying the point count method. This color etched or magnetically colored sample can be examined using an image analyzer which can speed up counting process.

11.3.2. Magne-Gage: Magnetic Adhesion Method

This method utilizes the ferromagnetic property of the ferrite to determine the ferrite content. It expresses the ferrite content in terms of ferrite number rather than volume % ferrite. Ferrite number was first developed in US as ANSI/AWS A4.2-74, according to Lefebvre[143]. It was found to overstate the %ferrite in weld metal[143, 144]. Ferrite number was found to be highly reproducible. The disadvantage is that it must be used in level surface in order to obtain accurate readings. Hence it is not suited for measuring ferrite number in the narrow HAZ due to the size of the magnet.

11.3.3. Eddy Current Method: Magnetic Induction Method

This is suitable for field use. It relies on low frequency alternating current through the field coil, generating an alternating magnetic field that penetrates into the specimen. The interaction between the field and specimen induces in the detection coil an alternating voltage, proportional to ferrite content in the volume of measurement; hence it determines ferrite content in terms of volume percentage. Feritscope® (Figure 3) uses the above principles and is used in the calibration procedure established and documented in ANSI AWS/A4.2-92 and ASTM A799-92. The accuracy of Feritscope® is affected by:

1) Electromagnetic properties of ferrite
2) Morphology of ferrite[145]
3) Distance between the probe pole and surface of specimen
4) Curvature of test specimen
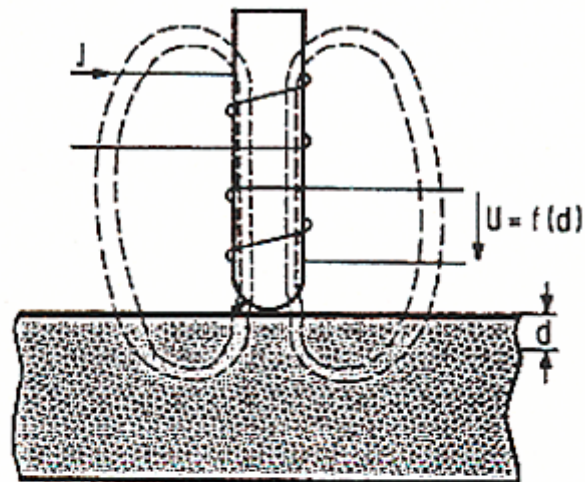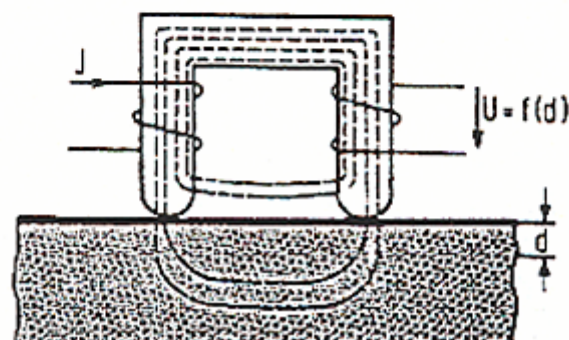
Figure 3: Ferrite Measurement with Single-and Two-Pole Probes Feritscope® (After Neumaier P. [145])

According to Lundin, the Feritscope® when properly calibrated, considering efficiency and instrument repeatability and reproducibility is identified as the most practical instrument for the determination of ferrite content in duplex[156].

11.3.4. Ferrite Number vs Ferrite Percent

Brantsma and Nijhof concluded that ferrite number was preferable over Ferrite percents for determining the ferrite content in the weld metal of duplex. But Kotecki[141] showed that in cast alloys it is the other way as the ferrite grains are much coarser and more regularly shaped than in the weld metal. Taylor[68] suggested a relationship:

% Ferrite = 0.55(EFN) + 10.6

Ferrite numbers in the range 0-28 are not applicable for this equation.

12. Weld Metal and Weldability

The weld metal microstructure differs from the parent material, as a result of variation in chemical composition and its total thermal history. The chemical composition of weld metal is very important.

12.1. Solidification and Austenite Formation

In the weld metal, ferrite solidification involves epitaxial growth from the parent material at the fusion boundary[146], i.e. the HTHAZ. The initial dendrite growth is oriented in relation to the thermal gradient[147], and produces a columnar ferritic structure. This provides the starting conditions for further solid state transformation and will dominate the final weld metal structure. The ferrite grain size and orientation together with ferrite content and morphology, influence weld metal properties.

Austenite precipitation depends on the weld metal composition. It also depends on the ferrite grain size and the cooling rate. Slow cooling rate results in more austenite formation, while fast cooling rate give less austenite. However, as the nucleation is

facilitated at grain boundaries, a small ferrite grain size, in principle, favors high austenite contents[149]. In general duplex weld metal has ferrite contents in the range of 30 - 70%.

12.2. Element Partitioning in Weld Metal

It is same as for parent material. For low heat input welding the substitutional elements (Cr, Ni, Mo etc) is almost equal in both phases whereas the interstitial elements controlling the reaction are heavily concentrated in the austenite. If higher heat input is given, slow cooling rate result and austenite transformation is mainly diffusion controlled with subsequent partioning of substitutional elements[146]. Multipass welding has a similar effect on partitioning as slow cooling[148].

12.3. Other Transformation

The as-deposited, non equilibrium, weld metal structure can be affected by additional thermal treatment, such as multipass welding and postweld heat treatment. In both cases, secondary austenite can precipitate from the ferrite which is supersaturated in nitrogen at lower temperatures. This contains lesser amount of Cr, Mo and N as compared to primary austenite.

Precipitation of intermetallic phases can occur in weld metal as well as LTHAZ. The precipitation is mainly in the ferrite/austenite and ferrite/ferrite boundaries. Exposures in the temperature range 700-900°C results in a more rapid precipitation in the weld metal than in the base metal due to higher alloy content of the ferrite. The phases observed are sigma, chi and R although sigma is dominant. At lower temperature of 500-600°C dominating phases are molybdenum rich R and Π phase.

12.4. Porosity

Too much nitrogen leads to weld metal porosity. But the nitrogen solubility in the liquid phase increases as the temperature drops, which ensures that there is no risk of pore formation during the liquid state.

Nitrogen contaminates the tungsten electrode which causes emission of very fine weld metal droplets from the weld pool[121] known as sparking. As the super duplex have a higher solubility limit, sparking and electrode wear is less likely for these steels. At higher nitrogen level weld metal spitting can take place, which can lead to a crevice on the parent steel and subsequent localized corrosion in service.

12.5. Solidification Cracking

Varestraint tests show that commercial duplex is less susceptible to weld metal cracking than austenitic alloys with primary austenitic solidification. If duplex solidify in a primary austenite solidification mode, which occurs when Cr_{eq}/Ni_{eq} ratio is below 1.5, severe partitioning of impurities such as S and P will occur and tend to form liquid films which effectively wet austenite/austenite grain boundaries, thus promoting weld fusion zone solidification cracking. If the weld metal chemistry shows a Cr_{eq}/Ni_{eq} ratio above 2, the solidification mode is highly ferritic and a cracking tendency also exits. A duplex solidification mode occurs when the ratio is 1.5 to 2 and it offers best hot cracking resistance.

12.6. HAZ Liquation Cracking

The susceptibility of duplex to liquation-related HAZ cracking is negligible according to Lippold et al.[32]. He said that the resistance of duplex is attributed to the low impurity level of duplex and that ferritic microstructures are generally resistant to grain boundary liquation due to the high diffusivity of alloying and impurity elements at elevated temperature.

12.7. Hydrogen Assisted Cold Cracking

The rate of hydrogen entry in steel increases as the potential becomes more negative, which is the case for cathodically protected components. In addition, lower pH solutions have higher hydrogen ion concentrations and so accelerate adsorptions. Once hydrogen is in steel, diffusion is activation controlled and it thus a function of temperature. Diffusion of hydrogen through austenite is slower than in ferrite by a factor of 10^4. It diffuses to ferrite austenite boundaries[150]. These sites act as hydrogen sinks. Hydrogen ingress into duplex is slow hence they travel a short distance beneath the surface unless exposed to elevated temperatures (>100 ° C).

Hydrogen can be adsorbed into the weld metal by[32, 151-155]:

1) Contamination of weld joint.
2) Presence of hydrogenous material in electrode coatings or submerged arc flux.
3) Use of hydrogen as shielding gas.
4) Moisture absorbed from the atmosphere

Presence of ferrite minimizes hot cracking but at the same time it increases the cold cracking also called as hydrogen cracking. Ogawa and Miura[152] showed that increasing Ni and N in the weld metal can reduce hydrogen cracking tendency. The diffusion of hydrogen in austenite is less as compared to that in ferrite. Hence the ferrite content would be less. But Shinozaki et al[151] pointed out that if the cooling rate is extremely rapid Cr_2N will form in addition to a high ferrite content which is detrimental to hydrogen cracking resistance.

High weld metal hydrogen contents can be avoided by baking SMAW electrodes at appropriate temperatures but inadequate drying can result in sufficient diffusible hydrogen to cause weld metal cracking in high ferrite welds. A product that has failed the Charpy test may be at the option of a producer, be given a full anneal and retested.

Class-Ove Pettersson - AB Sandvik Steel Sweden[115] tested the weld metal properties of two duplex specimens' 22Cr-8Ni-3Mo-N and 25Cr-10Ni-4Mo-N. He found that MIG/MAG welding gave better mechanical properties. The impact strength was higher compared to weld metal from MMA process due to low amount of micro slag inclusions. The CPT was at acceptable level. There was no need for adding nitrogen for MIG/MAG because of fast feeding rate of filler metal which continuously feeds pumps in nitrogen into the weld pool and at the same time keeps it cooler compared to TIG process.

12.8. Influence of Shielding Gases on Weld Metal Nitrogen and Ferrite Content

To carry out this test UNS 32750 was used. A backing bar of copper was used and MIG/MAG welding was used. The study confirmed that more nitrogen is lost in TIG welding than in MIG/MAG. For MIG/MAG more nitrogen enters the weld deposit when CO_2 is added to shielding gas. This affects the ferrite content.

12.9. Pulsed Arc Welding with Argon (99.996%) as Shielding Gas

If this is used then the weldment is free from spatter. Using an inert gas also results in an almost oxide free surface. The pulsed arc profile is wider and does not have the argon finger that is typical for spray arc welding. This gives more safety margin concerning defects such as lack of fusion.

12.10. Ferrite Decomposition in the Weld Metal

A Gregori and J.O.Nilsson[155] compared the microstructural stability at temperature above 700°C of weld metal of type 29Cr-8Ni-2Mo-0.39N and 25Cr-10Ni-4Mo-0.28N. Multipass welding was employed using the gas tungsten arc welding technique with a shielding gas of Ar+2%N_2. They found that weld metal 29Cr-8Ni-2Mo-0.39N was more stable than the weld metal 25Cr-10Ni-4Mo-0.28N. A lower

molybdenum concentration with a higher nitrogen concentration could explain the higher stability with respect to the intermetallic phases. The higher nitrogen content could also explain the higher stability against the formation of secondary austenite in weld metal type 29Cr-8Ni-2Mo-0.39N.

The properties of weld metal are largely influenced by the solidification mode and subsequent cooling of the welding pass as a consequence of the absence of controlled recrystallization.

Gregori and Nilsson performed the calculation of TTT and CCT diagrams, based on the experimental results obtained by the image analysis, assuming that the isothermal precipitation of intermetallic phases could be described by the Avrami equation of the type:

$$V/V_m(T) = 1-\exp(-b(T)t^{n(T)})$$

where

V = Volume fraction of intermetallic phase formed at time t and temperature T

$V_m(T)$ = Corresponding equilibrium fraction at temperature T

$b(T)$, $n(T)$ = Temperature-dependent quantities

It was seen that σ phase occurred preferentially in the region where ferrite had a vermicular appearance with narrow arms. Ferrite influenced the precipitation kinetics. No intermetallic phases were observed in weld metals in the as-welded condition. Secondary austenite was precipitated in the 25Cr-10Ni-4Mo-0.28N weld metal in the ferrite region. In this weld metal the Chi phase (χ) tended to precipitate in the narrow ferrite arms, while σ phase precipitated essentially, in the broad ferrite arms. It was seen that nucleation of σ phase was facilitated by the presence of χ phase.

Thermo-Calc calculation performed on the 25Cr-10Ni-4Mo-0.28N weld metal predicted that the solidification begins with the formation of ferritic dendrites and, at lower temperature a peritectic occurs at about 1350˚C resulting in a ferritic-austenitic microstructure. Further cooling below 1000˚C resulted in the precipitation of Cr_2N and σ phase.

In the CCT diagram the nose of the C curve relative to the intermetallic phase precipitation is located at 900˚C.

III. Experimental Procedure

In order to support the inclusion of ASTM A890-5A material in ASTM A923, eleven heats of 5A material in the form of test bars (Figure 4, 5, 6, 7) were received from four SFSA foundries in the foundry solution annealed condition. The foundry solution annealing treatment for all the materials submitted for testing in accordance with A923 is shown in Table 5. The material from the eleven heats was tested in accordance with ASTM A923 Methods A, B and C. While no minimum toughness for the charpy impact testing or test temperature is given, per Method B, for the 2507 wrought alloy (to be agreed upon by purchaser and supplier), a temperature of -50°F was chosen as a temperature that may be representative of an industry typical test temperature. The chemistry for the eleven heats is given in Table 6. Sufficient material from one heat from Foundry D was available for a full scope of heat treatment following the schedule used for the testing of the wrought material in the development of the ASTM A923 specification.

Table 5: Details of the A890-5A Material Procured

Foundry	Heats	Number of Bars per Heat	Solution Annealing by Foundry
A	331F, 285F, 144F	1	Heat to 2200°F, Hold 3 hours, Water Quench
B	S1507, S1508	2	Heat to 2050°F, hold 2 hours, furnace cool to 1950°F, hold 1 hour, Water Quench
C	41544, 41414, 44073, 41374, 45633	1	Heat to 2075°F, cool to 1940°F, Hold 1 hour, Water Quench
D	04J142	10	Heat to 2100°F, Hold 1 hour, Water Quench

Table 6: Chemical Composition of Test Bars from Various Foundries

A890-5A GRADE TEST BARS

| Elements	Foundry A			Foundry B		Foundry C					Foundry D
	Heat 1	Heat 2	Heat 3	Heat 1	Heat 2	Heat 1	Heat 2	Heat 3	Heat 4	Heat 5	Heat 1
	144F	285F	331F	S1507	S1508	45633	44073	41374	41414	41544	04J142
Carbon	0.019	0.024	0.019	0.03	0.03	0.016	0.0194	0.016	0.019	0.03	0.02541
Sulphur	0.006	0.006	0.006	0.025	0.025	0.001	0.0039	0.01	0.009	0.005	0.00689
Phosphor	0.004	0.023	0.004	0.022	0.021	0.021	0.024	0.02	0.02	0.02	0.01157
Nitrogen	0.26	0.25	0.25	0.16	0.13	0.1537	0.1629	0.1615	0.166	0.1532	0.13935
Mangane	0.69	0.78	0.69	0.75	0.95	0.74	0.4	0.46	0.42	0.5	0.59528
Silicon	0.36	0.38	0.36	0.71	0.58	0.43	0.59	0.54	0.48	0.63	0.75715
Chromiu	25.3	25.3	25.3	25.6	25.8	24.5	24.15	24.61	24.77	24.54	25.16827
Nickel	7.6	7.8	7.6	7.2	7	8	7.77	7.88	7.76	7.63	6.87326
Molybde	4.1	4.6	4.1	4.6	4.7	4.14	4.18	4.29	4.52	4.35	4.52612
Copper	NA	NA	NA	0.94	0.98	0.262	0.174	0.202	0.133	0.195	0.04285
Tungsten	NA	NA	NA	0.12	0.05	0.037	0.027	0.025	0.024	0.026	0.02137
Vanadiur	NA	NA	NA	NA	NA	0.086	0.058	0.05	0.05	0.067	0.04186
Cobalt	NA	NA	NA	NA	NA	0.086	0.044	0.037	0.033	0.042	0.04712
Titanium	NA	NA	NA	NA	NA	0.001	0.001	0.001	0.001	0.001	0.00047
Aluminu	NA	NA	NA	NA	NA	0.014	0.023	0.017	0.018	0.018	0.01261
Tantalum	NA	NA	NA	NA	NA	NA	NA	NA	NA	NA	0.0019
Niobium	NA	NA	NA	NA	NA	0.013	0.015	0.03	0.017	0.022	0.01735
Tin	NA	NA	NA	NA	NA	0.007	0.007	0.007	0.007	0.007	NA
Boron	NA	NA	NA	NA	NA	NA	NA	NA	NA	NA	NA
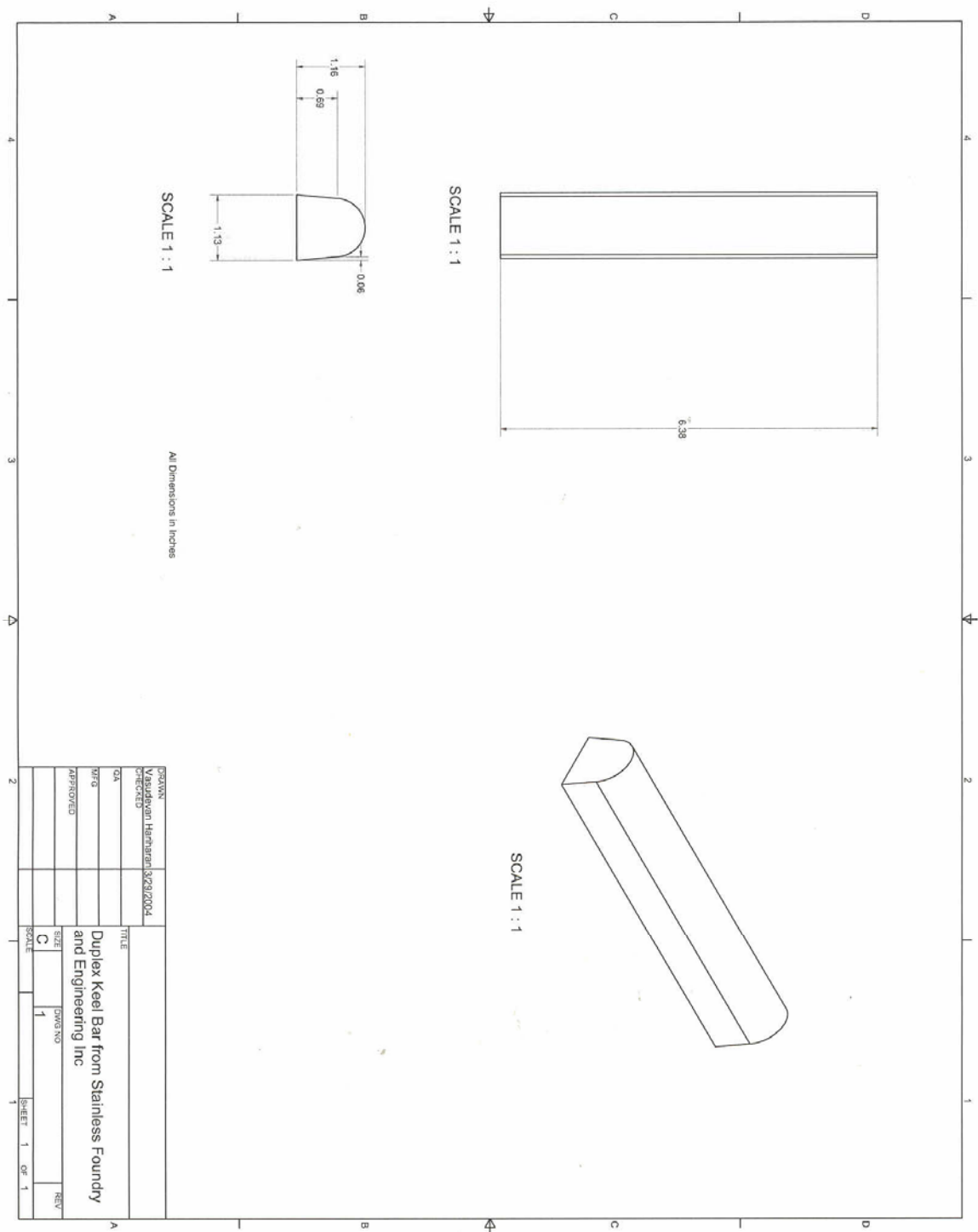
Figure 4: Duplex Keel Bar from Foundry A
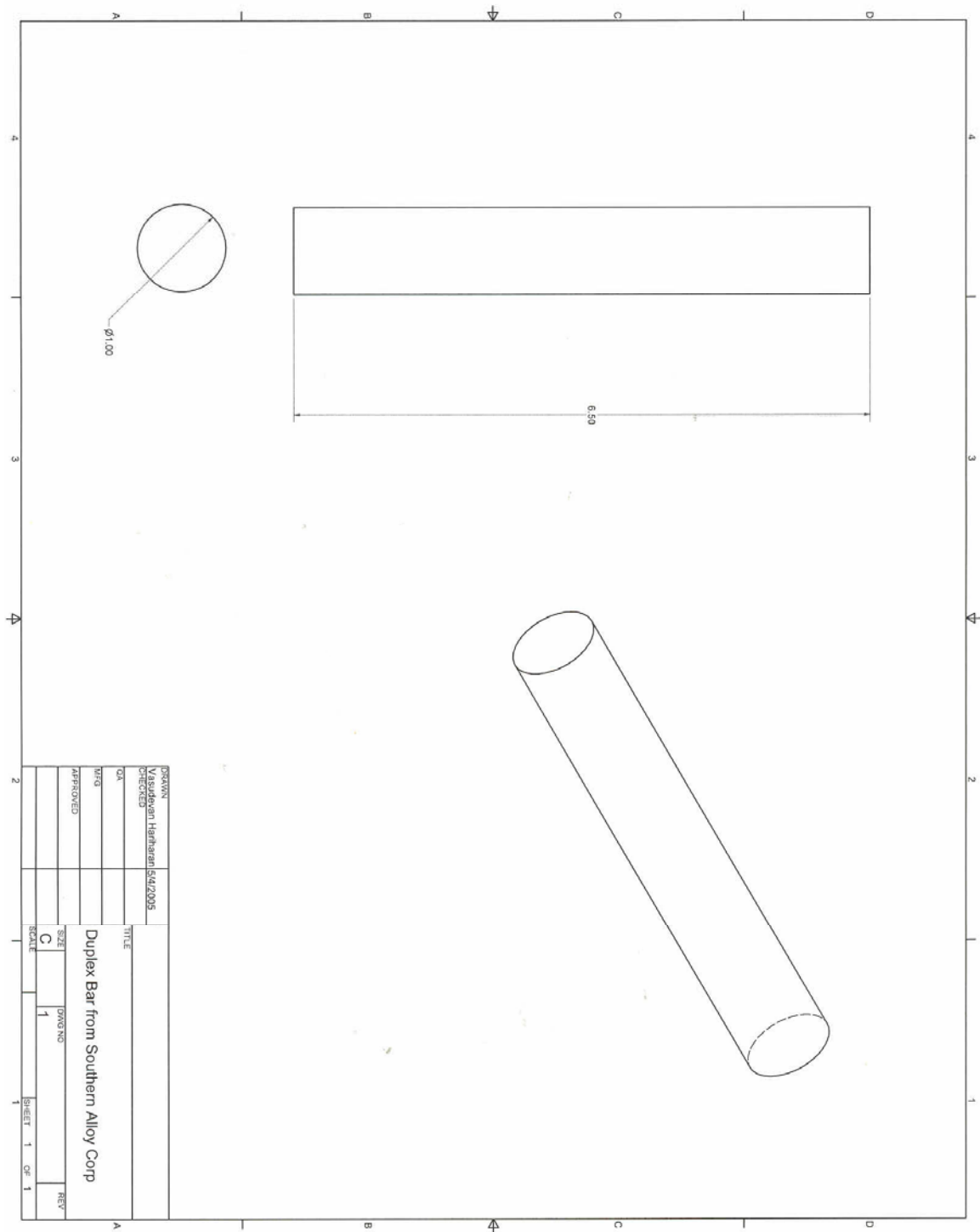
**Figure 5:** Duplex Bar from Foundry B
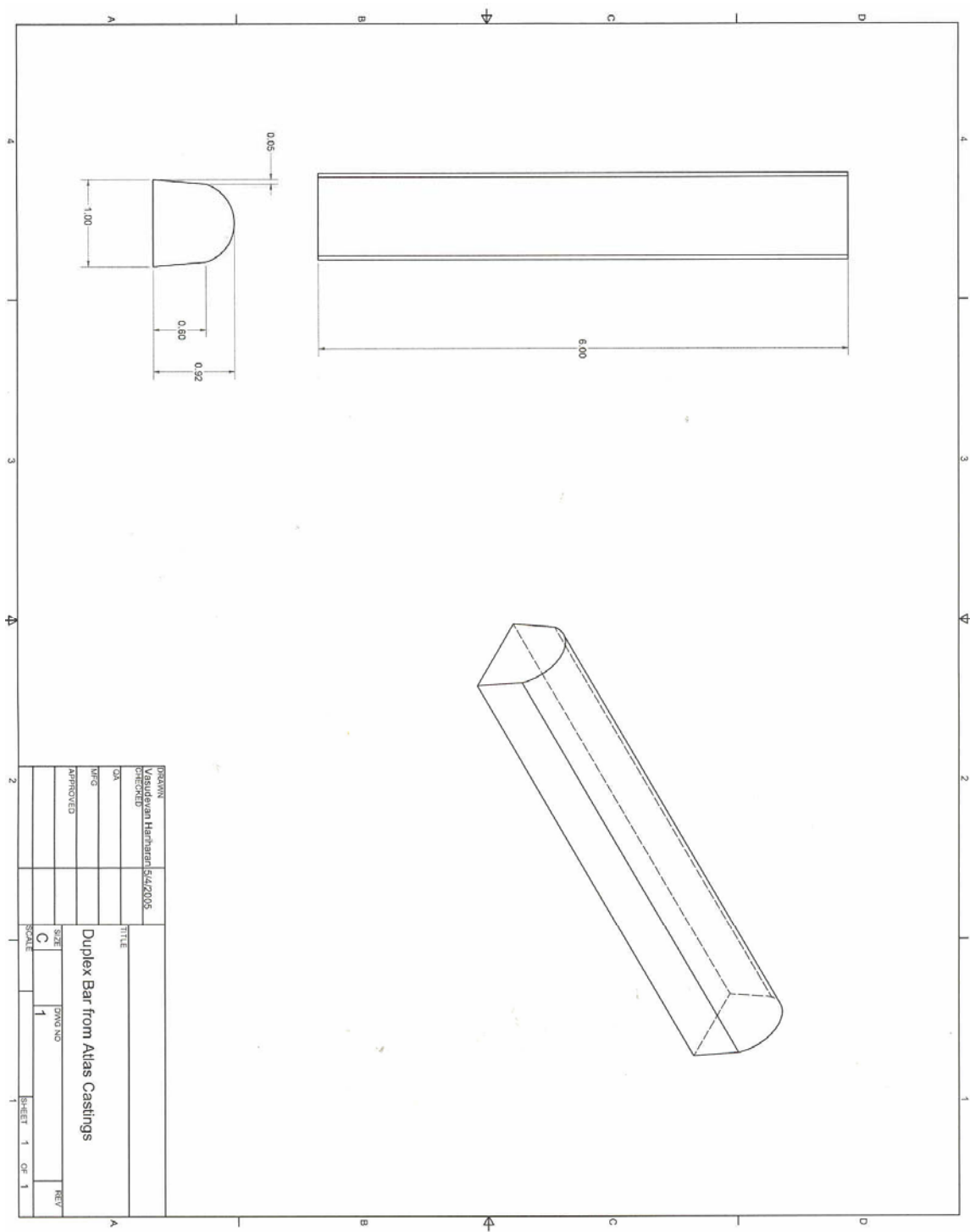
Figure 6: Duplex Bar from Foundry C

68
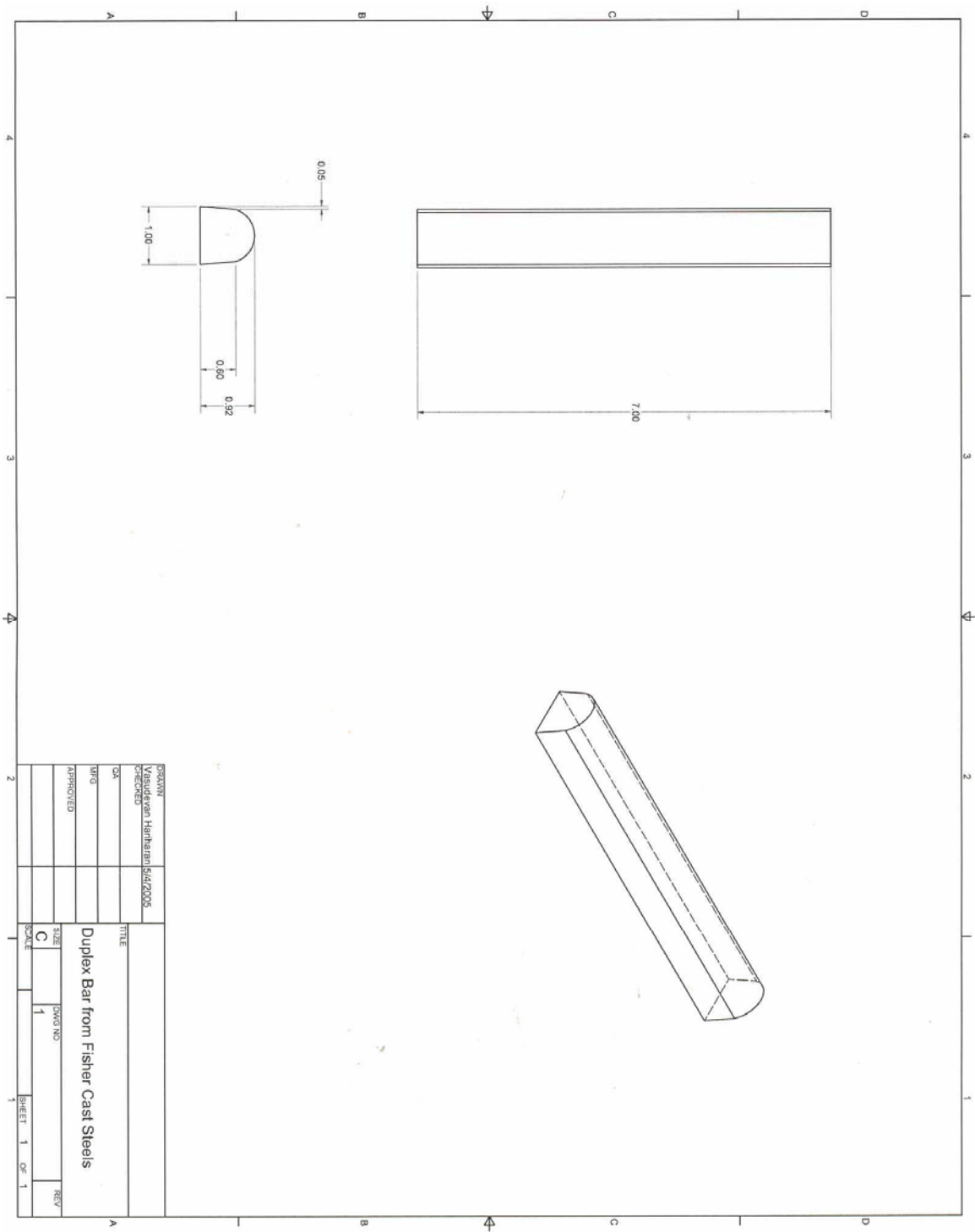
Figure 7: Duplex Bar from Foundry D

1. The Suitability of ASTM A923 for Detecting the Presence of Intermetallic Phases in Super Duplex Stainless Steel Castings

1.1. Heat Treatments

The blocks from Foundry A, B and C were not heat treated at the University of Tennessee. The various tests were carried out on them as cast solution annealed. The blocks from Foundry D were subjected to heat treatment as the material from the same heat was sufficient for conducting the full scope of heat treatment.

The heat treatment schedules were derived from the testing of wrought DSS to establish the A923 specification [117]. Eight heat treatment schedules were selected in order to produce a wide range of intermetallic phase precipitation; these heat treatments are shown in Table 7. The material was solution annealed at 2050°F (1120°C) minimum and then held for one hour according to ASTM A890/A890M-99 (Standard Specification for Castings, Iron-Chromium-Nickel-Molybdenum Corrosion-Resistant, Duplex (Austenitic/Ferritic) for General Application). These samples were furnace cooled to 1950°F and then the various heat treatment schedules was followed. Thermocouples were attached to the blocks when heat treated in order to measure the temperature of the samples accurately.

1.2. Testing Methods

1.2.1. Test Method B

This test method required Charpy impact testing at -50°F as a method for the detection of intermetallic phases in DSS.

Table 7: Heat Treatment Schedules

Heat Treatment	Stage 1	Stage 2
A	Heat Sample to 1950°F, Hold 30 min., Water Quench	
B	Heat Sample to 1950°F, Hold 30 min., Water Quench	Heat sample to 1550°F, Water Quench
C	Heat Sample to 1950°F, Hold 30 min., Water Quench	Heat sample to 1550°F, Hold 5 min., Water Quench
D	Heat Sample to 1950°F, Hold 30 min., Water Quench	Heat sample to 1550°F, Hold 10 min., Water Quench
E	Heat Sample to 1950°F, Hold 30 min., Water Quench	Heat sample to 1550°F, Hold 15 min., Water Quench
F	Heat Sample to 1950°F, Hold 30 min., Water Quench	Heat sample to 1550°F, Hold 20 min., Water Quench
G	Heat Sample to 1950°F, Hold 30 min., Air Cool	
H	Heat Sample to 1950°F, Hold 30 min., Slow Cool	

Two to four charpy impact samples were extracted from the material and notched. Figure 8 shows a standard charpy specimen. Notch Geometry for a Charpy Impact sample according to ASTM A370 is shown in Figure 10. The Charpy impact test apparatus is shown in Figure 9. This apparatus is a pendulum type of rigid construction that is capable of providing enough impact energy to break a notched sample in one blow.

The charpy samples were prepared in University of Tennessee and were sent to AMC-Vulcan, Inc. in Alabama where they were notched and tested as follows per ASTM A923. The samples were placed in an alcohol bath cooled with liquid nitrogen to maintain a temperature of $-50°F$ for a sufficient time to normalize the bars at temperature. Self-centering tongs were then used to remove the samples from the liquid alcohol bath. The samples were placed in the proper orientation in the Charpy impact test apparatus and the pendulum was then released. (This step must take no longer than 5 seconds to perform due to the low temperature that is being used). After impact the broken specimen were placed in a room temperature acetone bath.

If a test specimen shows a value below the specified minimum, one retest of two specimens is permitted. For acceptance both retest specimen show a value at or above the specified minimum value.

1.2.2. Test Method A

After the data package and the samples were retrieved from AMC Vulcan Inc. one half of a fractured Charpy sample from each block was tested as per Method A (sodium hydroxide etch test). The sodium hydroxide etch test may be used for the acceptance of material but not for rejection. This test method may be used with other evaluation tests to provide a rapid method for identifying those specimens that are free of detrimental intermetallic phases as measured in these tests.

All the samples were prepared by mounting them using epoxy resin and hardener in a ratio of 1:5. On all samples, cross-sectional surfaces were prepared to a metallographic finish suitable for examination at 400x after etching. This was achieved by grinding the mounted samples using 120-grit followed by 320, 400, 600, 800 and then
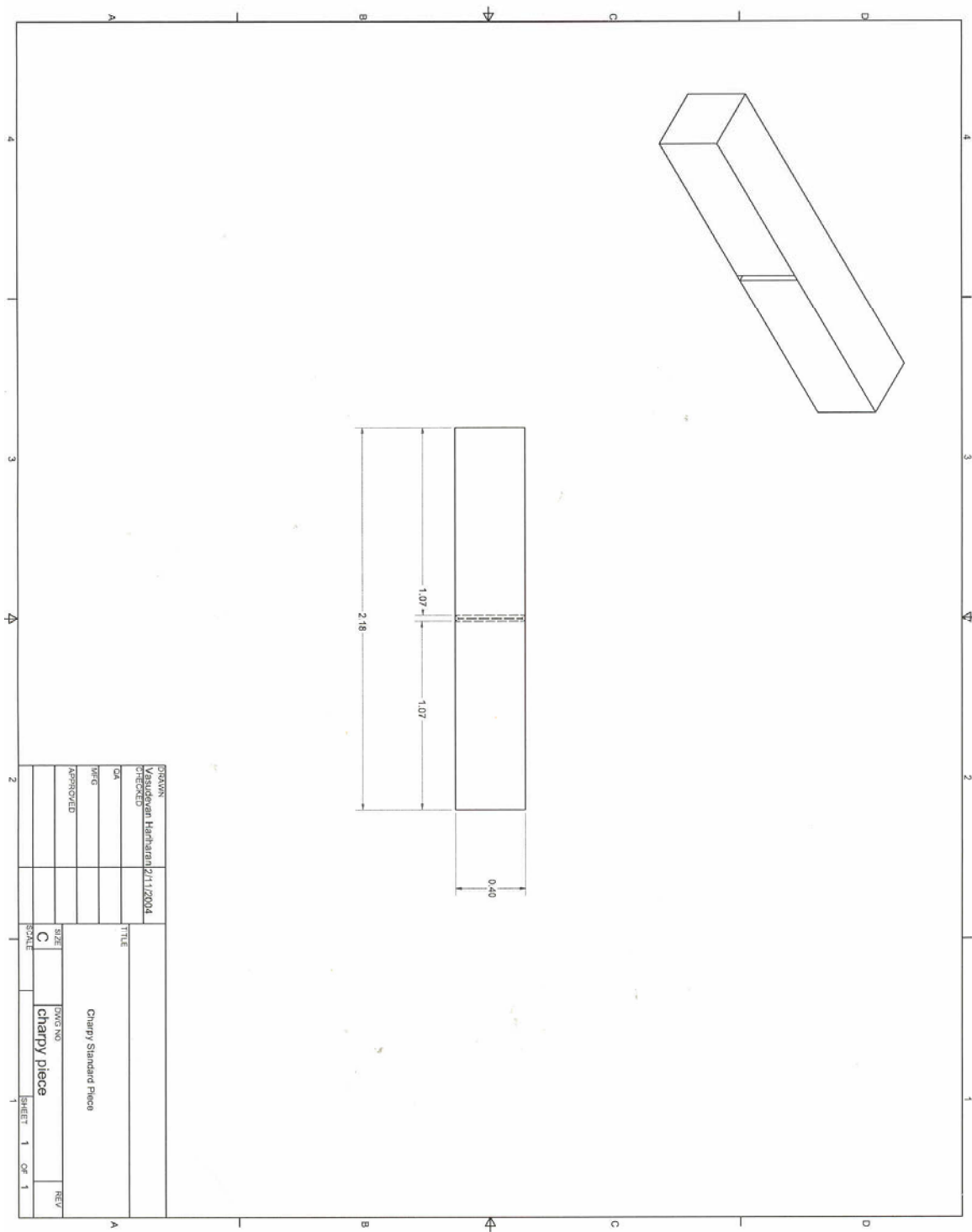
Figure 8: Standard Charpy Bar

73

Figure 9: Charpy Impact Testing Machine
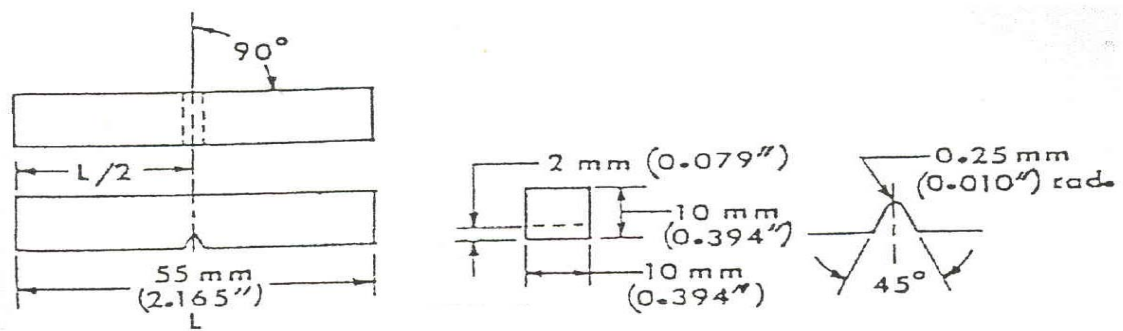
Figure 10: Charpy Impact Notch Geometry

polishing them using nylon cloth with Elgin Dymo of grade #6 followed by micro cloth using alumina powder of 0.05 microns. The etching solution was prepared by adding 40 g reagent grade sodium hydroxide (NaOH) to 100 g of distilled water. Samples were then electrolytically etched at 3 V dc for 15 seconds. Following etching, the specimens were rinsed thoroughly in hot water or in acetone, followed by air drying. The etched surfaces were examined at 400x using Optical Microscope and classified according to ASTM A923.

The cast material classification can be determined from the wrought material photomicrographs supplied in ASTM A923, with the exception of the centerline structure classification, which will only be applicable to wrought material, see Figures 11-14. ASTM A923 requires that any material showing other than an unaffected structure must be Charpy impact tested per Method B. The following was used to define/classify each microstructure:

1) Unaffected Structure (Figure 11) – The sample has been etched and the microstructure is without the revelation of any intermetallic phase. The austenite-ferrite boundaries are smooth.

2) Possibly Affected Structure (Figure 12) – The sample has been etched and isolated indications of possible intermetallic phase are noted. The austenite-ferrite boundaries show a fine waviness.

3) Affected Structure (Figure 13) – The indication of an intermetallic phase is readily revealed upon etching.

4) Centerline Structure (Figure 14) – The intermetallic phase is observed as a continuous or semi-continuous phase in the mid-thickness region of the sample, with or without the affected structure outside of the mid-thickness region, indicative of segregation. This structure is only applicable to wrought materials.

1.2.3. Test Method C

This test method is a ferric chloride corrosion test for detecting the presence of intermetallic phases in Duplex Stainless Steels. The presence or absence of corrosive attack in this test is not necessarily a measure of the performance of the material in other
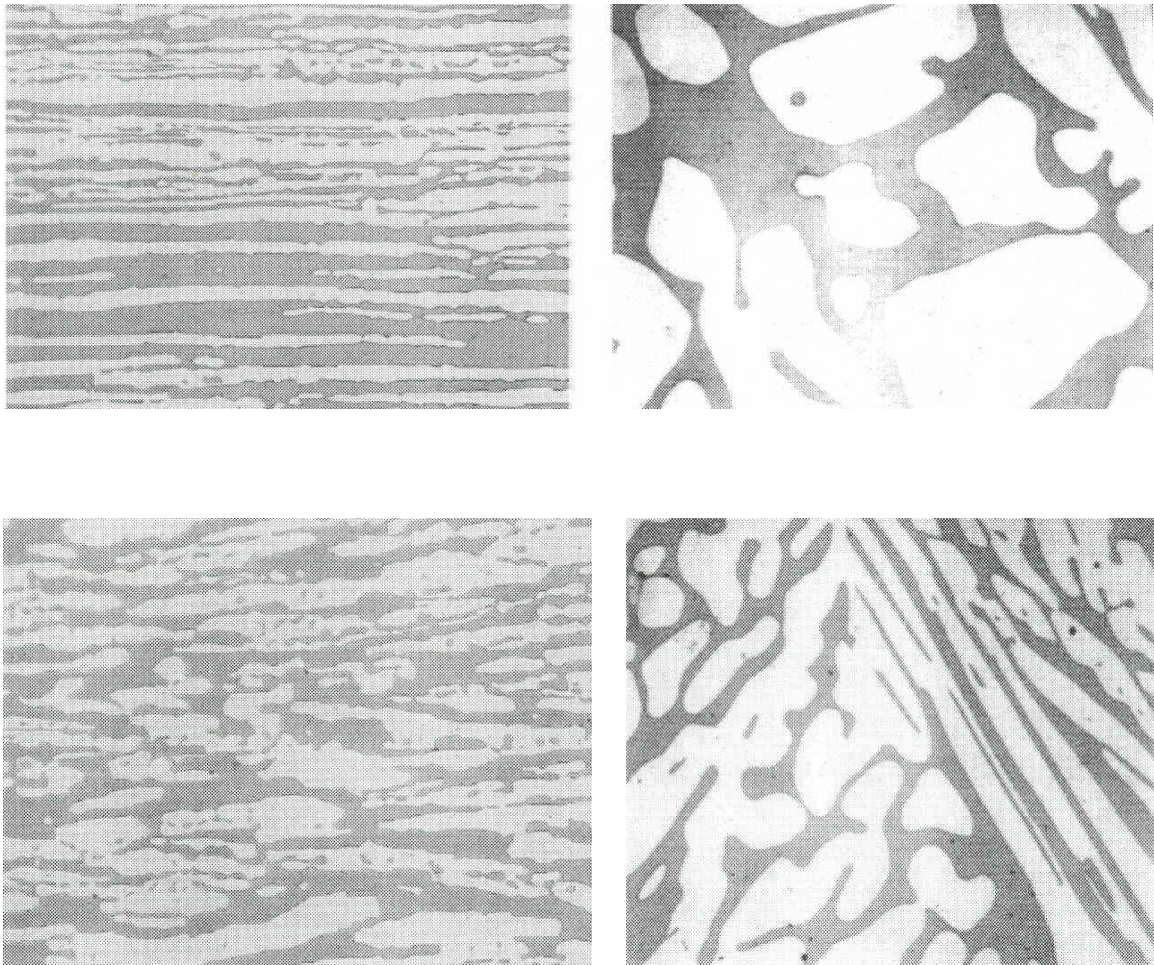
Figure 11: Unaffected Structure of ASTM A923
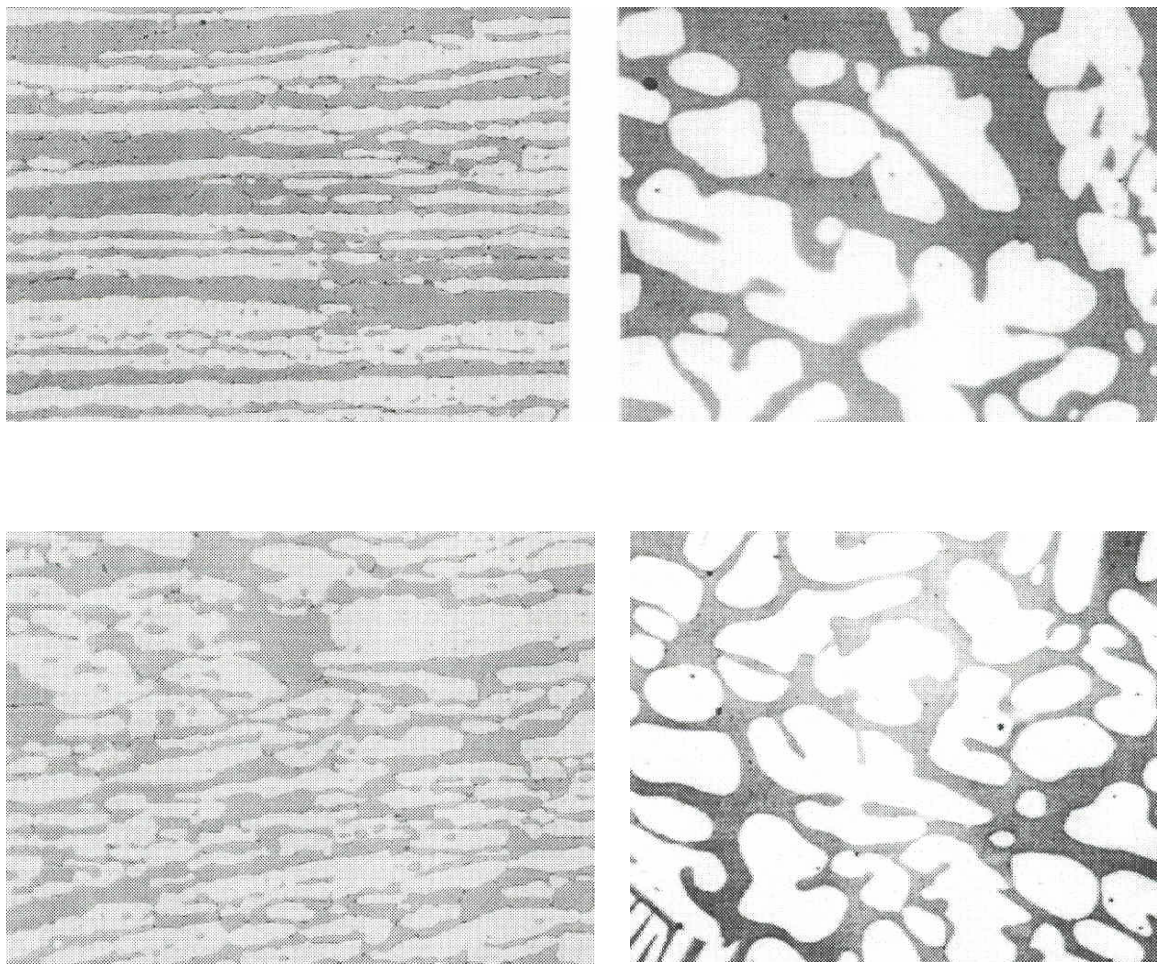
**Figure 12:** Possibly Affected Structure of ASTM A923
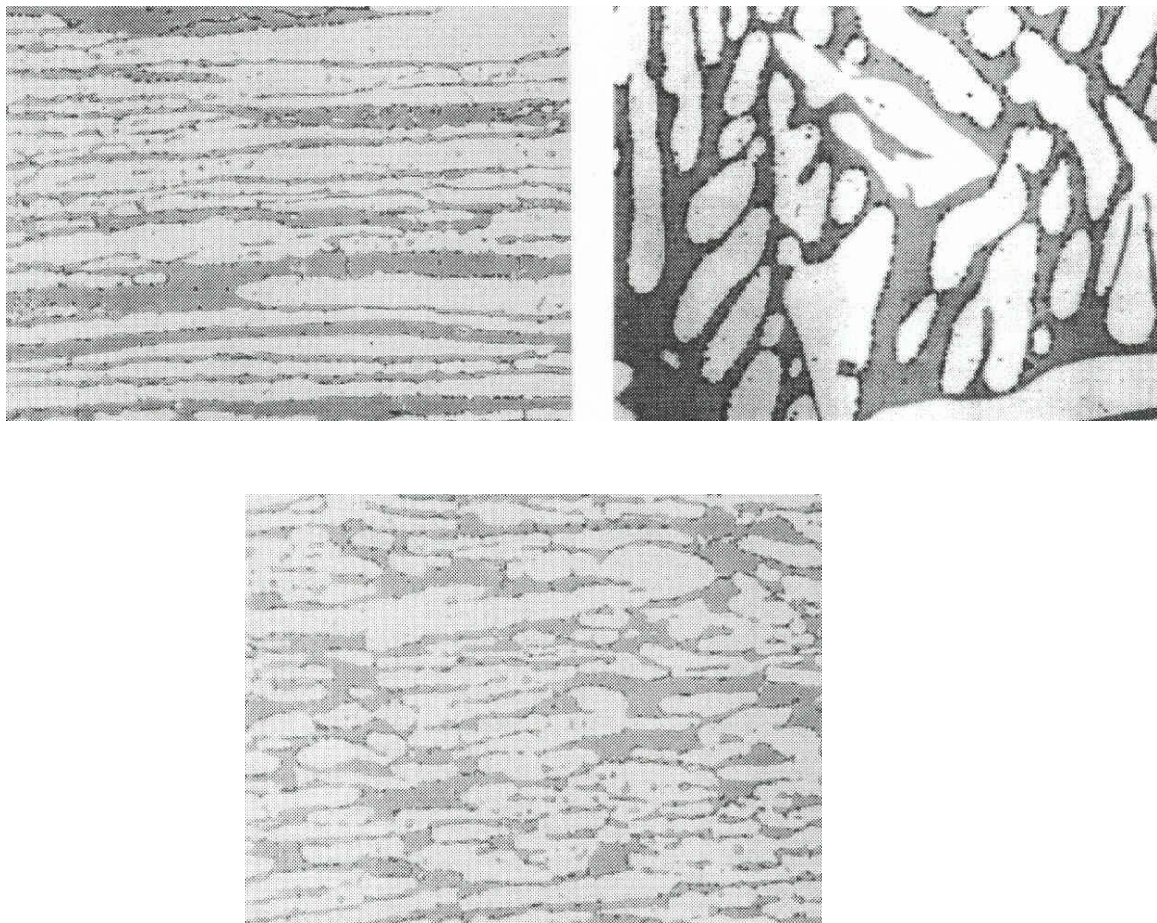
**Figure 13:** Affected Structure of ASTM A923
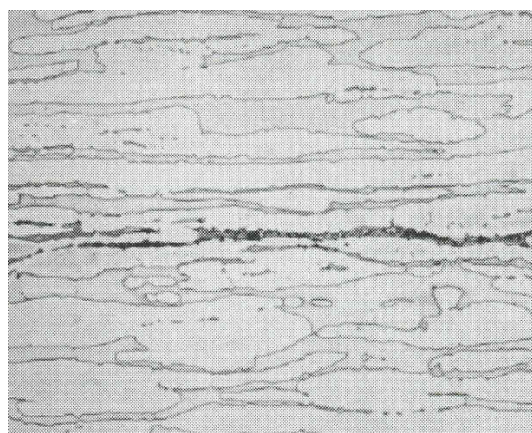
Figure 14: Centerline Structure of ASTM A923

corrosive environments; in particular, it does not provide a basis for predicting resistance to forms of corrosion not associated with the precipitation of intermetallic phases. One half of a fractured Charpy bar was used for this test. The bar was prepared by removing the fracture surface and grinding all surfaces to a 240-grit finish. Sharp edges of the specimen were rounded and care was taken to remove all burrs. Each specimen was labeled on the end by vibra-peening. Specimen weight was recorded to the 0.00001 g. Exposed surface area on the specimen was calculated after measuring each face. A test solution of 100 g reagent grade ferric chloride $FeCl_3$-$6H_2O$ dissolved in 900 ml of distilled water (6% $FeCl_3$ by weight) was used. The solution was filtered through filter paper to remove insoluble particles. The pH of the test solution was adjusted to approximately 1.3 prior to beginning the test by the addition of HCl or NaOH, as required. The test solution was then transferred to a 1000 ml, wide neck, glass beaker. The beaker was placed in a water bath as shown in Figure 15. Bath temperature was set at 40°C (107°F). After the test solution temperature reached the bath temperature the samples were placed in glass cradles and lowered into the solution. This test was performed at temperature for 24 hours. At the end of the 24 hour test period, the specimens were removed from the solution. These specimens were then rinsed with water, scrubbed with a soft bristle brush under running water to remove corrosive products, dipped in acetone, and then dried in air. Specimens were then re-weighed to 0.00001 g. The acceptance criterion for this test is that no specimen shall show a weight loss of more than 10 milligrams/decimeter/day (10 mdd), as calculated by:

Corrosion rate = weight loss (mg)/[specimen area (dm^2) x time (days)]

The corrosion rate was calculated in accordance with the weight loss and total surface area. Unless otherwise specified, the calculated corrosion rate shall not exceed 10 mdd. If the specimen shows a corrosion rate in excess of 10 mdd, one retest on two specimens is permitted. No retest specimen shall exhibit a corrosion rate in excess of 10 mdd.

Figure 15: Temperature Controlled Water Bath

2. Ferrite Measurement

Feritscope® was used to measure the ferrite content in all the Charpy samples. After the Charpy bars were machined, before sending those outside for conducting the impact toughness test ferrite content was measured. The Feritscope® uses the principle of magnetic induction method as presented in the literature review above. The Feritescope will measure the ferrite number from which we can calculate the volume % of ferrite from the formula suggested by Taylor[68]

$$\% \text{ Ferrite} = 0.55(\text{EFN}) + 10.6$$

Ferrite numbers in the range 0-28 are not applicable for this equation.

Five reading were taken from each Charpy sample and the mean of those five readings provided the ferrite number in that particular sample.

ASTM E562 Manual Point Count method was also used to measure the volume percentage of ferrite in order to compare the results with the results from the Feritscope®. Table 8 lists the heats used for this test. Each of these samples was prepared on the measurement face by polishing and etching. Figure 16 – 20 shows the microstructure of each sample used in this study.

Table 8: Heats for conducting ASTM E562 Manual Point Count

| Foundry	Heats
A	144
B	S1508
C	45633
D	04J142
	04J142 - D
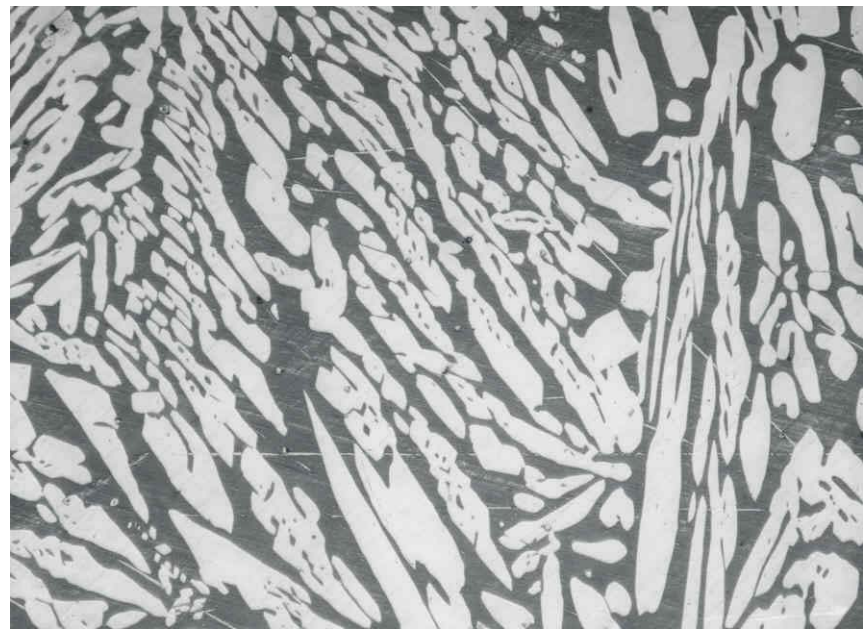
**Figure 16:** Microstructure of 144, NaOH, SA, 100x
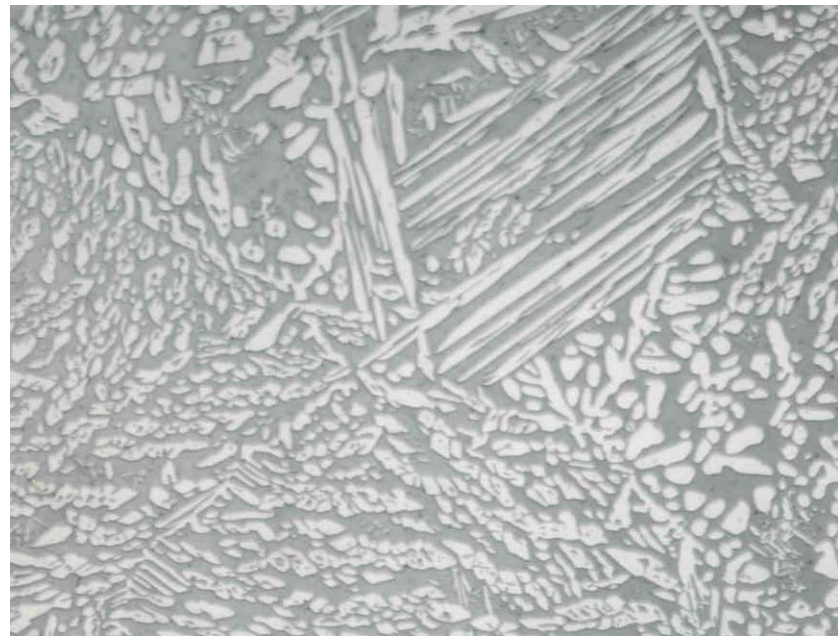
Figure 17: Microstructure of S1508, NaOH, SA, 100x

**Figure 18:** Microstructure of 45633, NaOH, SA, 100x
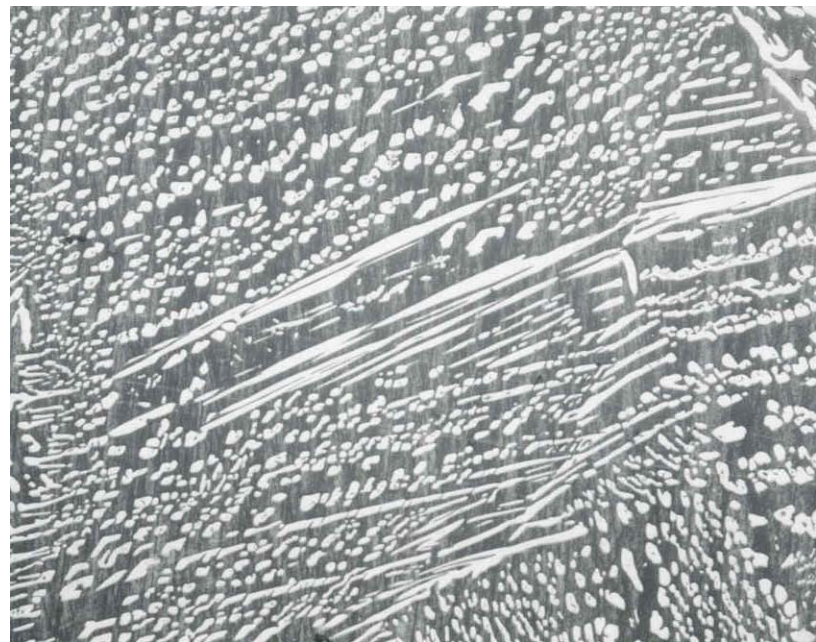
**Figure 19:** Microstructure of 04J142, NaOH, SA, 100x
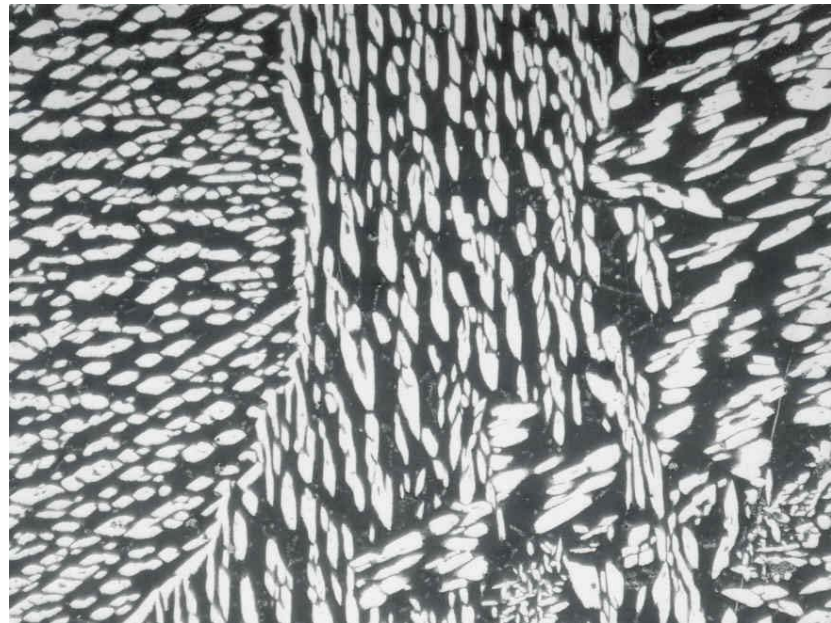
Figure 20: Microstructure of 04J142 – D, NaOH, 100x

Using the ASTM E562 a grid size, P_T was selected. The grid was then superimposed on the micrograph. The area to be counted was selected. The number of points, P_i falling within the ferrite was counted. The volume percentage of ferrite was calculated using the following equations:

P_T = Total number of points in the test grid

P_i = Point count on the ith field

$P_P(i) = P_i / P_T * 100$ = Percentage of grid points in the ferrite on the ith field

   n = number of fields counted

$P_P = 1/n \sum P_P(i)$ = Arithmetic average of $P_P(i)$

$s = [1/(n-1) \sum [P_P(i) - P_P]_2]_{1/2}$ = Estimate of standard deviation (σ)

95% CI = $\pm ts/\sqrt{n}$ = 95 % confidence interval

t = Multiplier related to the number of fields examined and used in conjunction with the standard deviation n of the measurements to determine the 95% CI, see (Table 1 of ASTM E562).

$V_V = P_P \pm 95\%$ CI = Volume fraction of ferrite as a percentage

% RA = (95% CI / P_P) = % Relative accuracy, a measure of statistical precision

3. Hardness Testing

The hardness values were measured on one half of a charpy sample taken from each block. Rockwell B and C values were used according to ASTM E92.

The sample on which hardness testing was carried out were ground to 600 grit finish in order to make the sample surface even and smooth so that there was no error in the reading. Hardness testing was not carried out on mounted samples because the indenter (ball bearing or diamond tip) pushed the sample into the mount while measuring giving us an incorrect reading.

4. Microstructural Analysis

After carrying out the above tests, Scanning Electron Microscopy was carried out using the Leo on all the mounted samples on which the test method A (Etch Test) was previously carried out. SEM was required in order to determine the presence of detrimental phases (higher magnification and resolution). Back scattered imaging gave a clear indication of various phases present in the sample. At a higher magnification it was easier to determine the type of secondary phase that was present by examining the microstructure.

The SEM which was used for this program is Leo 1525 manufactured by Leo, UK. The Leo 1525® workstation utilizes Gemini field emission column. The imaging was done by back scatter detector and secondary electron detector (SE2). The backscatter imaging was used for identifying the presence of different phases in the microstructure. SEM was also carried out on all the fracture surfaces in order to determine the presence of any cracks on the fracture surface as well as to determine whether it is brittle or ductile fracture. SEM was carried out on all the corrosion samples also, before and after they had undergone the test method C (Ferric Chloride Corrosion Test) in order to see the

difference in the surface. For these purposes SE2 detector was used. Following parameters were used while imaging:

Working distance = 15-20 mm

Applied voltage = 20 kV

Detector = SE2 and Backscatter

Magnification = Typically 500X or 1000X

Scanning speed = 4

For carrying out SEM (Figure 21) the samples were gold coated. SPI sputter coater was used for this purpose. This coater has six specimen mounts. The specimen mounts are secured to the holder by the set screws provided. After placing the glass chamber on top, the coating process begins. The air pressure is 2 psi, and the current passing through the plasma is 20 mA and time required to coat sufficient amount of gold is on the order 10 seconds. Typically coating thickness depends on cleanliness of sputtering system. The thickness of gold coating is calculated using the following formula:

$$d = K*i*V*t$$

where

  d = thickness of gold coating,

  K = constant for argon plasma system and equals 0.17

  i = plasma current

  V = applied voltage

  t = time in seconds

Thus for our application, the gold coating thickness can be calculated:

$$d = 0.17*20*10*1 = 34 \text{ A/ kV}$$

Figure 21: Leo 1525 Manufactured by Leo, UK

Energy Dispersive Spectroscopy was carried out on the material that was acquired from Foundry D in order to determine the variation in the amount of the chemical composition of various elements when the material is subjected to different heat treatment schedule. The EDS system is activated using RemCon 32; which opens the port to Link ISIS; the EDS software. The software also lets the user select the elements he thinks could be present in the sample. For carrying out EDS the working distance should be less than 8mm.

X-Ray Diffraction analysis was carried out using Philips X'pert. Prodiffractometer (Figure 22) at 45KV and 40mA. Diffraction patterns were acquired from the samples in a step mode with 0.05 degree step (2θ) and 2 seconds per point over diffraction angle (2θ) from 15 to 120 degrees. These patterns were used to find out the percentage of different phases present in the sample.

Figure 22: Philips X'pert. Prodiffractometer

IV. Results and Discussions

1. The Suitability of ASTM A923 for Detecting the Presence of Intermetallic Phases in Super Duplex Stainless Steel Casting A890-5A

1.1 Test Method A

The following tables (Table 9 and 10) show the classification of etch structures from Method A based on ASTM A923. Figure 23 – 41 shows the microstructure of the etch structures at 400x taken under the Optical Light Microscope. All the microstructures are labeled with their foundry heat ID followed by the etchant, SA (if foundry solution annealed) and magnification.

Table 9: Classification of Etch Structure for Foundry Solution Annealed Materials from Foundry A, B, C and D

Foundry	Specimen ID	Foundry Solution Annealed	Classification of Etch Surface
A	331	Heat to 2200°F, Hold 3 hours, Water Quench	Unaffected Structure
	185		Unaffected Structure
	285		Unaffected Structure
B	S1507	Heat to 2050°F, hold 2 hours, furnace cool to 1950°F, hold 1 hour, Water Quench	Unaffected Structure
	S1508		Unaffected Structure
C	41414	Heat to 2075°F, cool to 1940°F, Hold 1 hour, Water Quench	Unaffected Structure
	41544		Unaffected Structure
	44073		Unaffected Structure
	41374		Unaffected Structure
	45633		Unaffected Structure
D	04J142	Heat to 2100°F, Hold 1 hour, Water Quench	Unaffected Structure

Table 10: Classification of Etch Structure for Materials Heat Treated as shown from
Foundry D

Foundry	Specimen ID	Heat Treatment	Classification of Etch Surface
D	04J142 - A	A Heat to 1950°F, Hold 30 min., Water Quench	Unaffected Structure
	04J142 - B	B Heat to 1950°F, Hold 30 min., Water Quench, Heat to 1550°F, Water Quench	Affected Structure
	04J142 - C	C Heat to 1950°F, Hold 30 min., Water Quench, Heat to 1550°F, Hold 5 min., Water Quench	Affected Structure
	04J142 - D	D Heat to 1950°F, Hold 30 min., Water Quench, Heat to 1550°F, Hold 10 min., Water Quench	Affected Structure
	04J142 - E	E Heat to 1950°F, Hold 30 min., Water Quench, Heat to 1550°F, Hold 15 min., Water Quench	Affected Structure
	04J142 - F	F Heat to 1950°F, Hold 30 min., Water Quench, Heat to 1550°F, Hold 20 min., Water Quench	Affected Structure
	04J142 - G	G Heat to 1950°F, Hold 30 min., Air Cool	Affected Structure
	04J142 - H	H Heat to 1950°F, Hold 30 min., Slow Cool	Affected Structure
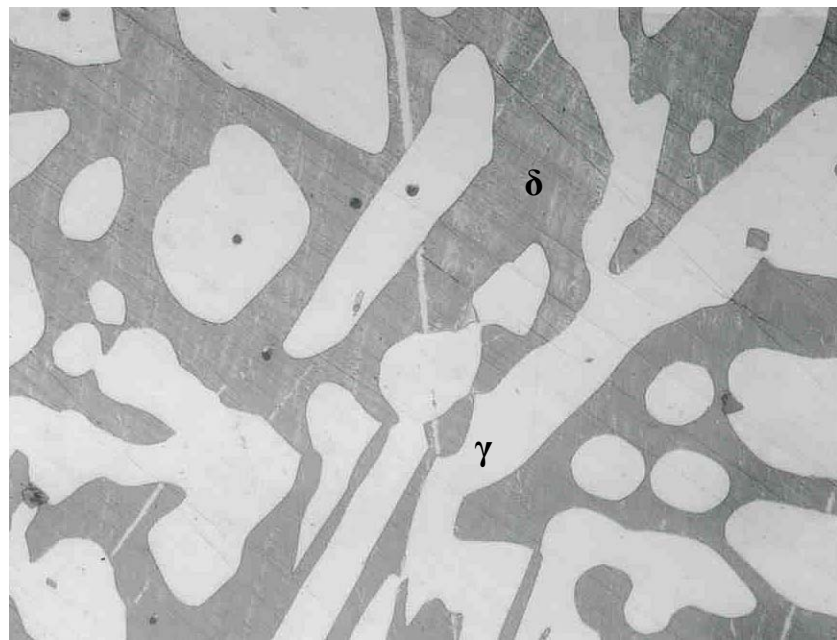
Figure 23: Microstructure of 144, NaOH, SA, 400x
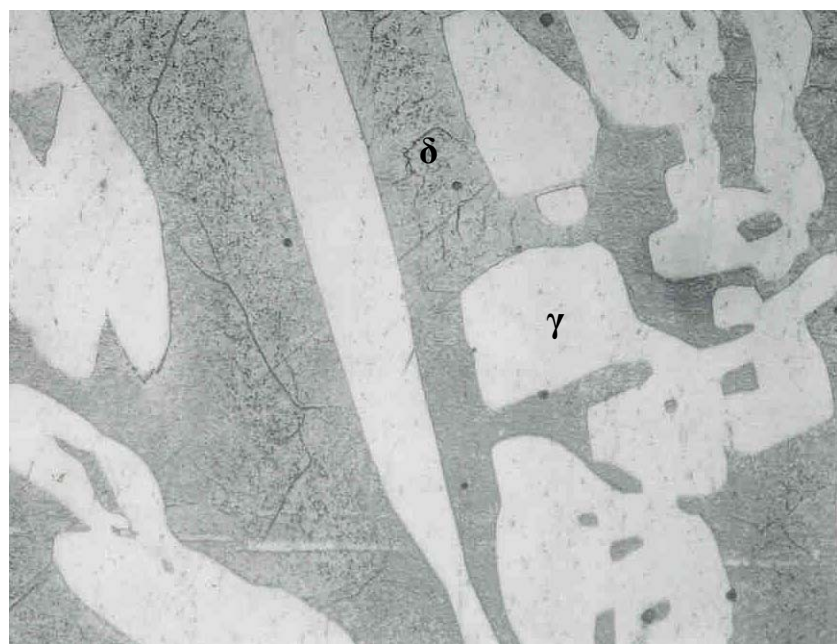
**Figure 24:** Microstructure of 285, NaOH, SA, 400x
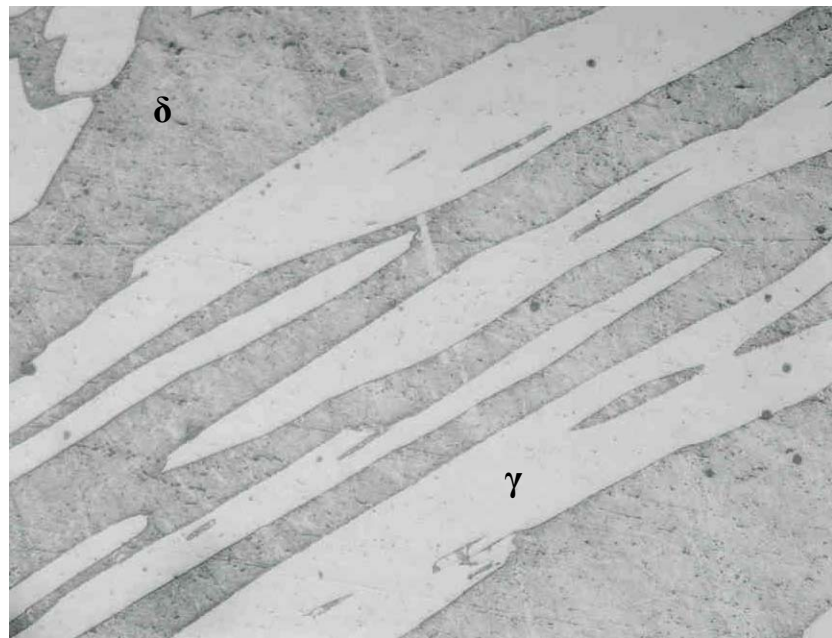
Figure 25: Microstructure of 331, NaOH, SA, 400x
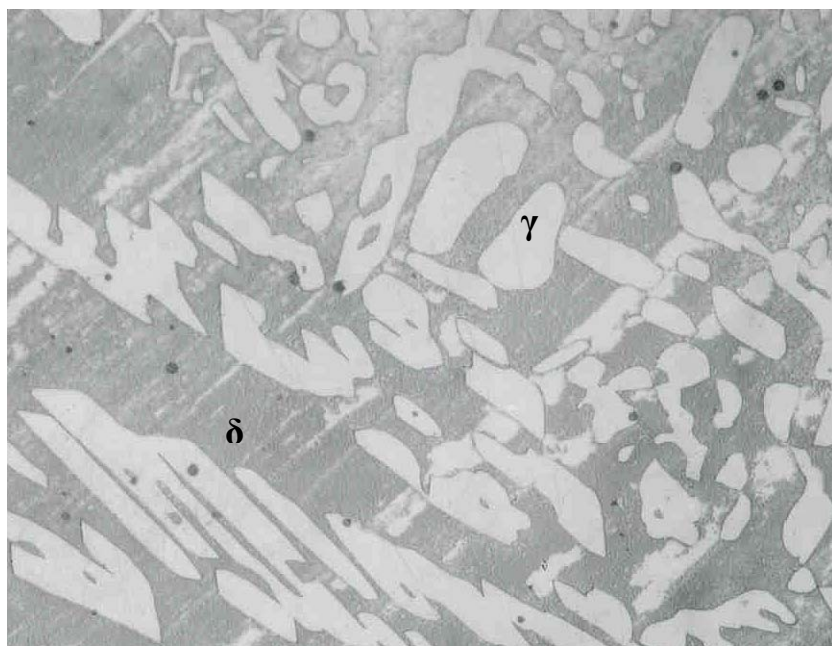
**Figure 26:** Microstructure of S1507, NaOH, SA, 400x
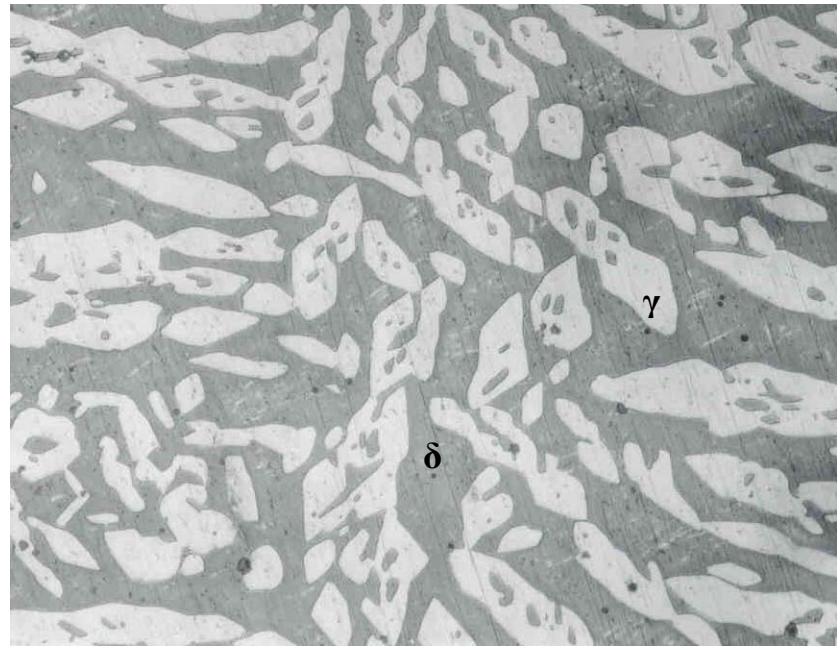
**Figure 27:** Microstructure of S1508, NaOH, SA, 400x
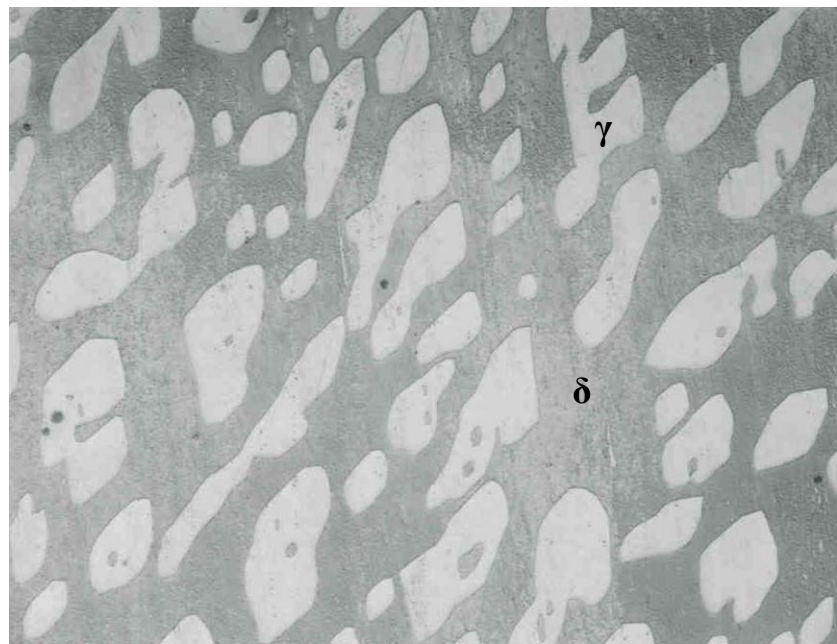
**Figure 28:** Microstructure of 41374, NaOH, SA, 400x
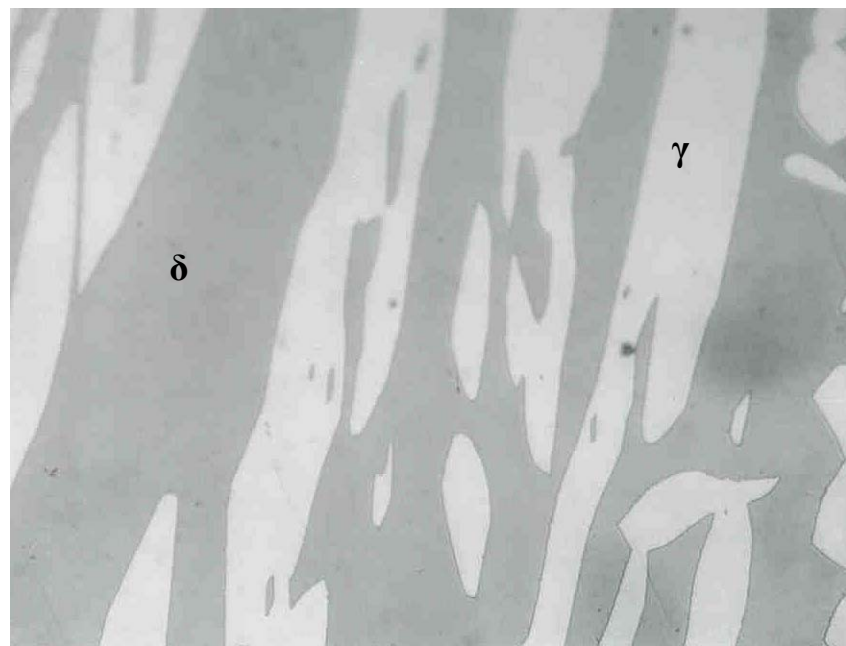
Figure 29: Microstructure of 41414, NaOH, SA, 400x
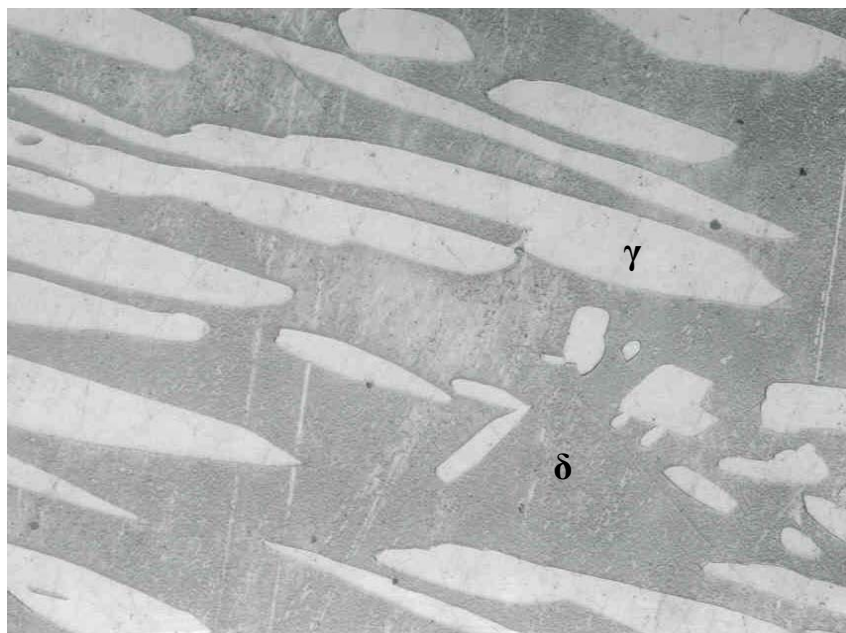
**Figure 30:** Microstructure of 41544, NaOH, SA, 400x
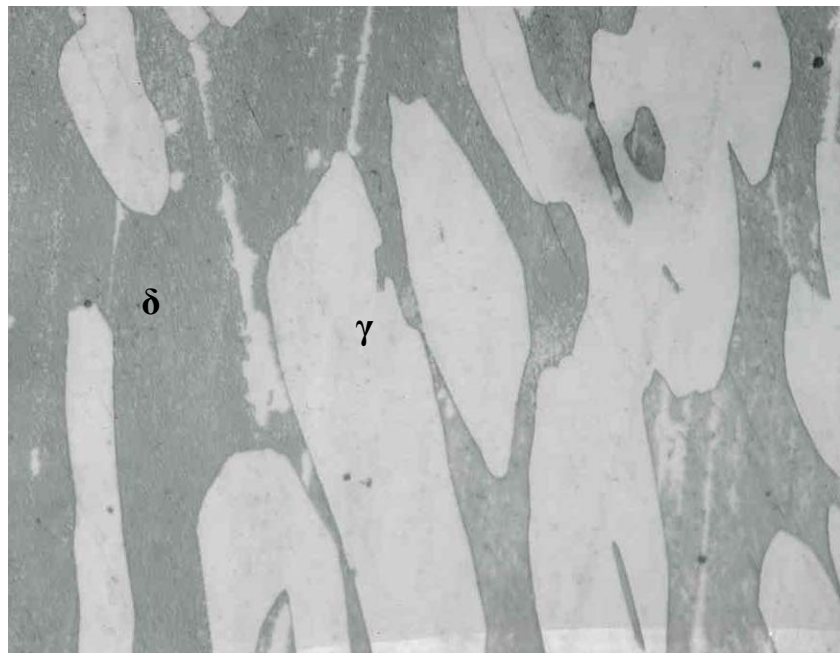
**Figure 31:** Microstructure of 44073, NaOH, SA, 400x
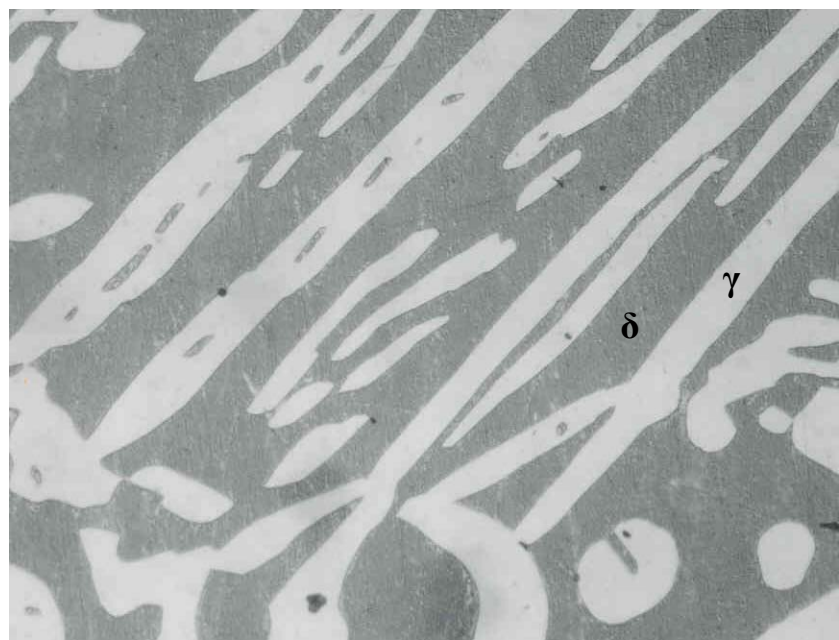

Figure 32: Microstructure of 45633, NaOH, SA,400x
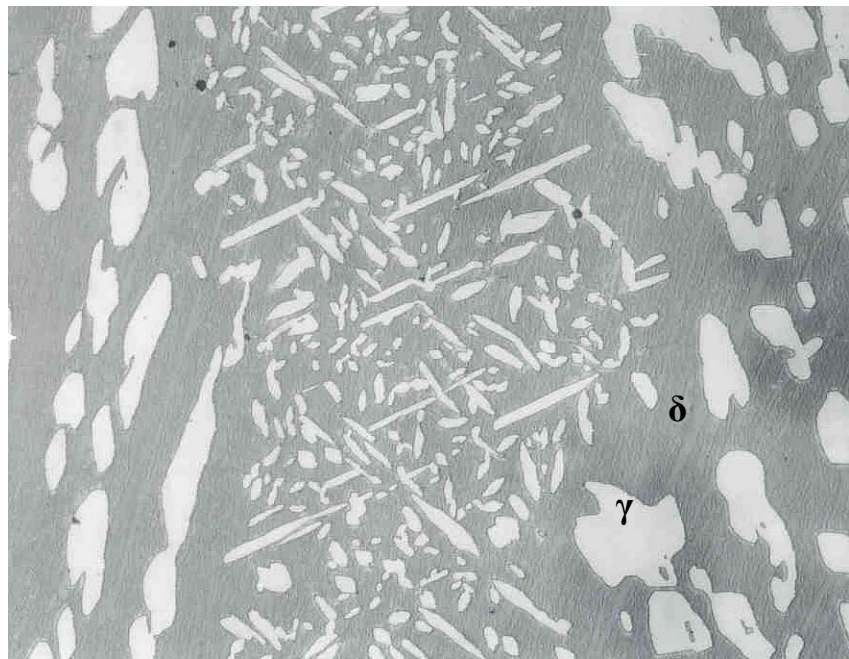
**Figure 33:** Microstructure of 04J142, NaOH, SA, 400x
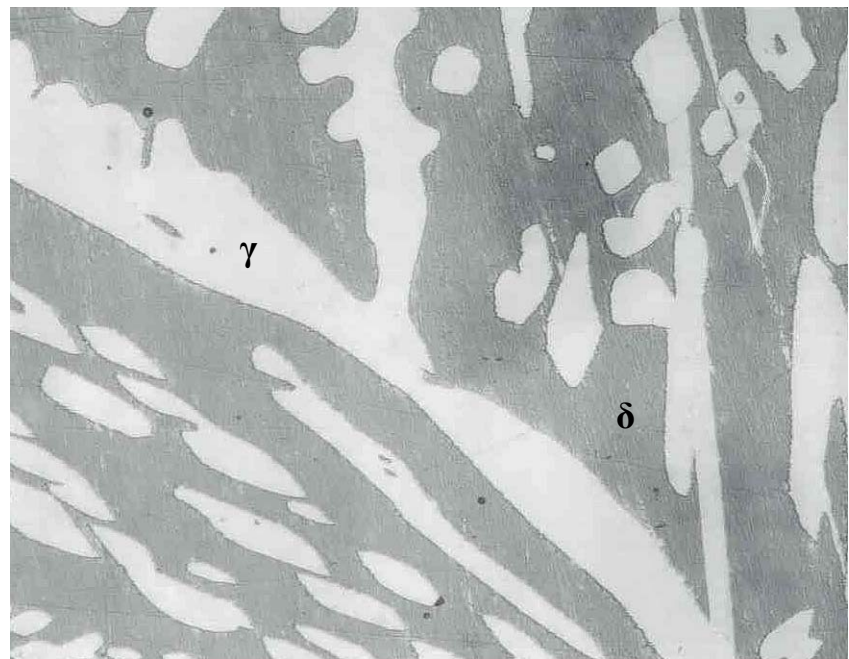
**Figure 34:** Microstructure of 04J142 – A, NaOH, 400x
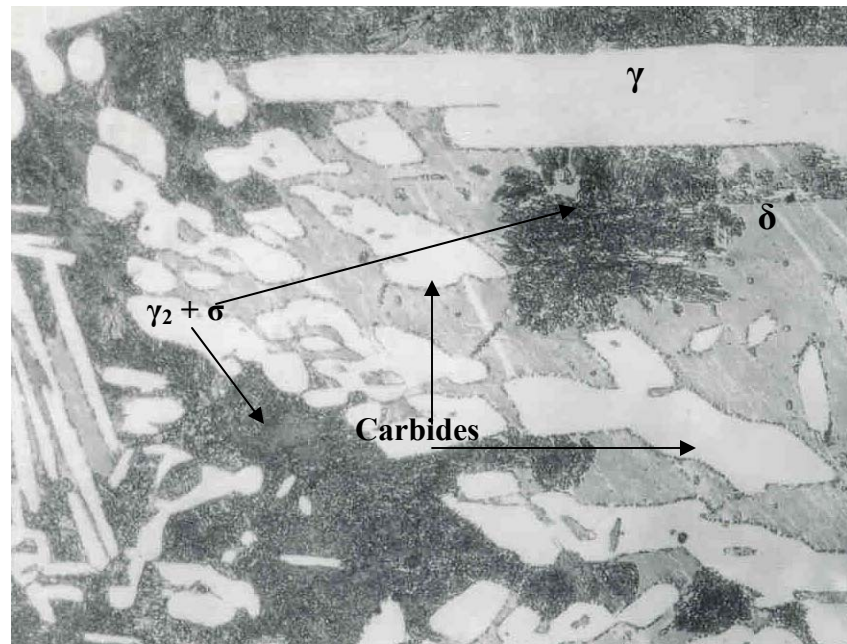
**Figure 35:** Microstructure of 04J142 – B, NaOH, 400x
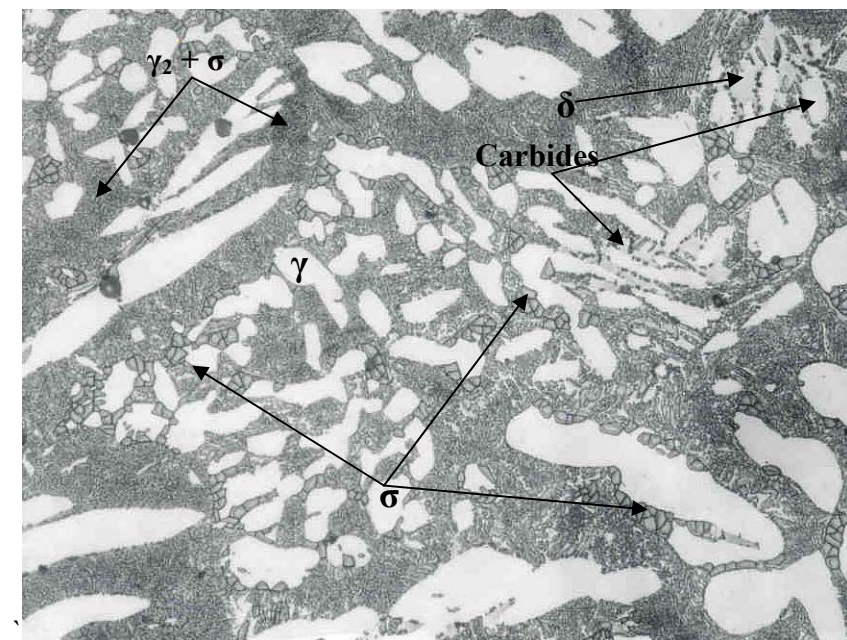
Figure 36: Microstructure of 04J142 – C, NaOH, 400x
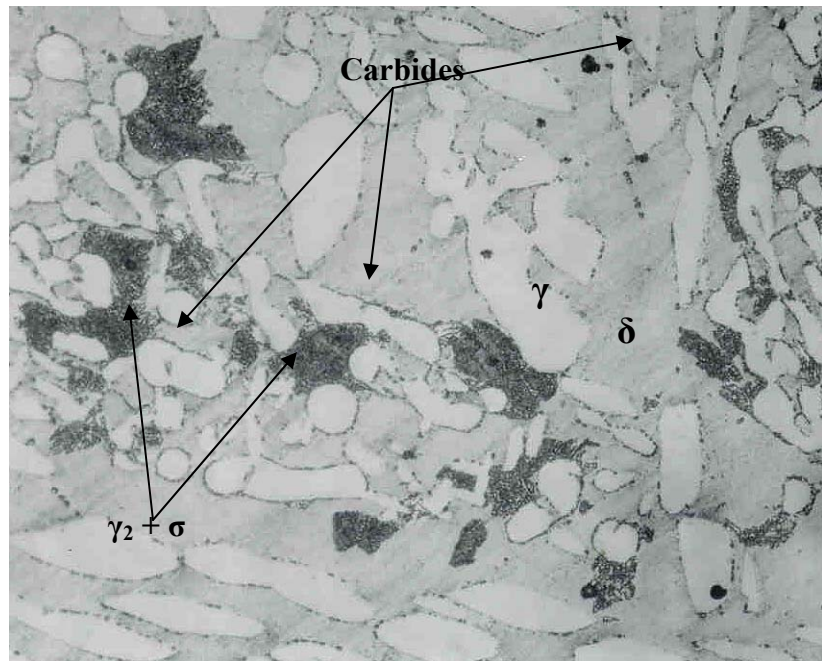
**Figure 37:** Microstructure of 04J142 – D, NaOH, 400x
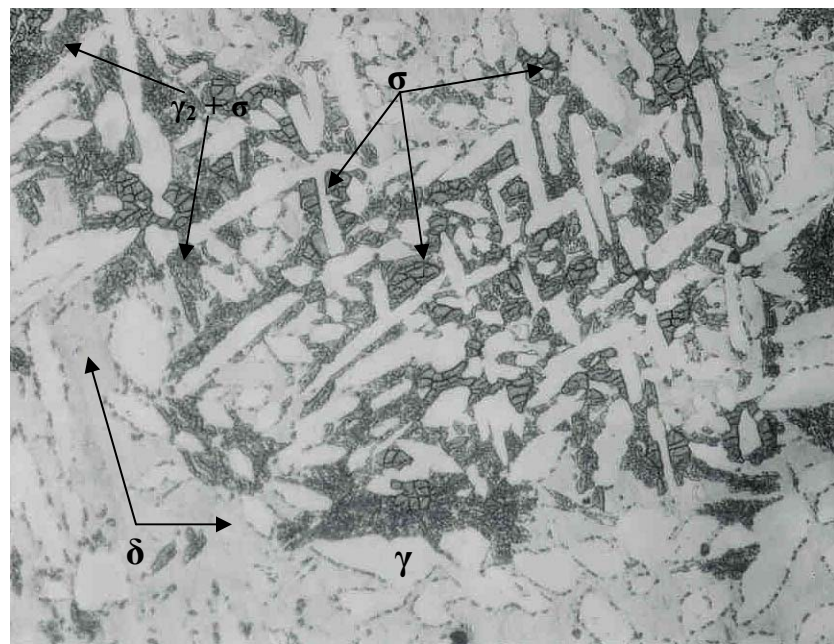
**Figure 38:** Microstructure of 04J142 – E, NaOH, 400x
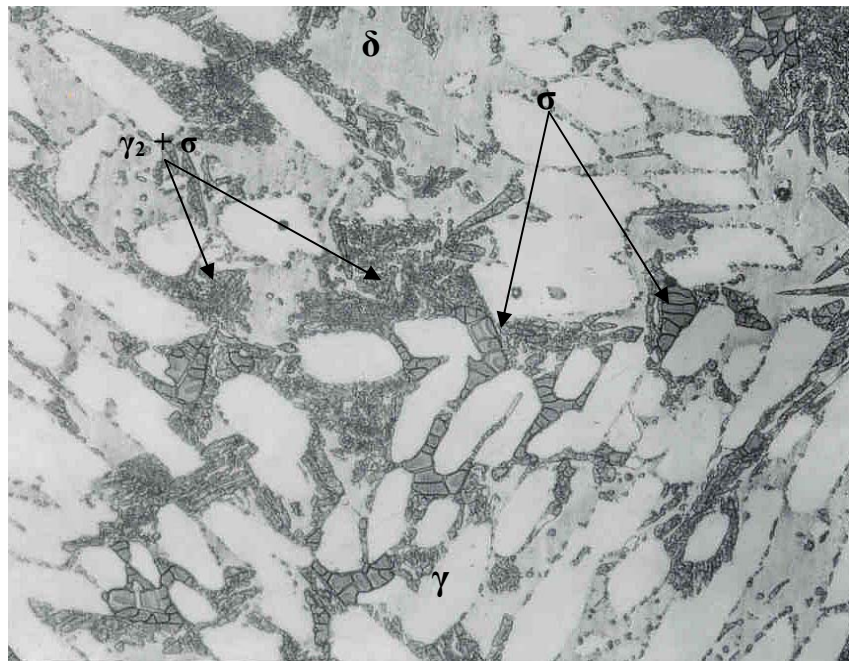
**Figure 39:** Microstructure of 04J142 – F, NaOH, 400x
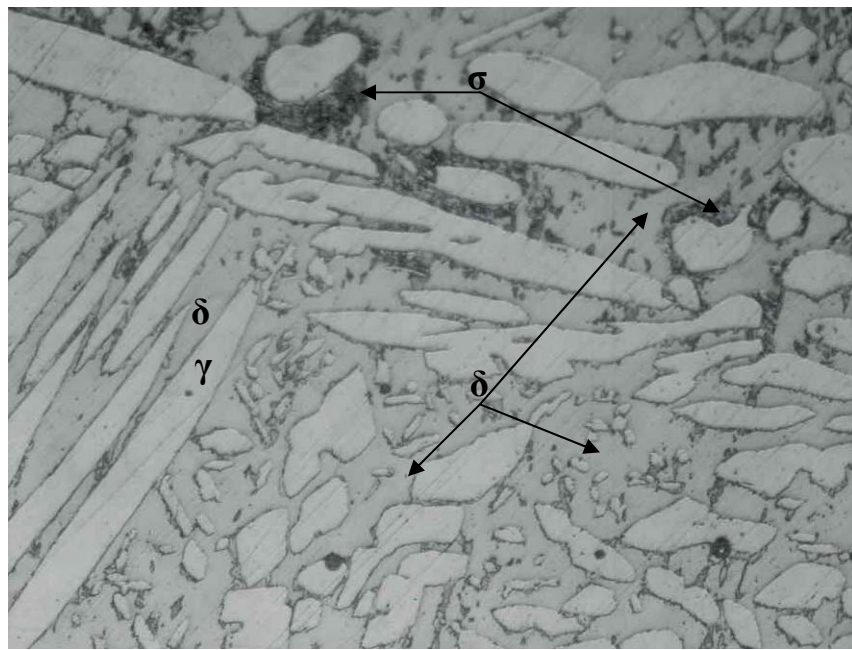
**Figure 40:** Microstructure of 04J142 – G, NaOH, 400x
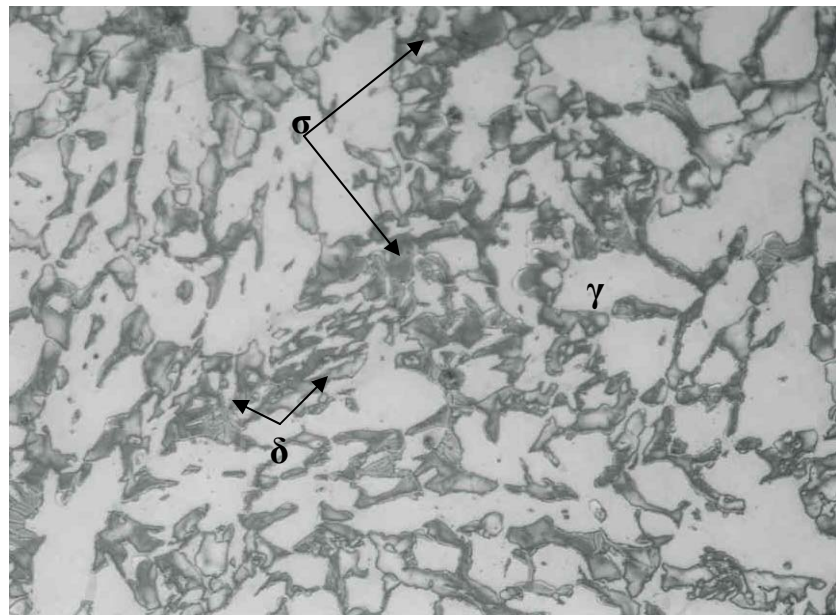
Figure 41: Microstructure of 04J142 – H, NaOH, 400x

In the case of Foundry D materials which were subjected to the full course of heat treatment schedule it was possible to compare the microstructure of solution annealed sample as received from the foundry with the microstructure of the samples which were subjected to different heat treatments. The as received solution annealed sample had an acicular structure[161]. After subjecting to different heat treatments the samples were rendered in an equiaxed structure as it can be observed from the microstructures.

1.2 Test Method B

Table 11 shows the -50°F Charpy Impact Toughness of all samples that were submitted by Foundry A, B, C and D. All materials were foundry solution annealed. Figure 42 is a graphical presentation of the average impact values for each lot.

Table 12 shows the Charpy Impact Energy of the samples that were made from material sent by Foundry D. Figure 43 is a graphical presentation of the average impact value for the Foundry D heat following the heat treatment schedule for wrought material used in the initial development of A923.

Table 11: Charpy Impact Toughness at -50°F for Foundry Solution Annealed Material

Foundry	Specimen ID	Impact Ft-Lbs
A	285	65.5
	285	76.5
	285	81.5
	285	75.5
	331	72
	331	61.5
	331	79
	331	77
	144	92
	144	135
	144	100
	144	91.5
B	S1507	94.5
	S1507	63
	S1507	78
	S1507	78.5
	S1508	65.5
	S1508	64
	S1508	78.5
	S1508	63
C	45633	99
	45633	136.5
	45633	146
	45633	129
	41414	123.5
	41414	113
	41414	138.5
	41374	134.5
	41374	142
	41374	131
	41374	113
	41544	145
	41544	135
	41544	144.5
	41544	146.5
	44073	148
	44073	155.5
	44073	149
	44073	157.5
D	04J142	69.5
	04J142	72
	04J142	75.5
	04J142	70
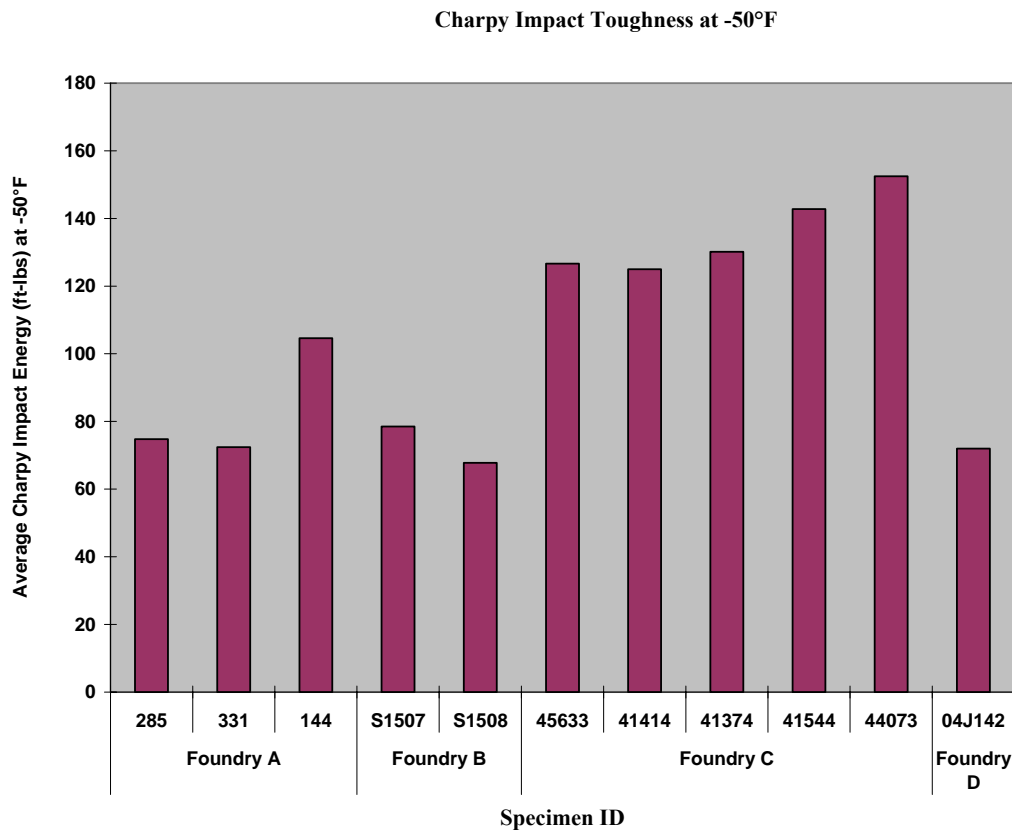
Charpy Impact Toughness at -50°F

Solution Annealing by Foundry

Foundry	Solution Annealing by Foundry
A	Heat to 2200°F, Hold 3 hours, Water Quench
B	Heat to 2050°F, hold 2 hours, furnace cool to 1950°F, hold 1 hour, Water Quench
C	Heat to 2075°F, cool to 1940°F, Hold 1 hour, Water Quench
D	Heat to 2100°F, Hold 1 hour, Water Quench

Figure 42: Charpy Impact Toughness of Foundry Solution Annealed Per A923 Test Method B at -50°F

Table 12: Charpy Impact Toughness at -50°F for Heat Treated Materials from Foundry D

Heat Treatment Schedule	Absorbed Energy (ft-lbs)
A Heat to 1950°F, Hold 30 min., Water Quench	90 71
B Heat to 1950°F, Hold 30 min., Water Quench, Heat to 1550°F, Water Quench	2.5 2
C Heat to 1950°F, Hold 30 min., Water Quench, Heat to 1550°F, Hold 5 min., Water Quench	1.5 1
D Heat to 1950°F, Hold 30 min., Water Quench, Heat to 1550°F, Hold 10 min., Water Quench	8 7.5
E Heat to 1950°F, Hold 30 min., Water Quench, Heat to 1550°F, Hold 15 min., Water Quench	2 1.5
F Heat to 1950°F, Hold 30 min., Water Quench, Heat to 1550°F, Hold 20 min., Water Quench	1.5 1.5
G Heat to 1950°F, Hold 30 min., Air Cool	11 9 9.5 10
H Heat to 1950°F, Hold 30 min., Slow Cool	2.5 2 2.5 2.5

Charpy Impact Toughness at -50°F

Heat Treatment Schedule

A - Heat to 1950°F, hold 30 minutes, WQ
B - Heat to 1950°F, hold 30 minutes, WQ, heat to 1550°F, WQ
C - Heat to 1950°F, hold 30 minutes, WQ, heat to 1550°F, hold 5 minutes, WQ
D - Heat to 1950°F, hold 30 minutes, WQ, heat to 1550°F, hold 10 minutes, WQ
E - Heat to 1950°F, hold 30 minutes, WQ, heat to 1550°F, hold 15 minutes, WQ
F - Heat to 1950°F, hold 30 minutes, WQ, heat to 1550°F, hold 20 minutes, WQ
G - Heat to 1950°F, hold 30 minutes, Air Cool
H - Heat to 1950°F, hold 30 minutes, Slow Cool

Figure 43: Charpy Impact Toughness at -50°F of Foundry D bars exposed to the Heat Treatment shown (As Per Background data for A923 wrought material)

1.3 Test Method C

Table 13 summarizes the results from the corrosion test on the materials procured from Foundry A, B, C and D. All of these materials were foundry solution annealed. Figure 44 shows the graphical view of corrosion rate of various heats.

Table 14 shows the corrosion test results of the material which was sent by Foundry D and subjected to the heat treatment schedule for wrought material in A923. Figure 45 shows the graphical view of the corrosion rate and the heat treatment schedule.

Table 13: Corrosion Rates for Foundry Solution Annealed Materials from Foundry A, B, C and D

Foundry	Specimen ID	Area of the Specimen	Weight of the Specimen	Weight after Testing	Corrosion Rates	Corrosion Results
A	331	195.312	15.85025	15.84881	0.073728	Pass
	144	185.546	14.95525	14.95519	0.003234	Pass
	285	224.515	17.99977	17.99811	0.073937	Pass
B	S1507	204.984	15.26527	15.26455	0.035125	Pass
	S1508	195.218	15.54399	15.54348	0.026125	Pass
C	41414	185.546	14.70874	14.70714	0.086232	Pass
	41544	195.593	16.12668	16.12647	0.010737	Pass
	44073	185.734	15.41645	15.41623	0.011845	Pass
	41374	195.312	15.65445	15.65424	0.010752	Pass
	45633	214.937	17.55149	17.54949	0.093051	Pass
D	04J142	175.874	14.53285	14.53261	0.013646	Pass
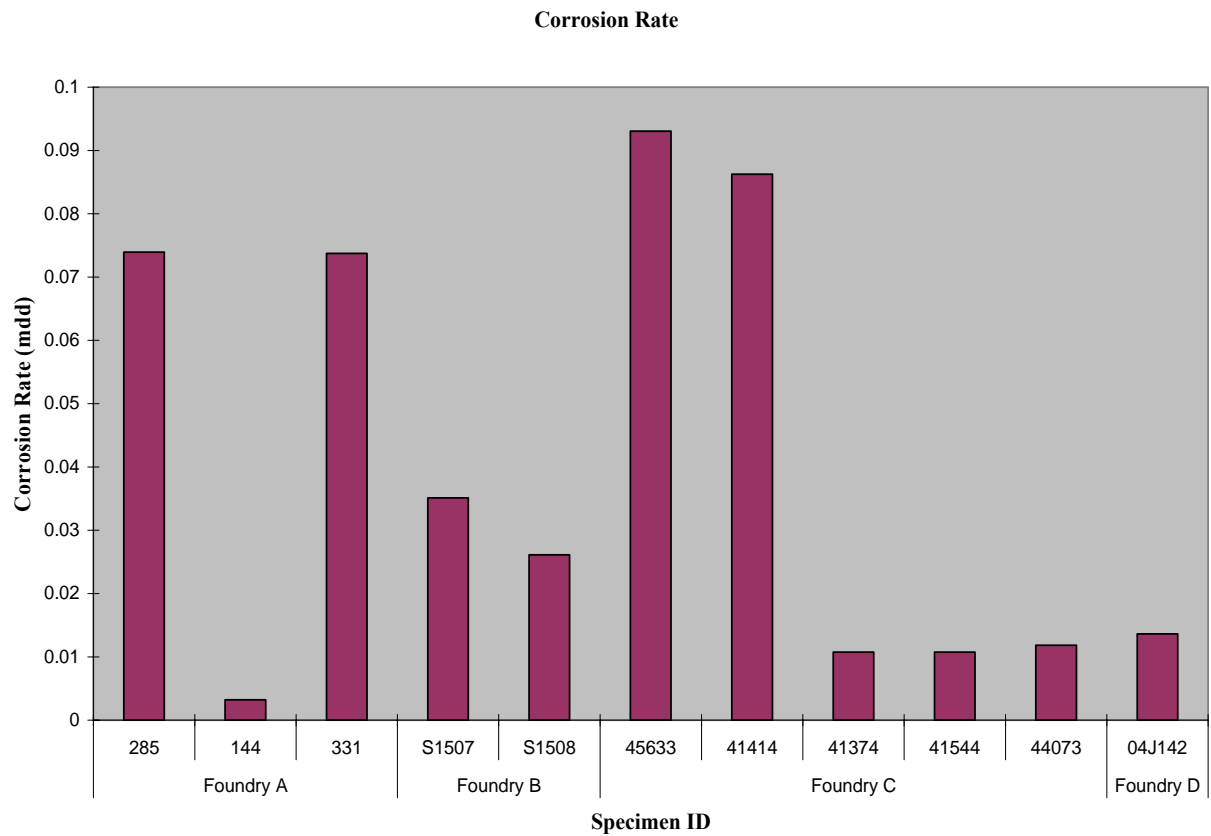
Corrosion Rate

Solution Annealing by Foundry

Foundry	Solution Annealing by Foundry
A	Heat to 2200°F, Hold 3 hours, Water Quench
B	Heat to 2050°F, hold 2 hours, furnace cool to 1950°F, hold 1 hour, Water Quench
C	Heat to 2075°F, cool to 1940°F, Hold 1 hour, Water Quench
D	Heat to 2100°F, Hold 1 hour, Water Quench

Figure 44: Corrosion Rate of Foundry Solution Annealed material from Foundry A, B, C and D (Acceptance Criteria – Weight loss ≤ 10 milligrams/decimeter/day (10 mdd))

Table 14: Corrosion Rates for Heat Treated Materials from Foundry D

Foundry	Specimen ID	Area of the Specimen	Weight of the Specimen	Weight after Testing	Corrosion Rates	Corrosion Results
D	04J142 - A	185.359	14.81757	14.81754	0.001618	Pass
	04J142 - B	166.11	13.8771	13.42999	26.9165	Fail
	04J142 - C	156.156	12.65836	12.23875	26.87121	Fail
	04J142 - D	175.781	14.27541	14.20991	3.726228	Pass
	04J142 - E	175.875	14.75958	14.54034	12.46567	Fail
	04J142 - F	175.781	14.63388	14.21803	23.65728	Fail
	04J142 - G	175.875	14.5804	14.54974	1.743284	Pass
	04J142 - H	195.594	16.55008	15.11975	73.1275	Fail

Heat Treatment Schedule

A - Heat to 1950°F, hold 30 minutes, WQ
B - Heat to 1950°F, hold 30 minutes, WQ, heat to 1550°F, WQ
C - Heat to 1950°F, hold 30 minutes, WQ, heat to 1550°F, hold 5 minutes, WQ
D - Heat to 1950°F, hold 30 minutes, WQ, heat to 1550°F, hold 10 minutes, WQ
E - Heat to 1950°F, hold 30 minutes, WQ, heat to 1550°F, hold 15 minutes, WQ
F - Heat to 1950°F, hold 30 minutes, WQ, heat to 1550°F, hold 20 minutes, WQ
G - Heat to 1950°F, hold 30 minutes, Air Cool
H - Heat to 1950°F, hold 30 minutes, Slow Cool

* Heat Treatment "A" sample showed corrosion rate equivalent to zero (≈0)

Figure 45: Corrosion Rate of material from Foundry D (Acceptance Criteria – Weight loss ≤ 10 milligrams/decimeter/day (10 mdd))

2. Evaluation and Correlation between the Test Methods of A923

All the materials from Foundry A, B, C and D were subjected to the test methods of A923. Test Method A was the Sodium Hydroxide Etch Test (visual identification of intermetallic phases). One half of fractured charpy sample was used to carry out the Sodium Hydroxide Etch Test. Solution Annealed samples from Foundry A, B, C and D was considered as unaffected structures. The heat treatment "A" sample from Foundry D (solution annealed in The University of Tennessee) also revealed an unaffected structure. The samples which underwent heat treatment schedules "B", "C", "D", "E", "F", "G" and "H" were all identified as affected structures. Heat Treatments "B" to "F" were subjected to two stages of heat treatment which is Heat to 1950 ºF, hold for 30 minutes and water quench followed by heat to 1550ºF, hold for different time periods before water quenching them. Heat Treatment "G" is the air cool sample which is heated to 1950 ºF, held for 30 minutes and then air cooled. Heat treatment "H" is the slow cool sample which is heated to 1950 ºF, held for 30 minutes and then furnace cooled.

From the Charpy Impact Test (Test Method B) it was found that foundry solution annealed samples from Foundries A, B, C and D had toughness as greater than 60ft-lbs (Figure 42). The material from Foundry C had the highest toughness. The Charpy impact energy was greater than 100ft-lbs for all the samples that were tested. There were two heats from Foundry B. Heat S1507 had porosity in the charpy samples that were machined but had a higher impact value than the other heat S1508. This may be because the porosity was not in the notched region of the sample. Out of the three materials from Foundry A, heat 144 had a comparatively greater toughness than the other heats 331 and 285. The heat treatment "A" sample from Foundry D (solution annealed at The University of Tennessee) also showed a toughness value greater than 60ft-lbs.

The samples from Foundry D were subjected to the full scope of heat treatment. After heat treatment the Charpy Impact Test was carried out. From Figure 43 it can be observed that the toughness dropped from 60ft-lbs to 1-10ft-lbs when the second stage of heat treatment was carried out (Heat to 1550ºF and hold for different time periods before

water quenching). Air cooled and slow cooled samples also showed a similar drop in toughness.

The Ferric Chloride Corrosion Test (Test Method C) was carried out on these fractured Charpy samples. It was seen that the foundry solution annealed samples from Foundry A, B, C and D passed. All these samples passed the acceptance criteria of weight loss $\leq$ 10 mdd by a wide margin (Figure 44). The heat treatment "A" sample from Foundry D (solution annealed at The University of Tennessee) also passed by a similar margin. The heat treatment "D" and "G" samples also passed. All the samples which underwent other heat treatment schedules failed the corrosion test (Figure 45).

From the results of the three test methods can be derived a correlation between the results. Also one can predict the best method which could be used to detect the presence of detrimental intermetallic phases. Test Method A can be used to visually detect the presence of an affected structure but cannot identify the type of intermetallic phases present. It was possible to visually deduce whether a sample is affected with a greater percentage of intermetallic phases when compared with another sample. The estimated percentage of intermetallic phases present in air cooled (Figure 40) sample (heat treatment "G" sample from Foundry D) was less when compared with slow cooled (Figure 41) sample (heat treatment "H" sample from Foundry D). It was visually confirmed that heat treatment "D" sample (Figure 37) had a lesser percentage of intermetallic phase when compared to heat treatment "B", "C", "E" and "F" samples (Figure 35-36, 38-39) which had similar percentage of intermetallic phase.

The Charpy Impact Test indicated that all the solution annealed materials (Figure 42) have high toughness. There was no precipitation of detrimental intermetallic phases. In these foundry solution annealed samples Figure 43 indicates that the second stage of the heat treatment process (heat treatment "B", "C", "D", "E" and "F") precipitated intermetallic phases and reduced the impact toughness considerably. During the second stage of heat treatment when the samples are heated to 1550°F, the heating process takes approximately an hour for the samples to reach this temperature after they were water quenched from 1950°F. It may be concluded that the intermetallic phases were precipitated during the heating stage (to 1550°F). There was an increase in the

110

toughness of heat treatment "D" sample as compared to the toughness of heat treatment "B" and "C" samples. The reason for this observation is unknown at this time.

There were no intermetallic phases for the samples from heat treatment schedule "A" (solution annealed at the University of Tennessee). This demonstrates that solution annealed samples do not contain any intermetallic phases but the subsequent heat treatment schedules result in the precipitation of intermetallic phases as noted in Table 4. The heat treatment "G" and "H" samples which were heated to 1950°F and then air cooled and slow cooled respectively also precipitated intermetallic phases. The air cooled sample contained lesser amount of intermetallic phases as compared to slow cool sample though both had low toughness (1-10ft-lbs). This indicates that precipitation of small amount of intermetallic phase reduce the toughness considerably (1-10ft-lbs). Air cooling and slow cooling precipitates intermetallic phases but when similar material is heated to the same temperature and water quenched no intermetallic phases are precipitated which indicates that solution treatment (1950°F) dissolves all the intermetallic phases which have been precipitated during heating. This is true only for first stage of heat treatment which is heat treatment "A" (Heating to 1950°F followed by water quenching). It can be concluded that heat treatment "A", intermetallic phases did not precipitate when the samples were water quenched, however intermetallic phases developed in the air to slow cooled samples.

The sample from Foundry D which underwent heat treatment schedule "D" had low toughness from the Charpy Impact Test (Test Method B) and also an affected structure in the Sodium Hydroxide Etch Test (Test Method A) but still passed the Ferric Chloride Corrosion Test (Test Method C). This demonstrates the ineffectiveness of Test Method C in detecting the presence of detrimental intermetallic phases.

The sample from Foundry D which underwent heat treatment schedule "G" also passed the Ferric Chloride Corrosion Test though it revealed an affected structure and low toughness. But the amount of intermetallic phase which was determined from the OLM image was less when compared to samples which had undergone other heat treatment schedules. In previous work A890-4A grade samples which had undergone heat treatment schedule "G" did not reveal the presence of intermetallic phase though they had

111

similar toughness[162]. From this it may be concluded that air cooling is not rapid enough to prevent the precipitation of intermetallic phases in A890-5A material.

From the results it can be concluded that Charpy Impact Test (Test Method B) is the best method out of the three to indicate the presence of detrimental intermetallic phase. From the toughness it is possible to predict the Sodium Hydroxide Etch Test (Test Method A) and Ferric Chloride Corrosion Test (Test Method C) results. The trend which was observed was that if the toughness is greater than 60ft-lbs then the samples had an unaffected structure and a high corrosion resistance (passed the acceptance criteria of weight loss $\leq$ 10 mdd by a wide margin). If the toughness was below 15ft-lbs then the samples revealed an affected structure and low corrosion resistance (weight loss $\geq$ 10 mdd). There was a 1:1 correlation between Test Method A and B. Though Test Method A is a direct method of detecting the presence of intermetallic phases, it cannot be confirmed whether the intermetallic phases present are detrimental or not. The lowering of toughness from Test Method B confirms whether the intermetallic phase present is detrimental. However, the toughness value of the material may also decrease if the percentage of ferrite is high. But this can be determined using Feritscope.

It can be concluded that the micrographs from A890-4A grade included in ASTM A923 are applicable for A890-5A grade to compare and detect the presence of detrimental intermetallic phase. The micrographs can be used to verify whether the A890-5A sample has an unaffected, affected or a possibly affected structure. It was also observed that when compared to A890-4A grade A890-5A grade is more sensitive to heat treatment. The A890-4A grade when subjected to Charpy Impact Test showed a gradual decrease in toughness with increasing hold time at 1550ºF. But the A890-5A grade material showed a significant drop in toughness from heat treatment schedule "A" to "B" when the second stage of the heat treatment process was followed (Heat to 1550ºF and hold for different time periods before water quenching). Qualitatively a greater amount of intermetallic phase is precipitated in the A890-5A material when compared to A890-4A grade for the same heat treatment schedule.

3. Ferrite Measurement

Feritscope® was used to measure the ferrite content in all the Charpy samples before carrying out toughness tests. Table 15 shows the average of volume ferrite in percentage in every heat calculated from the ferrite number.

From the above data it was seen that all the foundry solution annealed heats from Foundry A, B and C which had high toughness showed volume percentage of ferrite to be approximately 50.

Table 15: Ferrite Content in Volume Percentage

Foundry	Specimen ID	Ferrite Number	Volume % Ferrite
A	285	66.2	46.9
	144	53.7	40.2
	331	61.3	42.3
B	S1507	84	56.8
	S1508	65.1	46.4
C	45633	75.3	52.1
	41414	71.1	49.7
	41374	74.3	51.5
	41544	73.8	51.2
	44073	64.7	46.2
D	04J142	100.6	65.9
	04J142 - A	95.5	63.1
	04J142 - B	59.2	43.2
	04J142 - C	39.1	32.1
	04J142 - D	80.4	54.8
	04J142 - E	41.6	33.5
	04J142 - F	35.9	30.3
	04J142 - G	79.7	54.5
	04J142 - H	3.8	12.7

The foundry solution annealed material from Foundry D showed a significant variation in ferrite content with heat treatment schedules. The foundry solution annealed and heat treatment "A" samples (solution annealed at the University of Tennessee) showed ferrite content of approximately 65%, higher than the foundry solution annealed samples from other foundries even though they had similar toughness. The samples which underwent heat treatment "B", "D" and "G" showed an approximate volume percent of ferrite of 50 though they had low toughness. Heat treatment "B", "D" and "G" samples contained intermetallic phases. The other heat treatment samples had low ferrite content especially heat treatment "H" sample which showed the volume percent of ferrite to be approximately 12.7%. This was evident from the affected microstructures which showed that a large proportion of ferrite was converted into intermetallic phases.

Though there were few exceptions it could be concluded that with increasing presence of intermetallic phases in the microstructure the volume percentage of ferrite content is reduced as most of the ferrite is converted into intermetallic phases. Since heat treatment "B" samples exhibited ferrite of approximately 50% but had low toughness (Test Method B) and failed the Sodium Hydroxide Etch Test (Test Method A) and Ferric Chloride Corrosion Test (Test Method C) ferrite percent is not a good indicator of the absence of detrimental intermetallic phases.

4. ASTM E562 Ferrite Measurement – Standard Test Method for Determining Volume Fraction by Systematic Manual Point Count

Ferrite measurement was also carried out using a manual point count method stated in ASTM E562. Table 16 shows the average volume ferrite in percentage calculated using point count method and also Feritscope®.

Figure 46 shows a comparison between the volume percentage of ferrite measured using the Feritscope® and ASTM E562 Manual Point Count method.

Ferrite Measurement
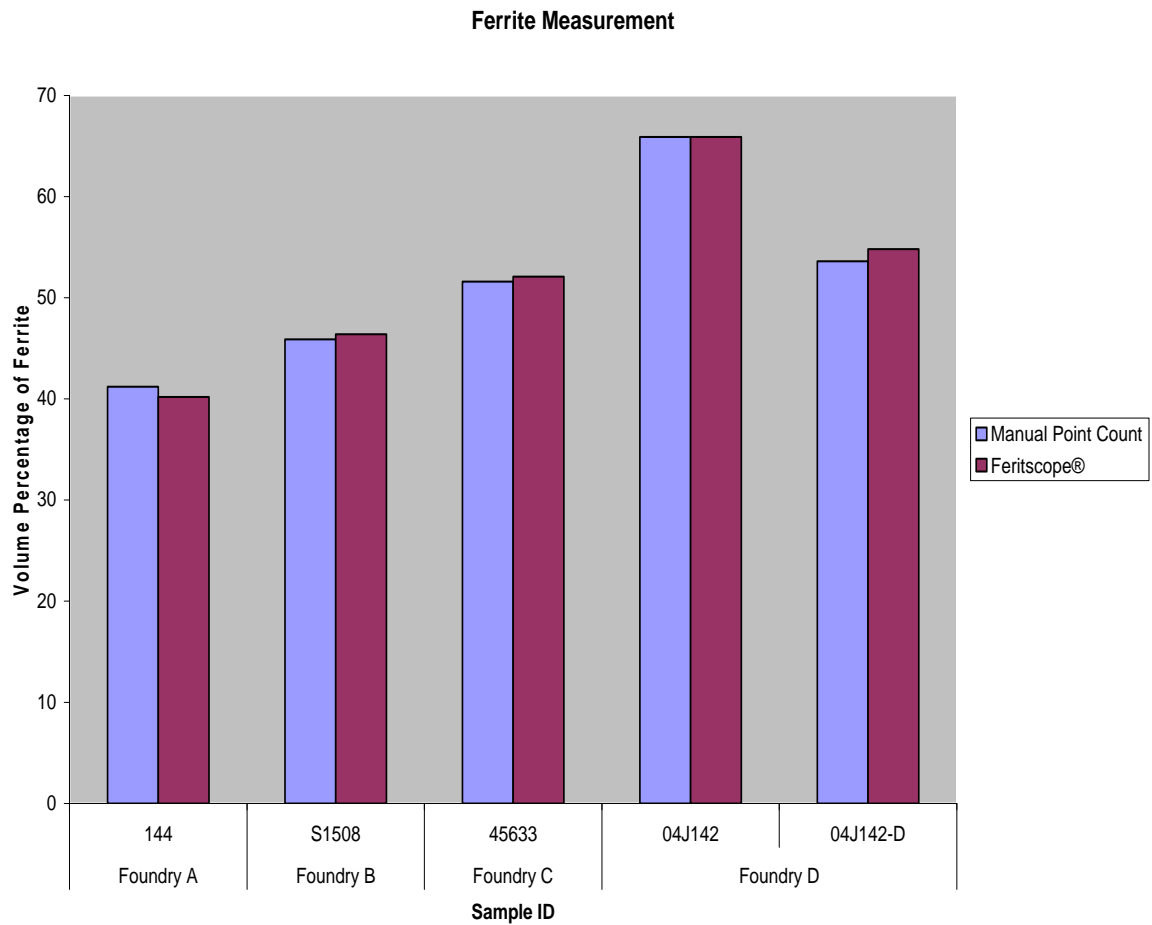
Figure 46: Comparison of Volume Percentage of Ferrite from the Feritscope® and per ASTM E562 Manual Point Count

Table 16: Volume Ferrite in Percentage from ASTM E562 Manual Point Count

Sample ID	Number of Fields (n)	% of Grid Points	Average volume % ferrite	Standard Deviation (s)	95% Confidence Limit	Volume % Ferrite using Point Count	Ferrite Number (Feritscope®)	Volume % Ferrite from Feritscope®
144	1	42.9						
	2	39.7						
	3	41.9						
	4	42.4						
	5	43.7	41.2	1.5	1.1	40.1 – 42.3	53.7	40.2
	6	39.3						
	7	40.3						
	8	41.9						
	9	40.7						
	10	39.6						
45633	1	55.2						
	2	52.3						
	3	51.1						
	4	52.9						
	5	51.6	51.6	1.7	1.2	50.4 – 52.8	75.3	52.1
	6	49.5						
	7	52.1						
	8	51.1						
	9	50.3						
	10	49.6						
S1508	1	46.2						
	2	45.4						
	3	47.6						
	4	49.1						
	5	44.8	45.9	1.8	1.3	44.6 – 47.2	65.1	46.4
	6	45.1						
	7	45.6						
	8	46.9						
	9	43.9						
	10	44.1						
04J142	1	66.7						
	2	69.1						
	3	64.9						
	4	63.4						
	5	65.9	65.9	2.1	1.4	63.8 - 68	100.6	65.9
	6	65.6						
	7	67.1						
	8	64.2						
	9	63.5						
	10	68.9						
04J142 - D	1	55.2						
	2	57.3						
	3	53.8						
	4	53.5						
	5	51.7	53.6	2.5	1.8	51.8 – 55.4	80.4	54.8
	6	53.7						
	7	56.6						
	8	54.5						
	9	50.5						
	10	49.6						

From the table we can infer that the volume percentage of ferrite calculated using Feritscope® falls within the 95% confidence limit for volume percentage of ferrite calculated using ASTM E562. The standard deviation measured from ASTM E562 ranged from 1.5 – 2.5%, which indicates that ferrite measurement by Point Counting per ASTM E562 shows similar results when compared with the Feritscope®.

There are few disadvantages of manual point count, which affect the accuracy of the results of ASTM E562:

1. Operator bias pays a role in counting the phases falling inside the grid.
2. Specimen Preparation: Surface defects or abnormalities due to polishing or etching can lead to difficulty in distinguishing between the phases.
3. Grid Preparation: Thickness of grid lines can cause difficulty in determining whether a phase actually lies at the intersection or not.

It can be concluded that the volume percentage of ferrite measurement from either method produces similar results but Feritscope® is more robust because it is easy to operate, eliminates operator bias and there are minimal requirements for specimen preparation[162,168].

5. Hardness Measurement

Hardness was measured on all the samples from various heats using both Rockwell B and C. Table 17 shows the hardness of all the heats and heat treatments.

From the above data one can derive a correlation between the toughness, ferrite content and the hardness. The hardness for all the heats from Foundry A, B and C was approximately between 94 to 103 and 18 to 26 on HRB and HRC scales respectively. For the samples from Foundry D the solution annealed and heat treatment "A" showed similar hardness. Heat treatment "B", "D" and "G" also showed similar hardness though

Table 17: Hardness Value Measured using Rockwell B and C

Foundry	Specimen ID	HRB	HRC
A	285	103.9	22.5
	144	94.1	18.9
	331	103	21.8
B	S1507	96.1	24.4
	S1508	96.1	21.9
C	45633	102.7	20.8
	41414	98.6	20.4
	41374	102.2	20.1
	41544	98.4	20.9
	44073	100.9	18.9
D	04J142	102.8	25.5
	04J142 - A*	99.1	20.4
	04J142 - B	101.9	24.9
	04J142 - C	106.1	30.8
	04J142 - D	101.6	20.1
	04J142 - E	106.8	29.9
	04J142 - F	108.6	29.9
	04J142 - G	102.7	22.1
	04J142 - H	109.9	35.2

* Refer to heat treatment schedule in Table 4

heat treatment "B", "D" and "G" samples contained intermetallic phase. This may be because from their OLM micrographs we were able to determine visually that there was only a small amount of intermetallic phase present as compared to samples which had undergone other heat treatment schedules. Samples from heat treatment schedules "C", "E", "F" and "H" showed greater hardness on both the scales because the presence of intermetallic phase increases the hardness of the material.

These results were similar to the results that were obtained for the ferrite content measurement. It may be possible to conclude that there was a direct relationship between the ferrite content and the hardness. As the ferrite content decreased due to the transformation of intermetallic phases there was an increase in the hardness. If the

volume percent of ferrite content is approximately 50, then the hardness is approximately between 94 to 103 and 18 to 26 in HRB and HRC scales respectively.

6. Evaluation of Fracture Surfaces from Test Method B

SEM was carried out on the fracture surfaces of one sample from each heat. The following figures (Figure 47 – 65) show SEM images of the fracture surfaces of the samples. All these samples are labeled with their specimen identity followed by its impact toughness and magnification.

.
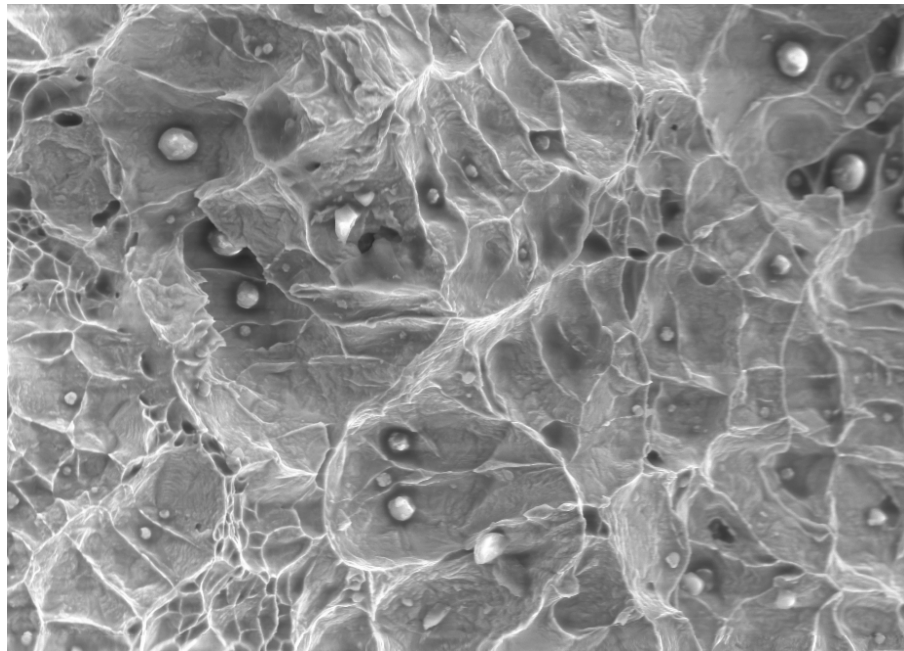
Figure 47: Fracture Surface of 04J142, 72ft-lbs, 500x
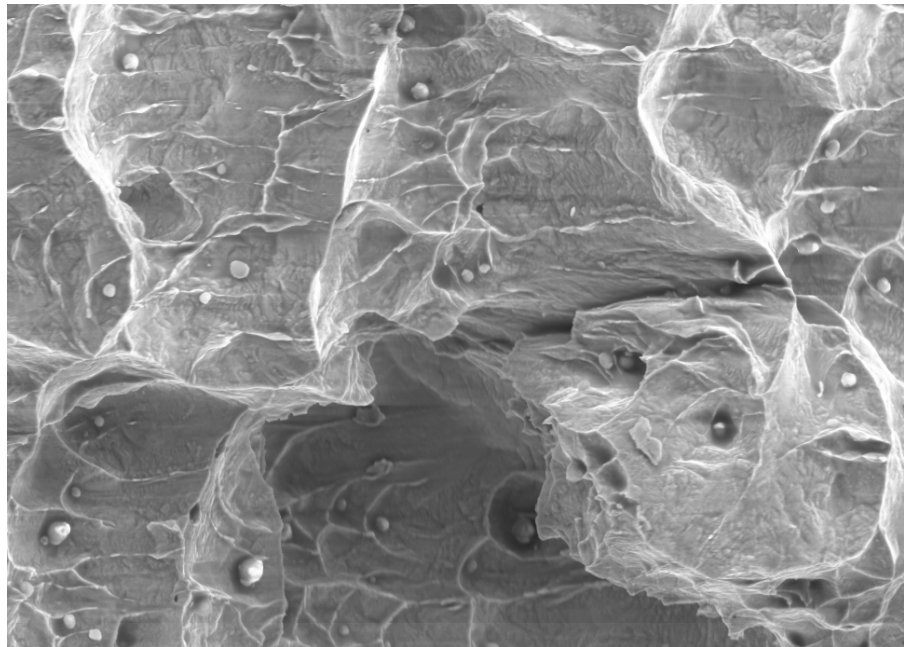
Figure 48: Fracture Surface of 04J142 – A, 80.5ft-lbs, 500x
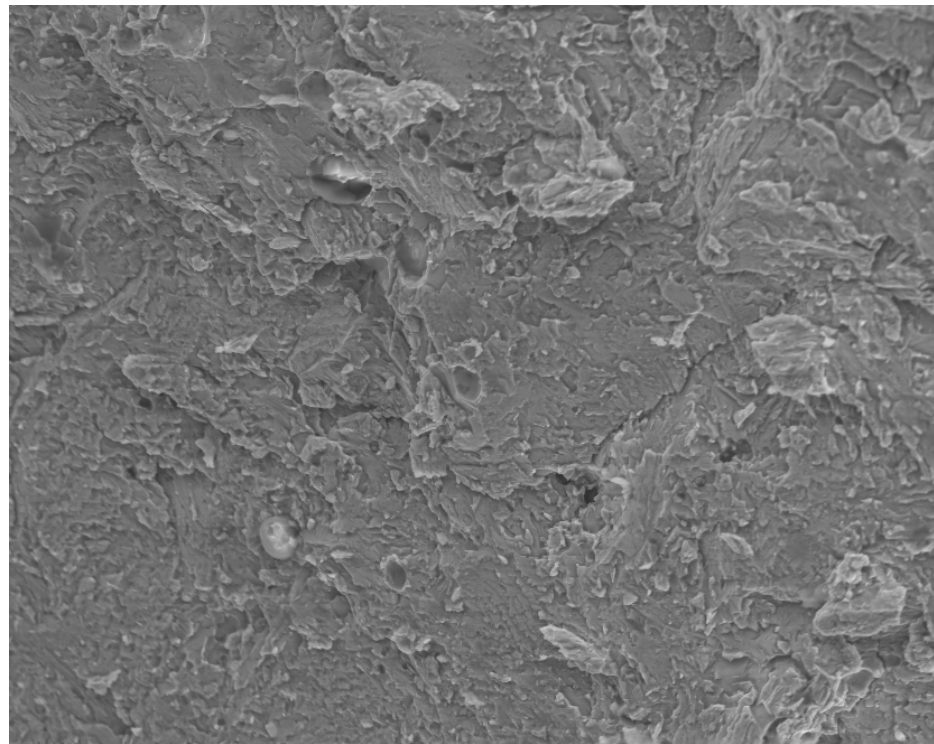
Figure 49: Fracture Surface of 04J142 – B, 2.5ft-lbs, 500x
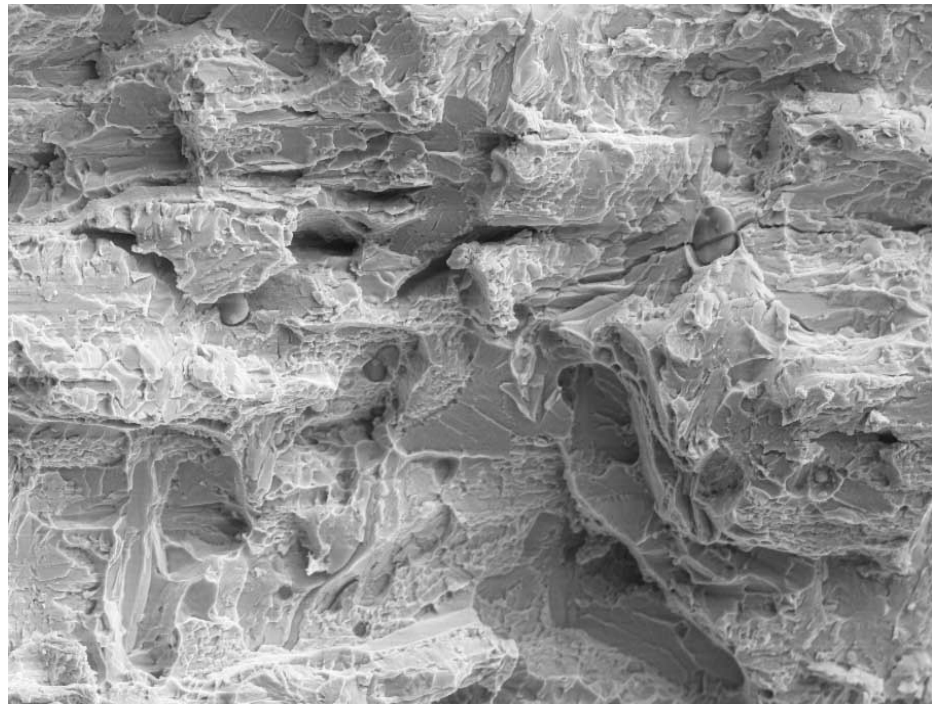
Figure 50: Fracture Surface of 04J142 – C, 1.5ft-lbs, 500x
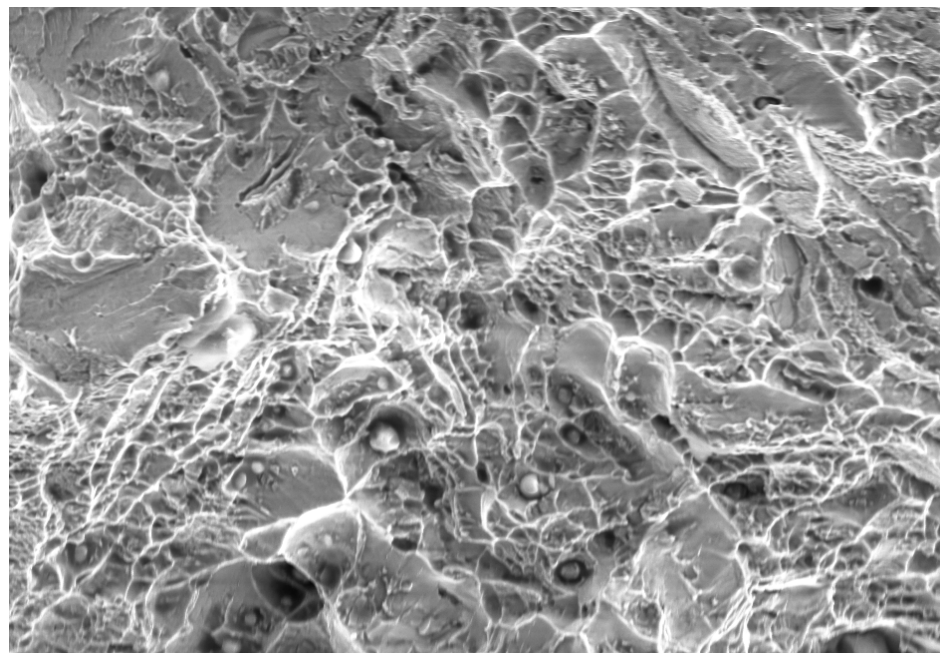
Figure 51: Fracture Surface of 04J142 – D, 7.5ft-lbs, 500x
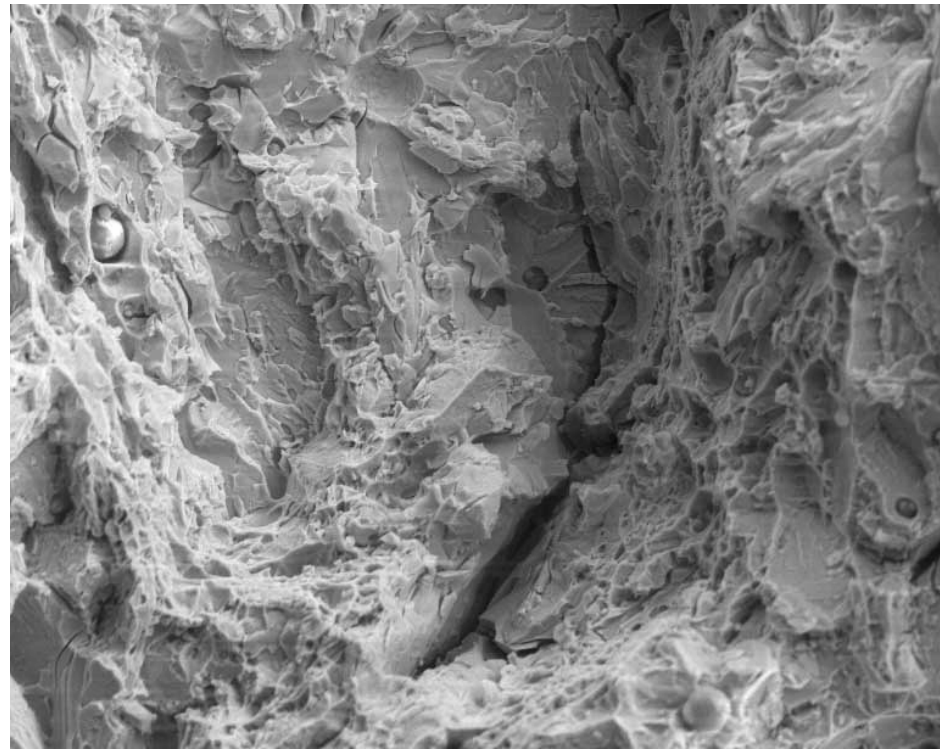
Figure 52: Fracture Surface of 04J142 – E, 1.5ft-lbs, 500x
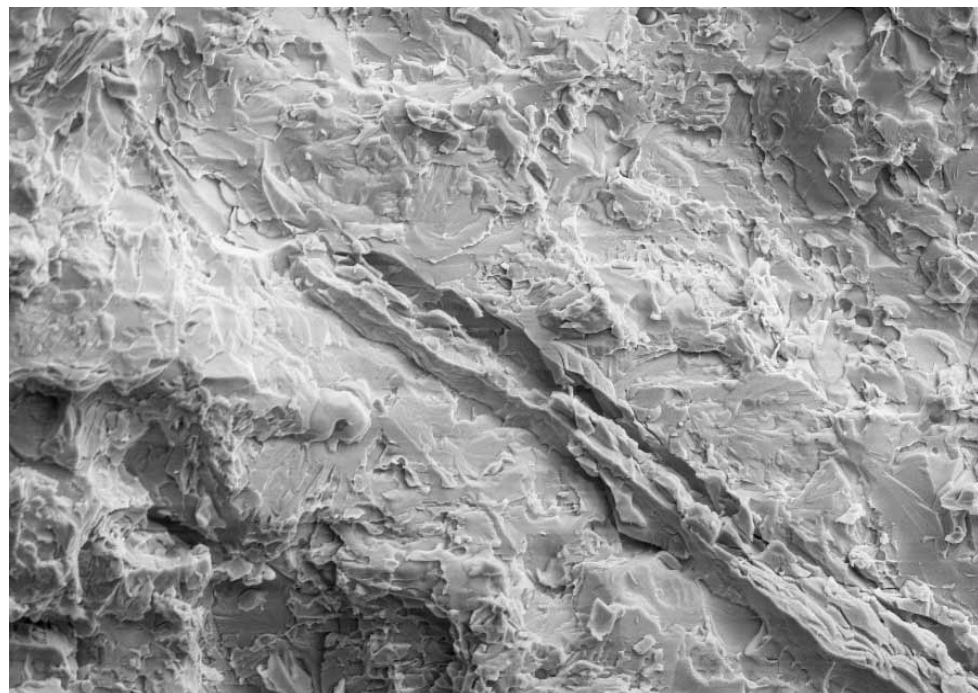
Figure 53: Fracture Surface of 04J142 – F, 1.5ft-lbs, 500x
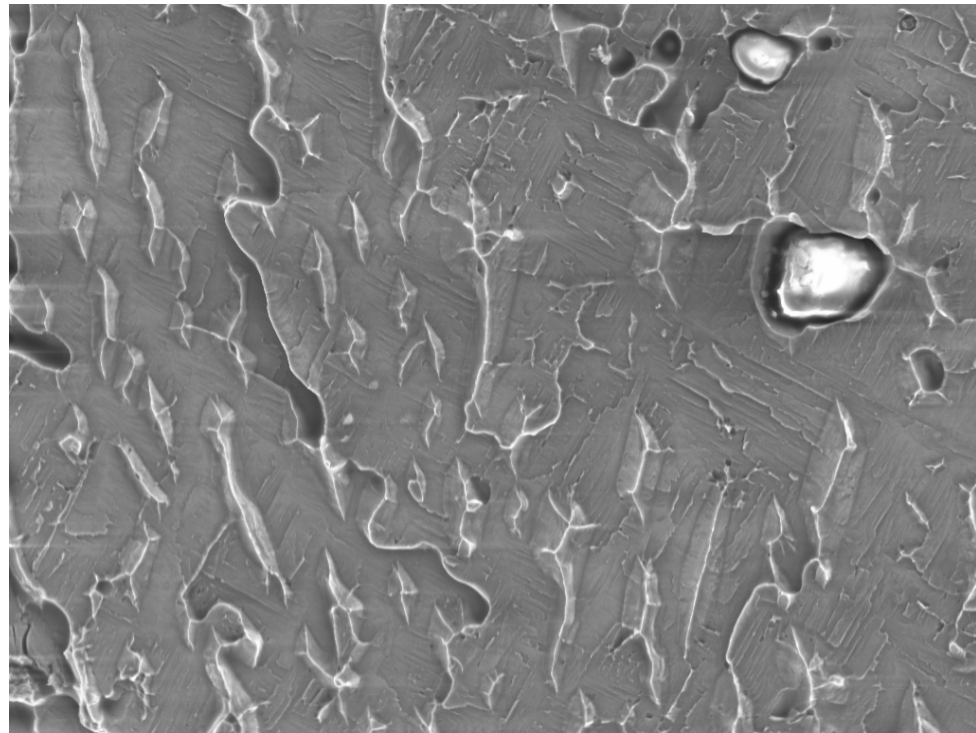
Figure 54: Fracture Surface of 04J142 – G, 9.5ft-lbs, 500x
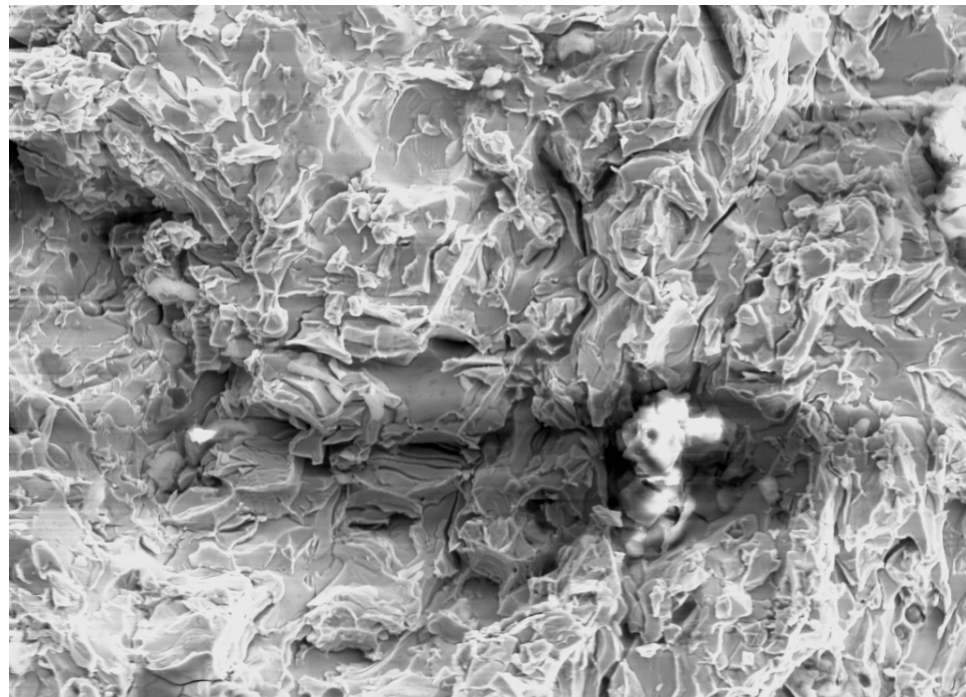
Figure 55: Fracture Surface of 04J142 – H, 2.5ft-lbs, 500x
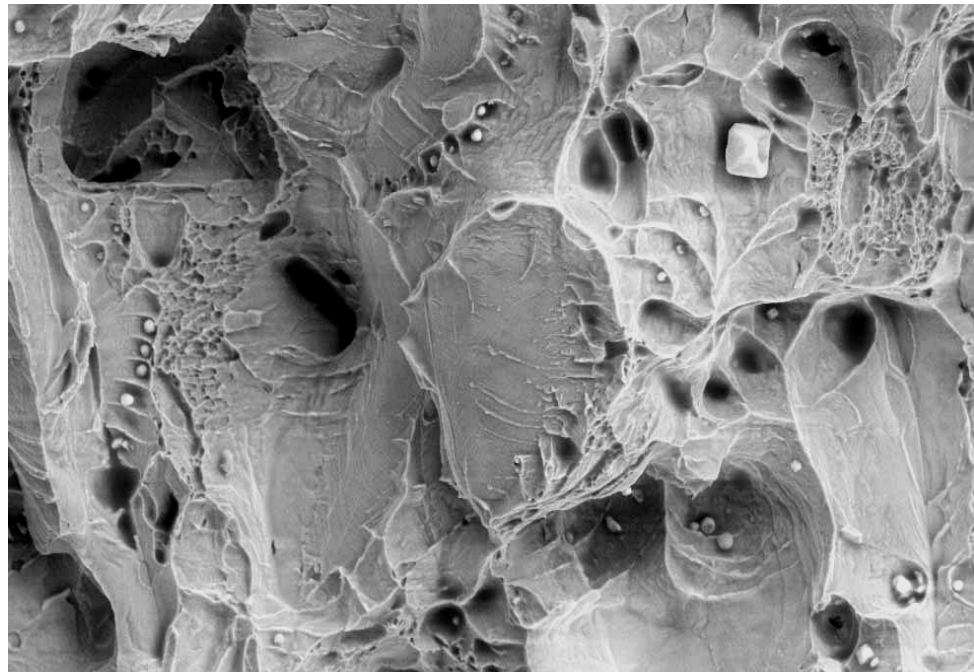
Figure 56: Fracture Surface of 331, 72.5ft-lbs, 500x
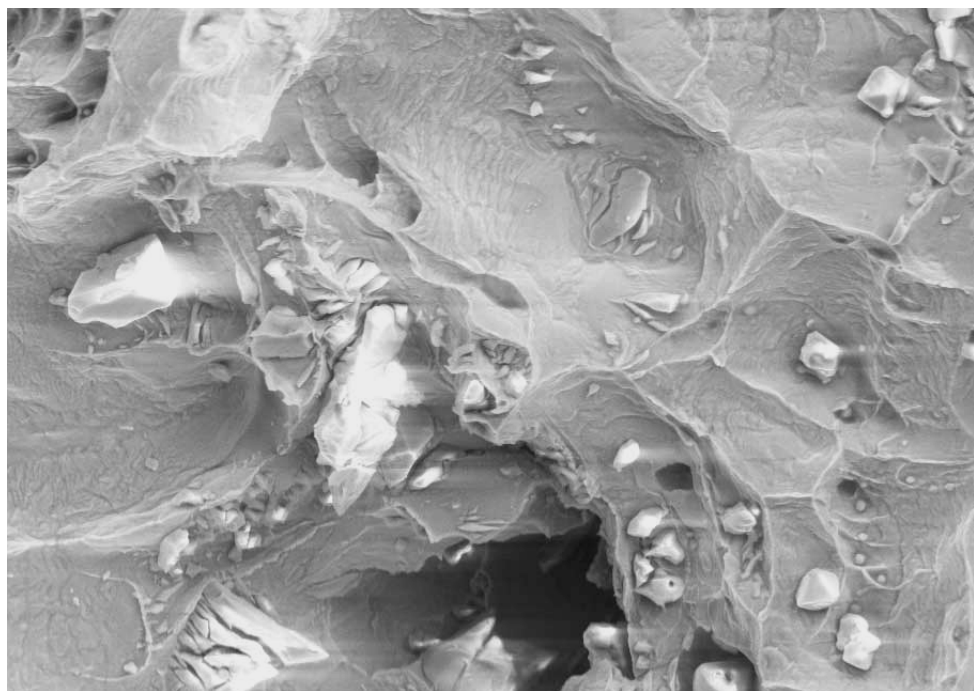
Figure 57: Fracture Surface of 144, 104ft-lbs, 500x
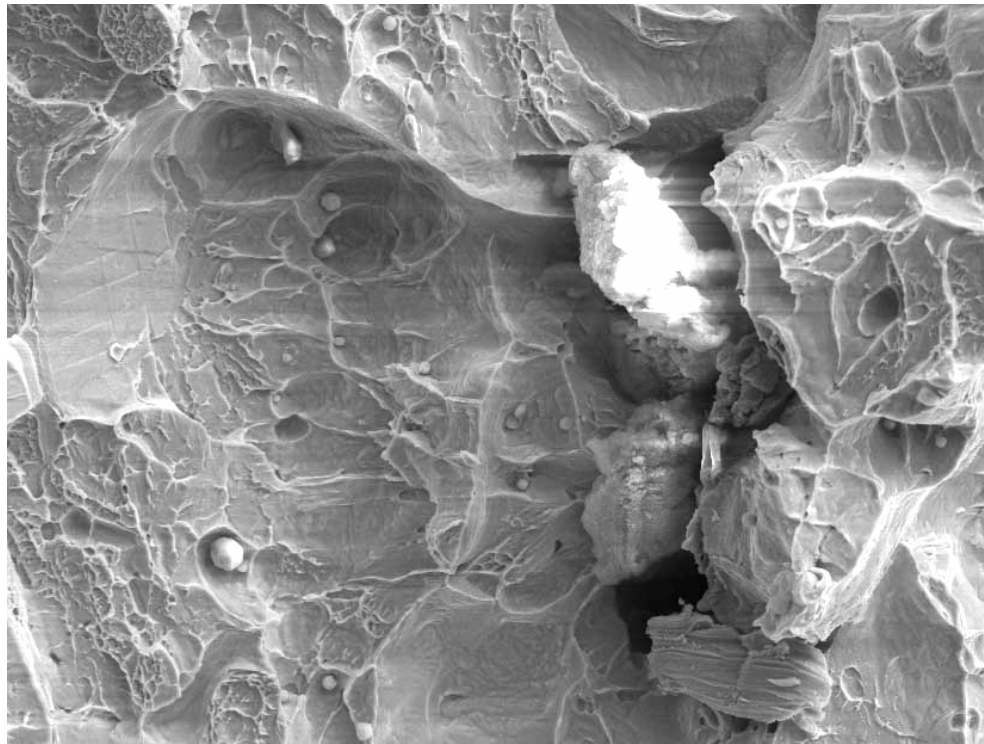
Figure 58: Fracture Surface of 285, 75ft-lbs, 500x
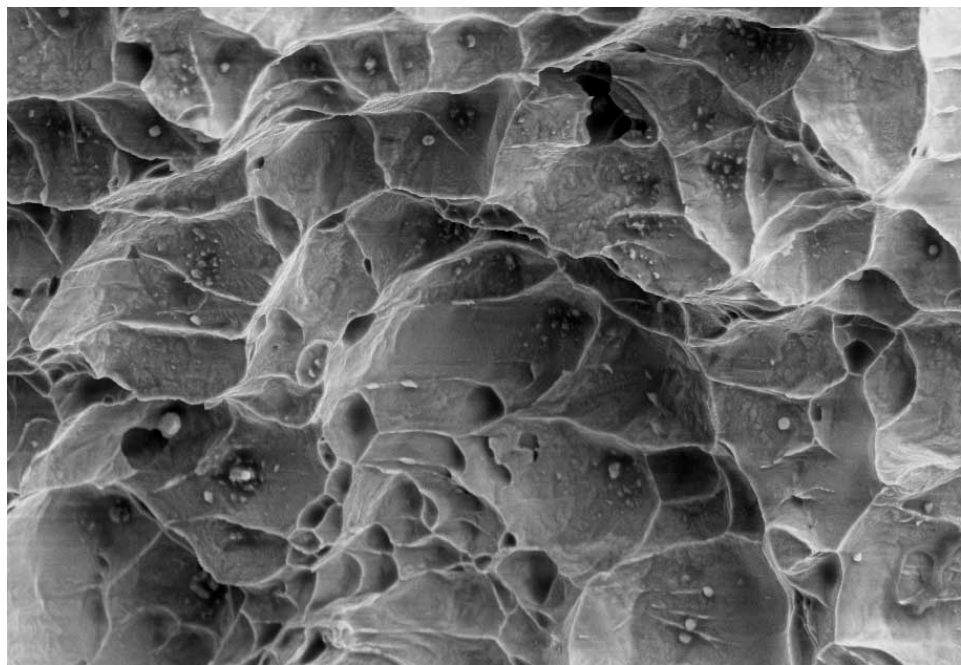
Figure 59: Fracture Surface of 41374, 130ft-lbs, 500x
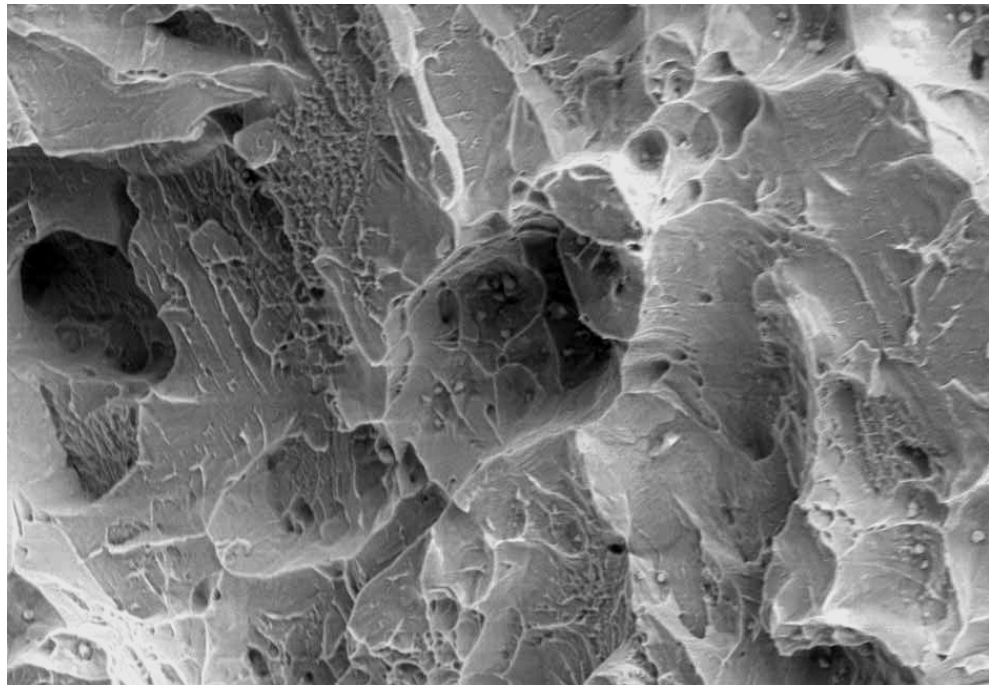
Figure 60: Fracture Surface of 41414, 125ft-lbs, 500x
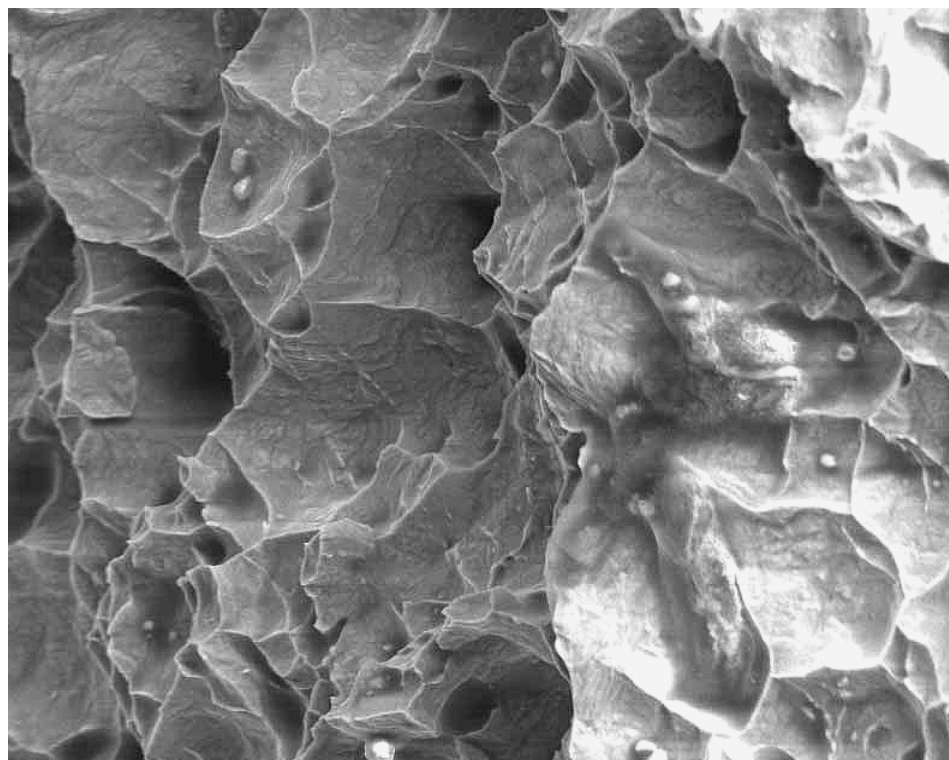
Figure 61: Fracture Surface of 41544, 143ft-lbs, 500x
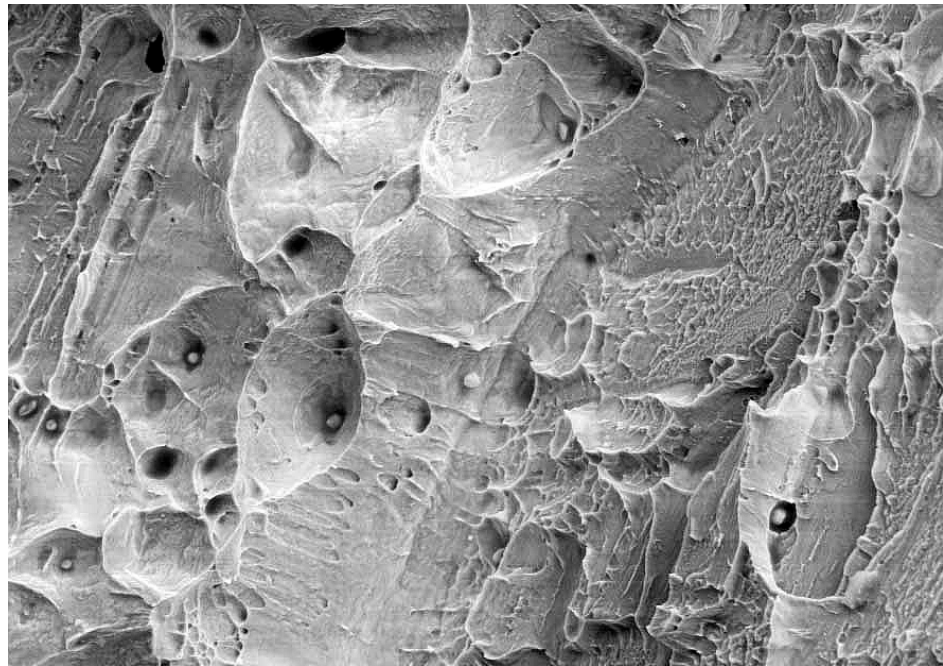
Figure 62 Fracture Surface of 45633, 126.5ft-lbs, 500x
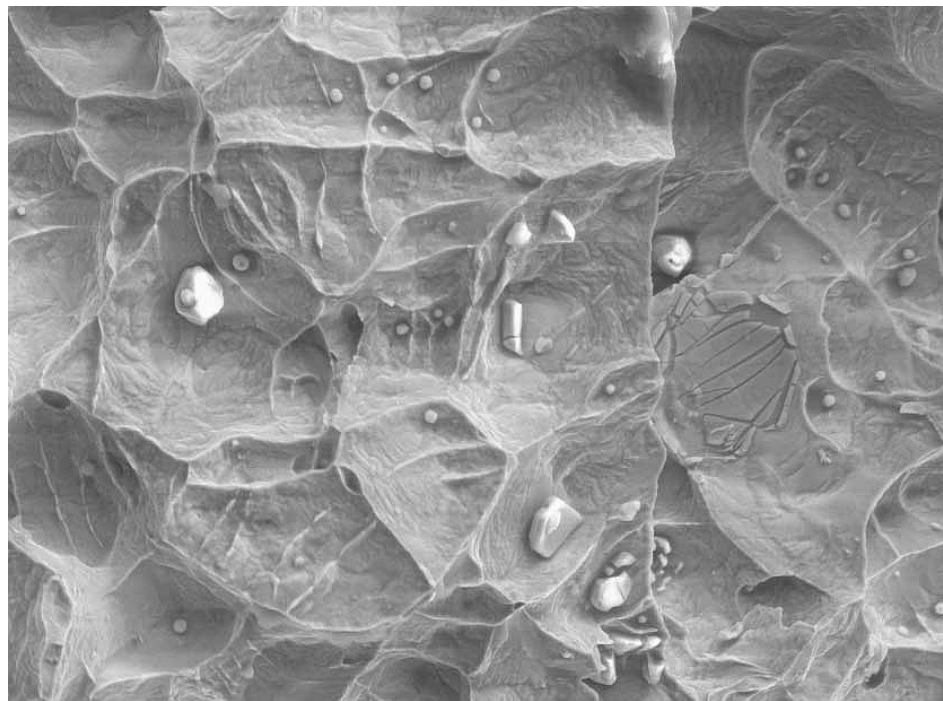
Figure 63: Fracture Surface of 44073, 152.5ft-lbs, 500x
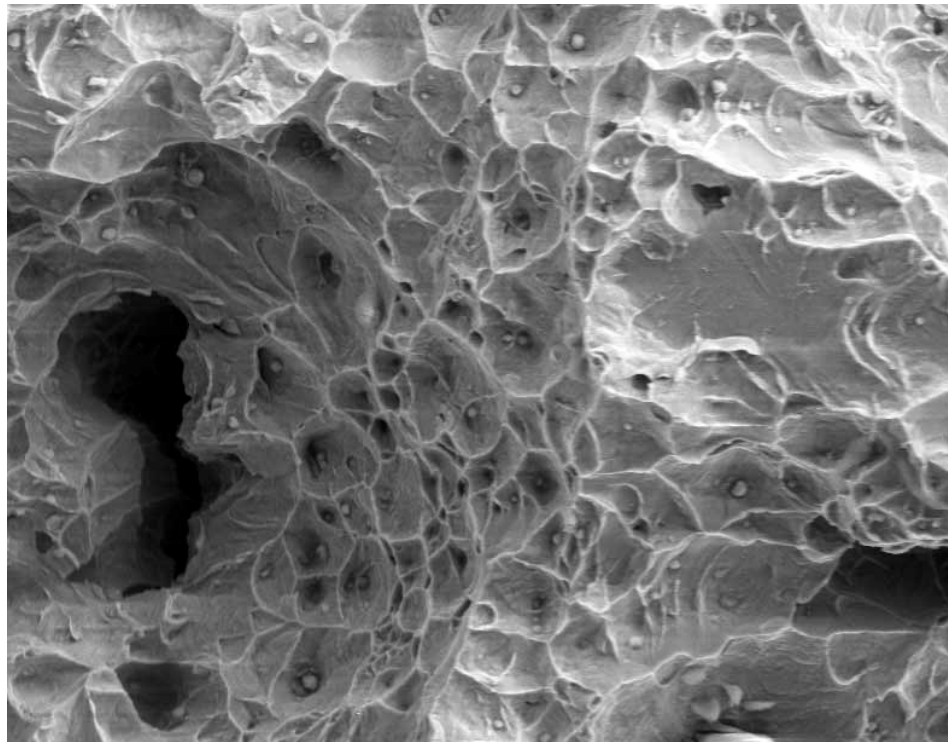
Figure 64: Fracture Surface of S1507, 78.5ft-lbs, 500x
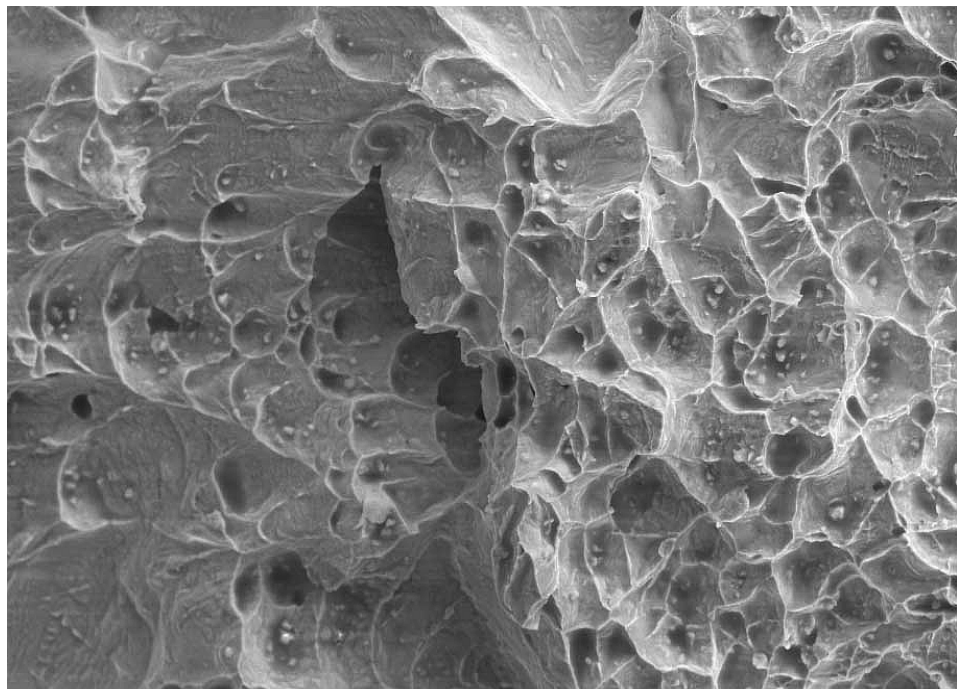
Figure 65: Fracture Surface of S1508, 68ft-lbs, 500x

The fractures can be categorized into two types – Ductile and Brittle. A ductile fracture is characterized by a dimpled surface. It is associated with high energy release. On the other hand brittle fracture is characterized by rapid crack propagation with low energy release. Brittle fractures display either cleavage (transgranular) or intergranular fracture. The fracture may have a bright granular appearance. The materials which undergo brittle fracture have greater hardness as compared to those which undergo ductile fracture.

From the SEM images it was observed that all the foundry solution annealed samples from Foundry A, B, C and D showed ductile fracture. All these samples had large dimpled ductile fracture surfaces. These samples had a high toughness. The heat treatment "A" sample (solution annealed at the University of Tennessee) from Foundry D also showed ductile fracture. The samples from other heat treatment schedules generally showed brittle fracture. Cleavage was evident on the fracture surface of heat treatment "G" sample. These samples had low toughness. Most of the samples which underwent brittle fracture had hardnesses greater than the solution annealed samples which showed ductile fracture.

7. Corrosion Analysis of Test Method C Samples using SEM

SEM was carried on all the ASTM A923 Test Method C samples before and after the corrosion test was performed. The following figures (Figure 66 – 84) show SEM images on all samples.

.
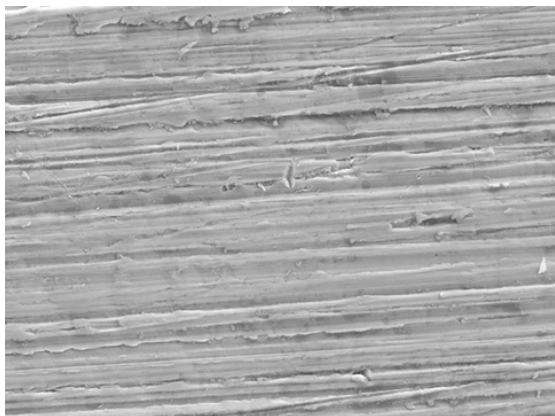
Figure 66: 04J142 (a) Before Corrosion, 1000x
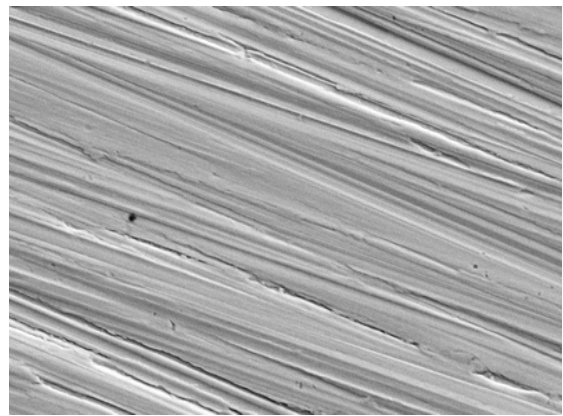
Figure 66: Continued (b) After Corrosion, 1000x
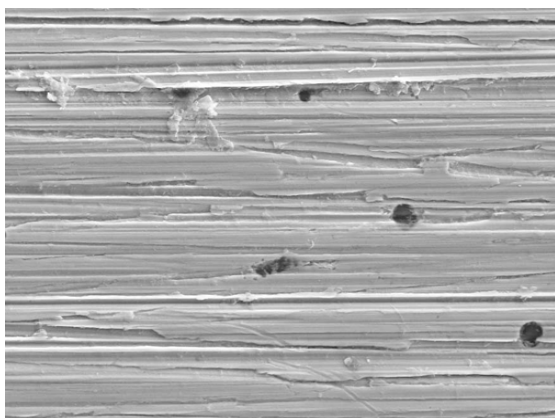

Figure 67: 04J142-A (a) Before Corrosion, 1000x
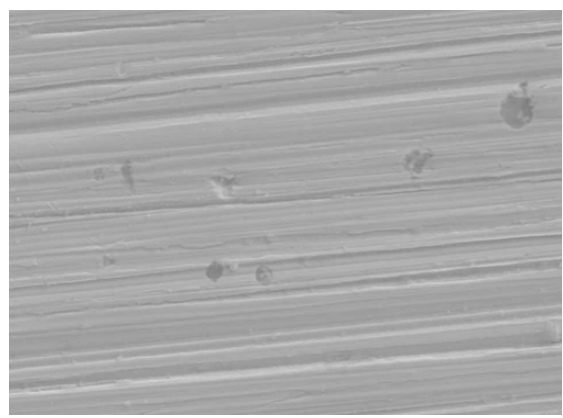
**Figure 67:** Continued (b) After Corrosion, 1000x
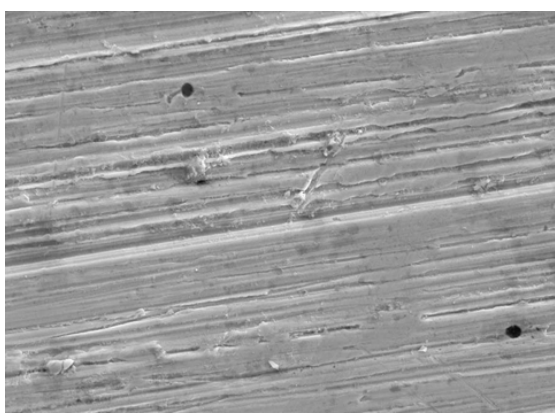
**Figure 68:** 04J142-B (a) Before Corrosion, 1000x

Cracks
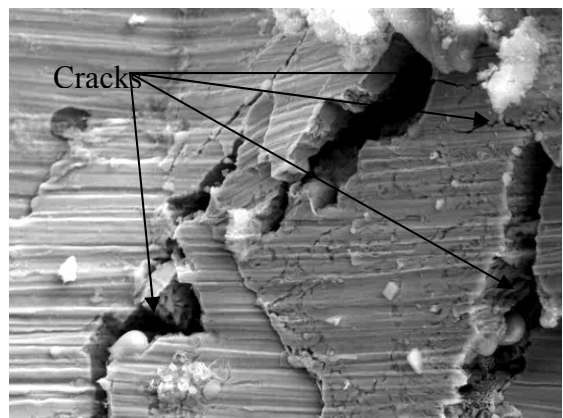
Figure 68: Continued (b) After Corrosion, 1000x
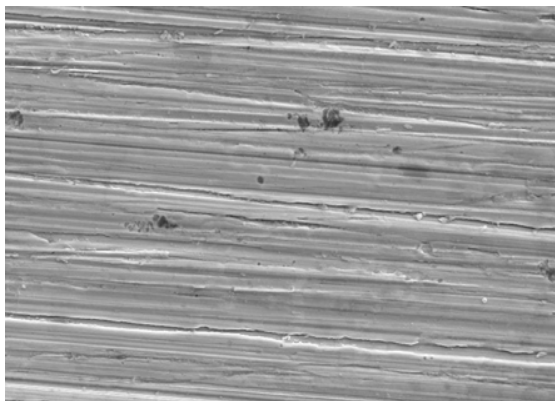
Figure 69: 04J142-C (a) Before Corrosion, 1000x   **Figure 69:** Continued (b) After Corrosion, 1000x
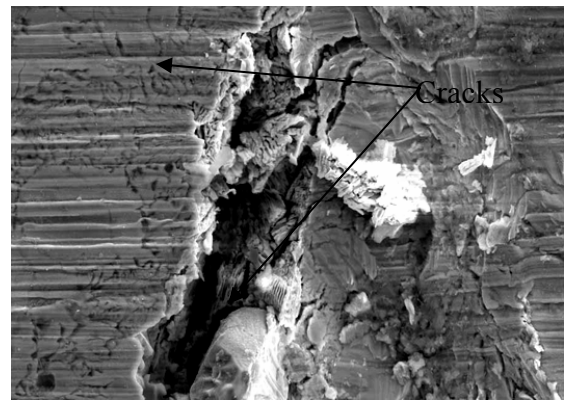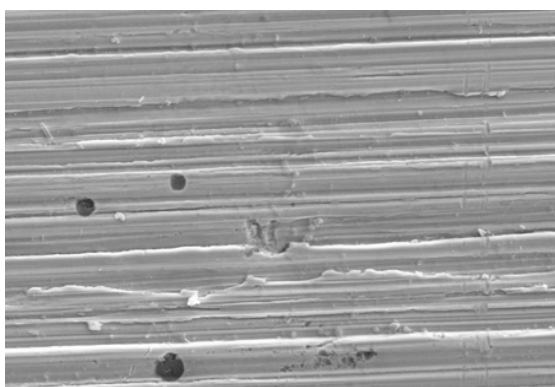
Figure 70: 04J142-D (a) Before Corrosion, 1000x   **Figure 70:** Continued (b) After Corrosion, 1000x
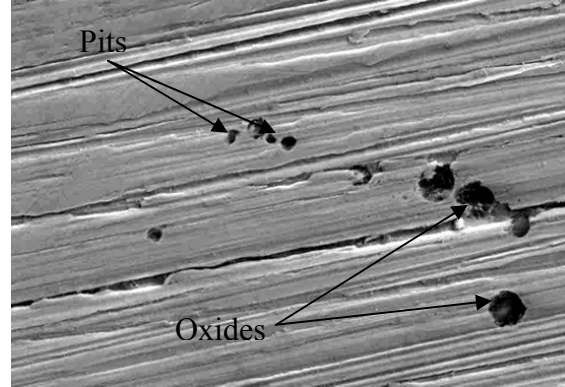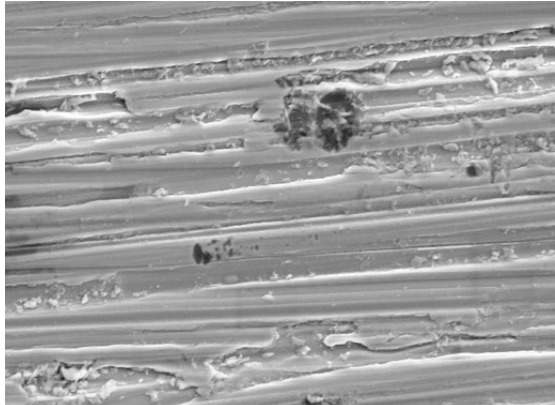
Figure 71: 04J142-E (a) Before Corrosion, 1000x   **Figure 71:** Continued (b) After Corrosion, 1000x
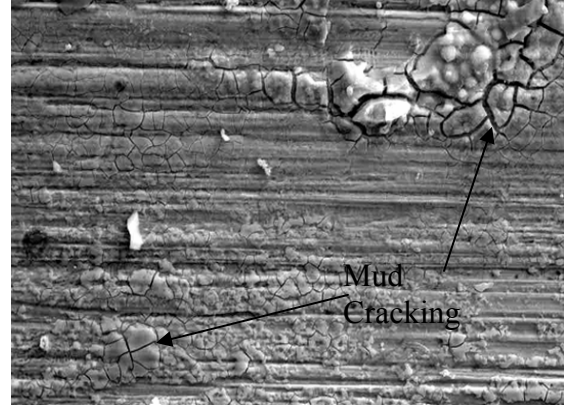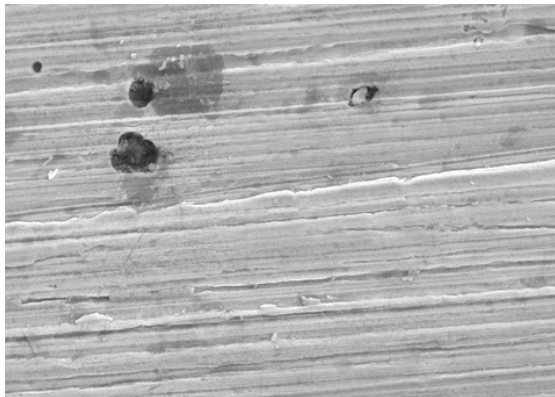
**Figure 72:** 04J142-F (a) Before Corrosion, 1000x
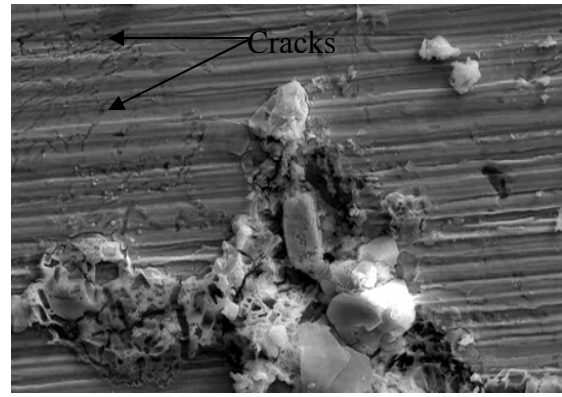
**Figure 72:** Continued (b) After Corrosion, 1000x
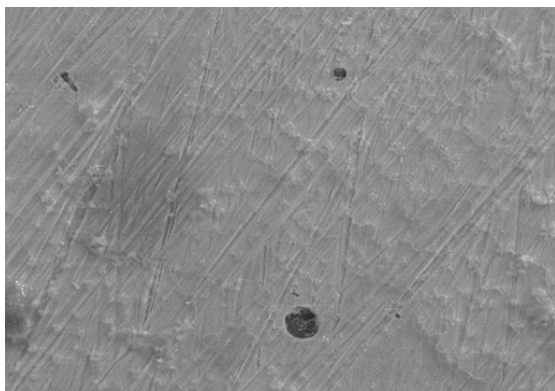
**Figure 73:** 04J142-G (a) Before Corrosion, 1000x
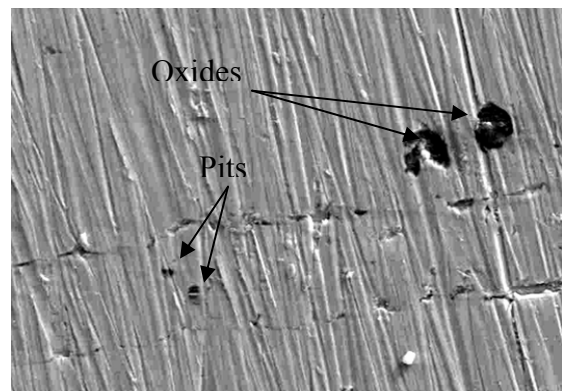
**Figure 73:** Continued (b) After Corrosion, 1000x
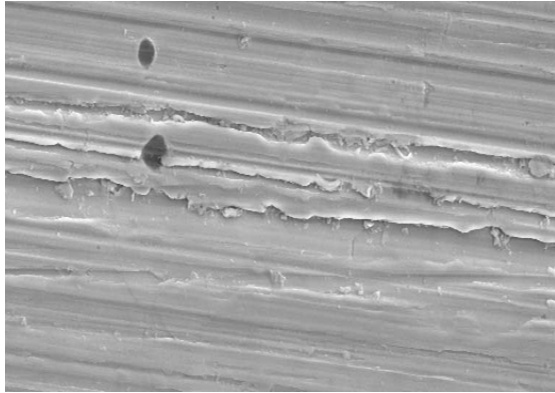
Figure 74: 04J142-H (a) Before Corrosion, 1000x
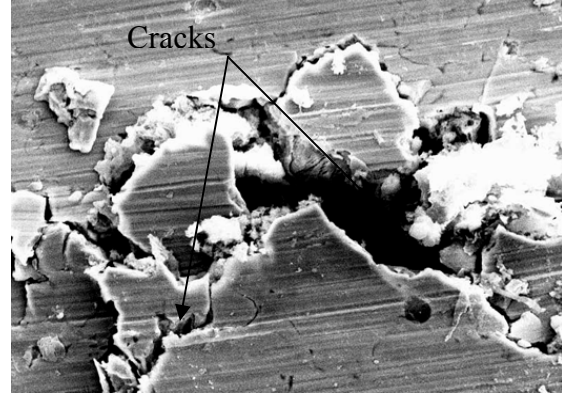
Figure 74: Continued (b) After Corrosion, 1000x
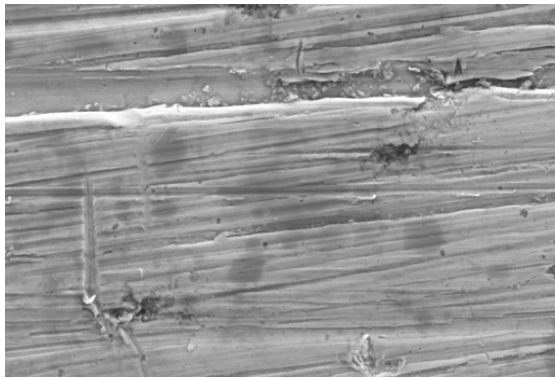
Figure 75: 144 (a) Before Corrosion, 1000x
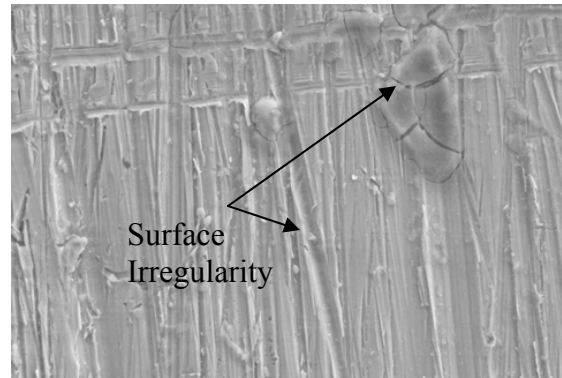
Figure 75: Continued (b) After Corrosion, 1000x
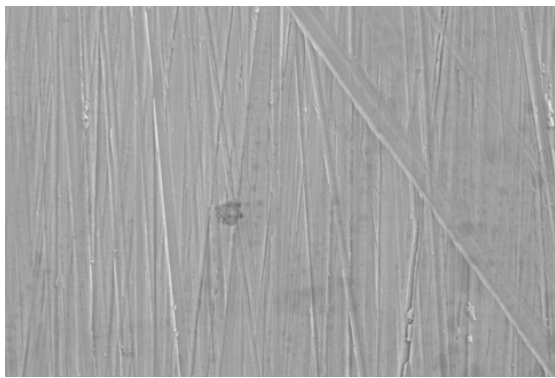
Figure 76: 285 (a) Before Corrosion, 1000x
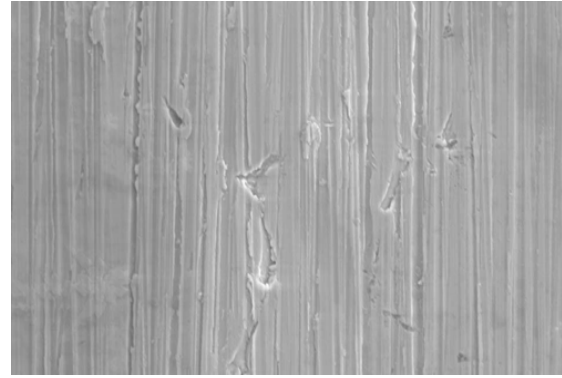
Figure 76: Continued (b) After Corrosion, 1000x
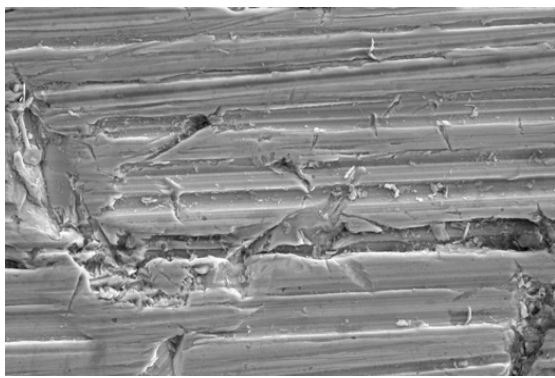
Figure 77: 331 (a) Before Corrosion, 1000x
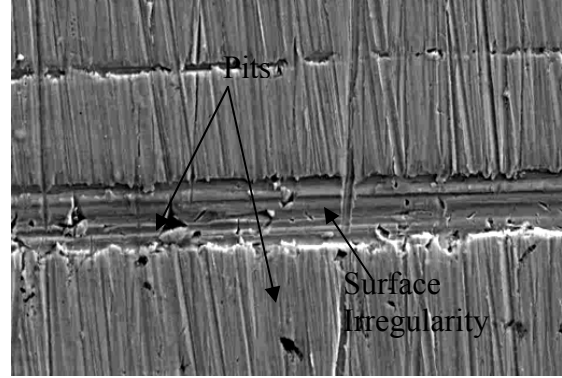
Figure 77: Continued (b) After Corrosion, 1000x

133
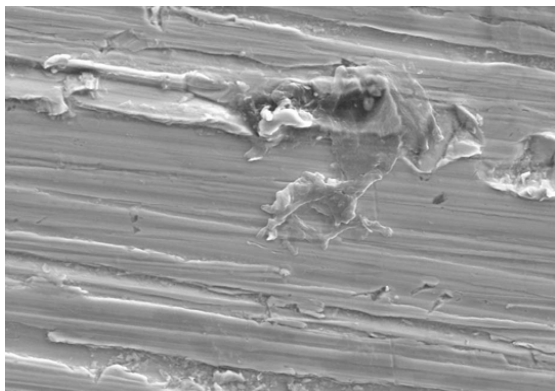
**Figure 78:** S1507 (a) Before Corrosion, 1000x
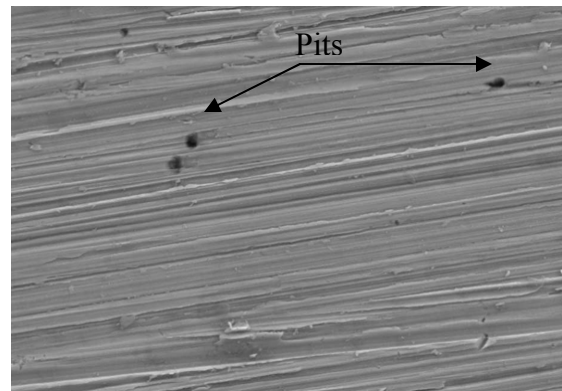
Figure 78: Continued (b) After Corrosion, 1000x
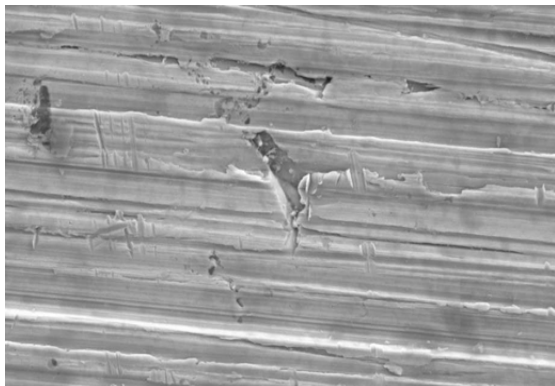
Figure 79: S1508 (a) Before Corrosion, 1000x
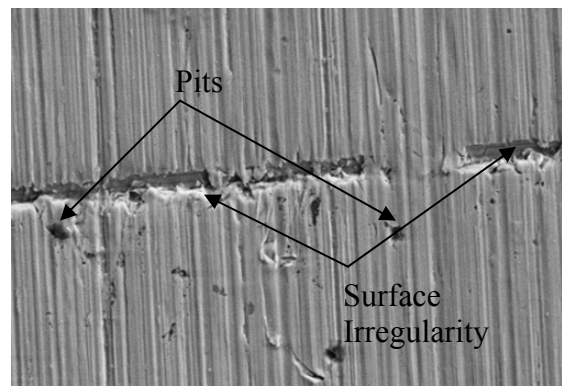
Figure 79: Continued (b) After Corrosion, 1000x
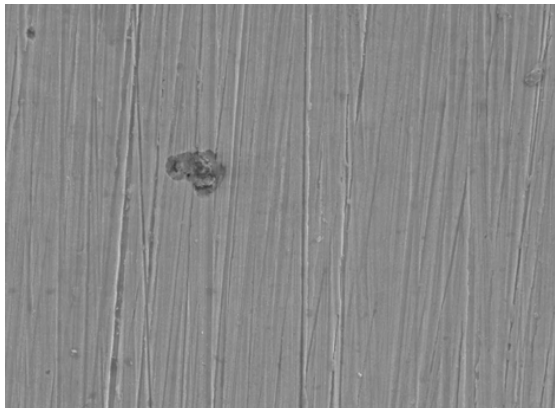
Figure 80: 41374 (a) Before Corrosion, 1000x
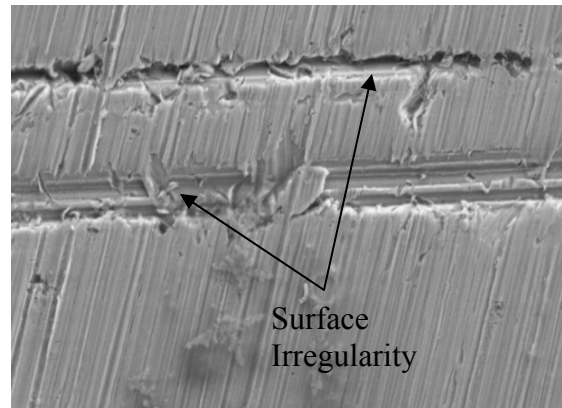
Figure 80: Continued (b) After Corrosion, 1000x
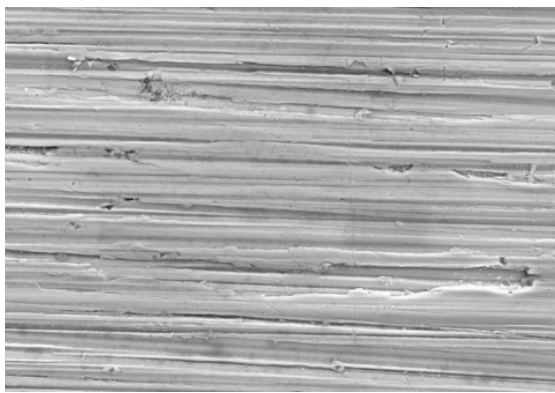
**Figure 81:** 41414 (a) Before Corrosion, 1000x
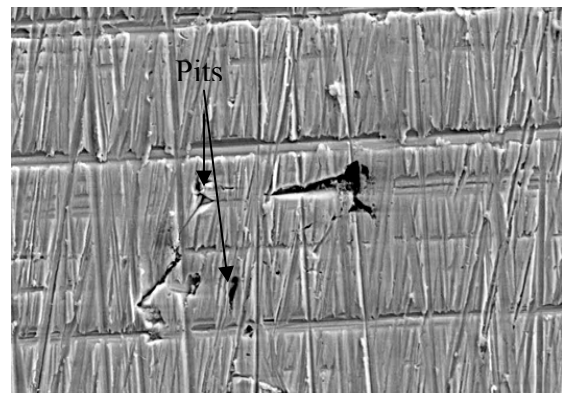
**Figure 81:** Continued (b) After Corrosion, 1000x
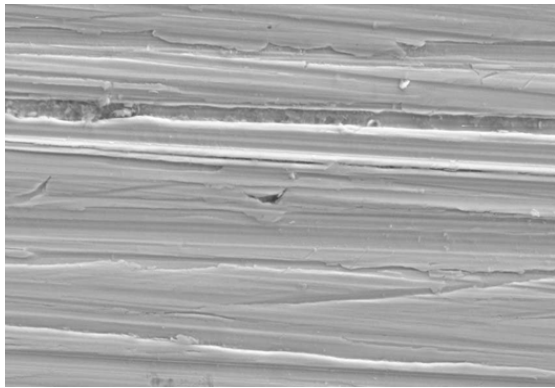
Figure 82: 41544 (a) Before Corrosion, 1000x
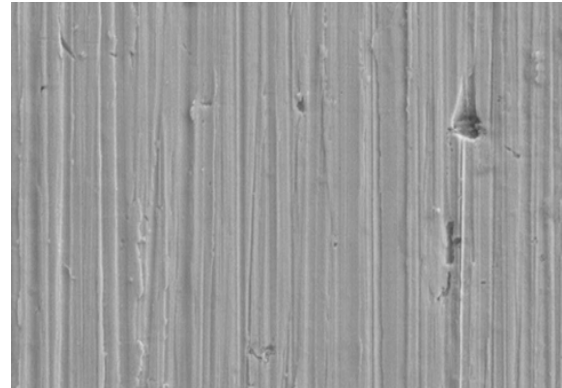

Figure 82: Continued (b) After Corrosion, 1000x
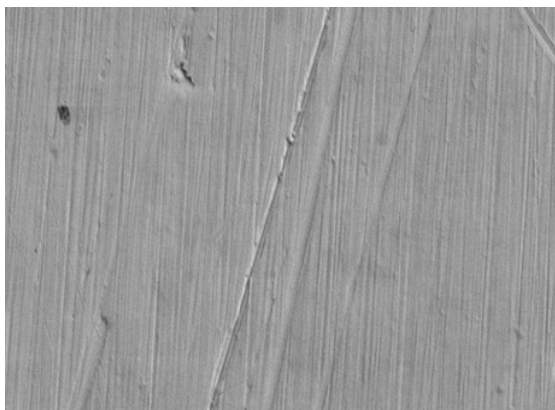

Figure 83: 45633 (a) Before Corrosion, 1000x
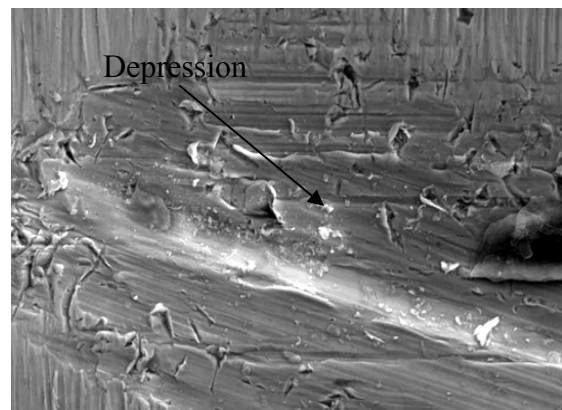

**Figure 83:** Continued (b) After Corrosion, 1000x

135
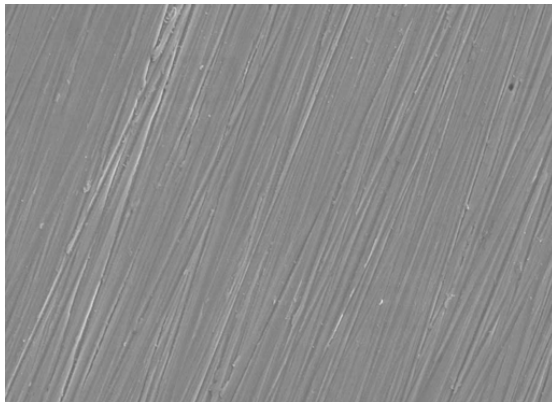
**Figure 84:** 44073 (a) Before Corrosion, 1000x   **Figure 84:** Continued (b) After Corrosion, 1000x
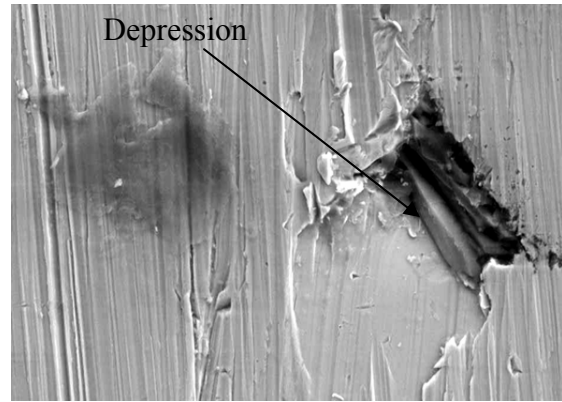
After carrying out SEM on the samples which were tested for corrosion resistance it was possible to correlate the results from the ASTM A923 Test Method C with the images that were obtained.

All the foundry solution annealed samples from Foundries A, B, C and D had been subjected to corrosion tests, passed Test Method C and when the SEM was carried out on these samples before and after they had subjected to corrosion, only pits, depressions and surface irregularities were found on these samples. Sample 331, from Foundry A showed pits and surface irregularities. Some surface irregularity was observed in this sample before the corrosion test was carried out but it was not well defined. The samples from heat S1507 and S1508 of Foundry B showed the presence of pits after the corrosion test was carried out. In the samples from Foundry C pits were present in sample 41414 and depressions in samples 45633 and 44073.

The heat treatment "A" sample (solution annealed at the University of Tennessee) passed the Test Method C as revealed by the SEM images which do not show any defects. The SEM images of heat treatment "B", "C", "E", "F" and "H" showed crack-like surface irregularities in the samples after corrosion testing. These samples failed the corrosion test. The sample from heat treatment "H" which showed a high corrosion rate had crack-like discontinuities throughout the surface of the specimen. Though heat treatment "D" and "G" passed the corrosion test, SEM images revealed pits and oxides on the corrosion surface.

136

It was observed that although the samples passed the corrosion Test Method C pits, oxides, surface irregularities and depressions were observed on the sample surface after the corrosion test was carried out. All these indications were highly localized. They were not distributed throughout the samples surface. It has been shown by Arthur H Tuthill[163] that the assumption of uniform weight loss over the full area of specimen in calculating the corrosion rate may be reasonable for carbon steel, however in the case of stainless steels it is misleading due to the fact that corrosion of stainless steel is highly localized as seen in the case of these samples also. This also indicates that Test Method C is a not a good method for determining the presence of detrimental intermetallic phase when compared to Test Method A and B.

Since these samples were not polished and etched to reveal the microstructure, as it was not required for Test Method C according to ASTM A923, it was not possible to determine which phases were present when indications were observed.

8. Verification of the type of Secondary Phases present in Foundry D samples using Scanning Electron Microscopy and Energy Dispersive Spectroscopy

SEM and EDS was carried out on the samples from Foundry D which were subjected to heat treatment schedule derived from the testing of wrought DSS. SEM and EDS was also carried out on the foundry solution annealed sample from Foundry D in order to compare its EDS results with the heat treatment "A" (Solution Annealed at the University of Tennessee) sample results. The following figures show the SEM images of these samples as well as the EDS results.

Element	Element %
Si	0.79
Cr	24.85
Fe	63.15
Ni	8.71
Mo	2.51

Element	Element %
Si	0.79
Cr	27.45
Fe	60.84
Ni	6.46
Mo	4.45
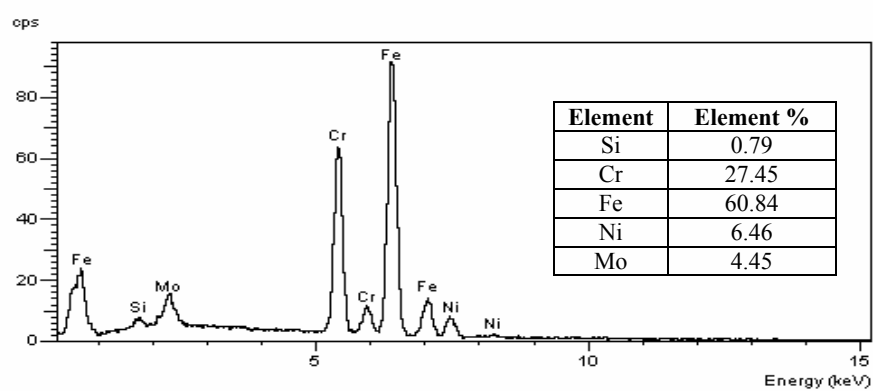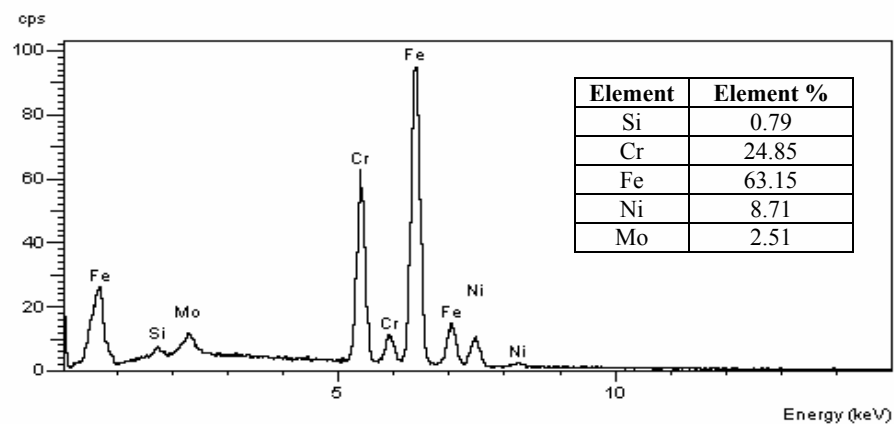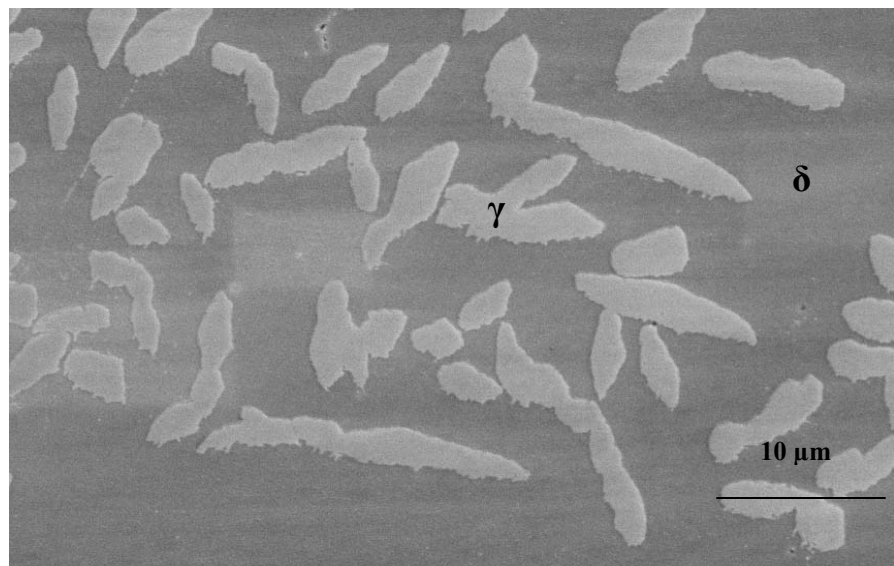
Figure 85: 04J142 (a) Secondary Electron SEM Image, 1000X (b) EDS on Austenite Phase (γ) (c) EDS on Ferrite (δ)

Element	Element %
Si	0.98
Cr	23.5
Fe	63.16
Ni	9.77
Mo	2.59

Element	Element %
Si	0.96
Cr	27.60
Fe	60.5
Ni	5.88
Mo	5.06
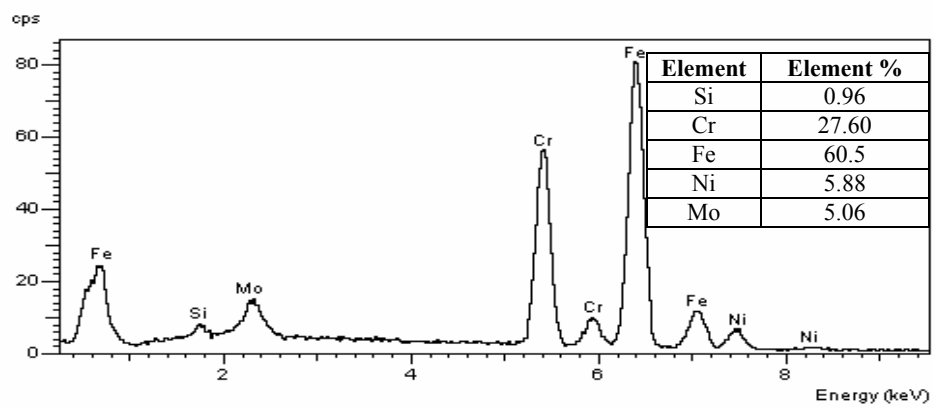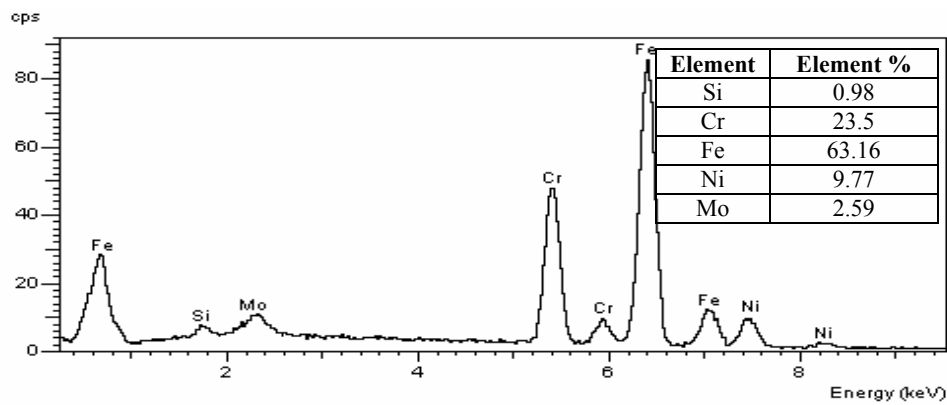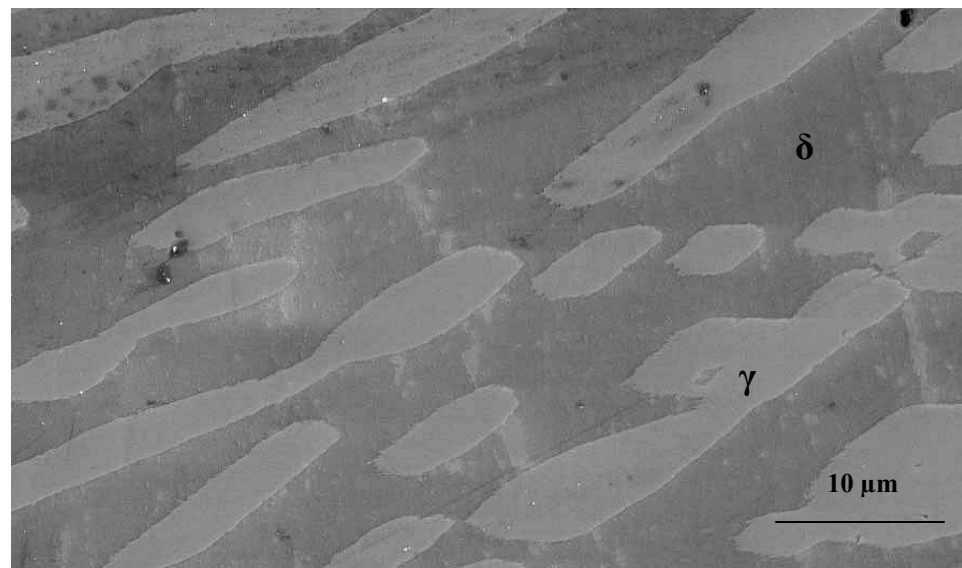
Figure 86: 04J142-A (a) Secondary Electron SEM Image, 1000X (b) EDS on Austenite Phase (γ) (c) EDS on Ferrite (δ)
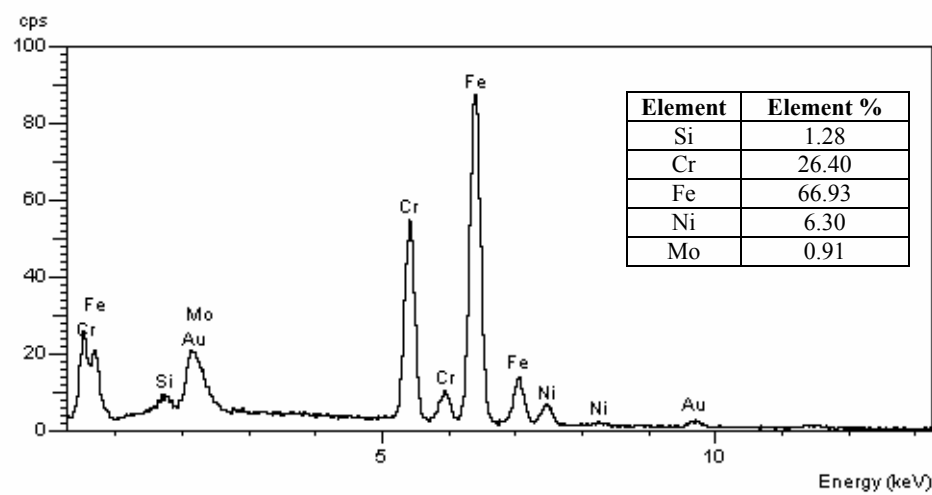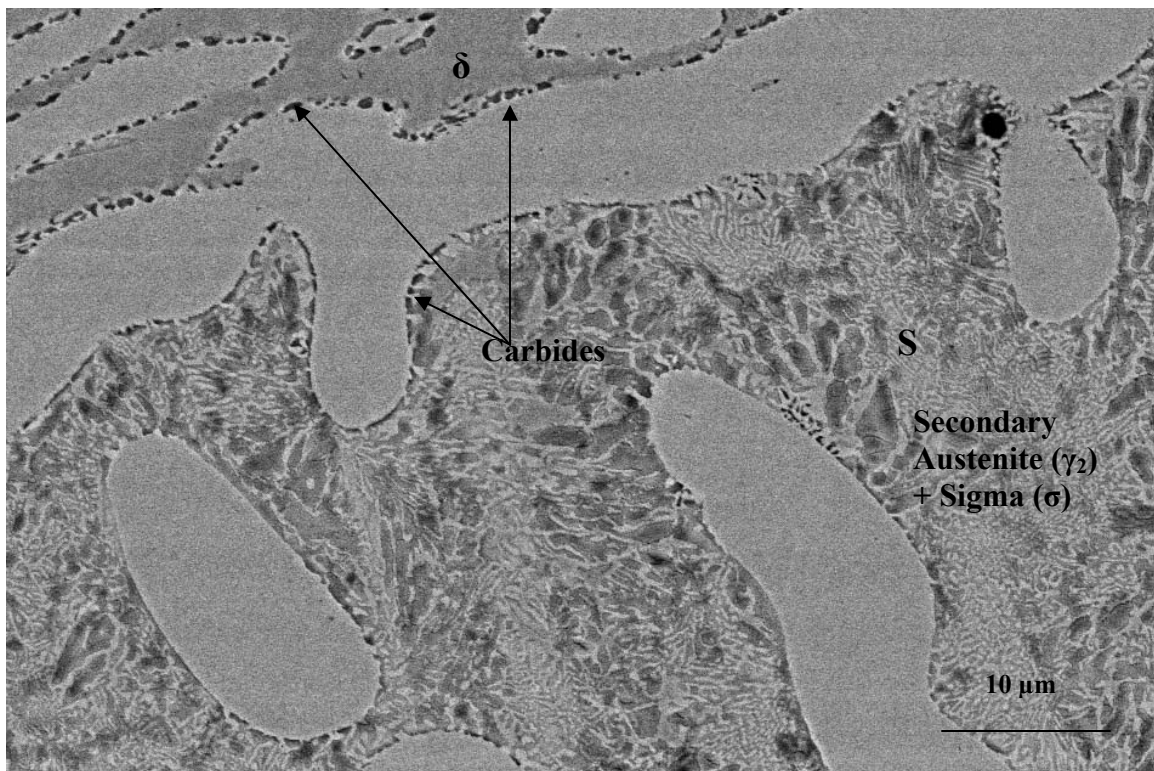
Figure 87: 04J142-B (a) Backscatter SEM Image, 1000X (b) EDS on
Secondary Phase (S)

Element	Element %
Si	1.09
Cr	26.53
Fe	66.22
Ni	7.36
Mo	1.21
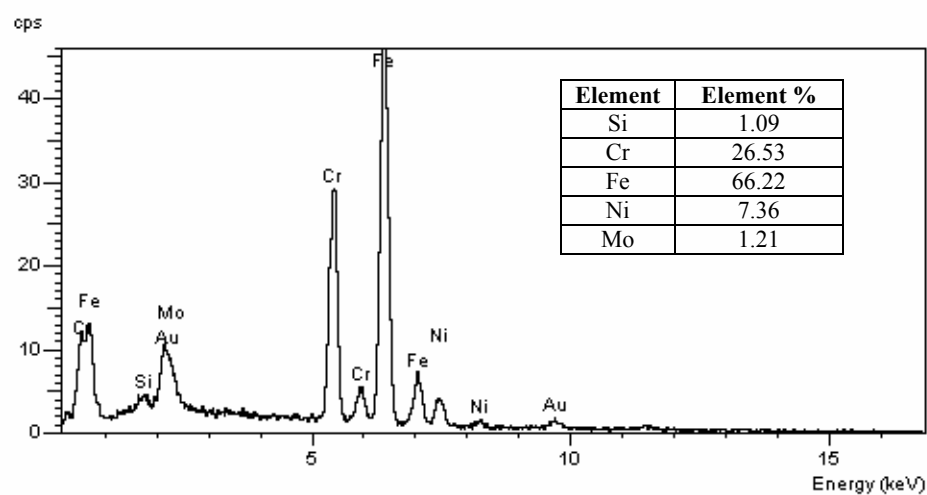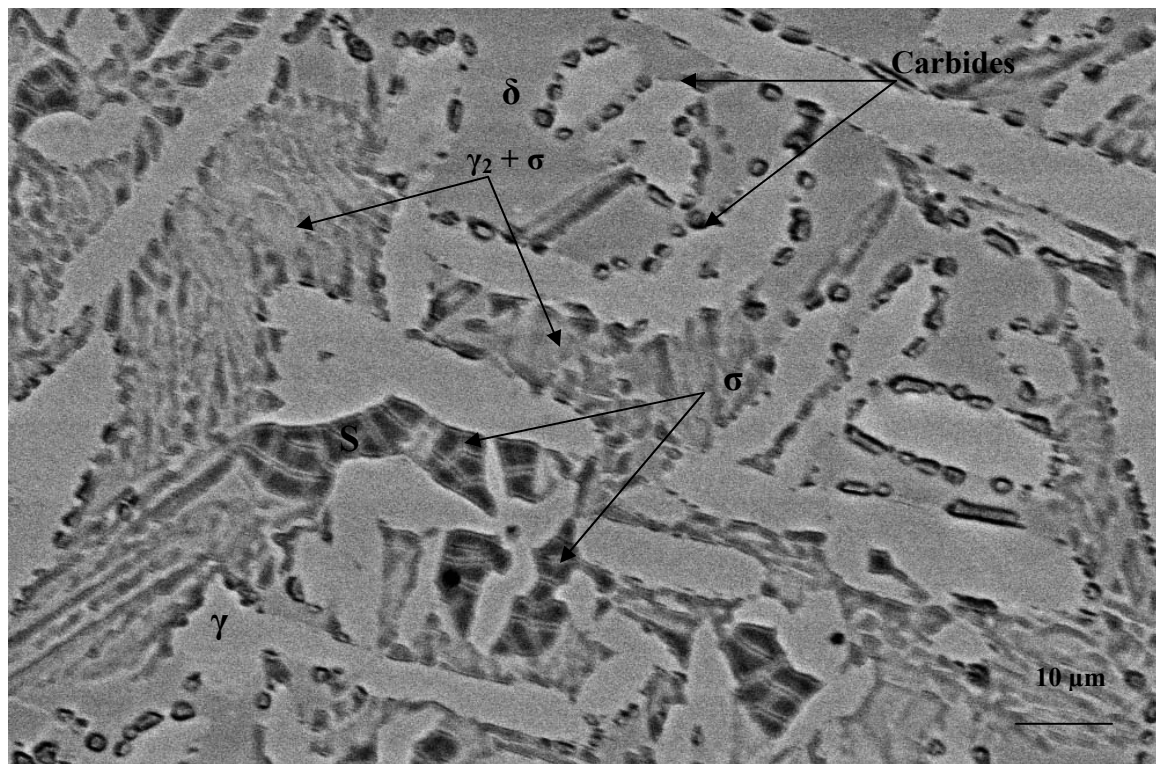
Figure 88: 04J142-C (a) Backscatter SEM Image, 1000X (b) EDS on Secondary Phase (S)
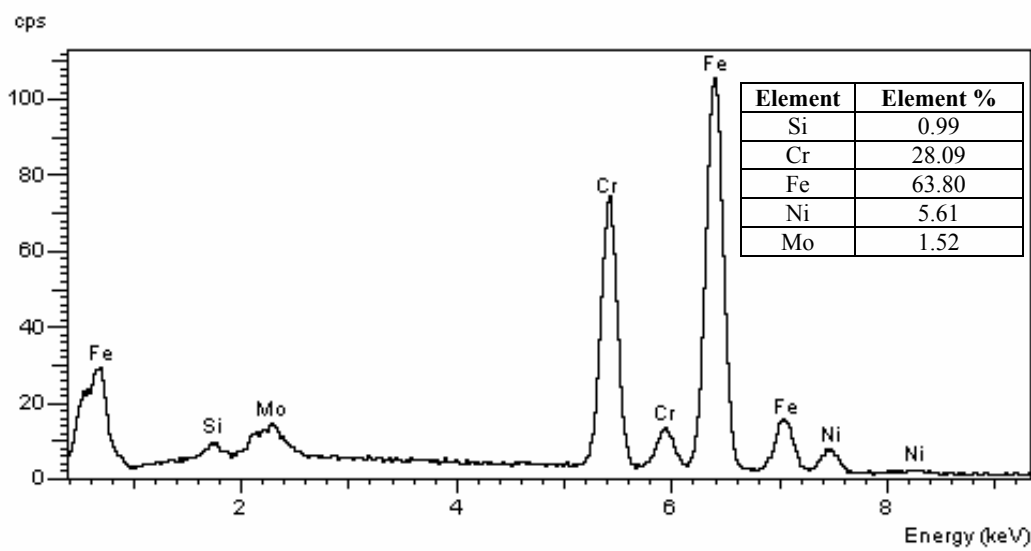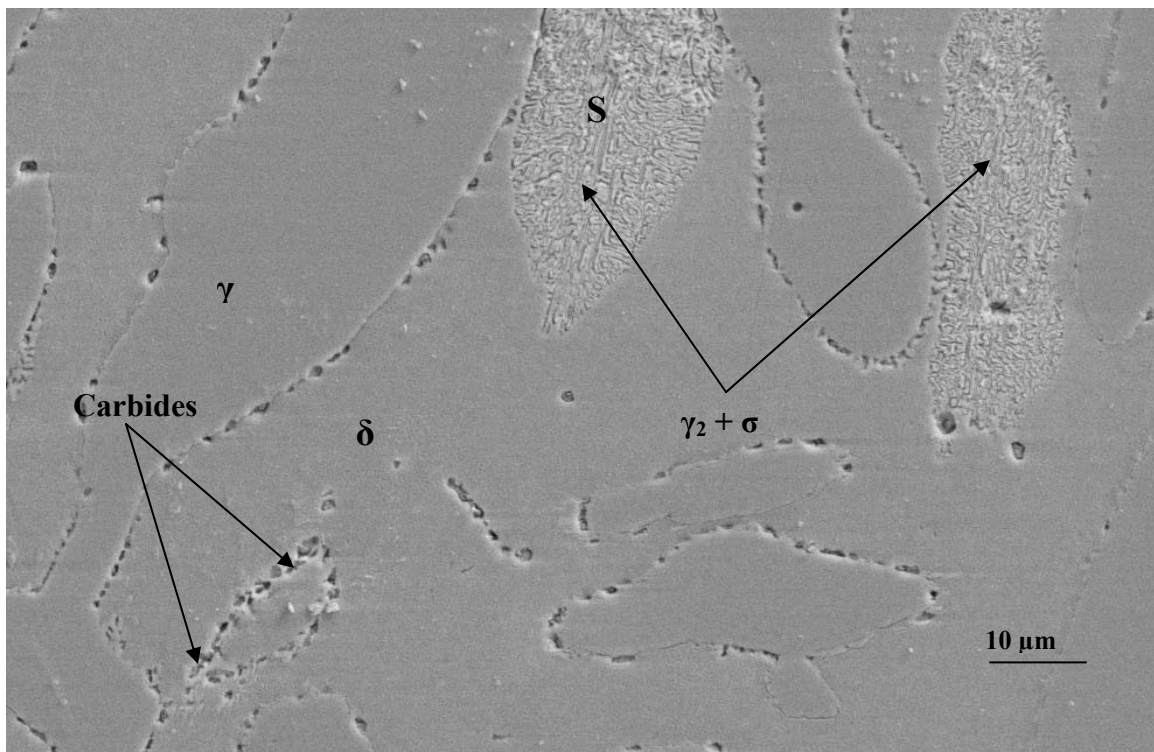
Figure 89: 04J142-D (a) Secondary Electron SEM Image, 1000X (b) EDS on Secondary Phase (S)
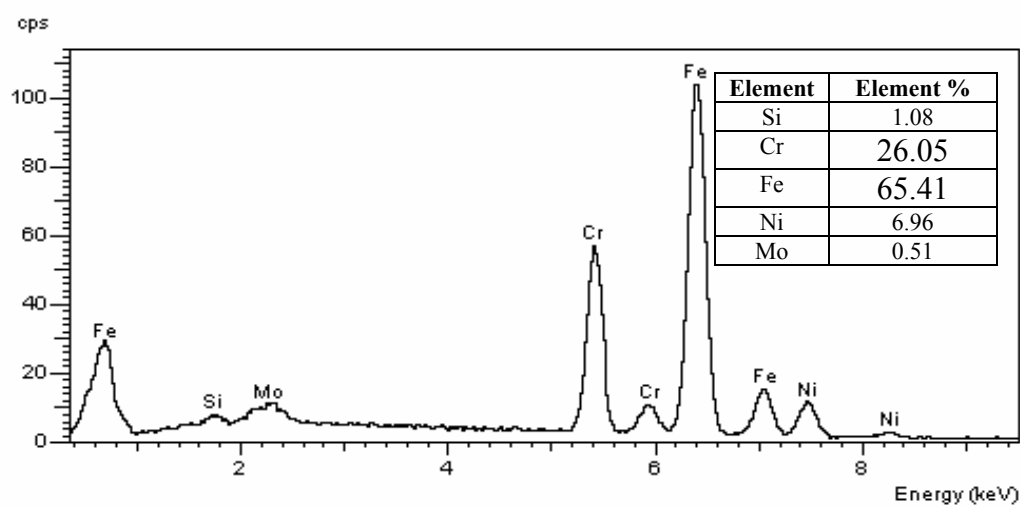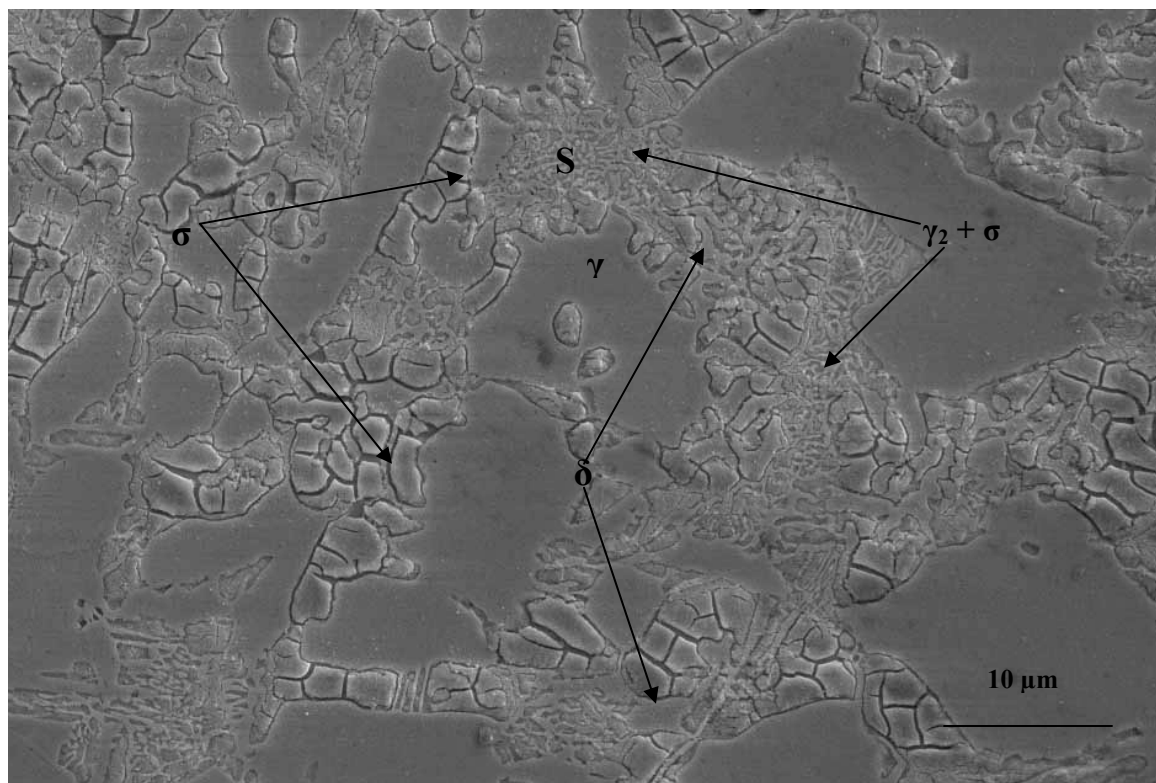
Figure 90: 04J142-E (a) Secondary Electron SEM Image, 1000X (b) EDS on Secondary Phase (S)

143

Element	Element %
Si	1.06
Cr	28.52
Fe	60.38
Ni	6.14
Mo	1.89
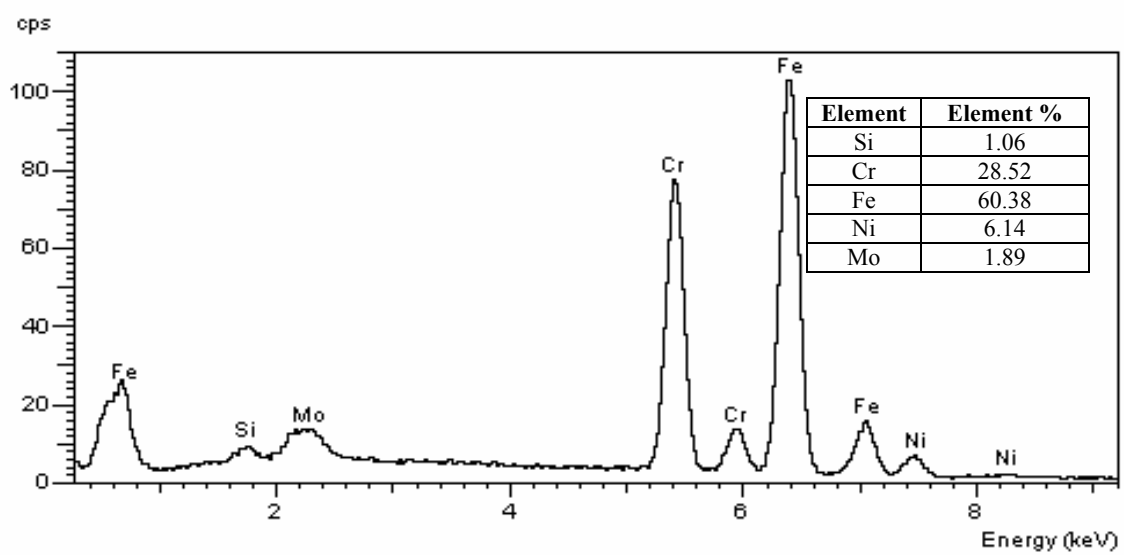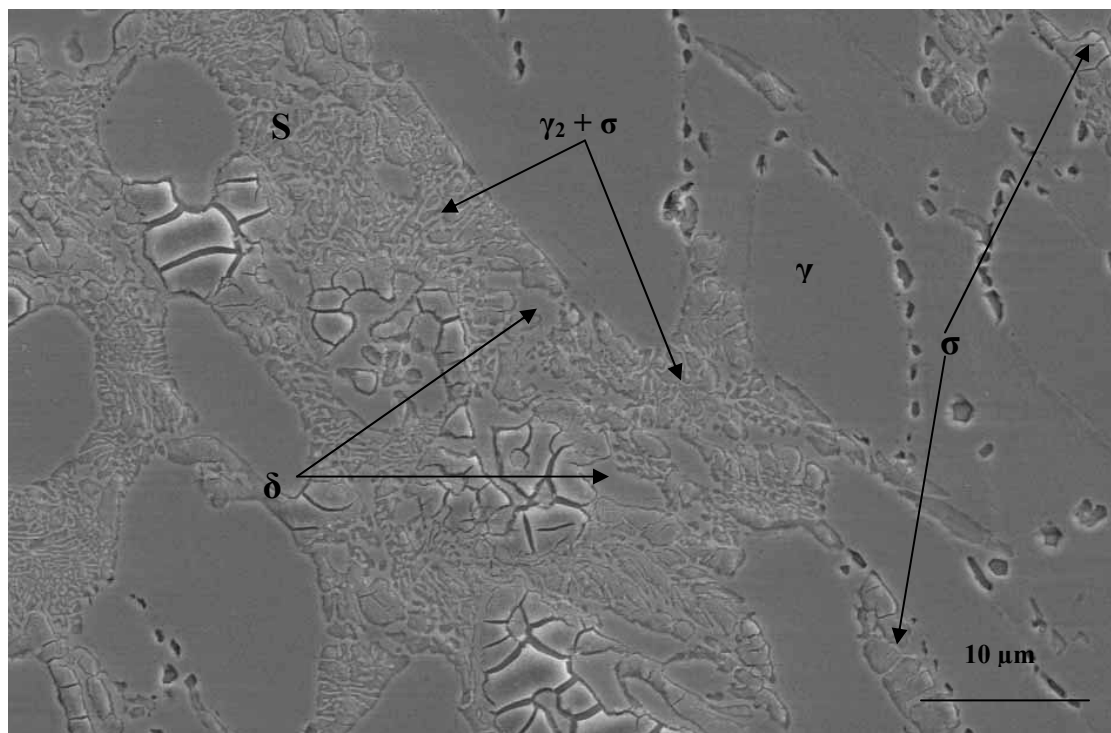
Figure 91: 04J142-F (a) Secondary Electron SEM Image, 1000X (b) EDS on Secondary Phase (S)

144
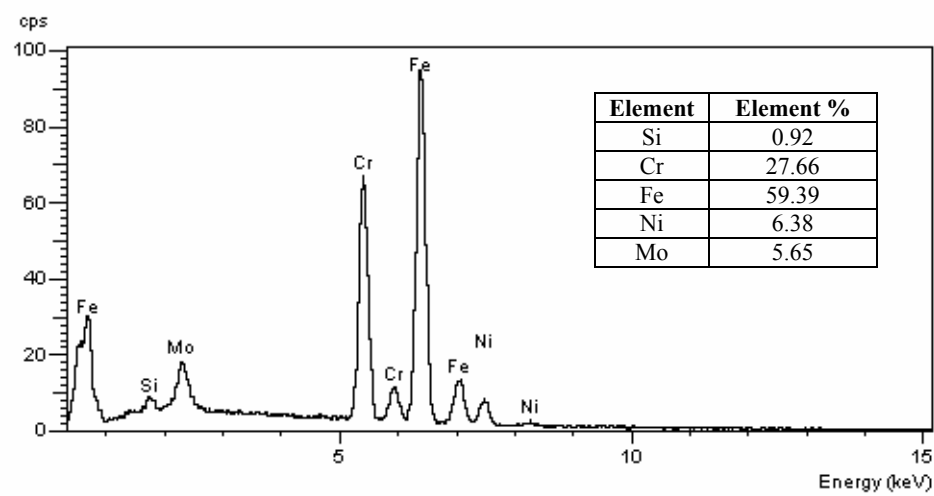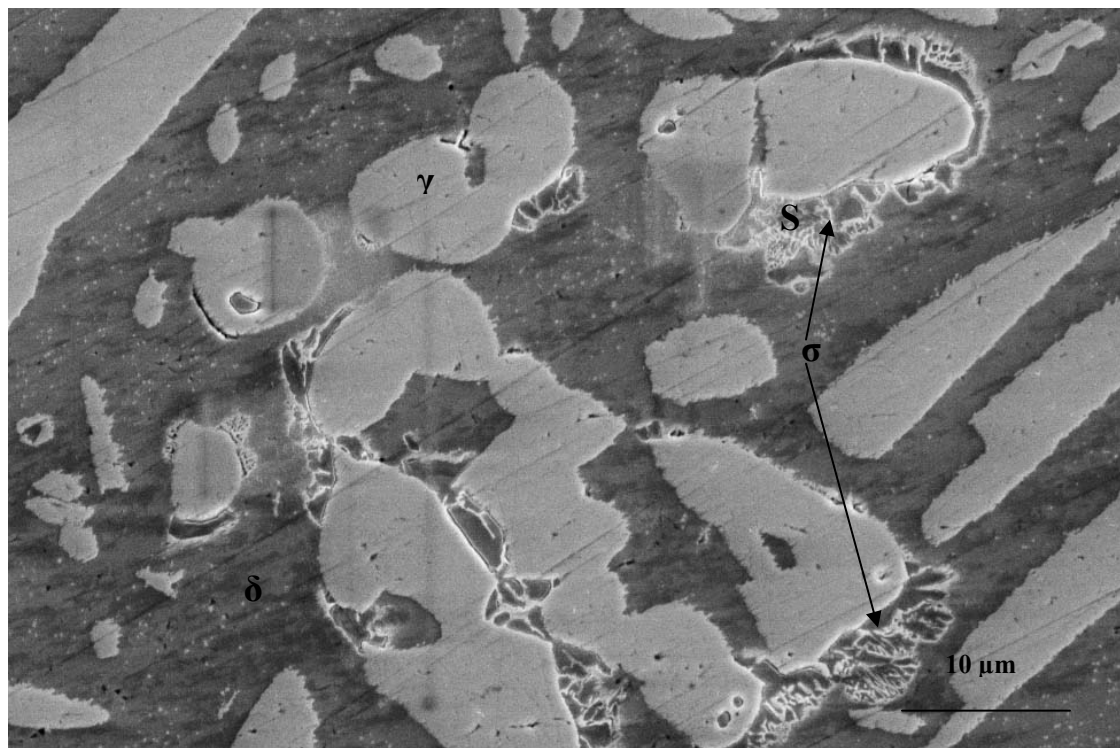
Figure 92: 04J142-G (a) Secondary Electron SEM Image, 1000X (b) EDS on
Secondary Phase (S)
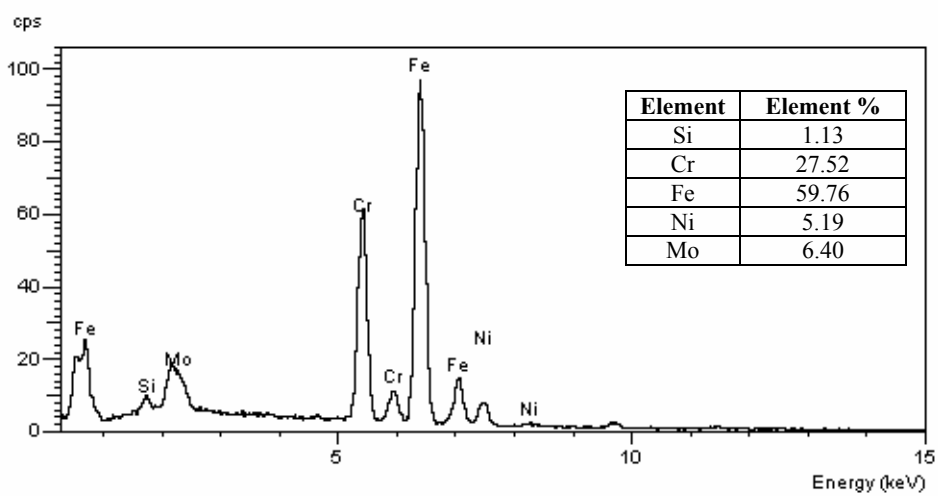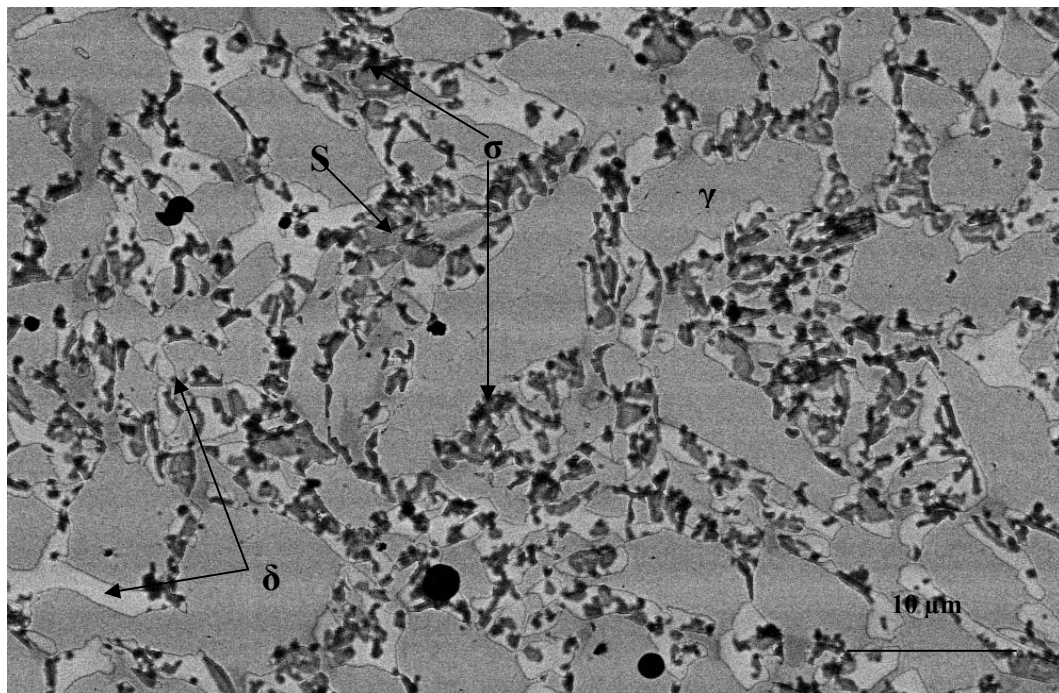
Figure 93: 04J142-H (a) Backscatter SEM Image, 1000X (b) EDS on Secondary Phase (S)

From the SEM micrographs the presence of intermetallic phases can be identified. All the samples which had undergone heat treatment schedule "B", "C", "D", "E", "F", "G" and "H" had intermetallic phases. Back scatter was carried out on some of the samples in order to more clearly identify the intermetallic phases as it is easier to differentiate between different phases using back scatter image compared to secondary electron image. By carrying out EDS on all these samples it was possible to identify the intermetallic phase as well as the composition. The solution annealed and the heat treatment "A" sample contained only austenite and ferrite phase. From EDS it was possible to identify the ferrite and austenite phase respectively. The austenite phase contained a lower percentage of chromium and molybdenum and higher nickel content as compared to the ferrite phase. Both the samples had similar chemical composition (Figure 85 and 86).

In the heat treatment sample "B", "C", "D", "E" and "F" $\gamma_2 + \sigma$ (Secondary austenite + Sigma) phases were identified. All these samples had undergone the second stage of heat treatment. The second stage is heating the sample to 843°C (1550°F) and holding for different time periods before water quenching. The $\gamma_2 + \sigma$ phases are precipitated between 700°C to 900°C. Growth of these phases into the δ phase can be observed in the SEM images. The precipitate of carbides could also be observed in samples from heat treatment "B", "C" and "D" samples along the γ/δ and γ/γ_2 interphase boundaries[157] as observed from the SEM images.

SEM images revealed that the heat treatment "D" sample contained lower amounts of intermetallic phase when compared to heat treatments "B", "C", "E" and "F". Also in contrast there was higher toughness for heat treatment "D" samples as evident in Figure 43. The heat treatment "G" sample which was air cooled also contained lesser amounts of intermetallic phases as evident from its SEM image (Figure 92). The SEM images of heat treatment "A", "G" and "H" samples indicated that as the toughness of these samples decreased in the order of "A"> "G">"H", intermetallic phases increased in the same order from zero in heat treatment "A" samples to a higher amount in heat treatment "H" samples.

In heat treated samples "C", "E", "F", "G" and "H" σ (Sigma) phase was observed on the γ/δ interphase boundaries. From the SEM image of heat treatment "H" sample it was observed that the amount of sigma present was high. This also explains the higher value of hardness of this sample on the Rockwell B and C scale because presence of sigma phase increases hardness. The amount of sigma present in the heat treatment "G" sample was less compared to heat treatment "H" sample. From this it can be concluded that slow cooling tends to transform more of ferrite into sigma as compared to air cooling.

There does not appear to be a correlation between volume percent ferrite and the precipitation of detrimental intermetallic phases. With the precipitation of intermetallic phase the volume percent of ferrite should decrease. This was observed only in heat treatment "C", "E", "F" and "G" samples. The volume percentage of ferrite was approximately 50 for heat treatment "B", "D" and "G" (Table 15) samples though intermetallic phases were observed in these samples. This suggests that volume percent of ferrite is not a good indicator of amount of detrimental intermetallic phases.

SEM was also carried out on the foundry solution annealed samples from Foundry A, B and C. The images are included in Appendix C.

9. Determination of Various Phases in the Samples using X-Ray Analysis

X- Ray analysis was carried out to determine different phases and the percentage of different phases present in the solution annealed and heat treated samples in order to compare the results with the Feritscope® data.

The following diffraction patterns (Figure 94 – 105) were acquired by running XRD on samples procured from four foundries. The γ – 200 (Austenite Peak) and δ – 002 (Ferrite Peak) peaks were used from these patterns for calculating the percentage of the phases present in these samples.

Figure 94: Diffraction Pattern of 285

Figure 95: Diffraction Pattern of 331

149
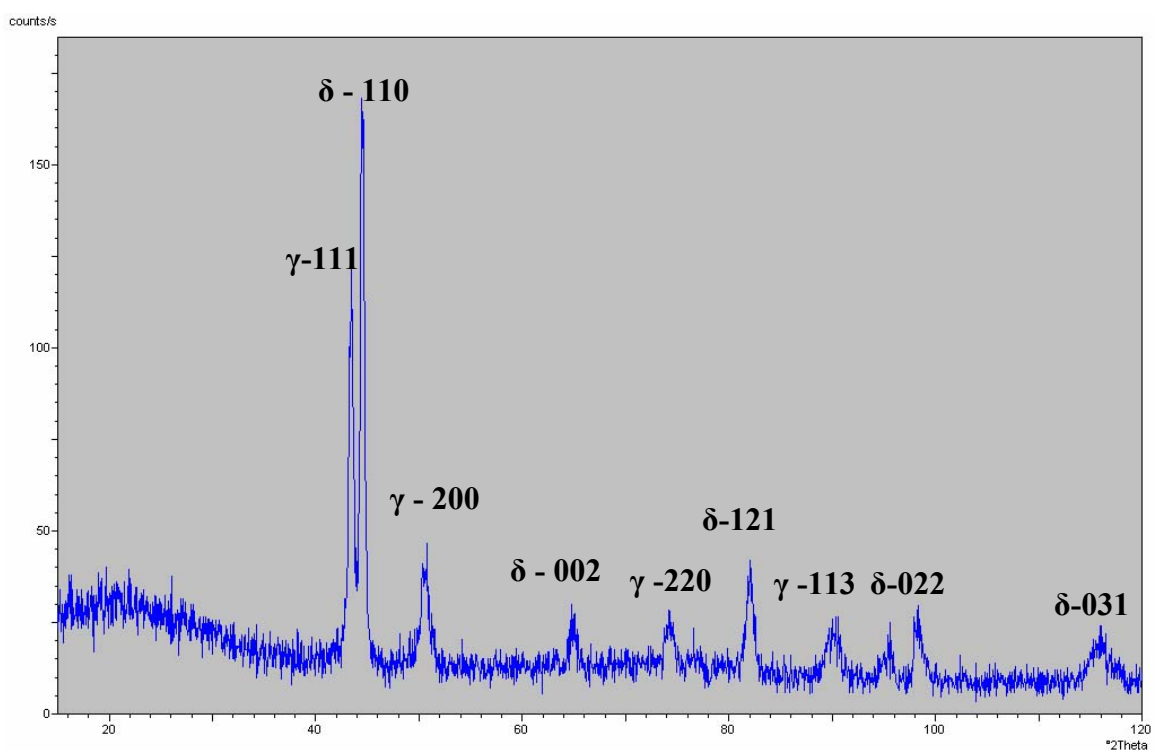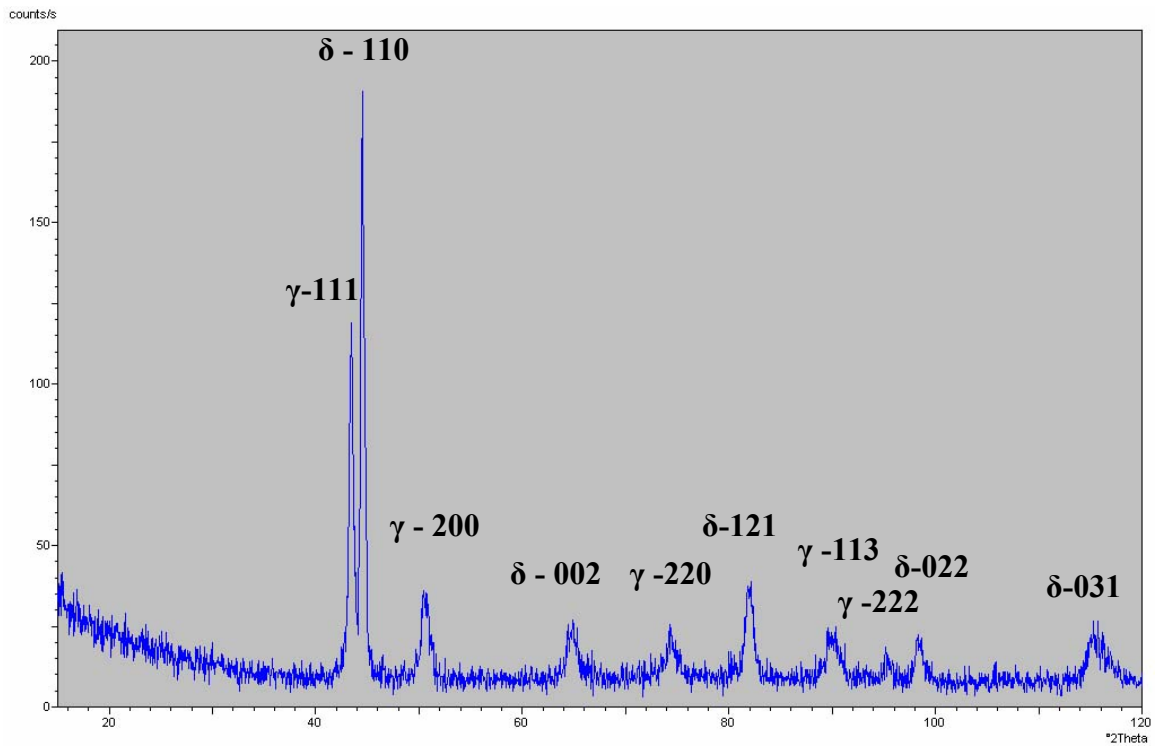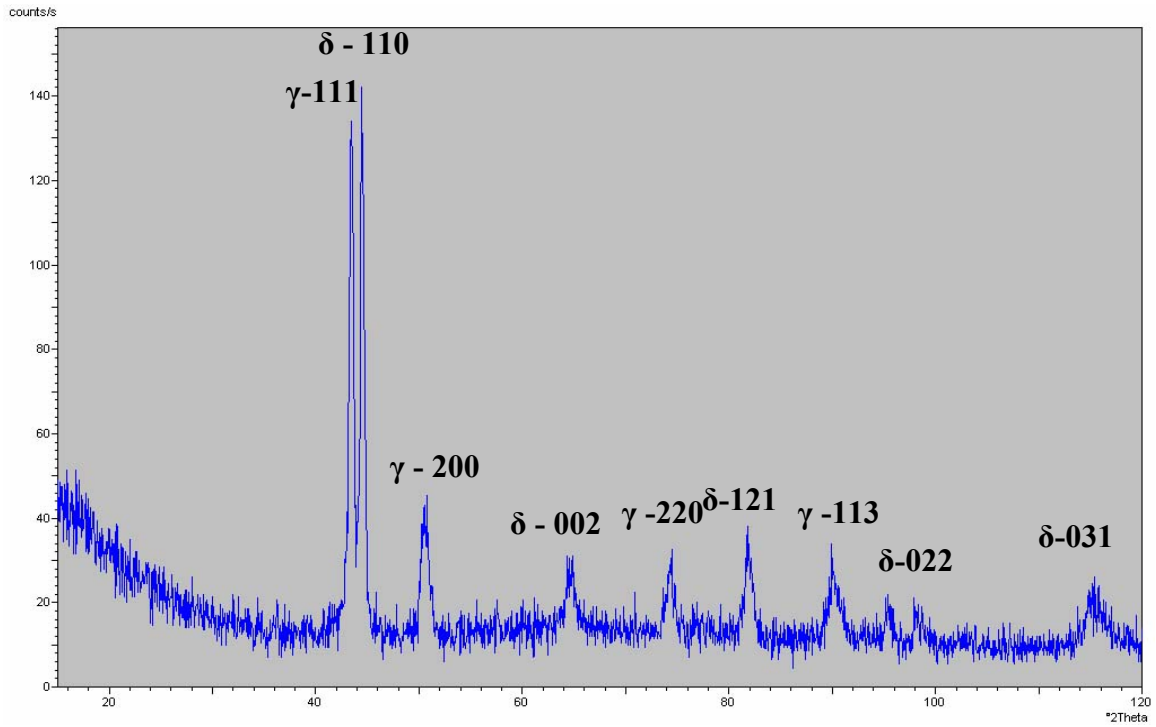
Figure 96: Diffraction Pattern of 144
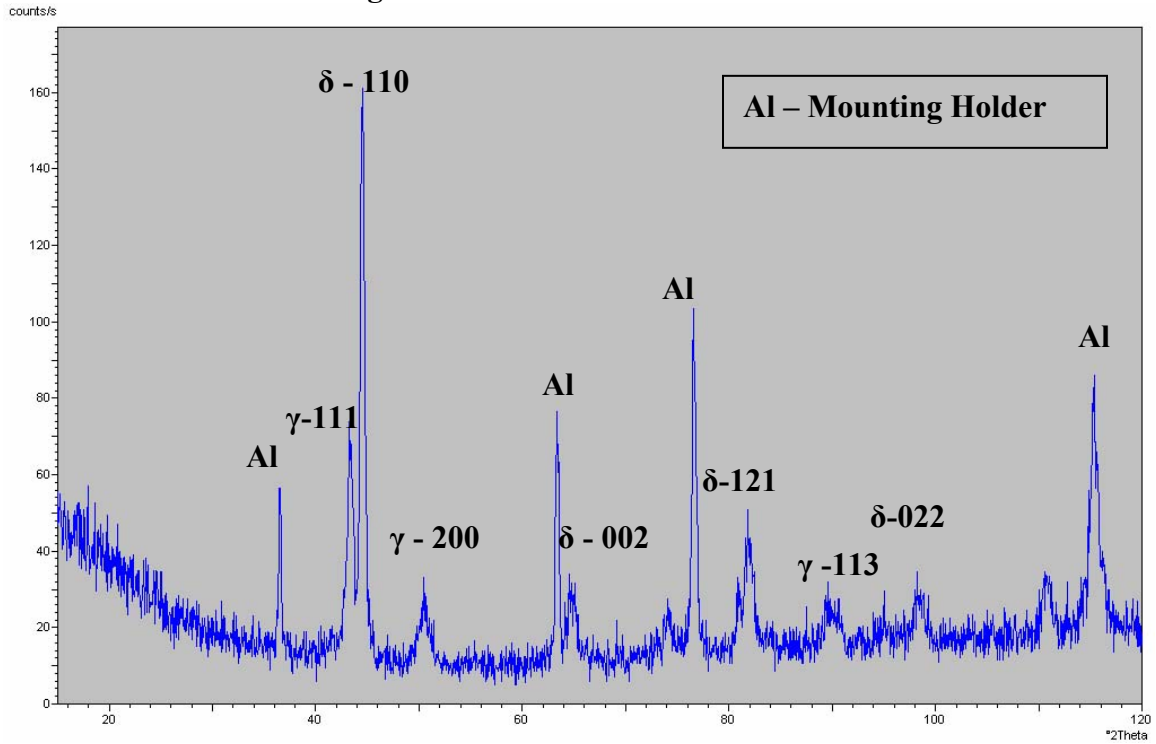
Figure 97: Diffraction Pattern of S1507

150
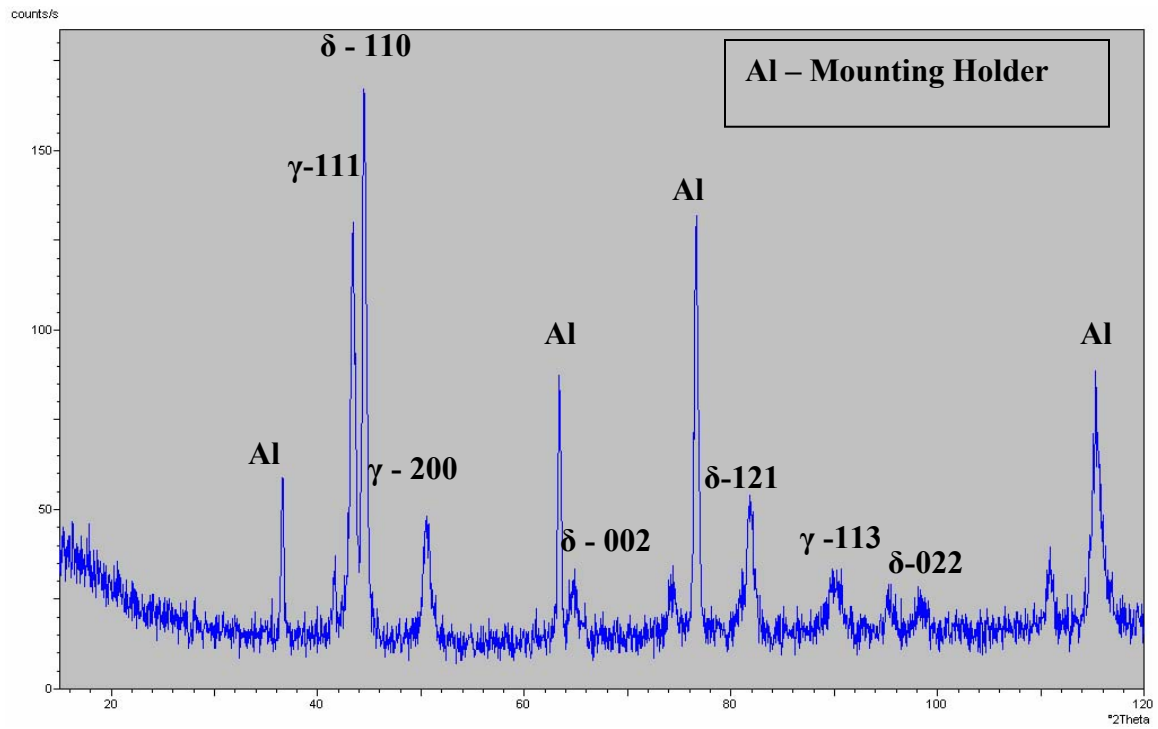
Figure 98: Diffraction Pattern of S1508
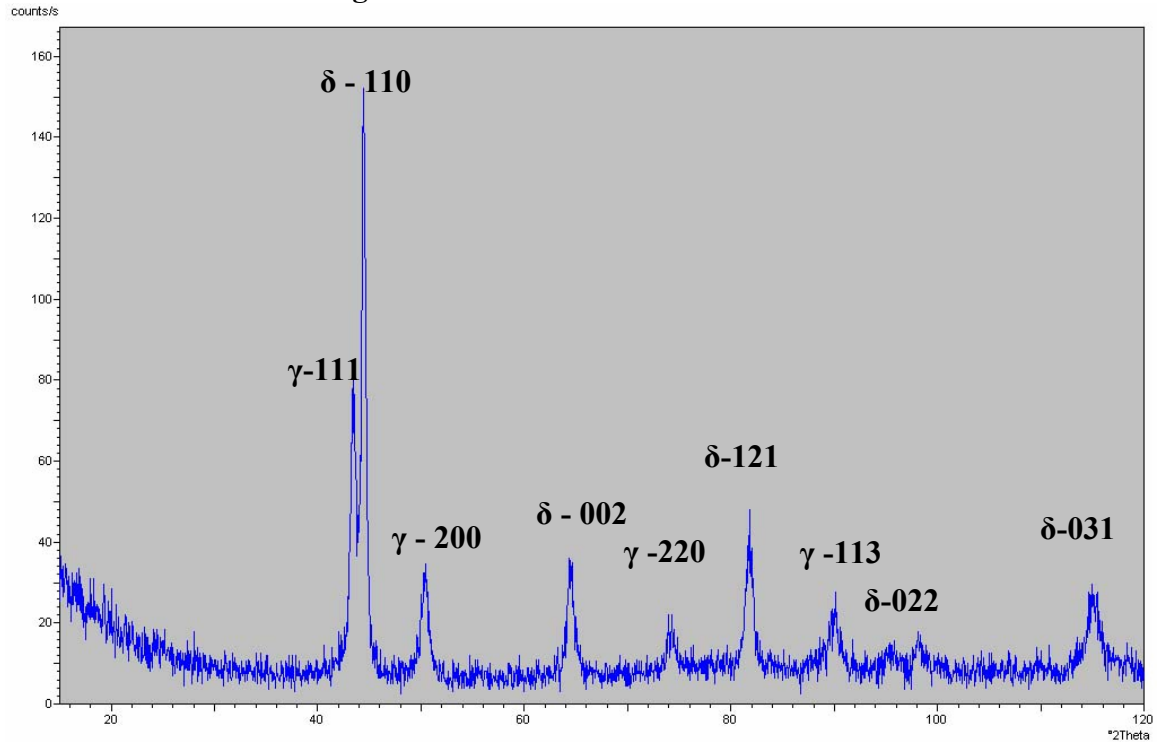
Figure 99: Diffraction Pattern of 41544

151
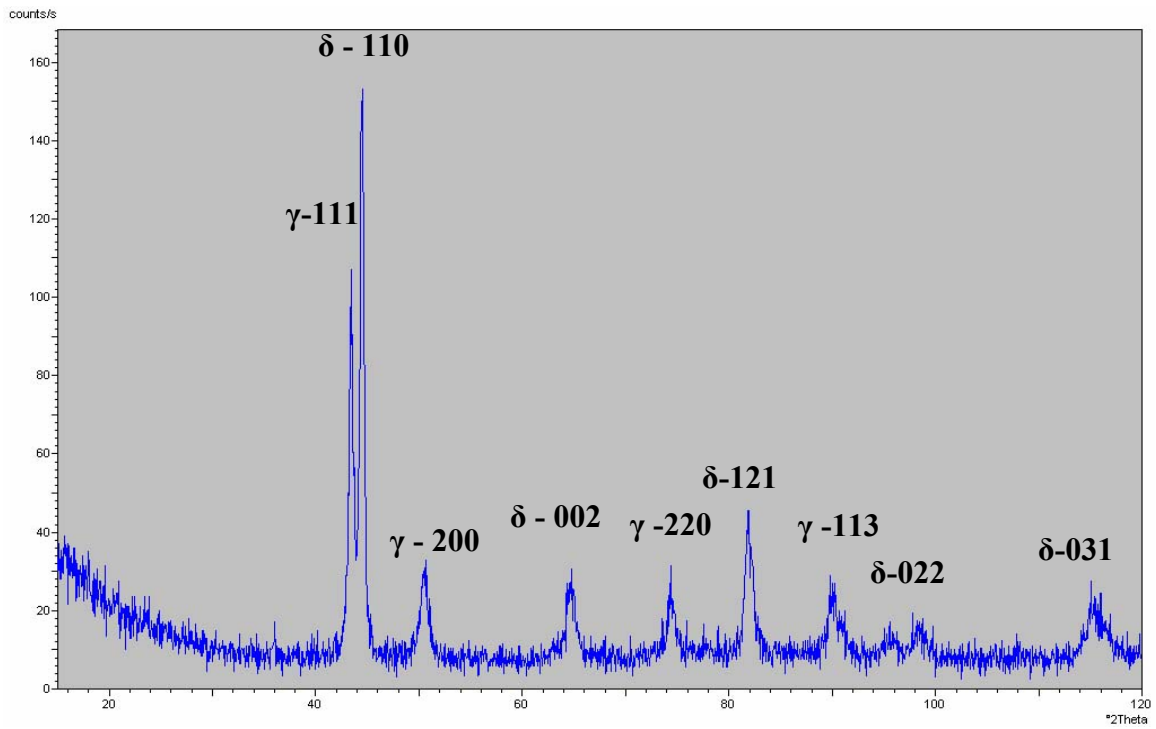
Figure 100: Diffraction Pattern of 44073
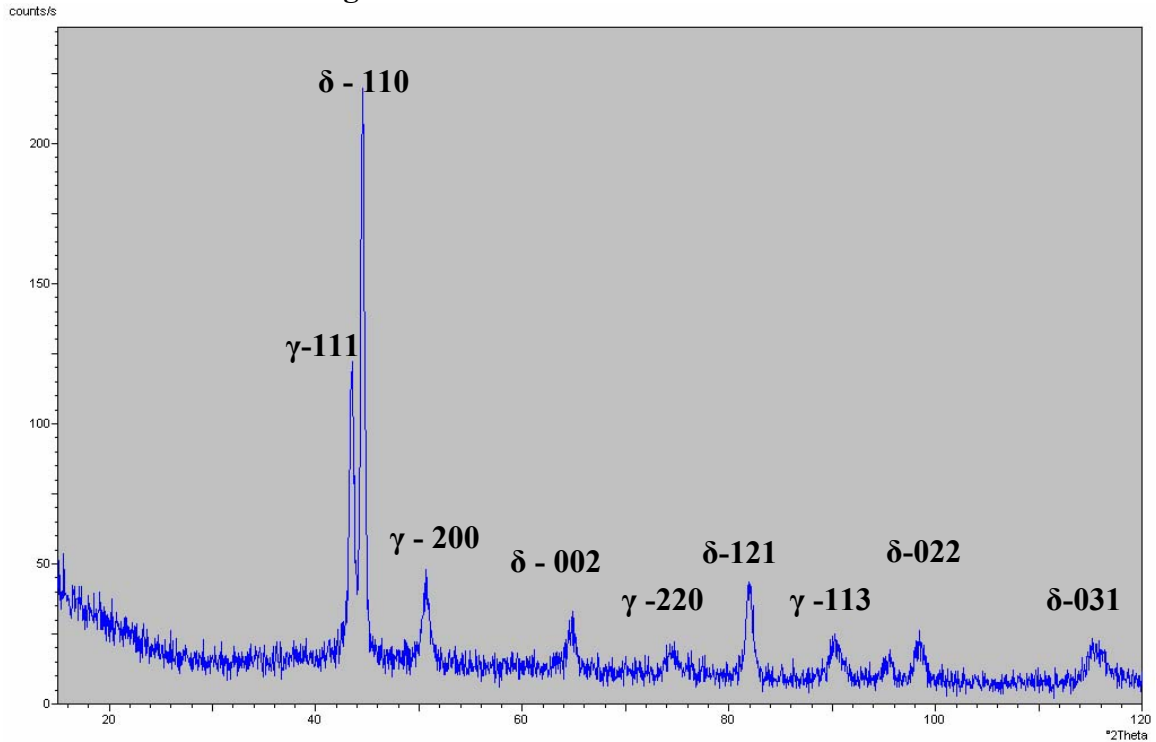
Figure 101: Diffraction Pattern of 41414

152

Figure 102: Diffraction Pattern of 45633

Figure 103: Diffraction Pattern of 41374

153
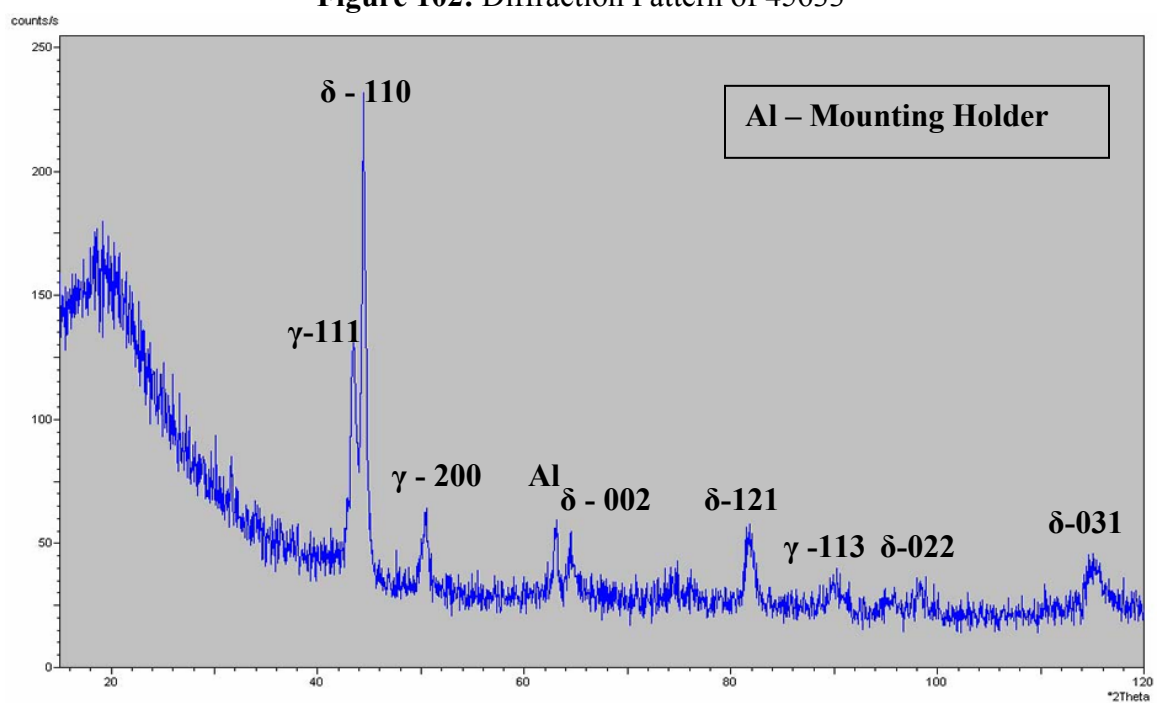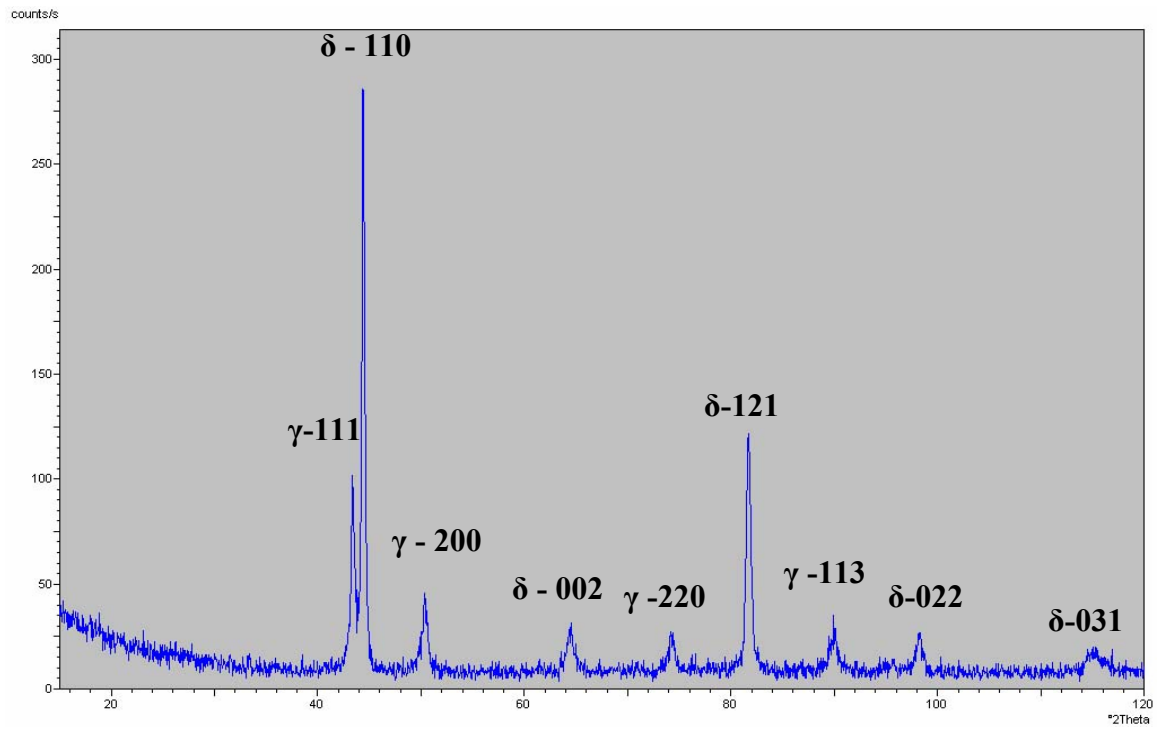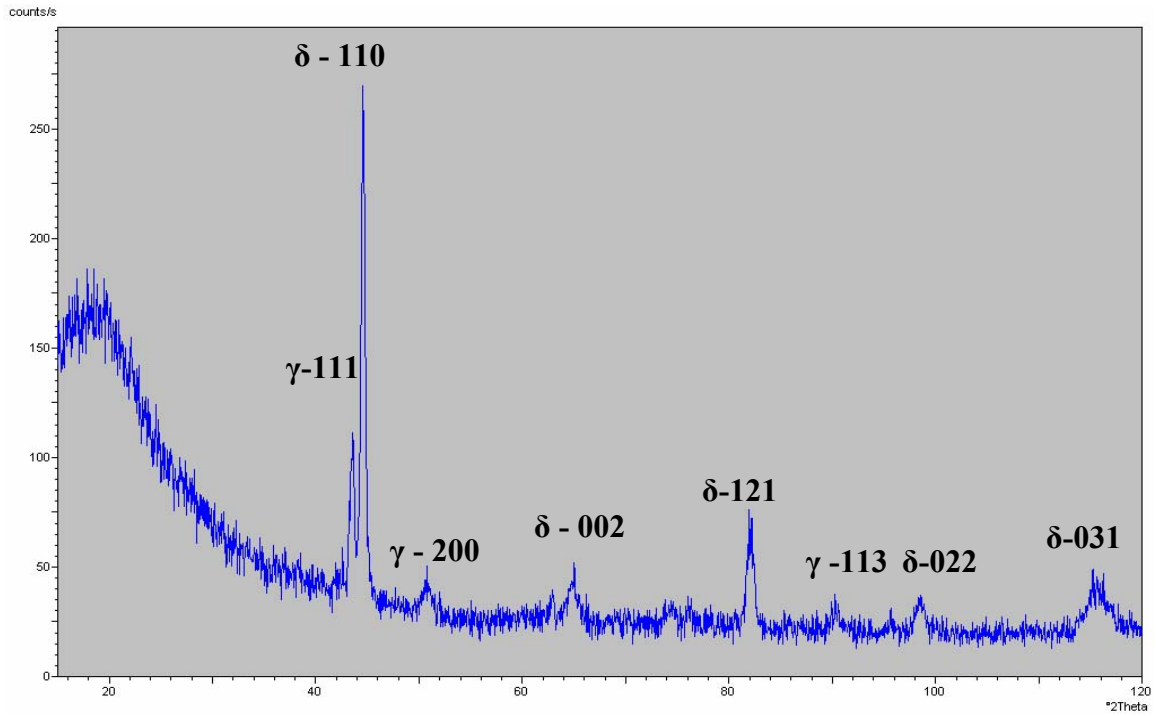
Figure 104: Diffraction Pattern of 04J142
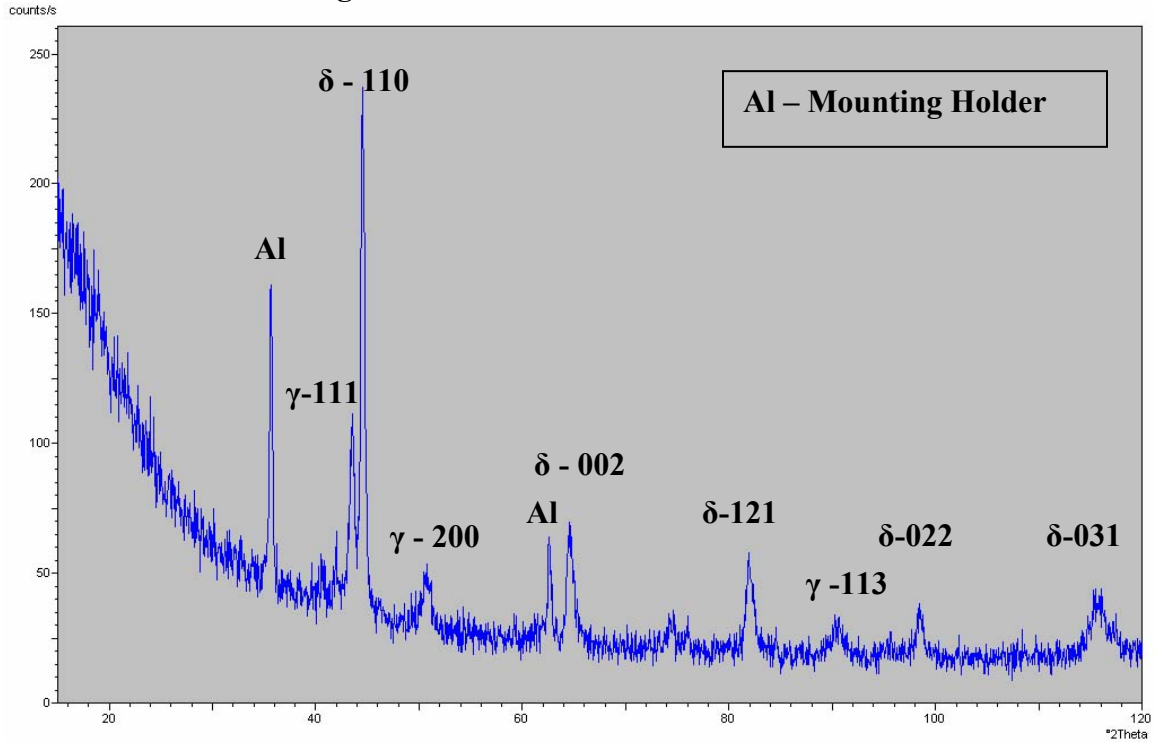
Figure 105: Diffraction Pattern of 04J142 – A

154

All the foundry solution annealed samples from Foundry A, B, C, D and heat treatment "A" sample from Foundry D contained only two phases: Austenite and Ferrite. The Direct Comparison Method[164] was used to calculate the percentage of different phases present in the sample from XRD. The (200) peak of austenite and (002) peak of ferrite was chosen to carry out the calculations because they fall in the same family of planes hence have the same multiplication factor which makes the calculation simple. The (110) peak of ferrite had the highest intensity, still we used the (002) peak because the (110) peak was too close to an austenite peak (111) and it is not desirable to use two close peaks for phase determination. In the samples S1508, S1507, 41374 and 04J142 – A additional peaks are seen other than the austenite and ferrite peaks. These peaks belong to the background material, which is Aluminum on which the sample was mounted to carry out X-Ray diffraction. These peaks are labeled as "Al". The following tables (Table 18 – 20) show the percentage of austenite and ferrite phase in the samples.

Table 18: Calculation of Lorentz Polarization Factor and Temperature Factor for Austenite Phase

Sample ID	Austenite Phase (γ)							
	Theta (θ)	d (Å)	Sinθ	Cosθ	$Sin^2\theta$	$Cos^2 2\theta$	LP	TF
285	25.2085	1.8086	0.4259	0.9047	0.1814	0.4060	8.5667	0.6321
331	25.1756	1.8107	0.4253	0.9050	0.1809	0.4071	8.5921	0.6328
144	25.1465	1.8128	0.4249	0.9052	0.1805	0.4081	8.6148	0.6334
S1507	25.2301	1.8070	0.4262	0.9046	0.1816	0.4052	8.5500	0.6316
S1508	25.3226	1.8009	0.4277	0.9039	0.1829	0.4021	8.4790	0.6296
45633	25.1719	1.8109	0.4253	0.9050	0.1809	0.4072	8.5950	0.6329
41414	25.3696	1.7978	0.4284	0.9035	0.1835	0.4004	8.4432	0.6286
41544	25.2066	1.8086	0.4258	0.9047	0.1813	0.4060	8.5681	0.6321
44073	25.2594	1.8051	0.4267	0.9043	0.1820	0.4042	8.5274	0.6310
41374	25.2461	1.8060	0.4265	0.9044	0.1819	0.4047	8.5376	0.6313
04J142	25.3701	1.7977	0.4284	0.9035	0.1835	0.4004	8.4430	0.6286
04J142-A	25.3927	1.7962	0.4288	0.9033	0.1838	0.3997	8.4258	0.6281

Table 19: Calculation of Lorentz Polarization Factor and Temperature Factor for Ferrite Phase

Sample ID	Ferrite Phase (δ)							
	Theta (θ)	D (Å)	Sinθ	Cosθ	Sin$^2\theta$	Cos^{2}2θ	LP	TF
285	32.3524	1.4394	0.5351	0.8447	0.2863	0.1825	4.8884	0.4848
331	32.4510	1.4355	0.5365	0.8438	0.2879	0.1799	4.8564	0.4829
144	32.3165	1.4408	0.5345	0.8451	0.2857	0.1835	4.9002	0.4855
S1507	32.4326	1.4362	0.5363	0.8440	0.2876	0.1804	4.8624	0.4832
S1508	32.4306	1.4363	0.5362	0.8440	0.2875	0.1804	4.8630	0.4832
45633	32.2163	1.4448	0.5331	0.8460	0.2842	0.1862	4.9333	0.4874
41414	32.4109	1.4371	0.5359	0.8442	0.2872	0.1809	4.8694	0.4836
41544	32.2455	1.4437	0.5335	0.8457	0.2846	0.1854	4.9236	0.4868
44073	32.3306	1.4403	0.5348	0.8449	0.2860	0.1831	4.8956	0.4852
41374	31.5267	1.4731	0.5228	0.8523	0.2734	0.2053	5.1718	0.5009
04J142	31.4512	1.4762	0.5217	0.8530	0.2722	0.2074	5.1991	0.5024
04J142-A	31.2902	1.4830	0.5193	0.8545	0.2697	0.2120	5.2580	0.5056

Table 20: Percentage of Ferrite and Austenite in the Diffraction Samples

Sample ID	R_δ/R_γ	I_δ/I_γ	C_δ/C_γ	% of Austenite	% of Ferrite
285	0.4208	0.5177	1.2300	44.8	55.2
331	0.4147	0.3360	0.8100	55.2	44.8
144	0.4192	0.5147	1.2200	44.7	55.3
S1507	0.4184	1.1830	2.8273	26.1	73.9
S1508	0.4233	0.4902	1.1579	46.3	53.7
45633	0.4251	0.5572	1.3107	43.3	56.7
41414	0.4267	0.4945	1.1588	43.2	56.8
41544	0.4256	1.0558	2.4806	28.7	71.3
44073	0.4245	0.8308	1.9569	33.8	62.2
41374	0.4622	0.9194	1.9890	33.4	62.6
04J142	0.4732	0.8327	1.7596	36.2	63.8
04J142-A	0.4830	2.2572	4.6731	17.6	82.4

For calculating the percentage of austenite and ferrite the following formulae[164] were used:

$$\frac{I_\delta}{I_\gamma} = \left(\frac{R_\delta}{R_\gamma}\right)\left(\frac{C_\delta}{C_\gamma}\right)$$

$$C_{\delta} + C_{\gamma} = 1$$

where,

I_δ = Intensity of ferrite peak
I_γ = Intensity of austenite peak
C_δ = Amount of ferrite phase
C_γ = Amount of austenite phase

$$R = \frac{1}{v}\left[|F_{hkl}|^2\, p\left(\frac{1+\cos^2 2\theta}{\sin^2 \theta \cos\theta}\right)\right]\left(e^{-2M}\right)$$

where,

v = Volume of the unit cell
p = Multiplicity Factor
$|F_{hkl}|$ = Structure Factor
e^{-2M} = Temperature Factor (TF)
$\dfrac{1+\cos^2 2\theta}{\sin^2 \theta \cos\theta}$ = Lorentz Polarization Factor (LP)

$$M = B_q\left(\frac{Sin\theta}{\lambda}\right)^2$$

where,

B_q = Assumed as 3
λ = Wavelength of incident beam (1.54056)

The lattice parameters for austenite and ferrite were taken as 3.58Å and 2.86 Å. The multiplicity factors for both austenite and ferrite peak was 6.

Table 21 shows a comparison between the percentage of ferrite calculated from X-Ray Diffraction and Feritscope®. Figure 106 shows a graphical comparison between the volume percentage of ferrite measured using the Feritscope® and X-ray Diffraction.

Table 21: Volume Percentage Ferrite from X-Ray Diffraction and Feritscope®

Foundry	Sample ID	Volume % Ferrite from X-Ray Diffraction	Volume % Ferrite from Feritscope®
A	285	55.2	46.9
	144	55.3	40.2
	331	44.8	42.3
B	S1507	73.9	56.8
	S1508	53.7	46.4
C	45633	56.7	52.1
	41414	56.8	49.7
	41374	62.6	51.5
	41544	71.3	51.2
	44073	62.2	46.2
D	04J142	63.8	65.9
	04J142 - A	82.4	63.1
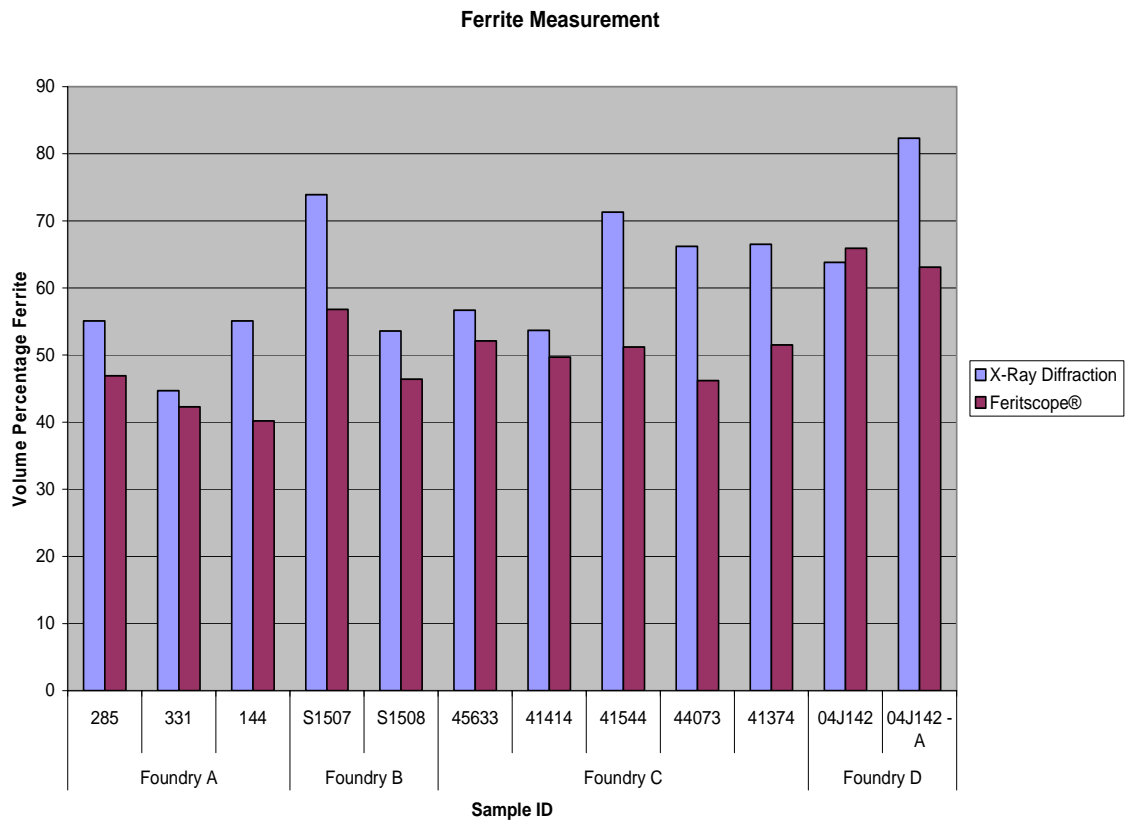
Figure 106: Comparison of Volume Percentage of Ferrite from Feritscope® and X-Ray Diffraction

From the above table we can infer that there is variation in the volume percentage ferrite calculated from the Feritscope® and the X-Ray Diffraction. The volume percentage of ferrite from X-ray Diffraction always overestimated the volume percentage of ferrite calculated from the Feritscope® except for the sample 04J142. This is because of preferred orientation of the crystals in a particular direction which results in the measured intensities of diffractions being incorrect. This affects the quantitative analysis of the various phases present. In the case of sample 04J142 the volume percentage ferrite calculated from the Feritscope® is more than the volume ferrite from X-Ray Diffraction by a small percentage. This may be because the ferrite calculated from the Feritscope® is an average of 10 values with some of the values being more than the volume percentage

ferrite calculated from X-Ray Diffraction. In all the other samples the maximum value calculated from the Feritscope® was less than the volume ferrite calculated from X-Ray Diffraction. It can be concluded that X-Ray Diffraction is not sufficiently sensitive for quantitative analysis of phases present.

X-Ray analysis was also carried out on the samples from Foundry D, which had intermetallic phases in them. Some of the diffraction patterns of the samples are shown below (Figure 107 and 108).

These diffraction patterns are similar to the patterns which were acquired for samples which did not have any intermetallic phases. The patterns does not show any peaks corresponding the intermetallic phases. This is because the percentage of different intermetallic phases present is low compared to the austenite and ferrite phase and X-Ray does not have the capability of showing up such peaks. It can be concluded that X-Ray Diffraction has a limitation in identification of phases. It has the capability of identifying phases like austenite and ferrite but cannot identify small amounts of intermetallic phases.
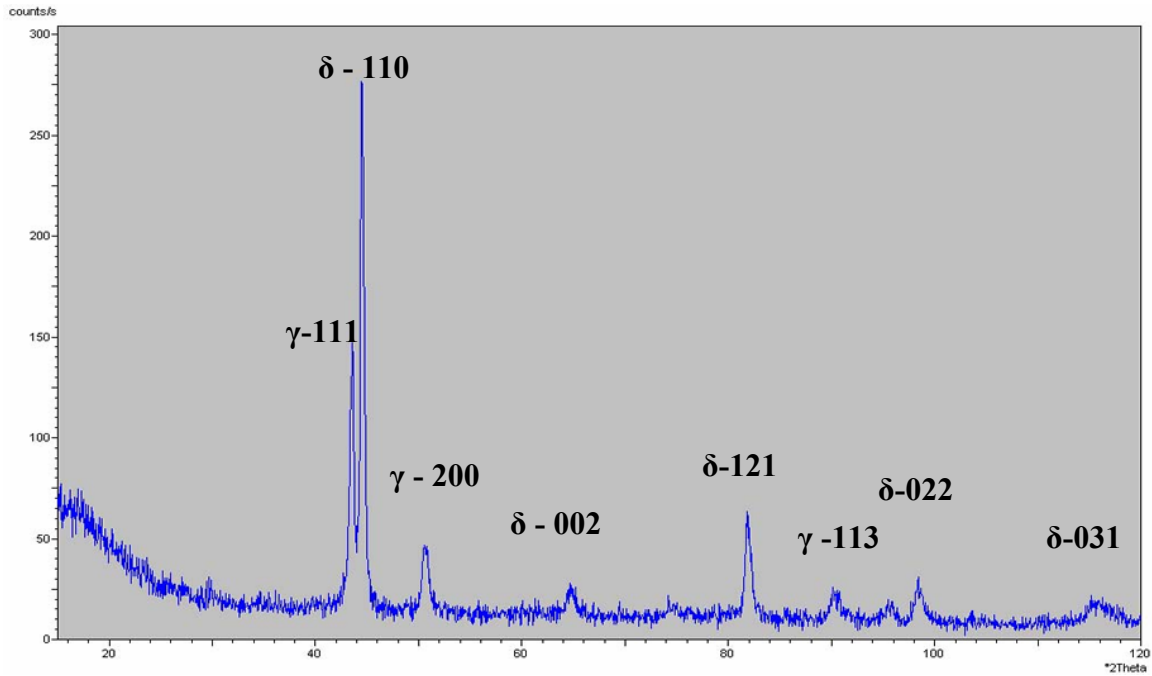
Figure 107: Diffraction Pattern of 04J142 – B
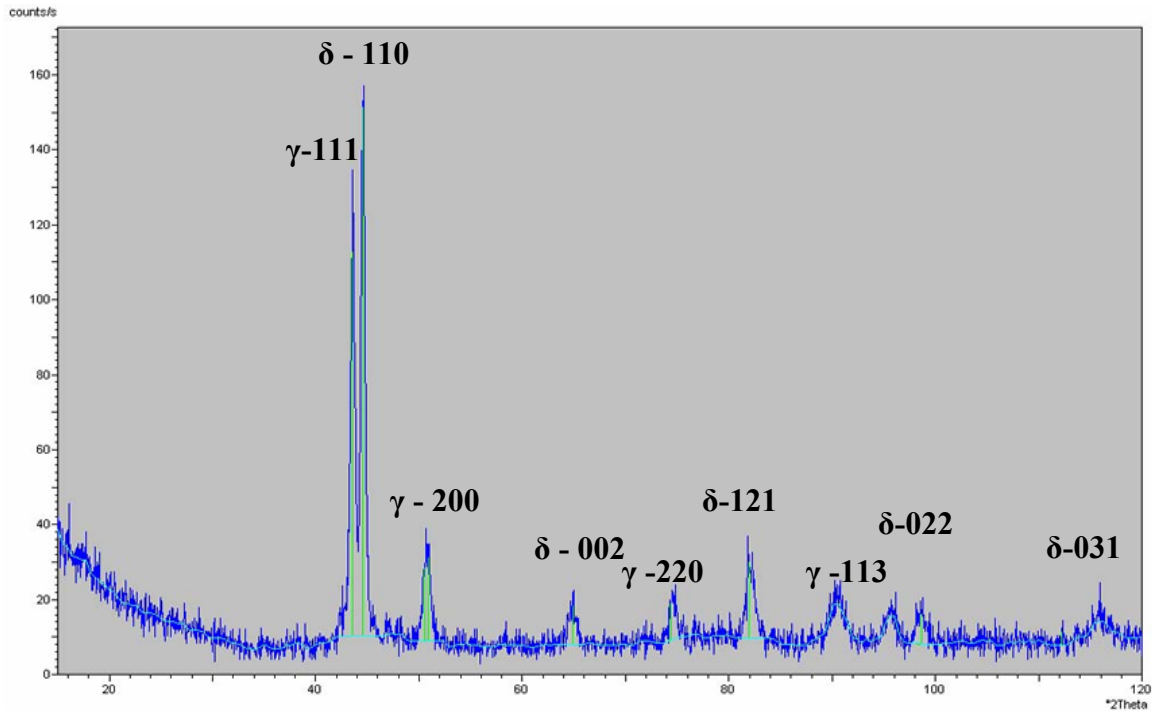
Figure 108: Diffraction Pattern of 04J142 – C

10. Comparison of Volume Percentage Ferrite calculated from the Feritscope®, ASTM E562 Manual Point Count and X-Ray Diffraction

The volume Percentage of ferrite can be calculated from three different techniques:

1. Feritscope®
2. ASTM E562 Manual Point Count
3. X-Ray Diffraction

Figure 109 shows the comparison between the volume percentage of ferrite measured using the Feritscope®, ASTM E562 Manual Point Count method and X-Ray Diffraction
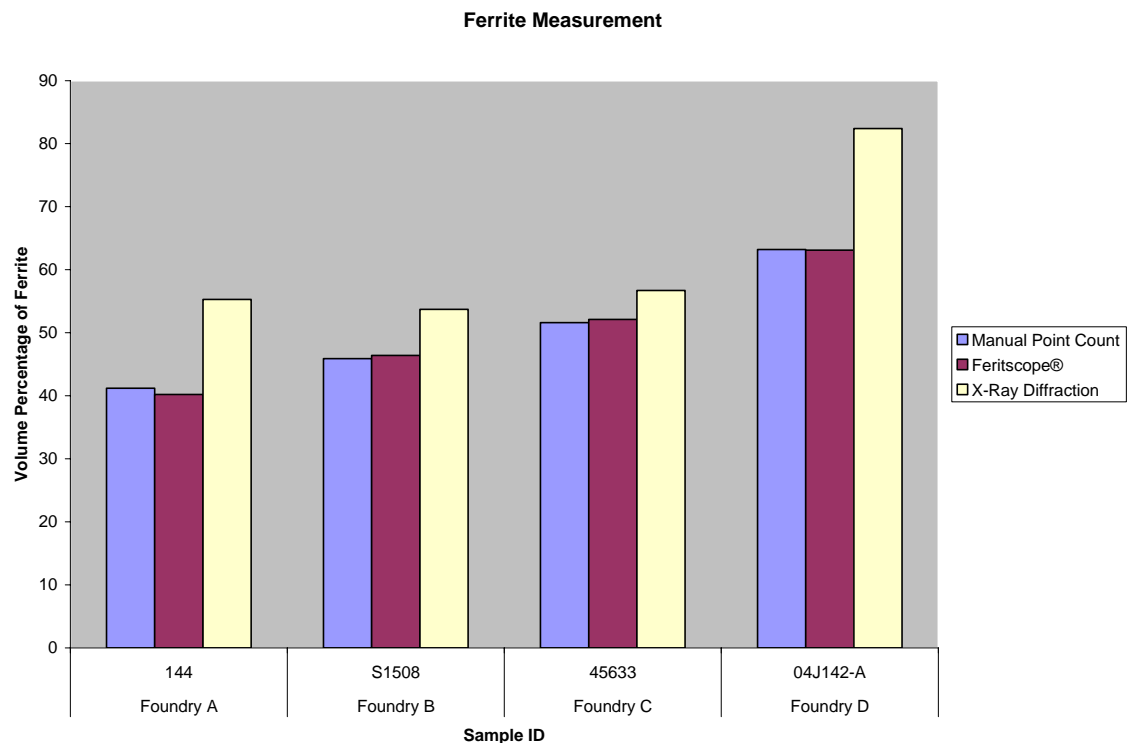
Figure 109: Comparison of Volume Percentage of Ferrite from the Feritscope®, ASTM E562 Manual Point Count and X-Ray Diffraction

The above figure indicates that the volume percentage of ferrite calculated from the Feritscope® and ASTM E562 Manual Point Count gives similar results. However, the volume percentage of ferrite calculated from X-Ray Diffraction shows a high variation when compared with the results from the Feritscope® and ASTM E562 Manual Point Count. The reasons for such results have been already discussed in sections 4 and 9. It can be concluded that the Feritscope® is the most appropriate method for calculating volume percentage of ferrite followed by ASTM E562 Manual Point Count. X-Ray Diffraction is not sufficiently sensitive for quantitative analysis of phases present.

V. Conclusions

A. Data Package

1a) A data package was developed based on the results which were acquired from various tests performed on the ASTM A890-5A cast Super Duplex Stainless Steel material procured from various foundries.

B. 1. The Suitability of ASTM A923 for Detecting the Presence of Intermetallic Phases in Super Duplex Stainless Steel Castings

1a) Since ASTM A923 Methods adequately identifies the presence of intermetallic phases in A890 – 5A grade Cast Super Duplex Stainless Steel A890 – 5A can be directly included in ASTM A923.

1b) The micrographs from the A890-4A grade (now in ASTM A923) are applicable for the A890-5A grade to compare and detect the presence of intermetallic phases. Using these micrographs one can verify whether an A890-5A sample has an unaffected, affected or a possibly affected structure.

2. Evaluation of the ASTM A923 Test Methods A, B and C

2a) All of the eleven foundry solution annealed heats from foundries A, B, C and D passed all the ASTM A923 Test Methods A, B and C. In addition, the heat treatment "A" samples (solution annealed at The University of Tennessee) from Foundry D also passed (all three ASTM A923 Test Methods.

2b) The samples which were subjected to heat treatment schedules "B", "C", "D", "E" and "F" (Heating to 1950ºF, hold for 30 minutes, Water Quench and then heat to 1550ºF, Water Quench after holding for 0, 5, 10, 15 and 20 minutes respectively) did not pass the ASTM A923 Test Methods. These samples underwent the second course of heat treatment (Heating to 1550ºF, holding for different time intervals

164

respectively, water quenching after water quenching from 1950ºF). The heating process took approximately an hour for the samples to reach the temperature of 1550°F. Intermetallic phases are expected to precipitate during the heating process to 1550°F as well as during the hold time at 1550°F. These heat treatment schedules were used for the testing of the wrought material and A890-4A grade cast Duplex Stainless Steel for the formulation of the ASTM A923 specification.

2c) During the first course of heat treatment (Heating to 1950°F, hold for 30 minutes and water quench) determination of precipitated detrimental intermetallic phases is virtually zero as anticipated.

2d) It was also observed that when compared to the A890-4A grade A890-5A grade is more sensitive to heat treatment. The A890-4A grade when subjected to Charpy impact test showed a gradual decrease in there toughness with increasing hold time at 1550ºF. But the A890-5A grade material showed a significant drop in toughness from heat treatment schedule "A" to "B" when second course of heat treatment process was followed (Heat to 1550ºF and hold for different time periods before water quenching).

2e) It was observed that from Test Method A one can visually detect the presence of an affected structure but cannot adequately identify the type of intermetallic phases present. However it is possible to visually deduce whether a sample is affected with a greater percentage of intermetallic phases when compared with another sample.

2f) The air cooled sample (from 1950°F) contained lesser amount of intermetallic phases as compared to slow cool sample though both had low toughness (1-10ft-lbs). This indicates that precipitation of even a small amount of intermetallic phase can reduce the toughness considerably (1-10ft-lbs).

2g) The heat treatment "G" samples (air cooled from 1950°F) revealed an affected structure though the amount of intermetallic phase which was visualized from the OLM image was less as compared to samples which had undergone other heat treatment schedules. They had low toughness. This was similar to ASTM A890-4A grade (previous test results) which indicated that air cooling was not sufficiently

rapid in preventing the intermetallic phase precipitation in A890-4A material. The same is true for ASTM A890-5A material.

2h) The samples from Foundry D which underwent heat treatment schedules "D" (Heat to 1950°F, hold 30 minutes, water quench, heat to 1550ºF, hold 10 minutes, water quench) and "G" (air cooled from 1950°F) had low Charpy toughness (Test Method B) and also an affected structure in the Sodium Hydroxide Etch Test (Test Method A) but still passed the Ferric Chloride Corrosion Test (Test Method C). This explains the ineffectiveness of Test Method C in detecting the presence of detrimental intermetallic phase.

2i) SEM images of corrosion samples proved that corrosion is localized; hence, the assumption of uniform weight loss over the full area of the specimen is not appropriate for calculating the corrosion rate. This indicates that possibly ASTM A923 Test Method C is not an appropriate method for predicting the presence of detrimental intermetallic phases in cast super duplex stainless steel.

2j) There was an increase in the toughness of heat treatment "D" (Heat to 1950°F, hold 30 minutes, water quench, heat to 1550ºF, hold 10 minutes, water quench) samples as compared to the toughness of heat treatment "B" (Heat to 1950°F, hold 30 minutes, water quench, heat to 1550ºF, water quench) and "C" (Heat to 1950°F, hold 30 minutes, water quench, heat to 1550ºF, hold 5 minutes, water quench) samples. The reason for this observation may be related to the heating time to 1550°F.

3. Determination of the best ASTM A923 Test Method for Detecting the Presence of Detrimental Intermetallic Phases

3a) A correlation was determined between the ASTM A923 Test Methods A, B and C in determining the presence of detrimental phases in the material.

3b) It was observed that if the toughness is greater than 60ft-lbs then all samples had an unaffected structure and a high corrosion resistance (passed the acceptance criteria of weight loss ≤ 10 mdd by a wide margin). If the toughness was below 15ft-lbs

then the samples always revealed an affected structure and exhibited low corrosion resistance (weight loss ≥ 10 mdd) except for heat treatment "D" and "G" samples which passed the Ferric Chloride Corrosion Test (Test Method C) indicating the ineffectiveness of Test Method C in determining the presence of detrimental intermetallic phases.

3c) There was a 1:1 correlation between Test Method A and B. Though Test Method A is a direct method of detecting the presence of intermetallic phases, it cannot be confirmed whether the intermetallic phases present are detrimental or not. The lowering of toughness from Test Method B confirms whether the intermetallic phase present is detrimental. However, the toughness of a material may also decrease if the percentage of ferrite is high. This can be determined using the Feritscope®.

3d) ASTM A923 Test Method B (Charpy Impact Test) was determined to be the best method out of the three test methods for predicting the presence of detrimental intermetallic phase in the material.

4. Evaluation by Ferrite and Hardness Measurement

4a) With increasing presence of intermetallic phase in the microstructure the volume percentage of ferrite content is reduced as most of the ferrite is converted into intermetallic phases.

4b) Since heat treatment "B" (Heat to 1950°F, hold 30 minutes, water quench, heat to 1550ºF, water quench) samples exhibited ferrite of approximately 50% but had low toughness (Test Method B) and failed the Sodium Hydroxide Etch Test (Test Method A) and Ferric Chloride Corrosion Test (Test Method C), ferrite percent is not a good indicator of the presence or absence of detrimental intermetallic phase. Heat treatment "D" (Heat to 1950°F, hold 30 minutes, water quench, heat to 1550ºF, hold 10 minutes, water quench) and "G" (Air cooled from 1950°F) samples also contained intermetallic phases and had low toughness but still had volume percentage ferrite of approximately 50%.

4c) As the ferrite content decreased there was an increase in the hardness. This is because as the ferrite content decreased as ferrite was converted into intermetallic phases which increased the hardness of the material. In general, the ferrite content decreases with an increase in the hardness because the ferrite is converted into intermetallic phases which have a higher hardness than ferrite.

5. Evaluation by SEM and EDS

5a) In the Charpy Impact Test the entire sample which showed brittle fracture had low toughness and all samples with ductile fracture showed high toughness. The solution annealed samples from Foundry A, B, C and D which had high toughness showed ductile fracture. The heat treated samples from Foundry D underwent brittle fracture except for heat treatment "A" (Heat to 1950°F, hold 30 minutes, water quench) sample which was solution annealed at the University of Tennessee.

5b) The chemical composition of the intermetallic phase was determined by carrying out EDS on the material from Foundry D after subjecting it to different heat treatment schedules.

5c) The type of intermetallic phase present in the samples was identified by examining the microstructure under SEM.

5d) The SEM images of heat treatment "A" (solution annealed at the University of Tennessee), "G" (air cooled from 1950°F) and "H" (furnace cooled from 1950°F) samples indicated that as the toughness of these samples decreased in the order of "A">"G">"H", intermetallic phase volume increased in the same order from zero in heat treatment "A" sample to a higher amount in heat treatment "H" sample. This result is directly influenced by the cooling rate.

6. X-Ray Diffraction Analysis

6a) The volume percentage of ferrite from X-ray Diffraction always overestimated the volume percentage of ferrite calculated from the Feritscope® due to the problem of

preferred orientation. This indicates that X-Ray Diffraction is not sufficiently sensitive for quantitative analysis of phases present.

6b) X-Ray Diffraction has the limitation in identification of phases. It has the capability of identifying phases like austenite and ferrite but cannot identify small amounts of intermetallic phases.

7. Comparison of Volume Percentage Ferrite measured using the Feritscope®, ASTM E562 Manual Point Count and X-Ray Diffraction

7a) From the comparison made between the Feritscope®, ASTM E562 Manual Point Count and X-Ray Diffraction it was concluded that the Feritscope® is the most suitable method from calculating the volume percentage of ferrite followed by ASTM E562 Manual Point Count method. X-Ray Diffraction is not an appropriate method for carrying out qualitative analysis of different phases present in a material.

7b) Feritscope® is more robust compared to ASTM E562 Manual Point Count which also gives similar results because it is easy to operate, eliminates operator bias and there are minimal requirements for specimen preparation.

VI. Future Work

The objective of this work was to determine the suitability of ASTM A923 "Standard Test methods for Detecting Detrimental Intermetallic Phase in Wrought Duplex Austenitic-Ferritic Stainless Steels" for 25 Cr Cast Super Duplex Stainless Steels (ASTM A890-5A).

This objective was successfully obtained. All the tests were carried out on the material which was procured from various foundries and a data package was developed to be sent to SFSA, DOE and the foundries. It was concluded that ASTM A923 Methods adequately identify the presence of secondary phases in ASTM A890-5A grade Cast Super Duplex Stainless Steels.

This work was also carried out on ASTM A890-4A grade material previously and the results led to the inclusion of the alloy in ASTM A923.

In the future the same work can be extended to ASTM A890-6A grade material in order to include this alloy also into ASTM A923.

References

References

1. Kåre Johansson, Statoil Norway, "Duplex Stainless Steels; Past, Present and Future", 6th World Conference & Expo October 2000, pp. 13-16.

2. Robert N Gunn, "Duplex Stainless Steels – Microstructures, Properties and Applications", pp. 1-3

3. Steel Founders' Society of America, "Duplex Stainless Steels – A state of Art Literature Review", March 2001, pp.2

4. Michel Verneau, Jean Pierre Audouard and Bernard Bonnefois, USINOR INDUSTEEL, 56 rue Clemenceau, BP 56, 71202 LE CREUSOT Cedex, FRANCE, Applications of superduplex UR 52N+ (UNS S32520) in chemical industries, 6th World Conference & Expo October 2000, pp.457-467(check)

5. C. Coussement and D. Fruytier, "An industrial application of duplex stainless steel in the petrochemical industry: A case study, failure analysis and subsequent investigation," Vol 1, pp. 522-529

6. C. Duret Thual and J.L.Moiron, "Duplex Stainless Steel wirelines for use in H_2S containing aqueous chloride environment," Vol 1, pp. 511-521

7. J.P. Audouard, C.Dernoncourt, G.Schweitzer and B.Vincent, "Duplex Stainless Steels for Chemical and Product ship Transportation," 6th World Conference & Expo October 2000, pp 469-484

8. Kåre Johansson, Statoil Norway, "Duplex Stainless Steels; Past, Present and Future", 6th World Conference & Expo October 2000, pp.19-22

9. Robert N Gunn, "Duplex Stainless Steels – Microstructures, Properties and Applications", pp. 7-8

10. Charles, J. "Super Duplex Stainless Steel: Structure and Properties," *Duplex Stainless Steels*. 1991.

11. Karlsson, L.and P., S., "Influence of Intermetallic Phases on the Corrosion Properties of Duplex Stainless Steel Weld Metals," *Welding International*, 1995. 9(7): pp. 554-562.

12. Karlsson,L., Ryen,L. and Pak,S., " Precipitation of Intermetallic Phases in 22% Cr duplex stainless weld metal," Welding Journal, 74(1), Jan. 1995, pp.28s-40s.

13. Nilsson,J.O. and Wilson, A., "Influence of Isothermal Phase transformation on Toughness and Pitting Resistance of Super Duplex Stainless Steel SAF 2507," Material Science and Technology, Vol 9, July 1993, pp.545-554

14. Nilsson, J.-O., "Overview: Super Duplex Stainless Steels," *Materials Science and Technology*, 1992. 8(8): pp. 686-700.

15. Charles, J. "Structure and Mechanical Properties of Duplex Stainless Steels," *Duplex Stainless Steels 94*. 1994.

16. Josefsson, B., Nilsson, J.-O., Wilson, A., "Phase Transformation in Duplex Steels and the Relation Between Continuous Cooling and Isothermal Heat Treatment," *Duplex Stainless Steels '91*, Vol. 1, pp. 67-78.

17. Wang, X.G.,Dumortier, D. and Riquier, Y., "Structural Evolution of Zeron 100 Duplex Stainless Steel between 550 and 1100°C," Duplex Stainless Steels 91, Vol 1, pp.127-134

18. Goldsmith HJ: Interstitial Alloys, Plenum Press, 1967, pp.167

19. Weiss B and Stickler R: Metallurgical transactions, 1972, pp.851

20. Charles, J. "Super Duplex Stainless Steel: Structure and Properties," *Duplex Stainless Steels*. 1991.

21. Machado, I.F., Padilha, A.F., "Precipitation Behavior of 25% Cr − 5.5% Ni Austenitic Stainless Steel Containing 0.87% Nitrogen," *Steel Research*, 67(7), July 1996, pp. 285-290.

22. Atamert, S., King, J.E., "Sigma Phase formation and its prevention in Duplex Stainless Steels," Journal of *Materials Science*, 12(14), July 1993, pp.1144-1147

23. Lai, J.K.L., Wong, K.W., Li, D.J., "Effect of Solution Treatment on the Transformation Behavior of Cold-Rolled Duplex Stainless Steels," *Materials Science and Engineering A*, 203(1-2), Nov. 1995, pp.356-364.

24. O.Smuk, P.Nenonen and H.Haenninen, "Study of the Mechanisms of the Secondary Phase Precipitation in P/M HIP Super Duplex Stainless Steels," 6th World Conference & Expo October 2000, pp. 395-404

25. Gooch, T.G., "Corrosion Resistance of Welds in Duplex Stainless Steels," *Duplex Stainless Steel 91*, 1991.

26. Thorvaldsson,T., Nilsson,J.O., ND Liu.P., "Microstructural Characterization of Stainless Steel – Industrial Applications," Micron and Microscopica Acta., 22(1/2), 1991, pp.185-186

27. Strutt A J, Lorimer G N, Roscoe C V, Gradwell K J: Conf Proc. Duplex Stainless Steels' 86 The Hague Nederlands Instituut voor Lastechniek, 26-28 Oct 1986, paper 3, 310-318.

28. Chance J, Coop W, Gradwell KJ, Roscoe CV: St Louis 82, vide ref.8, 371-398

29. Nilsson, J.-O., "Overview: Super Duplex Stainless Steels," *Materials Science and Technology*, 1992. 8(8): pp. 686-700.

30. Nilsson, J.-O., Wilson, A., Huhtala, T., Karlsson, L., Jonsson, P., "Structural Stability of Super Duplex Stainless Weld Metals and Its Dependence on Tungsten and Copper," Metallurgical and Materials Transactions A, 27A (8), Aug. 1996, pp. 2196-2208.

31. C.S.Lee,J.S.Ahn,K.A.Lee,K.T.Kim,C.G.Park and K.Y.kim, "Effect of Chi phase precipitation on the Mechanical Properties of Duplex Stainless Steels", 6th World Conference & Expo October 2000, pp. 785-793

32. Varol, I., Lippold, J.C., Baeslack III, W.A., "Welding of Duplex Stainless Steels," Key Engineering Materilas, Vol. 69 & 70, 1992, pp. 217-252.

33. Redjaïmia A,Metauer G, Gantois M: Beaune'91 vide ref.2, Vol.1,119-126

34. Nilsson J.O and Lui P, "Material Science and Technology", 1991, pp.853-861

35. Adhe, K.N., Kain, V., Madangopal, K., Gadiyar, H.S., "Influence of Sigma-Phase Formation on the Localized Corrosion Behavior of a Duplex Stainless Steel," *Journal of Materials Engineering and Performance*, 1996. 5(4): pp. 500-506.

36. Ravindranath, K., Malhotra, S.N., "Influence of Aging on Intergranular Corrosion of a 25%Cr-5%Ni Duplex Stainless Steel," *Corrosion*, 50(4), 1994, pp. 318-328.

37. Charles, J., "Composition and Properties of Duplex Stainless Steels," *Welding in the World*, Vol. 36, 1995, pp. 43-55.

38. Kuroda, T., Matsuda, F., "Role of Secondary Austenite on Corrosion and Stress Corrosion Cracking of Sensitized Duplex Stainless Steel Weldments," Transactions of *JWRI*, 23(2), 1994, pp. 205-211.

39. Hoffmeister, H. Lothongkum, G., "Quantitative Effects of Nitrogen Contents and Cooling Rates on δ-γ transformation, Chromium Nitride Precipitation and Pitting Corrosion after Weld Simulation of Duplex Stainless Steels," *Duplex Stainless Steel '94*, Vol. 1, 1994, Paper 55.

40. Karlsson, L., "Welding Super Duplex Stainless Steels," *Anti-Corrosion Methods and Materials*, 42(6), 1995, pp. 30-35.

41. Atamert, S., King, J.E., "Super Duplex Stainless Steels Part I: Heat Affected Microstructures," *Materials Science and Technology*, 7(2), pp. 137-145.

42. Kokawa H., Tsory E. and North T.H., "Nitride Precipitation in Duplex Stainless Steel Weld Metal," ISIJ International, 35 (10), 1995, pp. 1277-1283

43. Lindblom, B.E.S., Lundvist, B., Hannerz, N.E., "Grain Growth in HAZ of Duplex Stainless Steels," *Duplex Stainless Steel '91*, Vol. 1, Edited by J. Charles, S. Bernhardsson, pp. 373-381.

44. Blackburn MJ, Nutting J: J.I.S.I 1964, pp.610-613

45. Rouault A, Herpin P, Frauchart R: Ann.Chim, 1970, pp.461

46. Soylu B, Honeycombe RWK, "Material Science Technology," 1991, pp.137-145

47. Sriram, R., Thomas, D., "Pitting Corrosion of Duplex Stainless Steels," *Corrosion*, 45(10), Oct., 1989, pp. 804-810.

48. Hashimoto K, Asami K, Teramoto K, "Corrosion Science," 1979, pp.3-14

49. Sedriks AJ: Conc Proc Stainless Steels 84, Goteborg, Institute of Metals, 1985, 125-133

50. *SCRATA Materials Fact Sheets on Duplex Cr-Ni Steels*, Section D, Apr. 1991.

51. Charles J: Beaune 91, vide ref., Vol 1, pp.3-48

52. Halada GP, Clayton CR, Fritz JD and Kim D: Corrosion 95, Orlando, NACE, paper 95531

53. Nagano H, Kudo T, Inaba Y and Harada M: Mataux Corrosion Industrie, 1981, 23.1

54. Ogawa, T.a.K., T., "Effect of Composition Profiles on Metallurgy and Corrosion Behavior of Duplex Stainless Steel Weld Metals," *Welding Journal*, 1998. 68(5): pp. 181s-191s.

55. Miura, M., Koso, M., Hudo, T., Tsuge, H., "The Effects of Nickel and Nitrogen on the Microstructure and Corrosion Resistance of Duplex Stainless Steel Weldments," *Welding International*, 1990. 4(3): pp. 200-206.

56. Solomon HD and Levinson LM, "Acta Metallurgia," 1978, pp.429-442

57. Lu YC, Bandy R, Clayton CR, Newman RC, "Electrochemical Society.,"n1983, pp.1774

58. Bandy R et al, "Electrochemical Society", Book 1984

59. Newman RC, Franz E, "Journal of Electrochemical Society," 1984, pp.223

60. Osozawa K, Okato N, "Corrosion 86", Houston NACE, 1986

61. Fukuzaka T et al, "Trans I.S.I.J," 1980, pp.403

62. Charles J, "Weldability of New Ferrite and Stainless Steels," Cambridge, TWI, 1990

63. Lizlovs EA, "Climax Molybdenum Report RP," 1981

64. Anson D.R., Pomfret R.J., Hendry A. and Beattie G.T., "Castable High-Nitrogen Duplex Stainless Steels," Proceedings: The Institute of British Foundrymen 91st Annual Conference: Castcon 94

65. Kotecki DJ, Siewart TA: Welding Research Supplement, May 1992, pp.171-178

66. Roscoe CV, Gradwell KJ and Lorimer GW: Goteborg 84, vide ref. 6, pp. 563-577

67. Soulignac P and Dupoiron F: Stainless Steel Europe, 1990, pp. 18-21

68. Taylor R, "Duplex Stainless Steel Production," SFSA T&O conference, 1994

69. Sedriks AJ: International Metal Reviews, 1983, pp. 295

70. Kotecki, D.J., Siewert, T.A., "WRC-1992 Constitution Diagram for Stainless Steel Weld Metals: A Modification of the WRC-1988 Diagram," *Welding Journal*, 71(5), 1992, pp. 171s-178s.

71. Okamoto H: Conference Proceedings Applications of Stainless Steel 92, Stockholm Jernkontoret 1992, Vol 1, pp. 360-369

72. Farrar, R.A., "The Importanceof Microstructural Transformations for Welding and the Stability of Long Term Service Properties," *Welding in the World*, Vol. 36, 1995, pp. 143-151.

73. Bui N, Irhzo A, Dabosi F and Limouzin-Maire Y: Corrosion, 1983, pp. 491

74. Hertzman S., Nilsson M., Jargelius-Pettersson R.: "Influence of W and Cu on Microstructure, Mechanical Properties and Corrosion resistance of Weld Metal" Nov 1994, vide ref. 1, Vol. 1, paper 1.

75. J.S.kim, K.Y.Kim and J.S.Lee, "The Effect of W Modification of Duplex Stainless Steel on the Behavior of Precipitation of Secondary Phases and SCC," 6th World Conference & Expo October 2000, pp.251-259

76. Ogawa K, Okamoto H, Ueda M, Igarashi M and Mori T, " Effects of Tungsten on Pitting Corrosion Resistance and Impact Toughness in the HAZ of Duplex Stainless Steel – Study of Weldability of High – Tungsten Duplex Stainless Steel (1st Report)," Welding International, 10(6), 1996, pp.466-472

77. Atamert, S., King, J.E., "Elemental Partitioning and Microstructural Development in Duplex Stainless Steel Weld Metal," *Acta. Metall. Mater.*, 39(3), 1991, pp. 273-285.

78. Charles J: Beaune 91, vide ref., Vol 1, pp.151-168

79. Leffler B: Avesta Sheffield AB. Private Communication dated 3 January 1997

80. Charles J: Beaune 91, vide ref., Vol 1, pp.347-362

81. Niset M, Doyen R and Van Bemst A: Newyork 87, vide ref. 10, pp.96-104

82. Nyström M, Karlsson B and Wasén J: Chiba 91, vide ref. 11 Vol 1, pg 746-753

83. Nilsson J.O and Liu P, "Aging at 400-600°C of Submerged Arc Welds of 22Cr-3Mo-8Ni duplex stainless steel and its effect on toughness and microstructure," Materials Science and Technology, 7(9), 1991, pp. 853-862

84. Schmidt W: Thyssen Edelst Techn Ber 7 Band 1981 Heft, pp.55-71

85. John Ole Gjerb, Aker Maritime, Norway, "Cold Forming of Duplex Stainless Steel," 6th World Conference & Expo October 2000, pp. 163-172

86. Maehara Y: Conference Proceeding stainless Steel 91, Chiba ISIJ, 1991, Vol 1, pp. 647-654

87. Johansson J.O.: Swedish Institute for Metal Research, IM-2288

88. Bendall K: Stainless Steel Europe, February 1991, pp.22

89. Bernhardsson S: Beaune 91, vide ref., Vol 1, pp.185-210

90. C.A.Farina, U.Grassini and C.Aiello, "Experience and NDT controls with Duplex Stainless Steels in chemical and refinery plants," 6th World Conference & Expo October 2000, pp. 453-456

91. Langley Alloy Ltd: Brochure Ferralium 255, August 1995

92. Sandvik Steel: SAF 2507 reference list 1994

93. Avesta Sheffield: Corrosion handbook for Stainless Steels, Information 9401, ISBN 91-630-2122-6, 1994

94. Audouard JP, Charles J and Dupoiron F: Stainless Steel Europe, April 1992, pp.40-45

95. Bernhardsson S., "The Corrosion resistance of Duplex Stainless Steel"

96. Nicholls, J.M., "Corrosion Properties of Duplex Stainless Steels: General Corrosion, Pitting and Crevice Corrosion," *Duplex Stainless Steels 94*. 1994.

97. Francis R, "Weir Materials Ltd. Private Communication", 13 January 1997

98. Francis R, Irwin JB, Byrne G, "British Corrosion Journal", 1995, pp.237-242

99. Leffler B, "Marine Transportation of Chemicals an Application for Duplex Stainless Steels," Duplex Stainless Steel'91, Vol 1, pp.567-577

100. Gooch TG, Gunn RN, "Alloy Materials for Sour Services – A Critical Review" TWI Report 5607, July 1992

101. Francis R, "Conference Proceeding Duplex Stainless Steel," Glasgow, TWI 1994, Vol 3 paper KIV

102. Murata M. Mukai Y, Wang JB: "Conference Proceeding Advanced Technology in Welding," Tokyo, April 1990, Japan Welding Society, Vol II, pp.941-945

103. Lundin C.D., Buchanan R.A., Khan K.K., Lee I.S. and Gupta A, "The Weldability of High Alloy Cast and Wrought Materials: A Literature Review," Steel Founders' Society of America Special Report No.24 Dec. 1989

104. Ravindranath, K., Malhotra, S.N., "Influence of Aging on Intergranular Corrosion of a 25%Cr-5%Ni Duplex Stainless Steel," *Corrosion*, 50(4), 1994, pp. 318-328.

105. Otero, E., Merino, C., Fosca, C., Fernandez, P., "Electrochemical Characterization of Secondary Phases in Duplex Stainless Steel by EPR Test," *Duplex Stainless Steels, 94*. 1994

106. Merino, P., Novoa, X.R., Pena, G., Porto, E., Espada, L., "Intergranular Corrosion Susceptibility of Austenitic-Ferritic Duplex Stainless Steels: Application of Potentiokinetic Reactivation Tests," *Materials Science and Technology*, 1993. 9(2): pp. 168-171

107. Kajo Grubić and Ivan Juragac, "Laser Welding of Duplex Steel," 6th World Conference & Expo October 2000, pp.521-528

108. van Nassau, Meelker, H., Hilkes, J., "Welding Duplex and Super Duplex Stainless Steels," *Welding in the World*, 31(5), Sept./Oct. 1993, pp. 322-343.

109. Bekkers, K., "Practice in Welding Duplex and Super Duplex Stainless Steel Worldwide," *Welding in the World*, Vol. 36, 1995, pp. 111-123.

110. Noble, D.N., Gunn, R.N., "Welding of Duplex Stainless Steel – A Reader's Digest: Part 1," *Stainless Steel Europe*.

111. Fager, S. –A. Odegard, L., "Influence of Different Welding Conditions on Mechanical Properties and Corrosion Resistance of Sandvik SAF 2507," *Corrosion Review*, 11(3-4), 1993, pp.83-100.

112. Hilkes, J., Bekkers, K., "Welding Duplex Stainless Steel," *Welding Journal*, 74(11), Nov.1995, pp. 51-54.

113. Holmberg, B., "Welding of Super Duplex Steel Avesta 2507," *Welding Review International*, 11(1), 1992, pp. 22-27.

114. "Guidelines for Welding Zeron 100 Super Duplex Stainless Steel," Weir Materials, Ltd.

115. Claes-Ove Pettersson – AB Sandvik Steel Sweden, "The MIG/MAG Process, A Good Choice when Welding Duplex Stainless Steel", 6th World Conference & Expo October 2000, pp.513520

116. Geipl, H., "Gas Mixture MAG (GMA) Welding of Corrosion Resistant Duplex Steels – Effect of Shielding Gas and Process Variations," *Duplex Stainless Steels '91*, Vol. 2, 1991, pp 1027-1034.

117. Gouch, P.C., Farrar, J.C.M., "Factors Affecting Weld Root Run Corrosion Performance in Duplex and Super Duplex Pipework," *Duplex Stainless Steels '91*, Vol. 2, 1991, pp. 1009-1025.

118. Homberg, B., "Filler Metal Selection for Optimum Duplex Weldment Properties in Steel UNS 31803," *Duplex Stainless Steels '94*, Vol. 1, Part II, 1994, Paper 93.

119. Karlsson, L., Andersson, S.L., Huhtala, T., "New Ni-base Consumables for Welding of Duplex and Super Duplex Stainless Steels," *Duplex Stainless Steels '94*, Vol. 1, Part II, 1994, Paper 42.

120. Gunn, R.N., Anderson, P.C.J., "Development of Special Ar-He-N2 Gases for TIG Welding of Duplex and Superduplex Stainless Steels," *Duplex Stainless Steels '94*, Vol. 2, 1994, Paper 30.

121. Urmstom, S.A., Creffield, G.K., Cole, M.A., Huang, W., "Effect of Nitrogen Containing Shielding Gases on the Weldability and Corrosion Performance of Duplex Stainless Steels," *Duplex Stainless Steels '94*, Vol. 2, 1994, Paper 27.

122. Rabensteiner, G. Tosch, J., "The Specific Effect of Nitrogen in the Fabrication of a Super Duplex Stainless Steel Weld," *Duplex Stainless Steel '94*, Vol. 2, 1994, Paper 44.

123. Bradshaw, R., Cottis, R.A., "The Effect of Nitrogen Additions to Argon Shielding Gases on the properties of Duplex Stainless Steel GTA Welds," *Duplex Stainless Steels '94*, Vol. 2, 1994, Paper 31.

124. Bonnefois, B., Soulignac, P., Charles J., "Some Aspects of Nitrogen Introduction in the Duplex Weld Pool, "*Duplex Stainless Steels '91*, Vol. 1, 1991, pp. 469-478.

125. Stenbacka, N., Persson, K.A., Runnerstam, O., "Shielding Gas Technology when Ordinary and High Alloyed Stainless Steels," *Welding in the World*, Vol. 36, 1995, pp. 83-90.

126. Gunn RN: Concf Proc Duplex Stainless Steels'94, Glasgow, TWI, 1994, Vol 1, paper 32

127. Atamert, S., King, J.E., "Super Duplex Stainless Steels Part I: Heat Affected Microstructures," *Materials Science and Technology*, 7(2), pp. 137-145.

128. Bonnefois, B., Charles J., Dupoiron, F., Soulignac, P., "How to Predict Welding

Properties of Duplex Stainless Steels," *Duplex Stainless Steel '91*, Vol.1, 1991, pp. 347-361.

129. Cao, H.L., Hertzman, S., "The Realtionship between Impact Properties and Welding Simulated Microstructures in Three Duplex Stainless Steels," *Duplex Stainless Steel '91*, Vol. 1, 1991, pp. 363-372.

130. Lindbolm, B.E.S., Hannerz, N., "Austenite Reformation in HAZ of Ferritic Austenitic Steels," *Duplex Stainless Steels '91*, Vol. 2, 1991, pp. 951-958.

131. Dufrance, J.J., "Heat Affected Zone Simulation of Super Duplex Stainless Steel UNS S 32760 – Zeron 100," *Duplex Stainless Steel '91*, Vol. 2, 1991, pp. 967-975.

132. Draugelates, U., Schram, A., Boppert, C., Liu, J., "Investigation on the Effect of the Peak Temperature and Cooling Time on the Heat Affected Zone in Duplex Cast Steel," *Duplex Stainless Steel '91*, Vol. 2, 1991, pp. 977-984.

133. Ferreira, P.J., Hertzman, S., "δ-Ferrite Grain Growth in Simulated High Temperature HAZ of Three Duplex Stainless Steels," *Duplex Stainless Steel '91*, Vol. 2, Edited by J. Charles, S. Bernhardsson, pp. 959-966.

134. Lindblom, B.E.S., Lundvist, B., Hannerz, N.E., "Grain Growth in HAZ of Duplex Stainless Steels," *Duplex Stainless Steel '91*, Vol. 1, Edited by J. Charles, S. Bernhardsson, pp. 373-381.

135. Liljas M, "Welding Metallurgy of Duplex Stainless Steels," Duplex Stainless Steels'94, Vol 1, Key note paper KV 136. Radenkovic, G., Cvijovic, Z., Mihajlovic, D., "Effect of Quenching Temperature on the Microstructure and Properties of Cast Duplex Stainless Steel," *Acta Stereol*, 13(2), 1994, pp.439-444.

137. Kotecki, D.J., "Ferrite Control in Duplex Stainless Steel Weld Metal," *Welding Journal*, 65(10), 1986, pp. 352s-361s.

138. Kotecki, D.J., "Extension of the WRC Ferrite Number System," *Welding Journal*, 61(11), 1982, pp. 352-361. 65. Schaeffler, A., "Constitution Diagram

139. Delong, W.T., "Ferrite in Austenitic Stainless Steel Weld Metal," *Welding Journal*, 53(7), 1974, pp. 273s-286s.

140. Lake, F.B., "Effect of Cu on Stainless Steel Weld Metal Ferrite Content, " Paper

Presented at AWS Annual Meeting, 1990.

141. Kotecki, D.J., "Ferrite Measurement and Control in Duplex Stainless Steel Welds," Proc of Weldability of Materials, ASM International, Oct. 1990, pp.127-133.

142. Kotecki D.J., "Silicon Effect on Stainless Steel Metal Ferrite," IIW.DOC>II-C-779-86, 1986

143. Lefebvre, J., "Guidance on Specifications of Ferrite in Stainless Steel Weld Metal," *Welding in the World*, 31(6), Nov./Dec. 1993, pp. 390-406.

144. Kotecki D.J.,"Standards and Industrial Methods for Ferrite Measurement," Welding in the world, 36, 1995, pp. 161-169

145. Neumaier, P. "On-site Eddy Current Measurement of Ferrite Content in Austenitic and Duplex Steel Components," *Materials Evaluation*, 48(9), Sept. 1990, pp. 1065- 1072.

146. Atamert S and King JE, "Acta Metall Mater," 1991, pp.273

147. van Nassau L and Meelker H: Beaune '91, vide ref 3, Vol 1, pp.303-323

148. Ogawa T and Koseki T: Weldability of Materials, ASM, Oct 1990, Detroit, 135

149. Hertzman S and Symniotis E: Conf proc Stainless Steels, ISIJ, Chiba, 1991, Vol 2, pp.1085-1092

150. ASTM standard E562-95: Standard test method for determining volume fraction by systematic manual point count, ASTM, 1996

151. Shinozaki, K., Ke, L., North, T.H., "Hydrogen Cracking in Duplex Stainless Steel Weld Metal," *Welding Journal*, 71(11), 1992, pp. 387s-396s.

152. Ogawa, K., Miura, M., "Hydrogen Cracking in Duplex Stainless Steel Weldments," *Welding International*, 5(9), 1991, pp. 691-696.

153. Kotecki, D.J., "Phase Transformations and Weldability of Duplex Stainless Steels," *Proceedings: The First United States – Japan Symposium on Advances in Welding Metallurgy*, June 1990, pp. 251-263.

154. Hoffmeister, H., Volden, L., Grong, O., "Hydrogen Induced Weld Cracking of Duplex Stainless Steels as Affected by Shielding Gas Composition with TIG

Welding," *Duplex Stainless Steels '94*, Vol. 1, Part III, 1994, Paper 54.

155. Lundin, C.D. et al, "Measurement of Diffusible Hydrogen and Hydrogen Effects on the Weldability of 2205/2209 Duplex Stainless Steel."

156. Lundin C.D, Ruprecht S Wen S and Zhou G, "Comparison of ferrite measurement techniques as applied to duplex stainless steel castings utilizing point counting, magne gauge and Feritscope®," *6th World Conference* October 2000, pp 415-425.

157. Yoon-Jun Kim, L.Scott Chumbley and Brian Gleeson, "Transformation Diagrams of Intermetallic Phase Precipitation in Cast Duplex Stainless Steels CD3MN and CD3MWCuN."

158. Chwee-Sim Goh and Tick-Hon Yip, "Fatigue Deformation Induced Response in a Super Duplex Stainless Steel", *Metallurgical and Materials Transactions* Volume 33A-No.11 November 2002, pp 3433-3499

159. L Duprex, B.C.De Cooman and N. Akdut, "Flow Stress and Ductility of Duplex Stainless Steel during High-Temperature Torsion Deformation", *Metallurgical and Materials Transactions* Volume 33A-No.7 July 2002, pp 1931-1939

160. Robert N Gunn, "Duplex Stainless Steels – Microstructures, Properties and Applications", pp 93-96

161. Robert N Gunn, "Duplex Stainless Steels – Microstructures, Properties and Applications", pp 31-32

162. Steve W. Russell, "The Development of Qualification Standards for Cast Duplex Stainless Steel", *Master of Science Thesis*, April 2003, pp 108-109

163. Arthur H. Tuthill, "Corrosion Testing of Austenitic Stainless Steel Weldments", *Welding Journal*, May 2005, pp 36-40

164. B. D. Cullity, "Elements of X-ray Diffraction", Second Edition, pp 411-413

165. Yan Cui and Carl D. Lundin, "Effect of Microfissures on Fatigue Properties of Austenitic Stainless Steel Weld Metals", *Materials Letters*, 59(2005) 2942-2947

166. Yan Cui and Carl D. Lundin, "Evaluation of Initial Pitting Location in E316L Austenitic Stainless Steel Weld Metals", Materials Letters, 59(2005) 1542-1546

167. Yan Cui and Carl D. Lundin, "Austenite-Initial Corrosion Attack in 316L Weld Deposits", *Materials & Design*, 2005

168. Yan Cui and Carl D. Lundin, "Ferrite Measurement as a Function of the Larson-Miller Parameter for Austenitic Stainless Weld Metals after Creep Testing", *Metallurgical and Materials Transactions A*, Volume 35A, November 2004, 3631-3632

169. Yan Cui, Carl D. Lundin, Vasudevan Hariharan, "Mechanical Behavior of Austenitic Stainless Steel Weld Metals with Microfissures", *Materials Processing Technology*, 2005

170. Yan Cui and Carl D. Lundin, "Effect of Microfissures on Mechanical Properties of 308L Austenitic Stainless Steel Weld Metals", *Journal of Materials Science*, 40(2005) 1281 - 1283

Appendices

Appendix A - ASTM Specifications

1. **ASTM A 890M – 99:** "Standard Specification for castings, Iron-Chromium-Nickel-Molybdenum Corrosion Resistant, Duplex (Austenitic/Ferritic) for General Application"

2. **ASTM A800/A 800M – 91:** "Standard Practice for Steel Casting, Austenitic Alloy, Estimating Ferrite Content"

3. **ASTM A799/A 799 M – 91:** Standard Practice for Steel Castings, Stainless, Instrument Calibration, for Estimating Ferrite Content"

4. **ASTM A781 M – 94a:** "Standard Specification for Castings, Steel and Alloy, Common requirements for General Industrial Use"

5. **ASTM A 370:** "Standard Methods and Definitions for Mechanical Testing of Steel Products"

6. **ASTM A923 – 94:** "Standard Test for Determining the Detrimental Intermetallic Phase in Wrought Duplex (Austenitic/Ferritic) Stainless Steels"

7. **ASTM G48 – 92:** "Standard Test Method for Pitting and Crevice Corrosion Resistance of Stainless Steels and Related Alloys by use of Ferric Chloride Solution"

8. **ASTM A 262 – 93a:** "Standard Practice for Detecting Susceptibility to Intergranular Attack in Austenitic Stainless Steels"

9. **ASTM G 108 – 94:** "Standard Test Method for Electrochemical Reactivation (EPR) for Detecting Sensitization of AISI Type 304 and 304L"

10. **ASTM E18 – 03:** "Standard Test Method for Rockwell Hardness and Rockwell Superficial Hardness of Metallic Materials"

11. **ASTM E562 – 02:** "Standard Test Method for Determining Volume Fraction by Systematic Manual Point Count"

Appendix B

Table 22: Volume % Ferrite of Foundry Solution Annealed Samples from Foundry A, B, C and D

Foundry	Specimen ID	Ferrite Number	Volume % Ferrite
Foundry A	285	66.6	47.2
		68.7	48.4
		63.1	45.3
		66.3	47.1
	331	62	44.7
		59.4	43.3
		62.4	44.9
		61.2	44.3
	144	92	61.2
		54	40.3
		52.9	39.7
		54.9	40.8
Foundry B	S1507	77.3	53.1
		87.1	58.5
		83.1	56.3
		88.5	59.3
	S1508	66.6	47.3
		64.3	45.9
		64.4	46.1
		64.8	46.2
Foundry C	45633	71.8	50.1
		76.8	52.8
		76	52.4
		76.5	52.7
	41414	70.2	49.2
		69.6	48.9
		73.4	50.9
	41374	71.4	49.9
		70.9	49.6
		78.1	53.5
		76.7	52.8
	41544	75.1	51.9
		76.6	52.7
		70.3	49.3
		73.2	50.9
	44073	63.7	45.6
		69	48.5
		62.4	44.9
		63.8	45.7
Foundry D	04J142	102.5	66.9
		105	68.3
		96.6	63.7
		98.3	64.6

Table 23: Volume % Ferrite of Heat Treated Samples from Foundry D

Foundry	Specimen ID	Ferrite Number	Volume % Ferrite
Foundry D	04J142 - A	99	65.1
		91.9	61.1
	04J142 - B	57.5	42.2
		60.9	44.1
	04J142 - C	34.4	29.5
		43.7	34.6
	04J142 - D	79	54.1
		81.8	55.6
	04J142 - E	45	35.3
		38.3	31.6
	04J142 - F	36.2	30.5
		35.6	30.2
	04J142 - G	81	55.1
		77.8	53.4
		83.4	56.5
		76.9	52.9
	04J142 - H	3.6	12.5
		3.9	12.8
		4.1	12.8
		3.6	12.6

The volume percentage of ferrite was calculated using the formula:

Volume % of Ferrite = 0.55*(Ferrite Number) +10.6

The ferrite number was measured using Feritscope® on all the samples which had undergone charpy impact test. The values in Table 14 are the average of the ferrite number measured in all the samples.

Appendix C

Table 24: Hardness Values measured using Rockwell B and Rockwell C on Foundry Solution Annealed samples from Foundry A, B, C and D

Foundry	Specimen ID	HRB	HRC
Foundry A	285	104.1	22.9
		104.1	22.3
		103.6	22.3
	331	103.3	21.2
		103.2	22.1
		102.5	22.1
	144	83.1	19.7
		96.5	17.8
		102.6	19.1
Foundry B	S1507	84.7	24.1
		100.2	24.6
		103.5	24.5
	S1508	89.4	21.8
		96.9	21.7
		102.6	22.3
Foundry C	45633	102.4	20.8
		103.3	21.2
		102.5	20.5
	41414	72.6	19.3
		91	20.7
		102.2	21.1
	41374	101.9	19.4
		102.2	19.5
		102.5	21.5
	41544	92.9	20.4
		100.3	20.2
		101.9	22.2
	44073	100.8	18.1
		101	19.2
		101	19.6
Foundry D	04J142	100.9	25.1
		103.7	26.6
		103.9	24.7

Table 25: Hardness Values measured using Rockwell B and Rockwell C on Heat Treated samples from Foundry D

Foundry	Specimen ID	HRB Scale	HRC Scale
Foundry D	04J142 - A	97.6	20.9
		99.9	20.2
		99.6	20
	04J142 - B	98.5	22.1
		101.7	28.3
		105.7	24.4
	04J142 - C	106.3	30.7
		107.1	30.4
		104.9	31.4
	04J142 - D	101.1	20.9
		102.6	20.4
		101	19.1
	04J142 - E	100.1	25.7
		103.1	27.3
		105.1	27.8
	04J142 - F	109.4	30.7
		107.3	28.5
		109.1	30.5
	04J142 - G	104.4	29.7
		106.9	28.5
		107.4	27.8
	04J142 - H	105.5	33.5
		108.5	34.4
		109.3	34.6

Three values were measured on HRB and HRC scale on all the samples that were selected to undergo the hardness test. The values in Table 15 are the average of the hardness values measured on Rockwell B and Rockwell C scale.

Appendix D

SEM Images on Foundry Solution Annealed Samples from Foundry A, B and C
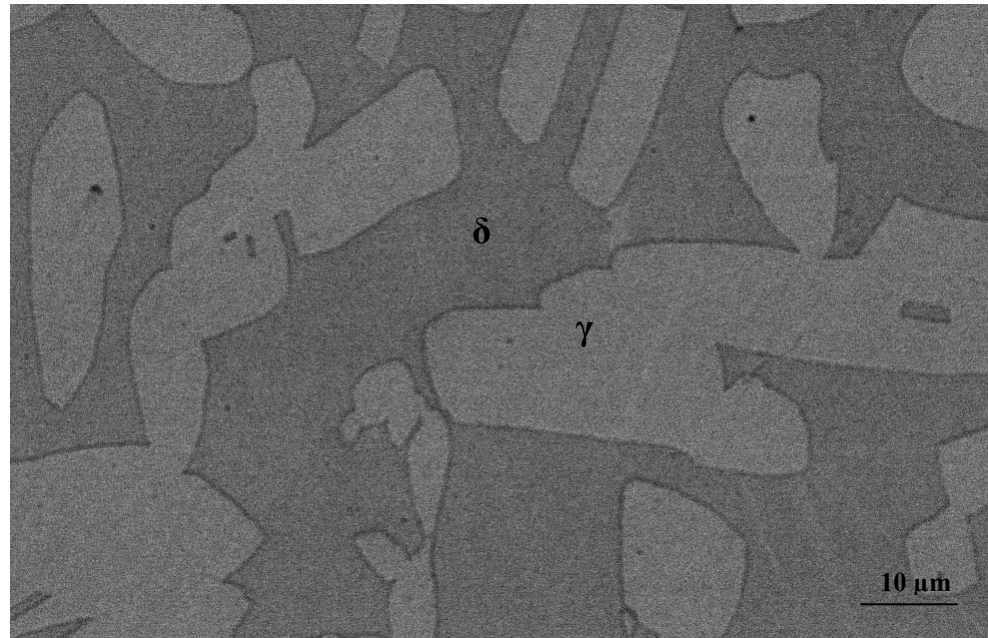
Figure 110: Backscatter SEM image of 285, 500x
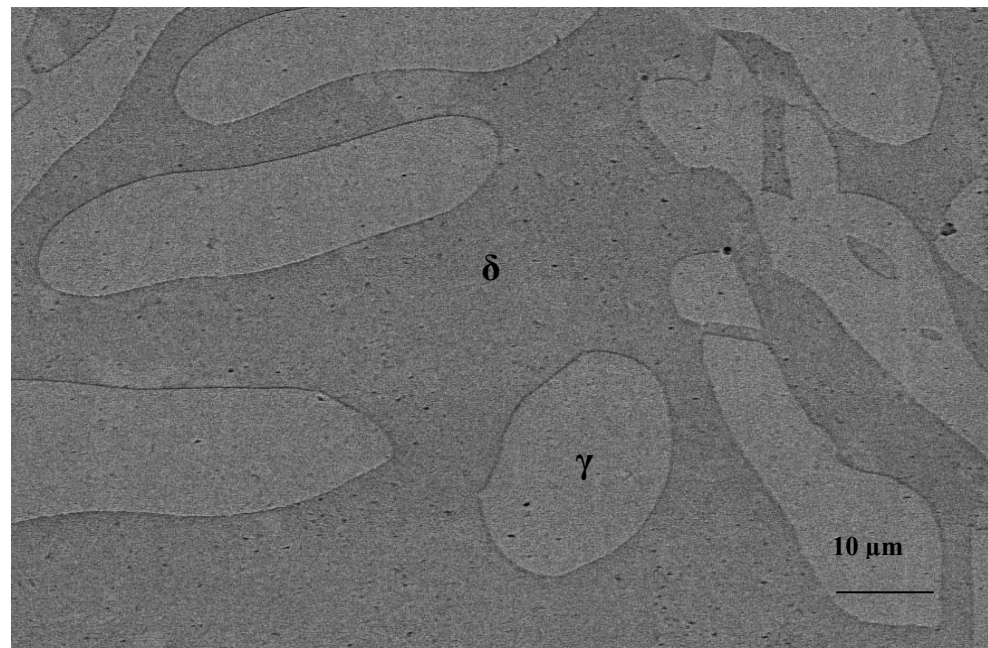
**Figure 111:** Backscatter SEM image of 331, 500x
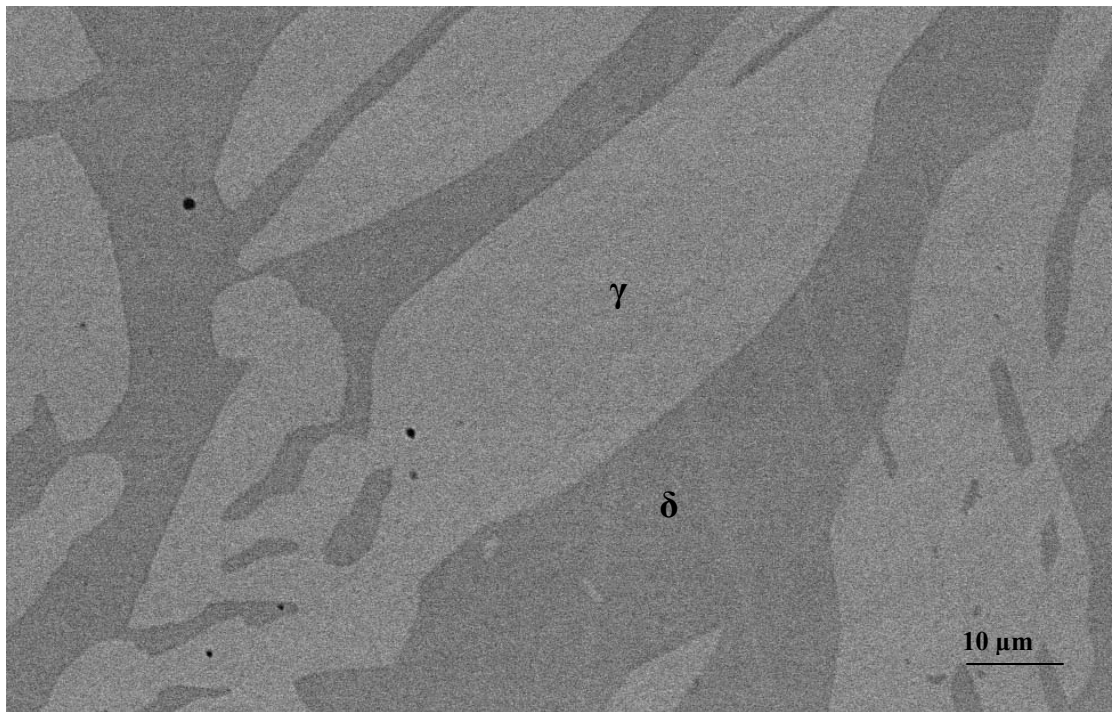
**Figure 112:** Backscatter SEM image of 144, 500x
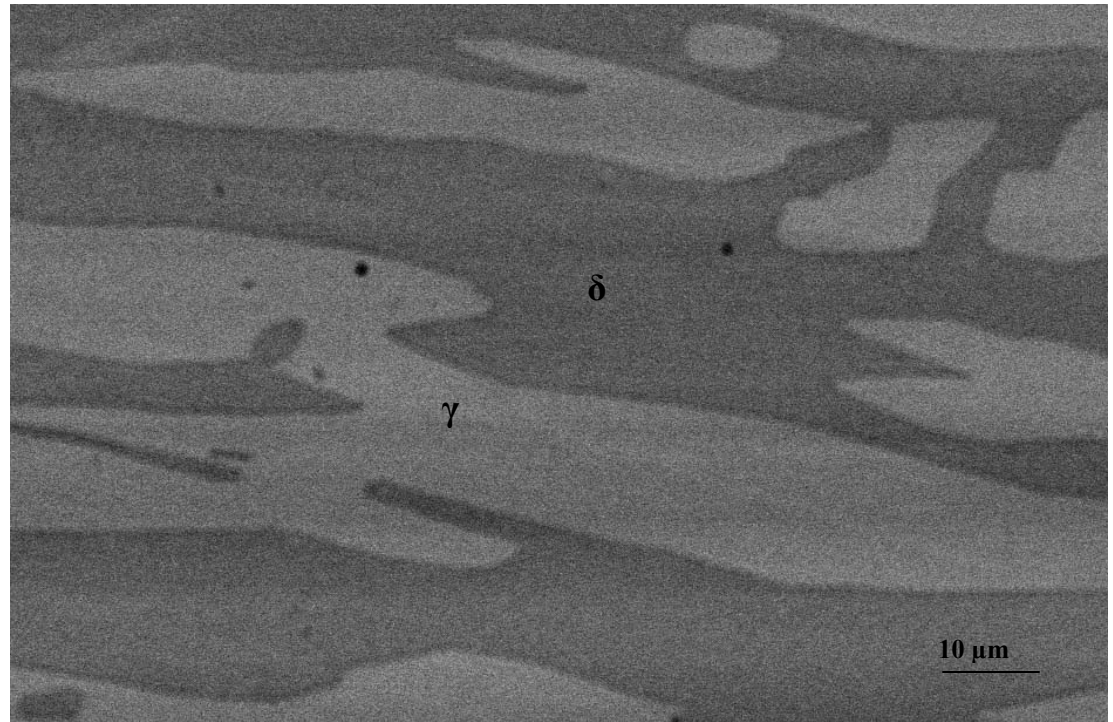
**Figure 113:** Backscatter SEM image of 41374, 500x
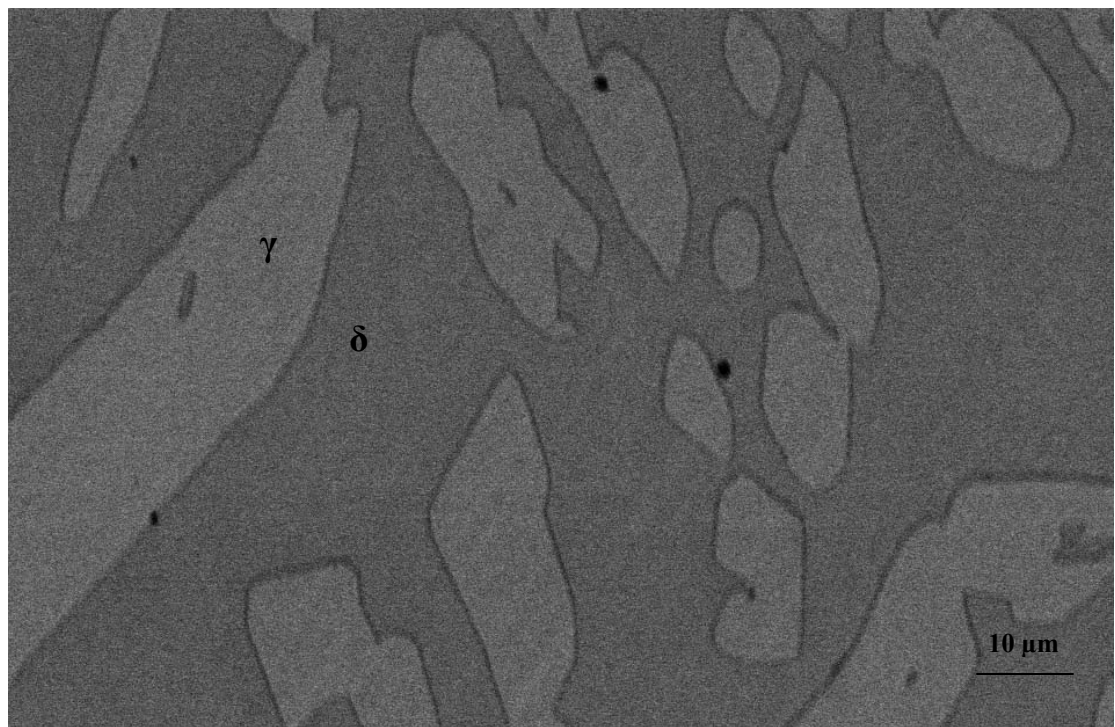
Figure 114: Backscatter SEM image of 41544, 500x
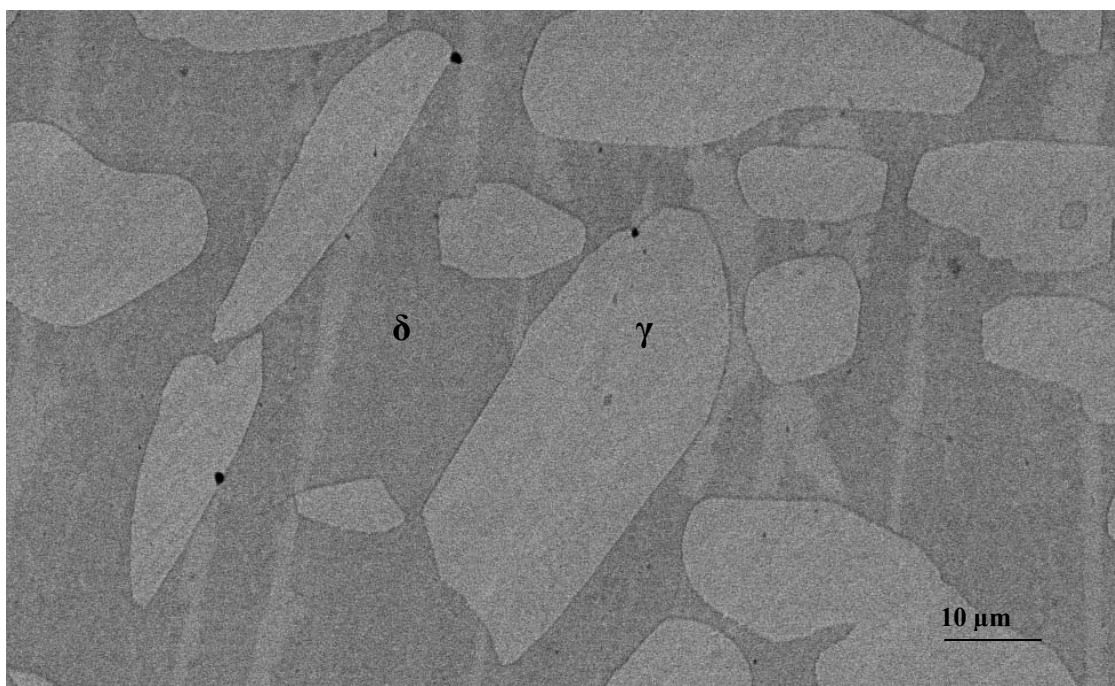

Figure 115: Backscatter SEM image of 44073, 500x
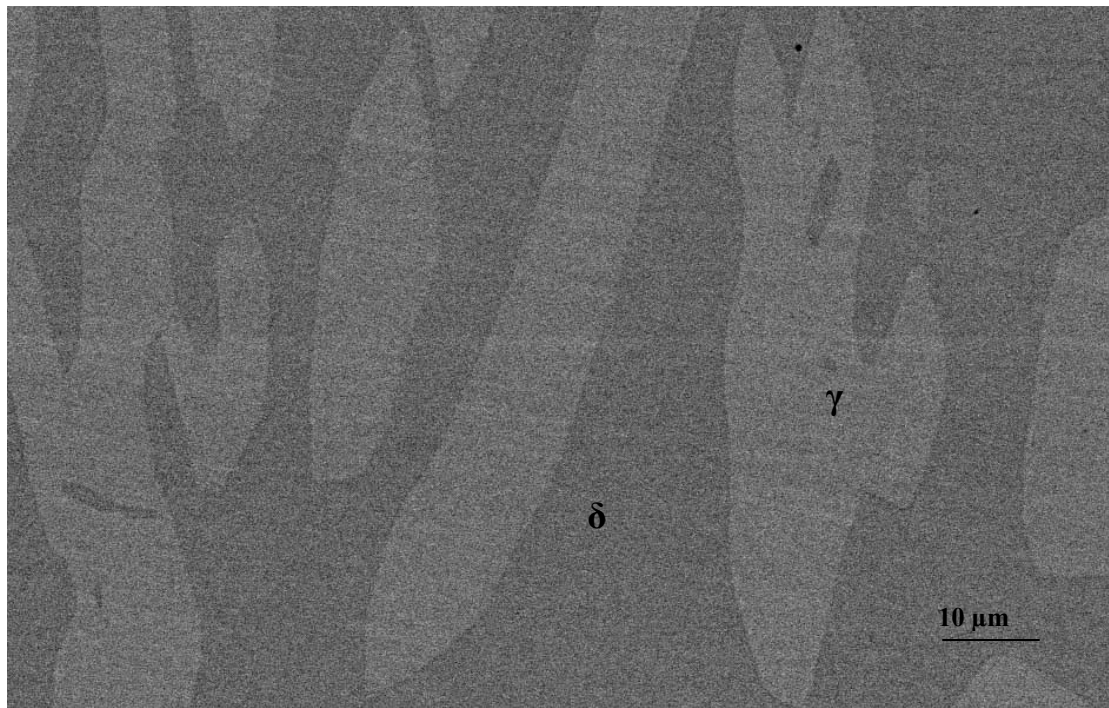
**Figure 116:** Backscatter SEM image of 41414, 500x
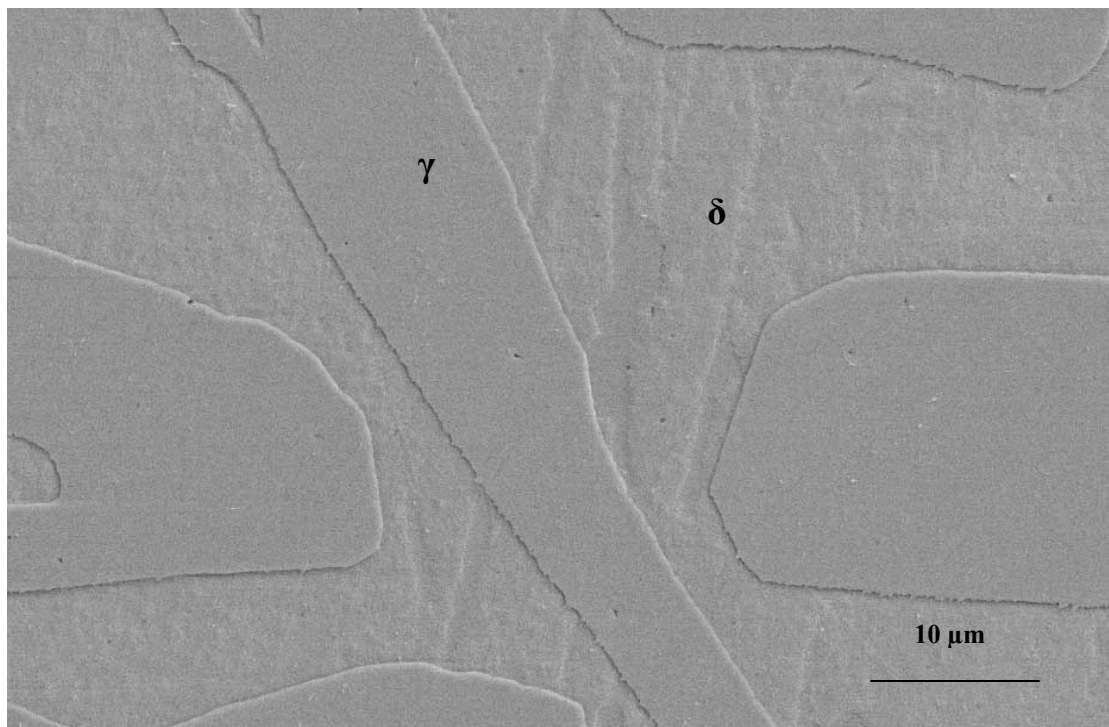
**Figure 117:** Secondary Electron SEM image of 45633, 1000x
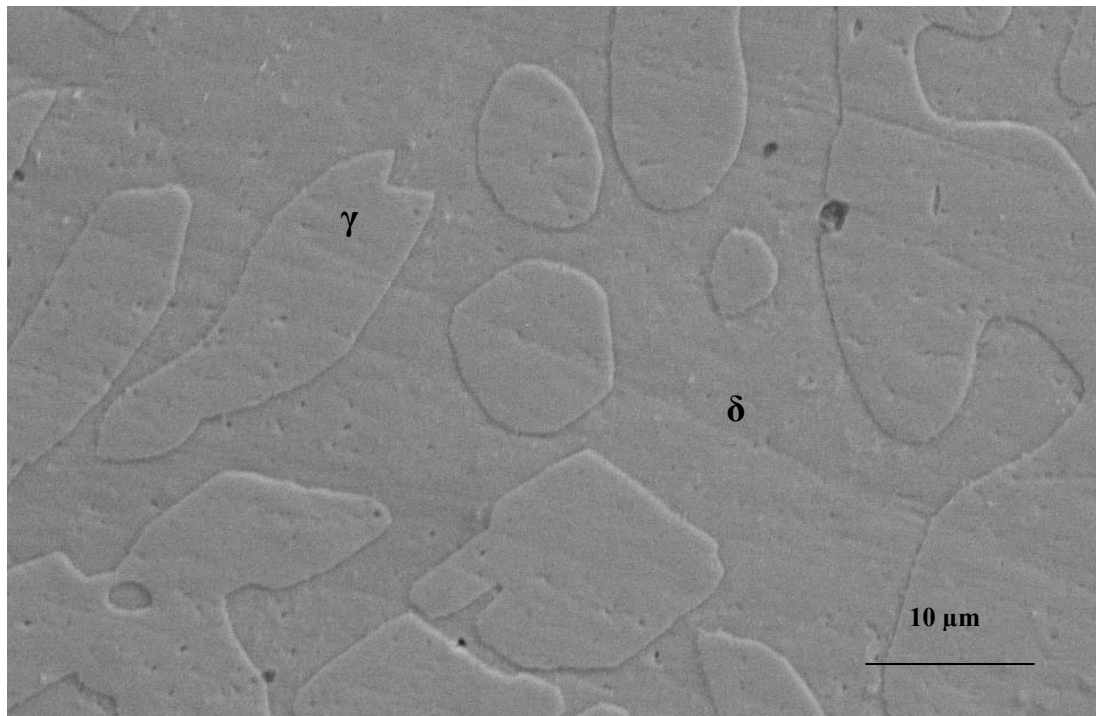
**Figure 118:** Secondary Electron SEM image of S1508, 1000x
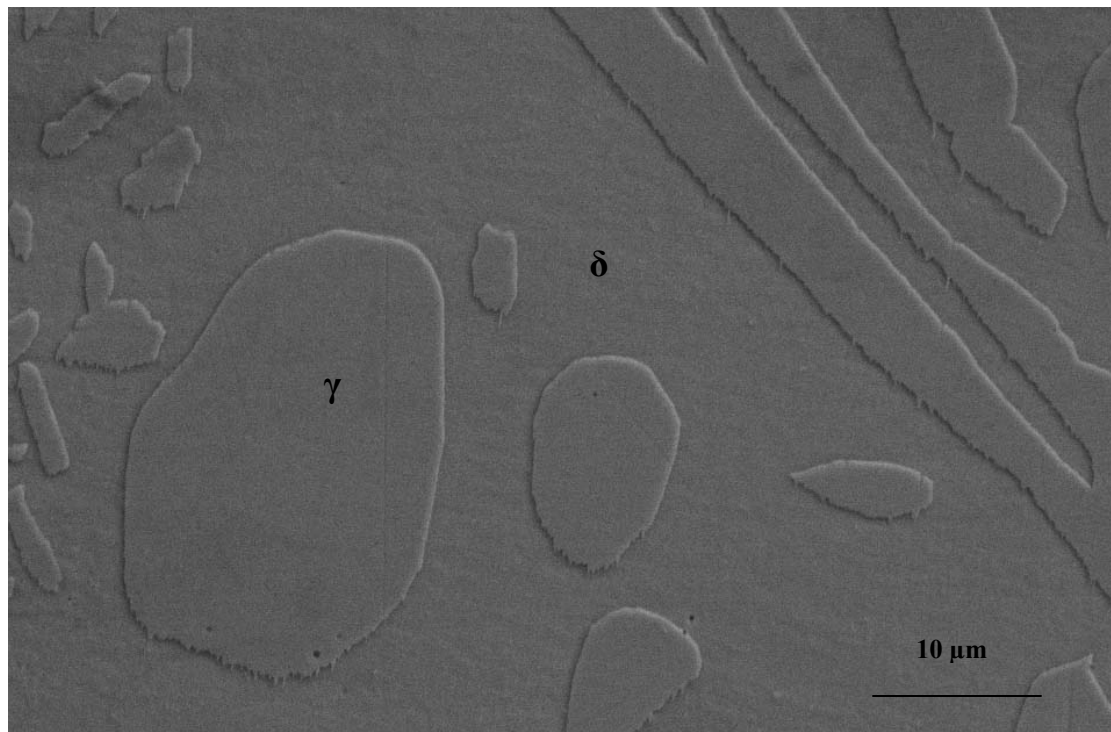
Figure 119: Secondary Electron SEM image of S1507, 1000x

Appendix E

Structure Factor for (200) Austenite and (002) Ferrite Peak

Austenite has FCC crystal lattice, hence it has its atoms are present at $000, \frac{1}{2}\frac{1}{2}\frac{1}{2}$ sites. Ferrite has BCC crystal lattice, hence it has its atoms are present at $000,$

$0\frac{1}{2}\frac{1}{2}, \frac{1}{2}0\frac{1}{2}, \frac{1}{2}\frac{1}{2}0$ sites.

For austenite (200) peak,

$$F_{hkl} = \sum_q f_q e^{i2\pi(hx_q + ky_q + lz_q)}$$

$$F_{hkl} = f_{Fe}(1 + e^{\pi i(h+k)} + e^{\pi i(k+l)} + e^{\pi i(l+h)})$$

$$F_{hkl} = 4f_{Fe}$$

$$\left|F_{hkl}\right|^2 = 16f^2_{Fe}$$

For ferrite (002) peak,

$$F_{hkl} = \sum_q f_q e^{i2\pi(hx_q + ky_q + lz_q)}$$

$$F_{hkl} = f_{Fe}(e^{i\pi(h+k+l)})$$

$$F_{hkl} = 2f_{Fe}$$

$$\left|F_{hkl}\right|^2 = 4f^2_{Fe}$$